

**Computational Analyses of *Mycobacterium tuberculosis*
Enzyme Inhibitors: A Study Involving Free Energy
Perturbations and Molecular Dynamics Simulations**

THESIS

Submitted in partial fulfilment
of the requirements for the degree of
DOCTOR OF PHILOSOPHY

by

PRIYANKA SURYADEVARA

ID No. 2012PHXF536H

Under the supervision of
Prof. P. YOGEESWARI



BITS Pilani
Pilani | Dubai | Goa | Hyderabad

BIRLA INSTITUTE OF TECHNOLOGY AND SCIENCE, PILANI
2016

**Computational Analyses of *Mycobacterium tuberculosis*
Enzyme Inhibitors: A Study Involving Free Energy
Perturbations and Molecular Dynamics Simulations**

THESIS

Submitted in partial fulfilment
of the requirements for the degree of
DOCTOR OF PHILOSOPHY

by

PRIYANKA SURYADEVARA

ID No. 2012PHXF536H

Under the supervision of
Prof. P. YOGEESWARI



BITS Pilani
Pilani | Dubai | Goa | Hyderabad

BIRLA INSTITUTE OF TECHNOLOGY AND SCIENCE, PILANI
2016

BIRLA INSTITUTE OF TECHNOLOGY AND SCIENCE, PILANI

CERTIFICATE

This is to certify that the thesis entitled “**Computational Analyses of *Mycobacterium tuberculosis* Enzyme Inhibitors: A Study Involving Free Energy Perturbations and Molecular Dynamics Simulations**” and submitted by **PRIYANKA SURYADEVARA** ID No. **2012PHXF536H** for award of Ph.D. of the Institute embodies original work done by her under my supervision.

Signature of the Supervisor:

Name in capital letters: **P. YOGEE SWARI**

Designation : **Professor**

Date:

ACKNOWLEDGEMENT

To complete a multiyear task, like PhD is not possible without the help and guidance of mentors, many seasoned experts, colleagues and other technical persons and my task was not an exception. It is a moment of gratification and pride to look back with a sense of contentment at the long traveled path, to be able to recapture some of the fine moments, to think of infinite number of people, some who were with me from the beginning, some who joined me at different stages during this journey, whose kindness, love and blessings has brought me to this day. I wish to thank each of them from the bottom of my heart.

*Words are insufficient to record my deep sense of gratitude to my esteemed teacher, mentor and guide **Prof. P. Yogeewari**, Professor, Department of Pharmacy, BITS Hyderabad for her constant inspiration with keen interest, parental affectionate behaviour and ever vigilant guidance, without which this task could not have been achieved. I appreciated the freedom she allowed, which permitted me to develop scientific thoughts and experimental skills independently. Her sincere involvement in my work has triggered and nourished my intellectual maturity that I will benefit from, for a long time to come.*

*I would also like to express my indebtedness to **Prof. D. Sriram**, Professor, Department of Pharmacy, BITS Hyderabad for his constant support, encouragement and supreme guidance in my entire research work at BITS. Without his valuable supervision and guidance this work would not be possible. The only way to thank him would be perhaps to strive to work similarly in years ahead, and continue the chain succession.*

*I gratefully acknowledge my DAC member **Prof. A. Sajeli Begum** for her understanding, encouragement and personal attention which have provided good and smooth basis for my Ph.D. tenure.*

*I take this opportunity to thank **Prof. V.S. Rao**, Acting Vice-Chancellor (BITS) and Director (BITS Hyderabad campus), for providing competent laboratory facilities and infrastructures to carry out my doctoral research work in the institute.*

I am thankful to **Prof. S.K. Verma**, Dean, Academic Research Division, BITS-Pilani and **Dr. Vidya Rajesh**, Associate Dean, Academic Research Division, BITS-Pilani, Hyderabad campus for their co-operation and encouragement at every stage of this research work.

I would like to express my gratitude to **Dr. Shrikant Y. Charde**, Head, Department of Pharmacy, BITS Hyderabad for providing me with all the necessary laboratory facilities and for having helped me at various stages of my research work.

I sincerely acknowledge the help rendered by **Prof. Punna Rao Ravi**, **Dr. V. Vamsi Krishna**, **Dr. Swati Biswas**, **Dr. Balaram Ghosh**, **Dr. Onkar Prakash Kulkarni**, **Dr. Arti Dhar**, and other faculty members at the BITS-Pilani, Hyderabad campus. It's my pleasure to acknowledge their constant moral support.

I owe a great deal of appreciation and gratitude to **Dr. Vinay Kumar Nandicoori**, Scientist, and his group at National Institute of Immunology, New Delhi, India for providing *Mycobacterium tuberculosis* clones for selected protein targets.

I take this opportunity to sincerely acknowledge the Department of Science & Technology (DST), Government of India, New Delhi, for providing financial assistance in the form of **INSPIRE Fellowship** which buttressed me to perform my work comfortably.

An attempt such as a Ph. D. is unattainable to achieve without the generous help and support of friends and colleagues. I would like to take this opportunity to thank those whom I was fortunate to know, work and form friendship with over the past few years. I owe a special mention of my friend, **Preeti**, without whom I definitely couldn't have completed this journey of research. You were the one always by my side in my good and hard times supporting and encouraging me towards my goals. It was really a wonderful journey and wish lot more to come with you. I would also like to thank **Ravali**, **Pavan Kumar**, **Sirisha**, **Chinmai**, **Prasanna** and **Jyothsna** for their awesome companionship through this journey.

It's my fortune to gratefully acknowledge the support of some special individuals. Words fail me to express my appreciation to all my friends **Ram**, **Hasitha**, **Vijay**, **Brindha**, **Jean**, **S. Ganesh**, **P. Ganesh**, **Bobesh**, **Shalini**, **Renuka**, **Mahibalan**, **Patrisha**, **Madhu**, **Gangadhar**, **Srikanth**, **Kaushik**, **Shubam**, **Radhika**, **S. Reshma**, **U. Priyanka**,

Prakruti, Nikhila, Prasanthi, Siva Krishna and for the time they had spent for me and making my stay at campus a memorable one. I take this opportunity to thank one and all for their help directly or indirectly. I express my thanks to our laboratory assistants, Mr. Srinivas, Mrs. Saritha, Mr. Rajesh, Mr. Ramu and Mrs. Rekha.

I express my entire honour to “My Parents” without whose blessing this task would not have been accomplished. I bow my head in utter humility and dedicate this piece of work to them from within my heart. My vocabulary is not wide enough to put my sentiments in words to repay them for what they have done to groom me in such a great fashion. This list would be incomplete without the mention of “My Family” because of who I am here today. I am happy to thank all my family members for their love and support and feel lucky to be a part of this wonderful family. I promise you to achieve higher positions in life and make you all proud.

It would be incomplete without the mention of my cousins Chaitu, Karunya, Manu, Vihari, Chinna babu, Chintu, Munna and Mintu with whom I explored most of the happiness and craziness in my life and hope to wish this throughout my journey. Happiness is till the moon with a new little angel into our family, Aanya, to whom I adore loads of love and blessings. You are the joy of my life baby.

Lastly, and above all, I would like to thank the God Almighty; for all that he has given to me.

Priyanka

ABSTRACT

In the present study, we attempted to develop novel *Mycobacterium tuberculosis* inhibitors by exploring pharmaceutically underexploited enzyme targets of the pathogen. Glutamine synthetase and glutamate racemase (MurI) were found to be crucial enzymes involved in the synthesis of mycobacterial cell wall. Malate synthase was observed to be one of the vital enzymes involved in the survival of MTB in dormant conditions within the host. Hence in the present study, three proteins targets, glutamine synthetase, glutamate racemase and malate synthase, were selected and focused for development of potential inhibitors against them that disrupt the vitality of the pathogen.

Utilizing the *in silico* structure based drug design protocol, (1*Z*)-3-methyl-N-[5-({2-[(5-methylisoxazol-3-yl)amino]-2-oxoethyl} sulfanyl)-1,3,4-thiadiazol-2-yl]but-2-enimidic acid (compound **6**) was identified as potential glutamine synthetase inhibitor with an IC₅₀ of **2.12 μM**. 3-(1-{2-[(2-methoxyphenyl)amino]-2-oxoethyl}-5-phenyl-1*H*-pyrrol-2-yl)propanoic acid was identified as *M. tuberculosis* glutamine synthetase lead compound, with IC₅₀ of 10.31 μM, for further structural optimization. In the study of glutamate racemase, a three dimensional protein model was developed due to the absence of its reported crystal structure. Compound 1-(benzamido)-N²,N⁴-diphenylazetidine-2,4-dicarboxamide, with IC₅₀ – 5.97 μM, was identified as lead compound against glutamate racemase through *in silico* virtual screening protocol which was further chemically derivatized. Similar to the methodology followed against glutamine synthetase, structure based drug design protocol was operated against malate synthase and compound 4-(1*H*-benzimidazol-2-yl)-N-benzylaniline was identified as a lead for structural optimization.

The leads identified against the three targets were subjected to further structural optimization based on the insights from both molecular docking and chemical synthesis to develop various analogues that displayed significant *in vitro* enzyme efficacy and bactericidal activity against *M. tuberculosis* H37Rv strain.

Of the synthesized series of 40 compounds against glutamine synthetase, compound **PSC10** emerged as the most potent compound with IC_{50} of **1.34 μ M**. Molecular dynamics simulations were carried out for glutamine synthetase–**PSC10** complex for 20 ns whose trajectory analysis revealed the stability of the complex attributing to the binding affinity of the compound. Free energy calculations supported the activity of **PSC10** with its high absolute free energy. The binding affinity of this compound was qualitatively analyzed using differential scanning fluorimetry experiments.

In case of targeting glutamate racemase, the developed model was validated and subjected to *in silico* virtual screening studies where compound 1-(benzamido)- N^2,N^4 -diphenylazetidene-2,4-dicarboxamide was identified as lead compound. Chemical derivatization of the lead resulted in compound **RV4** as the potent *M. tuberculosis* glutamate racemase inhibitor with an IC_{50} of **1.01 μ M** and minimum inhibitory concentration (MIC) of **1.56 μ M**. The activity of the compound was confirmed by differential scanning fluorimetry and molecular dynamics simulation studies.

Similarly, structural optimization of the identified lead against malate synthase resulted in compound **RP07** with an inhibitory concentration of **1.09 μ M** against MTB malate synthase. Differential scanning fluorimetry studies of the malate synthase-**RP07** complex revealed a positive shift in T_m of about 3.7 °C. The stabilizing effect of the compound was further studied using *in silico* simulation of the protein-ligand complex.

With new anti-TB agents desperately needed, we believe that the present class of inhibitors reported in this work would be interesting as potential leads to be worked for rational drug design against *M. tuberculosis* from pharmaceutical point of view.

TABLE OF CONTENTS

Contents	Page No.
<i>Certificate</i>	<i>i</i>
<i>Acknowledgements</i>	<i>ii-iv</i>
<i>Abstract</i>	<i>v-vi</i>
<i>List of Tables</i>	<i>xv-xvi</i>
<i>List of Figures</i>	<i>xvii-xxiii</i>
<i>Abbreviations</i>	<i>xxiv-xxviii</i>
Chapter 1 - Introduction	1-8
1.1.Epidemiology	1
1.2.Pathogenesis	2
1.3.MTB and its cell wall	2
1.4.Current drug therapy and resistance	4
1.5.Current TB drug development pipeline	7
Chapter 2 - Literature review	9-36
2.1. Glutamine synthetase as target for potential antimycobacterial drugs	9
2.1.1. Structural insight of MTB glutamine synthetase	11
2.1.2. Mechanism of action of MTB glutamine synthetase	12
2.1.3. Reported MTB glutamine synthetase inhibitors	13
2.1.3.1. Amino acid site targeting inhibitors	13
2.1.3.2. ATP binding site targeting inhibitors	15
2.1.3.2a. Imidazopyridine based inhibitors	15
2.1.3.2b. Diarylimidazole based Inhibitors	18
2.2. Glutamate racemase as target for potential antimycobacterial drugs	19
2.2.1. Role in bacterial cell wall synthesis	19
2.2.2. Moonlighting function of MurI	20
2.2.3. Relation between main and moonlighting functions of MurI	21
2.2.4. Structural insight of MurI	21
2.2.5. Reported glutamate racemase inhibitors	22
2.3. Malate synthase as target for potential antitubercular drugs	22
2.3.1. Structural information of MTB malate synthase	25

Contents	Page No.
2.3.2. Mechanism of action of MTB malate synthase	30
2.3.3. Reported inhibitors of MTB malate synthase	32
2.3.3.1. Phenyl-diketo acid derivatives	32
Chapter 3 - Objectives and Plan of work	37-41
3.1. Objectives	37
3.2. Plan of work	38
3.2.1. Designing of MTB glutamine synthetase and malate synthase inhibitors	38
3.2.1a. Structure based drug design approach	38
3.2.1b. Development of homology model for MTB glutamate racemase	38
3.2.2. Cloning, expression and purification of MTB GS, MurI and MS	39
3.2.2a: Cloning, expression and purification of MTB glutamine synthetase protein	39
3.2.2b: Cloning, expression and purification of MTB glutamate racemase protein	39
3.2.2c: Cloning, expression and purification of MTB malate synthase protein	39
3.2.3. Biological inhibitory assessment of designed hits against protein targets	39
3.2.3a. <i>In vitro</i> MTB glutamine synthetase enzyme inhibition assay	39
3.2.3b. <i>In vitro</i> MTB glutamate racemase enzyme inhibition assay	39
3.2.3c. <i>In vitro</i> MTB malate synthase enzyme inhibition assay	40
3.2.4. Synthesis and characterization	40
3.2.5. Evaluation of protein-inhibitor binding affinity using biophysical technique	40
3.2.6. <i>In vitro M. tuberculosis</i> screening by MABA assay	40
3.2.7. <i>In vitro</i> cytotoxicity screening by MTT assay	40
3.2.8. Molecular dynamics simulation studies	40

Contents	Page No.
3.2.9. Free energy perturbation studies	40
Chapter 4 – Materials and Methods	42-59
4.1. Identification of novel inhibitors targeting MTB acting through the inhibition of glutamine synthetase, glutamate racemase and malate synthase	42
4.1.1. Design of novel inhibitors for MTB glutamine synthetase, glutamate racemase and malate synthase	42
4.1.1.1. Structure based drug design approach	42
4.1.1.1a. Protein targets for MTB GS and MS	42
4.1.1.1b. Protein and ligand preparation	43
4.1.1.1c. Glide XP (Extra-Precision) docking	43
4.1.1.1d. E-pharmacophore generation	43
4.1.1.1e. Development of tertiary model for MTB glutamate racemase using homology modeling protocol	44
4.1.1.1f. Preparation of commercial database	45
4.1.1.1g. Molecular docking studies – Virtual screening workflow	45
4.1.1.1h. Molecular docking using GOLD	46
4.1.1.1i. Binding Energy calculations	46
4.1.1.1j. QikProp analysis	47
4.1.2. Synthesis and characterization	47
4.1.2.1. Synthetic protocol adopted for expansion of the lead against MTB glutamine synthetase obtained from e-pharmacophore based virtual screening	48
4.1.2.2. Synthetic protocol adopted for expansion of the lead against MTB glutamate racemase obtained from structure based virtual screening	48
4.1.2.3. Synthetic protocol adopted for expansion of the lead against MTB malate synthase obtained from e-pharmacophore based virtual screening	49

Contents	Page No.
4.1.3. <i>In vitro</i> biological assay and biophysical evaluation	50
4.1.3.1. Cloning, expression and purification of the target proteins	50
4.1.3.1a. Cloning, expression and purification of MTB glutamine synthetase	50
4.1.3.1b. Cloning, expression and purification of MTB glutamate racemase	51
4.1.3.1c. Cloning, expression and purification of MTB malate synthase	52
4.1.3.2. Enzyme kinetic studies	52
4.1.3.3. <i>In vitro</i> enzyme assays for target proteins	52
4.1.3.3a. <i>In vitro</i> glutamine synthetase inhibition assay	53
4.1.3.3b. <i>In vitro</i> glutamate racemase inhibition assay	53
4.1.3.3c. <i>In vitro</i> malate synthase inhibition assay	54
4.1.3.4. Biophysical characterization using DSF	54
4.1.3.5. <i>In vitro</i> antitubercular screening using MABA assay	55
4.1.3.6. <i>In vitro</i> cytotoxicity screening	55
4.1.4. Molecular dynamics simulation	55
4.1.4.1. RMSD analysis	56
4.1.4.2. RMSF analysis	57
4.1.4.3. Simulation interaction analysis	58
4.1.5. Free energy calculations	59
Chapter 5 – Results and discussion for development of MTB glutamine synthetase inhibitors	60-103
5.1. Design and development of MTB glutamine synthetase inhibitors	60
5.1.1. Design of glutamine synthetase inhibitors using structure based drug design	60
5.1.1.1. Selection of glutamine synthetase crystal structure and its binding site analysis	60
5.1.1.2. Protein active site validation and e-pharmacophore	62

Contents	Page No.
generation	
5.1.1.3. E-pharmacophore based screening of chemical databases	63
5.1.2. Molecular docking studies of the selected compounds	63
5.1.3. ADMET analysis of selected compounds	67
5.1.4. Binding energy calculations	68
5.1.5. <i>In vitro</i> enzyme inhibition studies	69
5.1.5.1. Enzyme kinetics of MTB glutamine synthetase	69
5.1.5.2. <i>In vitro</i> glutamine synthetase assay for selected compounds	69
5.1.6. Molecular dynamics simulations	73
5.1.6.1. Hydrogen bond analysis	76
5.1.7. Free energy perturbation (FEP) analysis	78
5.1.8. Hit expansion and lead optimization of the most active lead obtained from virtual screening	79
5.1.8.1. Development of 3-[1-(2-amino-2-oxoethyl)-5-phenyl-1 <i>H</i> -pyrrol-2-yl]propanoic acid derivatives as potential <i>M. tuberculosis</i> glutamine synthetase inhibitors	81
5.1.8.2. Molecular docking analysis of the synthesized compounds	82
5.1.8.3. <i>In vitro</i> glutamine synthetase inhibition assay, antimycobacterial potency and cytotoxicity studies for the synthesized compounds	82
5.1.8.3a. <i>In vitro</i> glutamine synthetase inhibition assay	82
5.1.8.3b. <i>In vitro</i> antimycobacterial screening for the synthesized compounds	87
5.1.9. Molecular dynamics simulation analysis	87
5.1.9.1. Simulation interaction analyses	93
5.1.10. Free energy perturbation studies	100
5.2. Highlights of the study	101
Overview of glutamine synthetase work	102

Contents	Page No.
Chapter 6- Results and discussion for development of MTB glutamate racemase inhibitors	104-138
6.1. Design of MTB glutamate racemase inhibitors	104
6.1.1. Development of 3D glutamate racemase model using homology modelling	104
6.1.1.1. Template search using BLASTp and sequence alignment	104
6.1.1.2. Generation of 3D MurI model using homology modelling	106
6.1.1.3. Validation of generated MurI homology model	106
6.1.1.4. Molecular dynamics simulations analysis for MurI model	108
6.1.2. Molecular docking studies using virtual screening	110
6.1.3. <i>In vitro</i> enzyme inhibition studies	112
6.1.3.1. Enzyme kinetics of glutamate racemase activity	112
6.1.3.2. <i>In vitro</i> enzymatic assay for the selected compounds	112
6.1.4. Lead expansion and optimization of the most active compound	113
6.1.4.1. Development of azetidine derivatives as potential <i>M. tuberculosis</i> glutamate racemase inhibitors	113
6.1.4.2. Molecular docking analysis of synthesized compounds	114
6.1.4.3. <i>In vitro</i> glutamate racemase inhibition assay, antimycobacterial potency and cytotoxicity studies for the synthesized compounds	115
6.1.4.3a. <i>In vitro</i> glutamate racemase inhibition assay	115
6.1.4.3b. Structure activity relationship (SAR) of the synthesized compounds	118
6.1.4.3c. <i>In vitro</i> antimycobacterial screening for the synthesized compounds	120
6.1.4.3d. <i>In vitro</i> cytotoxicity studies for the synthesized compounds	121

Contents	Page No.
6.1.5. ADMET analysis of the synthesized compounds	121
6.1.6. Biophysical characterization studies for MurI-RV4 complex	122
6.1.7. Molecular dynamics simulation analysis of MurI-RV4 complex	123
6.1.7.1. Simulation interaction analyses	130
6.2. Highlights of the study	137
Overview of glutamate racemase work	138
Chapter 7- Results and discussion for development of MTB malate synthase inhibitors	139-172
7.1. Design and development of MTB malate synthase inhibitors	139
7.1.1. Design of malate synthase inhibitors using structure based drug design	139
7.1.1.1. Selection of malate synthase crystal structure and its binding site analysis	139
7.1.1.2. Protein active site validation and e-pharmacophore generation	140
7.1.1.3. E-pharmacophore based screening of chemical databases	142
7.1.2. Molecular docking studies of the retrieved hits	142
7.1.3. <i>In vitro</i> enzyme inhibition studies	147
7.1.3.1. Enzyme kinetics of MTB malate synthase	147
7.1.3.2. <i>In vitro</i> malate synthase assay for the selected compounds	148
7.1.4. ADMET analysis	149
7.1.5. Hit expansion and optimization of the most active lead obtained from virtual screening	150
7.1.5.1. Development of 4-(1 <i>H</i> -benzimidazol-2-yl)- <i>N</i> -benzylaniline derivatives as potential <i>M. tuberculosis</i> malate synthase inhibitors	150
7.1.5.2. Molecular docking analysis of the synthesized compounds	154
7.1.5.3. <i>In vitro</i> malate synthase inhibition assay for the synthesized compounds	155
7.1.5.3a. Structure activity relationship (SAR) for the synthesized compounds	157
7.1.6. Biophysical characterization analysis	159
7.1.7. Molecular dynamics simulations	160
7.1.7.1. Simulation interaction analysis	166

Contents	Page No.
7.2. Highlights of the study	170
Overview of malate synthase work	172
Chapter 8- Recapitulation and Conclusion	173-176
8.1. Development of mycobacterial glutamine synthetase inhibitors	173
8.2. Development of mycobacterial glutamate racemase inhibitors	174
8.3. Development of mycobacterial malate synthase inhibitors	175
Future Perspectives	177
References	178-191
Annexures	192-195
Annexure I	192
Annexure II	194
Annexure III	195
Appendix	
List of publications and conferences	196-198
Biography of the candidate	199
Biography of the supervisor	200

LIST OF TABLES

Table No.	Description	Page No.
Table 2.1	Synthesized PDKA derivatives with their MTB malate synthase inhibitory profile	35
Table 5.1	Energy scores of each feature in the generated e-pharmacophore	63
Table 5.2	Glide score, glide energy, fitness and GOLD score for the selected 12 compounds	65
Table 5.3	Interactions of the selected 12 compounds at MTB glutamine synthetase ATP site	66
Table 5.4	<i>In silico</i> pharmacokinetic profile for the selected 12 compounds	67
Table 5.5	Binding energies of 12 compounds calculated using Prime MM-GBSA protocol	69
Table 5.6	Activity table showing IC ₅₀ values for the selected 12 compounds	70
Table 5.7	Solvation free energies calculated for the top 3 active compounds using FEP	78
Table 5.8	<i>In vitro</i> inhibitory activities of the synthesized analogues	83
Table 6.1	Top 5 crystal structures identical to MTB glutamate racemase obtained from BLAST	105
Table 6.2	Structures of selected seven compounds with their glide scores and glide energies	111
Table 6.3	Glide scores and MurI active site interactions of the synthesized azetidine derivatives	114

Table No.	Description	Page No.
Table 6.4	<i>In vitro</i> inhibitory activities of the synthesized analogues	116
Table 6.5	<i>In silico</i> pharmacokinetic profile for the synthesized compounds	121
Table 7.1	Scores of each feature in the generated e-pharmacophore	142
Table 7.2	Glide scores, glide energy and fitness for selected 21 compounds against MTB MS	143
Table 7.3	Activity profile of the selected 6 benzimidazole derivatives against MS	148
Table 7.4	Interactions of active 6 compounds at MTB malate synthase active site	148
Table 7.5	<i>In silico</i> ADME properties for the selected 6 benzimidazole inhibitors of MTB MS	150
Table 7.6	<i>In vitro</i> inhibitory activities of the synthesized analogues	155

LIST OF FIGURES

Figure No.	Description	Page No.
Figure 1.1	Cell wall arrangement of <i>M. tuberculosis</i>	03
Figure 1.2	Current chemotherapy available to cure tuberculosis. The pink cross marks indicate the resistance developed <i>M. tuberculosis</i> against specified drugs thereby developing in to XDR TB	05
Figure 1.3	Current tuberculosis drug development pipeline	07
Figure 2.1	Pictorial representation depicting role of glutamine synthetase in nitrogen metabolism and PLG synthesis	10
Figure 2.2	Mechanism of phagosome-lysosome fusion	11
Figure 2.3	Crystal structure of MTB glutamine synthetase with a close view of ligand bound at the ATP binding site	12
Figure 2.4	Reported MTB glutamine synthetase inhibitors targeting amino acid binding site	14
Figure 2.5	(P) SAR for imidazopyridine based inhibitors of MTB GS (Q) Most active compound of imidazopyridine series reported by Odell <i>et al.</i> (A, B, C) Generic structures of various compounds synthesized by Nordqvist <i>et al</i>	16
Figure 2.6	(a) Most active compound of the synthesized imidazopyridine series by Nordqvist <i>et al.</i> (b) inhibitor co-crystallized with MTB GS by Nordqvist <i>et al.</i> (c) interaction profile of inhibitor b at MTB GS active site as shown by Nordqvist <i>et al</i>	17
Figure 2.7	SAR for various diarylimidazole based MTB GS inhibitors reported by Nilsson <i>et al</i>	18
Figure 2.8	Schematic representation of glyoxylate shunt showing the reaction catalyzed by malate synthase	24
Figure 2.9	Interaction profile of glyoxylate at the MTB MS binding site	26
Figure 2.10	Interaction profile of acetyl Co A (left) and malate (right) at the malate synthase binding site	26
Figure 2.11	Binding of coenzyme A to the active site of GlcB. Surfaces were made around the protein atoms and colored according to the electrostatic potential.	28
Figure 2.12	Stereo view of interaction of malate at malate synthase active site	28

Figure No.	Description	Page No.
Figure 2.13	PDKA inhibitor and its contacts to MTB malate synthase	30
Figure 2.14	Schematic representation of the substitutions attempted over phenyl-diketo acid.	33
Figure 2.15	Comparing binding of PDKA analogs to GlcB	34
Figure 5.1	Interaction profile of the crystal ligand at the active site of glutamine synthetase (PDB code – 4ACF)	61
Figure 5.2	e-Pharmacophore generated for the crystal ligand from MTB glutamine synthetase crystal structure (PDB code – 4ACF)	62
Figure 5.3	Structures of selected 12 compounds selected from asinex against MTB GS	64
Figure 5.4	Enzyme kinetics plot for L-glutamate	70
Figure 5.5	Dose response curve for compounds 6, 1 and 12	71
Figure 5.6	Interaction profile of (a) compound 3, (b) compound 6 and (c) compound 10	72
Figure 5.7	Interaction profile of (a) compound 7 and (b) compound 9	72
Figure 5.8	Interaction profile of the top 3 active compounds: (a) compound 6 (green), (b) compound 1 (orange) and (c) compound 12 (purple) at the MTB glutamine synthetase active site	73
Figure 5.9	(a) RMSD plot of glutamine synthetase in bound states with compounds 6, 1 and 12 as a function of time. (b) RMSD plot of glutamine synthetase in its free state	74
Figure 5.10	RMSF plot for all atoms of glutamine synthetase in its free state resulted from 10 ns simulation trajectory plotted in comparison with that of the crystallographic B factor	74
Figure 5.11	RMSF plot of glutamine synthetase in bound state with compounds 6, 1 and 12	76
Figure 5.12	Hydrogen bonding analysis for glutamine synthetase bound states with ligands (a) compound 6, (b) compound 1 and (c) compound 12 plotted as a function of time	77
Figure 5.13	Interaction profile of comp. 4 for lead optimization studies	80
Figure 5.14	Dose response curve for compound PSC10	86
Figure 5.15	Interaction profile of the most active synthesized analogue PSC10 at the active site of glutamine synthetase	88
Figure 5.16	RMSD plot of glutamine synthetase in bound state with compound PSC10	88

Figure No.	Description	Page No.
Figure 5.17	RMSD plot of compound PSC10 plotted in complex with glutamine synthetase	89
Figure 5.18	RMSF plot for C-alpha atoms of glutamine synthetase-PSC10 complex. Green lines indicate the residues interacting with compound PSC10	90
Figure 5.19	RMSF plot for the compound PSC10 with respect to its each atom during simulation	90
Figure 5.20	The 2D representation of the compound PSC10 shows the rotatable bonds of the compound with different color scheme. Torsion angle and torsion potential plotted for each rotatable bond of compound PSC10 are shown in radial and bar plot respectively	92
Figure 5.21	Interaction profile of the compound PSC10 with glutamine synthetase showing the strength of each interaction	93
Figure 5.22	Timeline representation of the interactions and contacts (H-bonds, Hydrophobic, Ionic, Water bridges) between the compound PSC10 and glutamine synthetase. The top panel shows the total number of specific contacts between MTB GS with compound PSC10 over the course of the trajectory. The bottom panel shows residues interacting with the ligand in each frame	94
Figure 5.23	Top panel of the figure shows the residues of glutamine synthetase involved in hydrogen bonding with compound PSC10. The stacked bar plots indicate the strength of the bond during the simulation time period. The bottom panel shows hydrogen bonding residues interacting with the ligand in each frame	95
Figure 5.24	Top panel of the figure shows the residues of glutamine synthetase involved in hydrophobic interactions with compound PSC10. The stacked bar plots indicate the strength of the bond during the simulation time period. The bottom panel shows residues interacting with the ligand in each frame	96
Figure 5.25	Top panel of the figure shows the residues of glutamine synthetase involved in ionic bonds with compound PSC10. The stacked bar plot indicate the strength of the ionic bond during the simulation time period. The bottom panel shows the residue interacting via ionic bond with the ligand in each frame	97
Figure 5.26	Top panel of the figure shows the residues of glutamine synthetase involved in water mediated hydrogen bonding with compound PSC10. The stacked bar plots indicate the strength of the bond during the simulation time period. The bottom panel shows	98

Figure No.	Description	Page No.
	residues interacting via water bridge interactions with the ligand in each frame	
Figure 5.27	Plot representing various ligand properties analyzed during the simulation of glutamine synthetase-compound PSC10 complex	99
Figure 6.1	Sequence alignment of MTB MurI over the selected template	105
Figure 6.2	(a) Three dimensional structure of glutamate racemase developed with D-glutamate at its active site; (b) interaction profile of D-glutamate at the active site. Pink lines indicate the hydrogen bonds	107
Figure 6.3	Ramachandran Plot for the developed glutamate racemase protein model	108
Figure 6.4	The root mean square deviation plot for MTB glutamate racemase showing for (a) C-alpha atoms of protein and all residues of the protein and (b) backbone atoms of the protein	109
Figure 6.5	Enzyme kinetics plot for D-glutamate	112
Figure 6.6	Interaction profile of compound B5 at glutamate racemase active site	113
Figure 6.7	Dose response curve for compound RV4 (IC50 – 1.01 μ M)	118
Figure 6.8	DSF experiment for compound RV4 showing an increase in thermal stability between the recombinant MTB GS protein (pink) and MTB GS protein-ligand complex (green)	123
Figure 6.9	Interaction profile of compounds (a) RV4 and (b) RV8	123
Figure 6.10	RMSD plot of glutamate racemase in bound state with compound RV4	125
Figure 6.11	RMSD plot of glutamate racemase in bound state with compound RV4 with respect to the simulation trajectory frame	125
Figure 6.12	RMSD plot of compound RV4 plotted in complex with glutamate racemase	126
Figure 6.13	RMSF plot for C-alpha atoms of glutamate racemase-RV4 complex. Green lines indicate the residues interacting with compound RV4	126
Figure 6.14	RMSF plot for the compound RV4 with respect to its each atom during simulation	127
Figure 6.15	Representation of rotatable bonds of compound RV4 with different color scheme	128
Figure 6.16	Torsion angle and torsion potential plotted for each rotatable bond of compound RV4	129

Figure No.	Description	Page No.
Figure 6.17	Interaction profile of the compound RV4 with glutamate racemase showing the strength of each interaction	131
Figure 6.18	Timeline representation of the interactions and contacts (H-bonds, Hydrophobic, Ionic, Water bridges) between the compound RV4 and glutamate racemase. The top panel shows the total number of specific contacts between MurI with compound RV4 over the course of the trajectory. The bottom panel shows residues interacting with the ligand in each frame	131
Figure 6.19	Top panel of the figure shows the residues of glutamate racemase involved in hydrogen bonding with compound RV4. The stacked bar plots indicate the strength of the bond during the simulation time period. The bottom panel shows hydrogen bonding residues interacting with the ligand in each frame	133
Figure 6.20	Top panel of the figure shows the residues of glutamate racemase involved in hydrophobic interactions with compound RV4. The stacked bar plots indicate the strength of the bond during the simulation time period. The bottom panel shows residues interacting with the ligand in each frame	134
Figure 6.21	Top panel of the figure shows the residues of glutamate racemase involved in water mediated hydrogen bonding with compound RV4. Stacked bar plots indicate the strength of the bond during the simulation time period. Bottom panel shows residues interacting via water bridge interactions with the ligand in each frame	135
Figure 6.22	Plot representing various ligand properties analyzed during the simulation of glutamate racemase-compound RV4 complex	136
Figure 7.1	Interaction profile of crystal ligand at malate synthase binding pocket (PDB code – 3S9Z)	141
Figure 7.2	e-Pharmacophore generated for crystal ligand of malate synthase (PDB code – 3S9Z)	141
Figure 7.3	Enzyme kinetics plot for (a) glyoxylate and (b) acetyl Co A	147
Figure 7.4	Interaction profile of top two active compounds (a) compound Bm13 (pink) and (b) compound Bm1 (purple) at the active site of MTB malate synthase	151
Figure 7.5	Electrostatic surface view of MTB malate synthase with compounds Bm1 (pink) and Bm13 (green) at its active site	151
Figure 7.6	(a) Structure of the designed lead with substituents. (b) Interaction profile of lead at the MTB malate synthase active site	153

Figure No.	Description	Page No.
Figure 7.7	Dose response curve for compound RP07	157
Figure 7.8	DSF experiment for compound RP07 showing an increase in thermal stability between the recombinant MTB MS protein (pink) and MTB MS protein-ligand complex (green)	159
Figure 7.9	Interaction profile of the compound RP07 at malate synthase active site	161
Figure 7.10	RMSD plot of glutamine synthetase in bound state with compound RP07	161
Figure 7.11	RMSD plot of malate synthase in ligand free state	162
Figure 7.12	RMSD plot of compound RP07 plotted in complex with malate synthase	162
Figure 7.13	RMSF plot for C-alpha atoms of malate synthase-RP07 complex. Green lines indicate the residues interacting with compound RP07	164
Figure 7.14	RMSF plot for the compound RP07 with respect to its each atom during simulation	164
Figure 7.15	The 2D representation of the compound RP07 shows the rotatable bonds of the compound with different color scheme. Torsion angle and torsion potential plotted for each rotatable bond of compound RP07 are shown in radial and bar plot respectively	165
Figure 7.16	Interaction profile of the compound RP07 with malate synthase showing the strength of each interaction	166
Figure 7.17	Timeline representation of the interactions and contacts (H-bonds, Hydrophobic, Ionic, Water bridges) between the compound RP07 and malate synthase. The top panel shows the total number of specific contacts between MTB MS with compound RP07 over the course of the trajectory. The bottom panel shows residues interacting with the ligand in each frame	167
Figure 7.18	Top panel of the figure shows the residues of malate synthase involved in hydrogen bonding with compound RP07. The stacked bar plots indicate the strength of the bond during the simulation time period. The bottom panel shows hydrogen bonding residues interacting with the ligand in each frame	168
Figure 7.19	Top panel of the figure shows the residues of malate synthase involved in hydrophobic interactions with compound RP07. The stacked bar plots indicate the strength of the bond during the simulation time period. The bottom panel shows residues interacting with the ligand in each frame	169

Figure No.	Description	Page No.
Figure 7.20	Top panel of the figure shows the residues of malate synthase involved in water mediated hydrogen bonding with compound RP07. The stacked bar plots indicate the strength of the bond during the simulation time period. The bottom panel shows residues interacting via water bridge interactions with the ligand in each frame	170

LIST OF ABBREVIATIONS

α	:	Alpha
Å	:	Angstrom
β	:	Beta
μ l	:	Microlitre
μ M	:	Micromolar
δ	:	Chemical shift
Π	:	Pi
^{13}C NMR	:	Carbon Nuclear Magnetic Resonance
^1H NMR	:	Proton Nuclear Magnetic Resonance
A	:	Hydrogen bond acceptor
ADME	:	Absorption, distribution, metabolism, excretion
ADP	:	Adenosine diphosphate
AG	:	Arabinogalactan
ATP	:	Adenosine Triphosphate
BLAST	:	Basic local alignment search tool
BITS	:	Birla Institute of Science and Technology
CFU	:	Colony Forming Unit
CG	:	Conjugate Gradient
CHARMM	:	Chemistry at Harvard Macromolecular Mechanics
CHN	:	Carbon Hydrogen Nitrogen
CNS	:	Central Nervous System
CoA	:	Coenzyme A
CO ₂	:	Carbon dioxide
D	:	Hydrogen bond Donor
DCM	:	Dichloromethane
DMF	:	Dimethylformamide
DMSO	:	Dimethyl Sulphoxide
DNA	:	Deoxyribonucleic acid

D,L-PPT	:	D,L-phosphinothricin
DTNB	:	5,5`-dithio-bis(2-nitobenzoic acid)
DTT	:	Dithiothreitol
DOTS	:	Directly Observed Treatment, Short course
DSF	:	Differential Scanning Fluorimetry
EDC	:	1-Ethyl-3-(3-dimethylaminopropyl) carbodiimide
ELISA	:	Enzyme-linked immunosorbent assay
FBS	:	Fetal Bovine Serum
FDA	:	Food and Drug Administration
FEP	:	Free energy perturbations
GB	:	Generalized Born
GDH	:	Glutamate dehydrogenase
GOLD	:	Genetic Optimisation for Ligand Docking
GlcB	:	Malate synthase G
GLIDE	:	Grid based Ligand Docking and Energetics
GR	:	Glutamate Racemase
GS	:	Glutamine Synthetase
HEPES	:	4-(2-Hydroxyethyl)piperazine-1-ethanesulfonic acid
hERG	:	The human ether-á-go-go-related gene
HIV	:	Human Immunodeficiency Virus
HOBT	:	Hydroxybenzotriazole
HPLC	:	High Pressure Liquid Chromatography
HTVS	:	High-throughput Virtual Screening
IC ₅₀	:	Half maximal Inhibitory Concentration
ICL	:	Isocitrate lyase
INH	:	Isoniazid
IPTG	:	Isopropyl β-D-1-thiogalactopyranoside
H	:	Hydrophobic feature
kDa	:	Kilo Daltons
KH ₂ PO ₄	:	Potassium dihydrogen phosphate

K _i	:	Inhibitor constant
K _m	:	Kinetic constant
KMnO ₄	:	Potassium permanganate
L-RMSF	:	Ligand Root Mean Square Fluctuation
LAM	:	Lipoarabinomannan
LB broth	:	Luria-Bertani broth
LCMS	:	Liquid Chromatography-Mass Spectrometer
MABA	:	Microplate Alamar Blue Assay
MeOH	:	Methyl hydroxide
MD	:	Molecular Dynamics
MDR TB	:	Multidrug Resistant Tuberculosis
MTD	:	Maximum Tolerated Dose
mg	:	Milligram
MgCl ₂	:	Magnesium chloride
MgSO ₄	:	Magnesium sulphate
MIC	:	Minimum Inhibitory Concentration
ml	:	Millilitre
mmol	:	Millimole
MA	:	Mycolic acid
MC	:	Monte Carlo
MDCK	:	Madin-Darby Canine Kidney cells
MS	:	Malate synthase
MSO	:	L-methionine-(S)-sulfoximine
MTB	:	<i>Mycobacterium tuberculosis</i>
MTT	:	(4,5-dimethylthiazol-2-yl)-2,5-diphenyltetrazolium bromide
N	:	Negative ionisable
NaCl	:	Sodium chloride
NAD	:	Nicotinamide Adenine Dinucleotide
NADH	:	Nicotinamide adenine dinucleotide hydrated
NADPH	:	Nicotinamide adenine dinucleotide phosphate
NAG	:	N-acetyl glucosamine

NH ₄ Cl	:	Ammonium chloride
NaOH	:	Sodium hydroxide
Ni-NTA	:	Nickel-nitroloacetic acid
nM	:	Nano molar
nm	:	Nanometre
OADC	:	Oleic acid, Albumin, Dextrose, Catalase
OPLS	:	Optimized Potentials for Liquid Simulations
ORF	:	Open Reading Frame
PAGE	:	Polyacrylamide Gel Electrophoresis
PCR	:	Polymerase Chain Reaction
PDB	:	Protein Data Bank
PDKA	:	Phenyl diketo acid
PG	:	Peptidoglycan
PHASE	:	Pharmacophore Search Engine
PLG	:	Poly L-glutamate
PLP	:	Pyridoxal 5-phosphate
pM	:	Picomolar
PMSF	:	Phenylmethyl sulfonyl fluoride
PPT	:	Phosphinothricin
p-TSOH	:	P-Toluenesulfonic acid
QPlogBB	:	QuickProp predicted Blood Brain partition coefficient
QPlogCaco	:	QuickProp predicted Caco-2 cell permeability
QPlogHERG	:	QuickProp predicted the human Ether-a-go-go-Related gene
QPlogP	:	QuickProp predicted Partition coefficient
R	:	Aromatic ring
RB	:	Rotatable Bond
RFU	:	Relative Fluorescence Units
RMP	:	Rifampicin
RMSD	:	Root Mean Square Deviation
RMSF	:	Root Mean Square Fluctuation
rpm	:	Rotation per minute

Rt	:	Room Temperature
RT-PCR	:	Real time Polymerase Chain Reaction
SA	:	Surface Area
SAR	:	Structure-Activity Relationship
SASA	:	Solvent Accessible Surface Area
SD	:	Steepest Descent
SDS	:	Sodium Dodecyl Sulphate
SP	:	Standard Precision
TB	:	Tuberculosis
TCA	:	Tricarboxylic acid
TDR TB	:	Totally Drug Resistant Tuberculosis
TEA	:	Triethanol amine
TFA	:	Trifluoroacetic acid
TI	:	Thermodynamic Integration
TLC	:	Thin Layer Chromatography
T _m	:	Melting temperature
UV	:	Ultra Violet
V _{max}	:	Maximum velocity
VSW	:	Virtual Screening Workflow
WHO	:	World Health Organisation
XDR TB	:	Extensively Drug Resistant Tuberculosis
XP	:	Extra Precision
ZnSO ₄	:	Zinc sulphate

Chapter 1

INTRODUCTION

The battle of humankind with tuberculosis dates back to antiquity. Tuberculosis (TB) is a chronic infectious disease standing in second place next to HIV causing mortality. Tuberculosis was acknowledged a global health emergency by the World Health Organization (WHO) in 1993 [Wilson S.M.H., 2003]. The disease is caused by *Mycobacterium tuberculosis* (MTB), which is an acid fast bacterium. The bacterium is an obligate aerobic bacillus with slow rate of division. TB is an air-borne disease which is transmitted as highly infectious aerosol. The pathogen typically affects lungs, but can also infect other vital parts of the body such as intestines, brain, spinal cord and kidneys. The outcomes from the exposure of the pathogen to the human body ranges from the destruction of pathogen by host's immune system to development of active primary TB by the individual [Flynn J.L. *et al.*, 2001]. The symptoms of the active TB infection include chest pain, prolonged cough producing sputum, chills, night sweats, fatigue and loss of appetite [Bennett J.E *et al* 2014]. However, the majority of individuals infected with MTB have a non-contagious form of infection, known as latent tuberculosis. This form of infection does not show any symptoms and possess 5-10% risk of development of active TB during the lifetime of an infected individual [Clark-Curtiss J.E. and Haydel S.E., 2003].

1.1. Epidemiology

The Global Tuberculosis Report 2014 by World Health Organization (WHO) estimated that almost 9 million people developed TB in 2013 and 1.5 million people died from disease also including 3.6 lacs deaths from HIV infected people. More than half of the reported TB cases in the year were in South-East Asia and Western Pacific regions (56%) and Africa (25%). India and China had accounted 24% and 11% of total cases respectively. About 60% of TB cases and deaths occur among men, but the burden of disease among women is also high. This implied that there were shortcomings of current treatment strategies for TB and limited

effectiveness of public health systems [WHO Report, 2014]. A new emerging issue is co-infection of HIV and MTB. According to the WHO report, an estimated 1.1 million (13%) of the 9 million people who developed TB in 2013 were HIV-positive. Globally, around one fourth of TB deaths were due to HIV and this was about to one-third of new HIV-positive TB cases.

1.2. Pathogenesis

TB infection begins when the mycobacteria reach the pulmonary alveoli, where they invade and replicate within endosomes of alveolar macrophages. Macrophages identify the pathogen as foreign material and attempt to eliminate it by phagocytosis. During this process, the bacterium is enveloped by the macrophage and stored temporarily in a membrane-bound vesicle called phagosome. In the process of killing the pathogen, phagosome combines with lysosome to create a phagolysosome. Within the macrophage the bacteria inhibit many cellular mechanisms preventing the fusion between phagosomes and lysosomes [Houben E.N., *et al.*, 2006]. MTB is able to reproduce inside the macrophage and will eventually disrupt the immune cell. When a large number of macrophages get infected, they fuse together and form multinucleated giant cells called Langhans cells. These infected macrophages are surrounded by other immune cells creating a compartment called granuloma [Pieters J., *et al.*, 2008]. Usually macrophages, T lymphocytes, B lymphocytes and fibroblasts aggregate to form granulomas, which are surrounded by lymphocytes [Grosset J., *et al.*, 2003]. Mostly, the granulomas formed will be suppressed by the host immune system thereby restricting the replication of bacteria. In such cases the pathogen enters a dormant state within the granulomas, within which the pathogen virulence factors and the host immune response are in balance. Suppression of the immune system leads to the bacterial reactivation and its replication thereby turning into active TB infection.

1.3. MTB and its cell wall

Two factors: *persistence* and *resistance* have made the treatment of tuberculosis disease difficult [Clemens D.L. and Horwitz M.A., 1996]. The term persistence depicts the survival success of MTB irrespective of the use of antibiotics. It is this persistence phenomenon, because of which the treatment of disease is extended and the use of current antibiotics require long courses of treatment. Another term resistance depicts the occurrence of genetic mutations that result in an innate loss of susceptibility to antibiotics. The principle

component of mycobacteria contributing to its persistent and resistant nature is its highly lipophilic cell wall which determines the virulence of the pathogen.

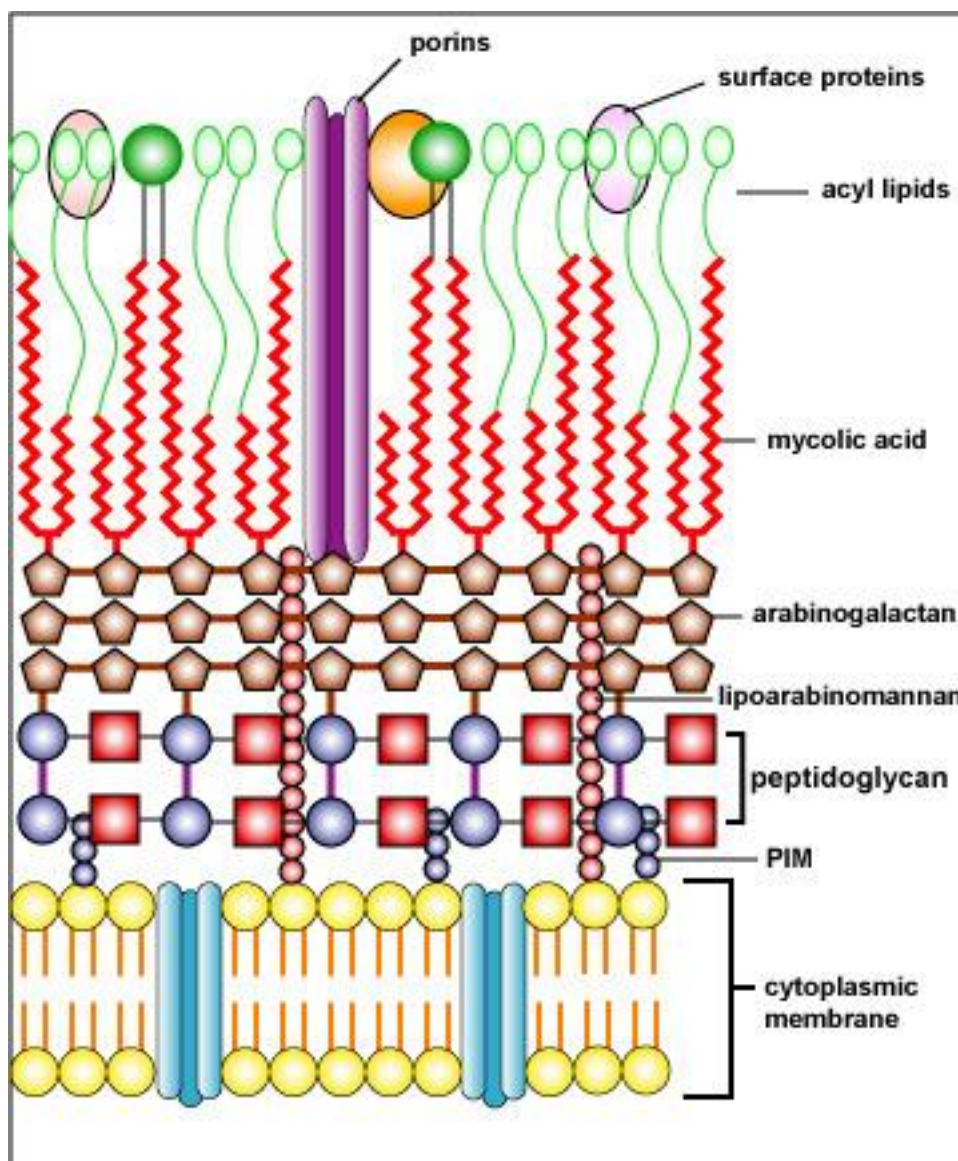


Figure 1.1: Cell wall arrangement of *M. tuberculosis* [www.quizlet.com/10261163/medical-microbiology-flash-cards/].

The mycobacterial cell wall consists of an inner layer and outer layer that surround the plasma membrane [Brennan P.J., 2003]. The cell wall arrangement of MTB is shown in **Figure 1.1**. The outer layer consists of both lipids and proteins. The lipids are freely associated with cell wall with some long- and short- chain fatty acids. The lipid-linked polysaccharides associated with the outer cell wall consist of lipoarabinomannan (LAM),

lipomannan, phosphatidyl inositol mannosides. These outer proteins and lipids are soluble components of cell wall and have been referred to as the signaling and effector molecules of mycobacteria because of their role in interacting with the host immune system. The inner component consists of peptidoglycan (PG), arabinogalactan (AG) and mycolic acids (MA) covalently linked together to form a complex called PG-AG-MA complex that extends from the plasma membrane outward in layers, starting from peptidoglycan to mycolic acids. This complex of mycobacteria is referred to as the most essential component of cell wall and is highly insoluble. Most of the drugs aimed at the disruption of mycobacteria target this complex.

Peptidoglycan is a versatile material rigid enough to provide a scaffold for bacteria to maintain their shape and protect them from osmotic turgor pressure. The structure of peptidoglycan is unique to bacteria, hence an excellent target for therapeutics. This layer consists of many peptides and repetitive units of glycan strands like N-acetyl glucosamines (NAGs) linked to N-acetyl muramic acid (NAM) [Benson T.E., 1996; Holtz J.V., 1998]. Arabinogalactan is the major polysaccharide of the mycobacterial cell wall. It is important for cell integrity and for anchoring the impermeable MA layer to the PG layer. Ag is composed of arabinan and galactan, both in the relatively uncommon furanose form [McNeil M., 1987]. Mycolic acids are unique α -branched lipids found in cell walls of mycobacterium [Asselineau J., *et al.*, 1950]. Mycolic acids are strong hydrophobic molecules that form lipid shell around the organism that affects permeability property in cell surface [Takayama K., *et al.*, 2005]. Mycolic acids prevent mycobacteria from the attack of cationic proteins, lysozyme and oxygen radicals in phagocytic granule. The high lipid content of the mycobacterial cell wall make the bacteria impermeable to many agents, attributes to the resistance of the bacteria towards many antibiotics, resistant to host immune system, resistant towards acidic/alkaline environment and survival of the bacteria under stress conditions in the dormant form [Jarlier V. and Nikaido H., 1994].

1.4. Current drug therapy and resistance

Tuberculosis is one of the most explored infectious diseases in the field of drug discovery. Most of the first-line agents currently being used in the treatment of tuberculosis have been discovered in the early 1950's. Of all the drugs, streptomycin was the first discovered

effective antitubercular agent [Singh B. and Mitchison D.A., 1954]. It is an aminoglycoside, which interfere with the protein biosynthetic pathway, interacting with the 30S subunit of the ribosome [Schatz A., *et al.*, 1944; Jones D., *et al.*, 1944]. Later, isoniazid (INH), one of the most potent anti-tubercular agents was discovered which inhibit the mycolic acid synthesis, a crucial component of MTB cell wall [Bernstein J., *et al.*, 1952] as shown in **Figure 1.2**. Though these agents were effective against MTB, the treatment period was a major fall back with these agents which also exceeds a year sometimes.

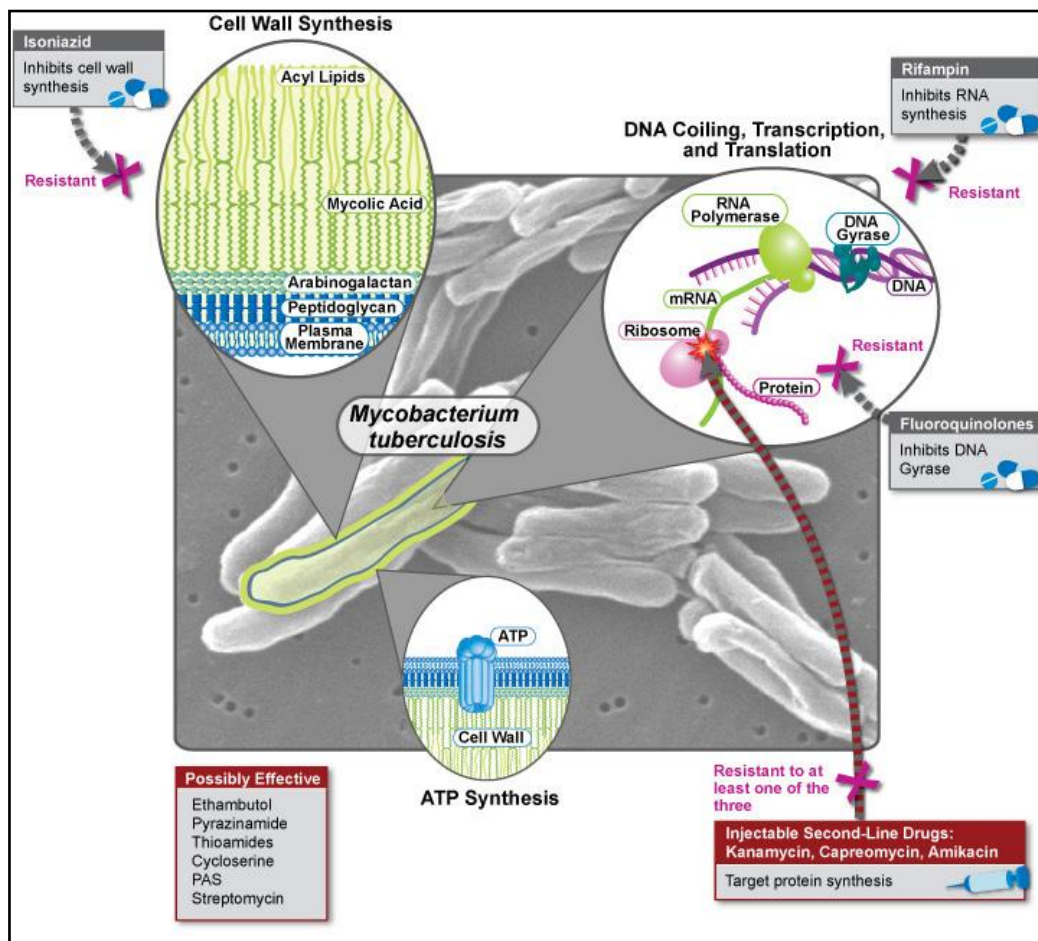


Figure 1.2: Current chemotherapy available to cure tuberculosis. The pink cross marks indicate the resistance developed *M. tuberculosis* against specified drugs thereby developing in to XDR TB. [www.niaid.nih.gov]

The major breakthrough in the field of antitubercular drug discovery can be considered as the discovery of pyrazinamide, which significantly reduced the treatment period to 6 months. Later, ethambutol was discovered as antitubercular agent during the screening of a

series of diamine analogues [Thomas J.P., *et al.*, 1961]. The final drug of first-line agents, rifampicin/rifampin (RMP) was discovered as an effective anti-TB agent against both replicating and non-replicating MTB [Binda G., *et al.*, 1971]. This mainly inhibits the RNA synthesis by binding to the β -subunit of DNA-dependent polymerase.

The second line drugs are only used to treat disease that is resistant to first line therapy. Some of the second line agents include aminoglycosides (amikacin, kanamycin), polypeptides (capreomycin, viomycin, enviomycin), fluoroquinolones (ciprofloxacin, moxifloxacin), thioamides (ethionamide, prothionamide), cyclosterine and terizidone. The third line agents are also available which include drugs that may be useful but have doubtful or unproven efficacy which include rifabutin, clarithromycin, linezolid, thioacetazone etc.

In spite of the availability of many effective antitubercular agents, treatment of tuberculosis is always an aspect of challenge. This is because of the resistance developed by the bacteria against these agents. Mycobacterium is popularly known for its high rate of mutation which continuously changes its physiology. Hence, the treatment for TB is given in combination therapy which reduces the chances of development of resistance against the particular drug. The combination therapy, consists of isoniazid, pyrazinamide and rifampicin or different combinations, lasts from 6-8 months depending upon the recovery of the individual. But still the problem prevails in the treatment due to the emergence of new strains of mycobacteria which are resistant to this therapy too. Such strains include – MDR TB, XDR TB and TDR TB. The genetic diversity of drug-resistant MTB indicates that the drug resistance has been evolving due to inappropriate drug treatment [Trauner A., *et al.*, 2014].

Multi-drug resistant tuberculosis (MDR TB) is defined as TB that is resistant at least to isoniazid and rifampicin. Isolates that are multi-resistant to any other combination of antitubercular drugs but not to INH and RMP are not classed as MDR TB [Iseman M.D., 1998]. The term MDR-TB was associated with high mortality rates occurred among HIV-infected patients [WHO report, 2013]. The treatment is quite complicated and it requires second-line drugs some of which are less effective, more toxic and expensive than first-line drugs. Extensively-drug resistant (XDR TB) is defined as MDR TB that is resistant to quinolones and also to any one of kanamycin, capreomycin or amikacin [WHO. 2006]. The principles of treatment for MDR TB and XDR TB are the same with the difference lying in

the high mortality rate associated with XDR TB than that of MDR TB.

1.5. Current TB drug development pipeline

Current TB drugs were developed 40-45 years ago, against which mycobacteria developed resistance. However, treatment of TB requires long treatment duration and with combination of drugs. The treatment of resistant TB is difficult because less potent and more toxic drugs are required for longer duration. In recent years, several promising TB drugs have been identified and developed and new regimens that combine these drugs with existing drugs have been studied with the aim of reducing treatment duration [Zumla A., *et al.*, 2013]. Some of the recent developments include identification of moxifloxacin and levofloxacin both with equally good efficacy and safety in the early phase of treatment of MDR TB [Falzon D., *et al.*, 2011]. Current TB drug pipeline is shown in **Figure 1.3**.

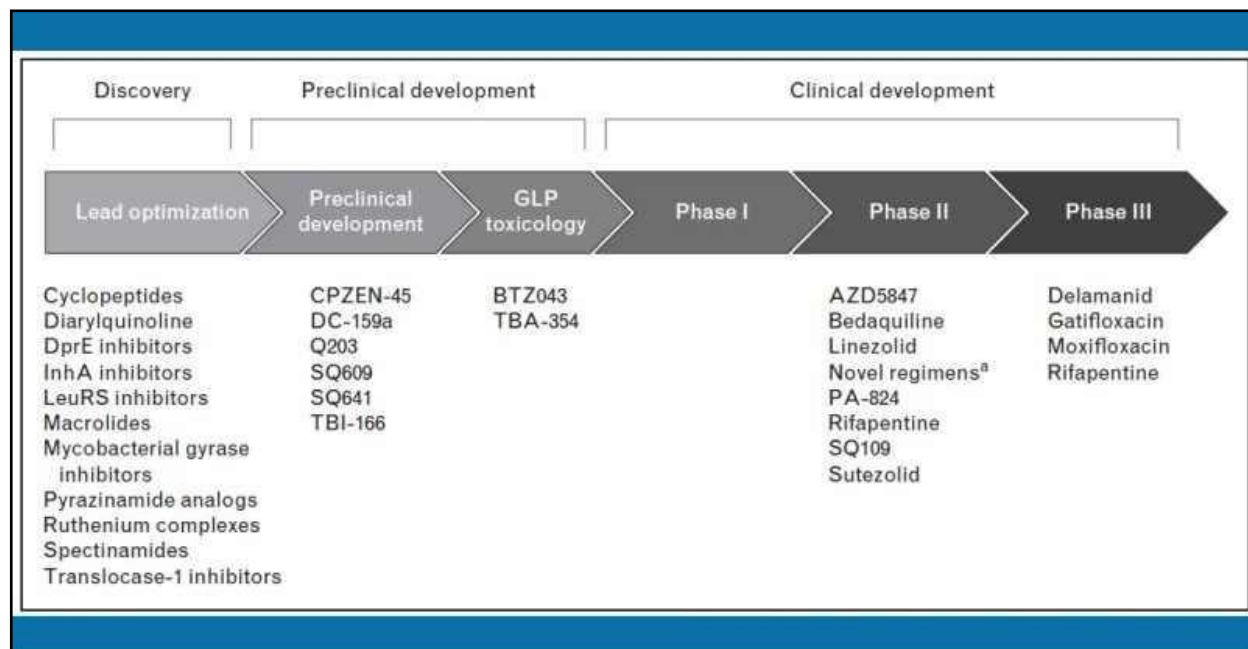


Figure 1.3: Current tuberculosis drug development pipeline [Kwon Y.S., *et al.*, 2014].

Bedaquiline (TMC-207), a diarylamine, is a potent new drug target which acts as an adenosine triphosphate synthase (ATPase) inhibitor [Andries K., *et al.*, 2005]. It was recently approved by U.S. FDA for the treatment of MDR-TB as a part of new combination therapy. It has very low minimum inhibitory concentration (MIC) against MTB and potent bactericidal activity in murine model exceeding INH and RMP [Andries K., *et al.*, 2005].

Delamanid (OPC-67683) and **PA 824**, new nitroimidazoles, inhibit mycolic acid synthesis

and are currently in phase 3 trials for the treatment of MDR-TB [Matsumoto M., *et al.*, 2006].

Clofazimine, an antileprotic drug, and combination therapy with meropenem and clavulanate showed positive effects over inhibition of cultures of MDR TB [Gopal M., *et al.*, 2013; Hugonnet J.E., *et al.*, 2009]. **SQ109**, an analog of ethambutol, has activity against both drug-susceptible and drug-resistant TB by targeting MmpL3 in MTB thereby inhibiting its protein synthesis [Sackstedes K.A., *et al.*, ., *et al.*, 2012]. SQ109 is currently in phase II clinical trials.

Benzothiazinones derivatives, **PBTZ169** and **BTZ043** are in late stage of clinical development. Both drugs inhibit the enzyme, decaprenyl phosphoryl- β -D-ribose 2' epimerase (DprE1) in MTB [Makarov V., *et al.*, 2009]. Inhibition of this enzyme prevents the formation of decaprenyl phosphoryl arabinose- a key precursor for biosynthesis of cell wall arabinans, resulting in cell lysis and bacterial death [Makarov V., *et al.*, 2009]. BTZ043 is active against MTB, drug-susceptible, MDR and XDR TB [Pasca M.R., *et al.*, 2010]. Synergic effects were also found when BTZ043 was combined with bedaquiline [Lecharties B., *et al.*, 2012].

Chapter 2

LITERATURE REVIEW

In the search of new TB drugs that can overcome the increasing spread of MDR and XDR-TB and emergence of drug resistance along with the problem of mycobacterial persistence, highlights the need to develop novel TB drugs that are active against drug resistant bacteria and also more importantly, kill persistent bacteria and shorten the length of treatment. It can be approached from the identification and validation of novel targets. One such attractive strategy is to inhibit **glutamine synthetase (GS)**, an ATP-dependent enzyme. The other target that can be handy in inhibiting MTB is **glutamate racemase (MurI)**. The other target is **malate synthase (MS)** from *M. tuberculosis*. The major problem associated with TB is that the TB bacteria survive in the human host for decades evading the immune system in a latent or persistent state. In such conditions, the *glcB* gene that codes for malate synthase enzyme catalyzes the condensation of glyoxylate with acetyl CoA resulting in the formation of L-malate and also it is over-expressed under hypoxic and nutrient starvation conditions. At present, as there is no suitable drug available to treat dormant tuberculosis; it is essential to identify drug candidates that could potentially treat dormant TB. These three targets are the focus of the present study.

2.1. Glutamine synthetase as target for potential antimycobacterial drugs

Of many enzymes important for the vitality of mycobacteria, glutamine synthetase (GS) is one of such enzymes which are involved in various major activities of pathogen. Glutamine synthetase catalyses the formation of glutamine in which glutamate and ammonia act as substrates [Liaw S.H. and Eisenberg D., 1994]. The energy for this reaction is provided in the form of ATP (adenosine triphosphate) which results in formation of ADP (adenosine diphosphate) and Pi (inorganic phosphate). Glutamine synthetase is found in pathogenic (*M. tuberculosis*, *M. bovis* and *M. avium*) and non-pathogenic forms of mycobacteria (*M. smegmatis*, *M. gilvum* and *M. vanbaalenii*) [Harth G., *et al.*, 1994]. The enzyme was also

found to be involved in the extracellular synthesis of glutamine, which is involved in the formation of an important cell wall structure, poly L-glutamic acid/glutamine which is a characteristic of pathogenic mycobacteria [Harth G., *et al.*, 1994]. The role of glutamine synthetase in cell wall synthesis is shown in **Figure 2.1**. This enzyme was also found to influence the cellular ammonia level within the infected host cells thereby inhibiting the phagosome-lysosome fusion, a primary defense mechanism of the host cell (**Figure 2.2**) [Gordon A.H., *et al.*, 1980].

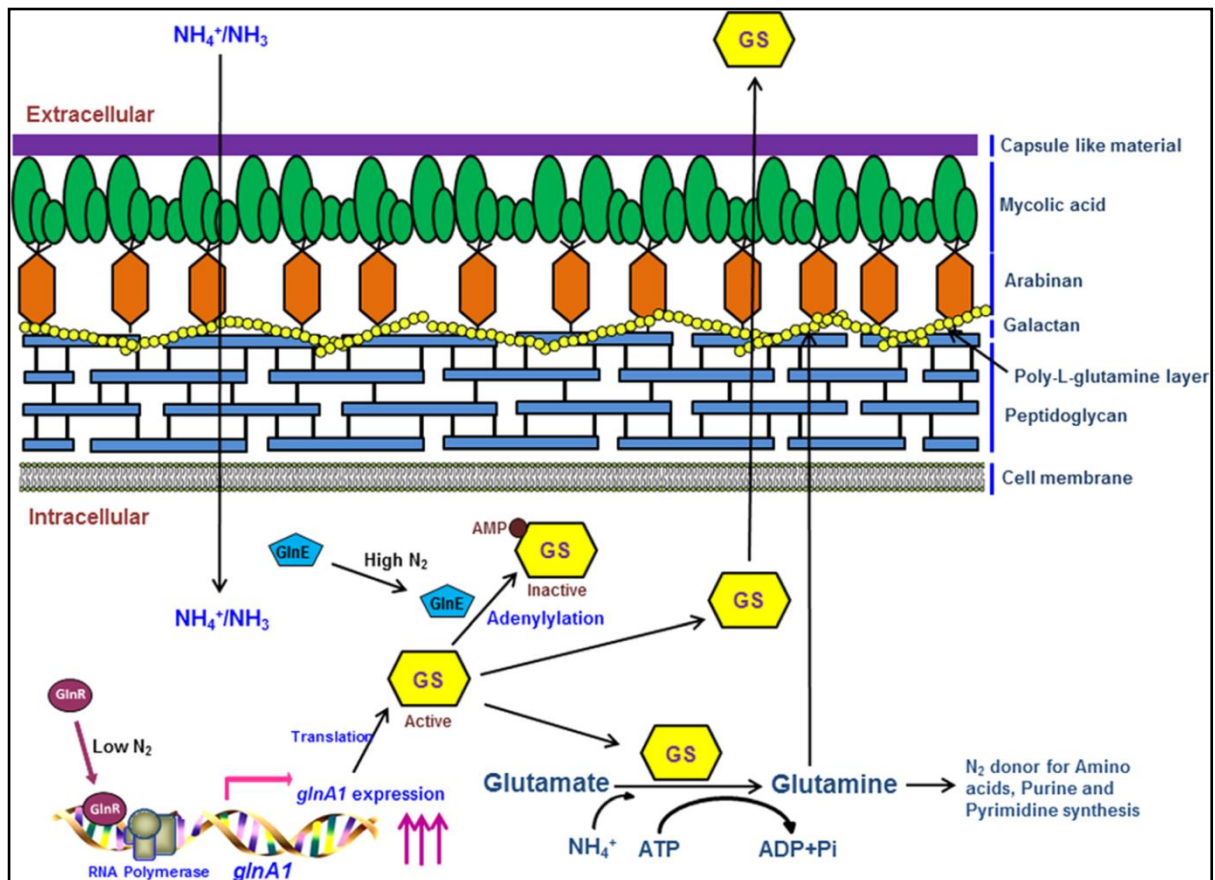


Figure 2.1: Pictorial representation depicting role of glutamine synthetase in nitrogen metabolism and PLG synthesis [Tripathi D., *et al.*, 2013].

Though MTB GS is the most explored enzyme among all mycobacterial glutamine synthetases, GS from other pathogenic mycobacteria like *M. bovis* and from non-pathogenic *M. smegmatis* are also being studied extensively. Studies revealed that the glutamine synthetase coded by *glnA1* is crucial for stress tolerance and resistance of cell wall in *M. bovis* [Chandra H., *et al.*, 2010]. Poly L-glutamate (PLG) synthesized by GS plays a major

role in *M. bovis* pathogenicity which was proved by mutational studies of *glnA1* [Chandra H., *et al.*, 2010]. This PLG synthesis was regulated by the amount of nitrogen availability. During high nitrogen growth conditions, the expression and activity of GS was found to be decreased drastically and which was vice versa [Tripathi D., *et al.*, 2015]. But in *M. smegmatis*, the absence of PLG in the cell wall was reasoned for the low expression level of *glnA1* which makes the bacteria non-pathogenic [Tripathi D., *et al.*, 2015].

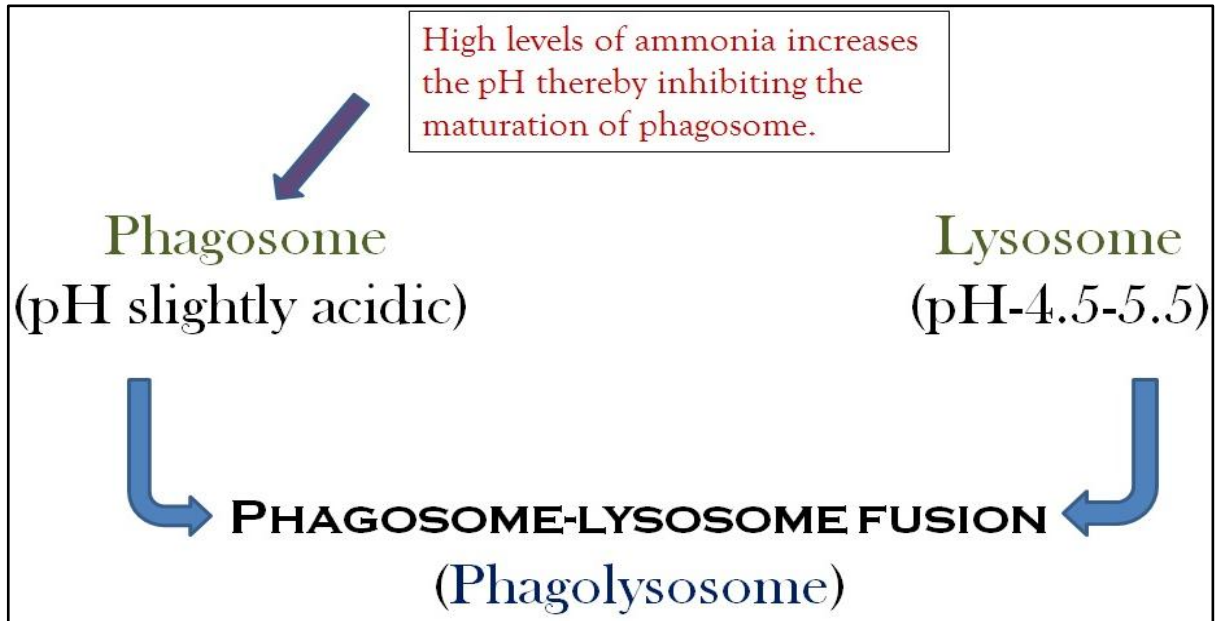


Figure 2.2: Mechanism of phagosome-lysosome fusion.

2.1.1. Structural insight of MTB glutamine synthetase

Glutamine synthetase is a dodecamer (contains 12 monomers) arranged in two parallel hexagonal rings, each with six monomers as shown in **Figure 2.3** [Krajewski W.W., *et al.*, 2005]. Each subunit has two sites, an amino acid binding site where the glutamate accommodates during the catalyzation and another is the ATP binding site. The amino acid binding site accommodates glutamate during the conversion of glutamate to glutamine, where the energy is supplied in the form of ATP that will be binding at the ATP site [Nordqvist A., *et al.*, 2008]. The amino acid binding site also accommodates three magnesium ions (Mg^{2+}) which has key role in the glutamine anabolism [Nordqvist A., *et al.*, 2008]. L-methionine-(S)-sulfoximine (MSO), is a previously known inhibitor of MTB glutamine synthetase (MTB GS) ($IC_{50} \sim 5 \mu M$) whose antibacterial activity was proven by *in vivo* models of guinea pig [Harth G. and Horwitz M.A., 1999; Harth G. and Horwitz M.A., 2003]. It was found that MSO

selectively acts against the pathogenic forms of mycobacteria and was even found to inhibit the growth of *M. tuberculosis* and *M. avium* in the human phagocytes [Harth G. and Horwitz M.A., 1999]. MSO was found to act on glutamine synthetase through its amino acid binding site which shares high similarity with a distantly related enzyme present in human [Krajewski W.W., *et al.*, 2005]. However, the transcriptional profiling studies and western analysis showed that *M. tuberculosis* offered resistance in response to the MSO inhibition by up regulating either GlnA1 or GlnA3, thereby restraining its development as an antitubercular drug [Carroll P., *et al.*, 2011]. ATP binding site offered far better prospects in the field of drug design against glutamine synthetase [Mowbray S.L., *et al.*, 2014]. No resistance towards designed inhibitors against this site has been observed till date. Recent studies reported some of the ATP competitive inhibitors of MTB GS including their crystallographic data [Gising J., *et al.*, 2012; Nordqvist A., *et al.*, 2012].

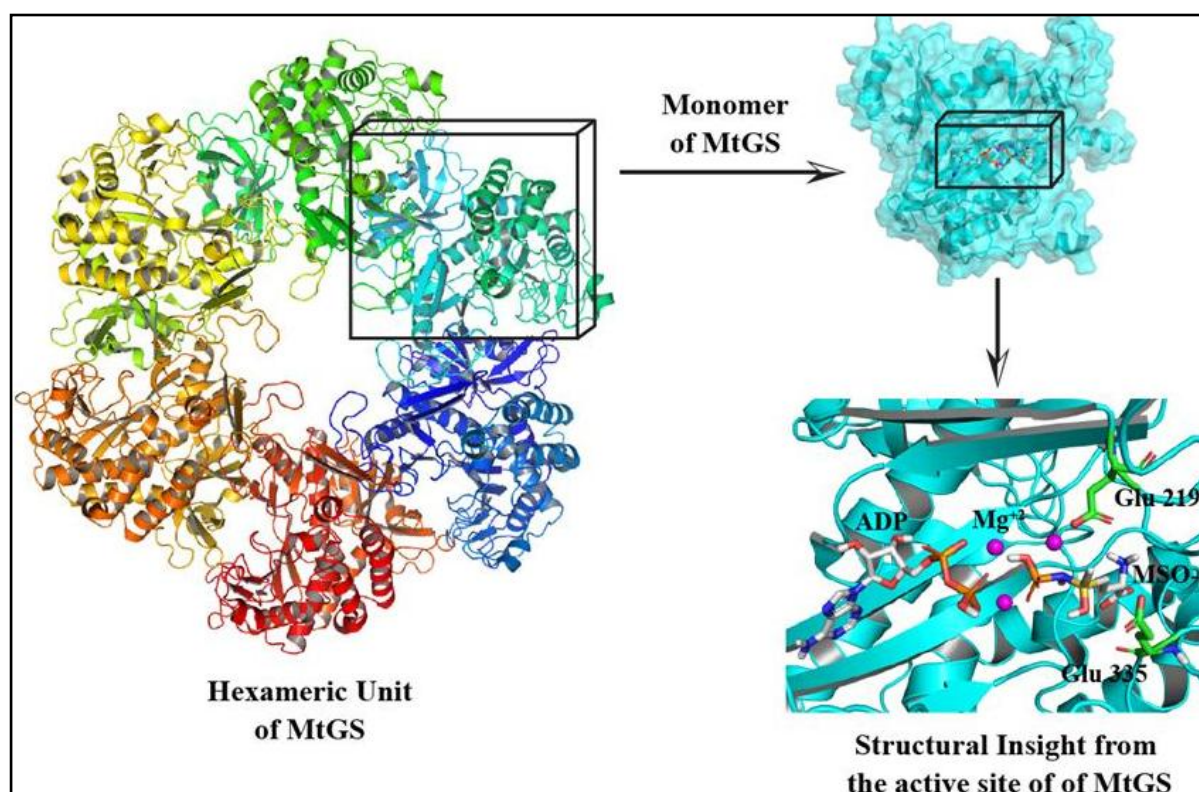


Figure 2.3: Crystal structure of MTB GS with a view of ligand bound at ATP binding site.

2.1.2. Mechanism of action of MTB glutamine synthetase

The first step in GS catalysis is the ordered binding of ATP and glutamate [Eisenberg D., *et al.*, 2000]. There are some differences in the binding of the nucleotide base according to the

literature available till date. However, these differences are not expected to have direct consequences for the reaction mechanism. The next step is the formation of the activated intermediate γ -glutamyl phosphate by means of the transfer of the terminal phosphate of ATP to glutamate. Three magnesium ions are intimately involved in balancing the overwhelming negative charge of both substrates and neighboring protein. The residues coordinating these ions are completely conserved throughout the known GS sequences (Fig. 2B). It has been proposed that magnesium ion coordination is a common catalytic motif among ATP-dependent ligases, increasing the reactivity of the γ -phosphate group of ATP and stabilizing the γ -glutamyl intermediate [Krajewski W.W., *et al.*, 2005]. Subsequent binding of ammonium is thought to occur near the side chain of Glu219; the position is occupied by the methyl group of MSO-P upon binding to GS (Fig. 2C). Thus, the inhibitors act by blocking the ammonium-binding site which prevents further reaction. Multiple interactions with active-site metals, as well as protein, ensure that ADP and phosphorylated inhibitor remain tightly bound [Krajewski W.W., *et al.*, 2005].

2.1.3. Reported MTB glutamine synthetase inhibitors

Glutamine synthetase, being one of the crucial enzymes necessary for the vitality of pathogenic mycobacteria, is an excellent target in the world of antitubercular drug development. Till date, there are a few inhibitors reported against MTB GS belonging to various chemical classes targeting either its amino acid site or the ATP binding site. The initial identification of inhibitors started by exploring the amino acid site which was later focused over the ATP site. The reported MTB GS inhibitors till date targeting both the sites are described in the following sections.

2.1.3.1. Amino acid site targeting inhibitors

In 1999, Harth *et al.* first demonstrated the inhibitory activity of L-Methionine-S-sulfoximine (MSO) and D,L-phosphinothricin (PPT), two well characterized prokaryotic and eukaryotic glutamine synthetase inhibitors, against *M. tuberculosis* glutamine synthetase [Harth G. and Horwitz M.A., 1999]. Both MSO and PPT were found to be inhibiting MTB growth with K_i of 1.1 μ M and 0.6 μ M respectively [Harth G. and Horwitz M.A., 1999]. The structures of both the inhibitors are shown in **Figure 2.4**. Of both the inhibitors, L-methionine-S-sulfoxamine (MSO) was found to be potent against MTB glutamine synthetase. MTB GS was found to be 100 fold more sensitive towards L-methionine-S-sulfoxamine when compared to

the mammalian GS. L-methionine-S-sulfoxamine, when tested over MTB, rapidly inhibited the extracellular glutamine synthetase when compared to the cellular glutamine synthetase demonstrating its inability to cross the mycobacterial cell wall [Harth G. and Horwitz M.A., 1999]. The compound was found to be inhibiting pathogenic mycobacteria but not the non-pathogenic ones signifying its specificity towards extracellular glutamine synthetase when compared with that of cellular glutamine synthetase. Also, the compound was observed with bacteriostatic activity against MTB present within the host human mononuclear phagocytes. Further, the *in vitro* determination of poly-L-glutamate/glutamine content in MTB cultures treated with L-methionine-S-sulfoxamine showed decreased amount of poly-L-glutamate/glutamine portraying the possibility of involvement of extracellular glutamine synthetase in the construction of poly-L-glutamate/glutamine cell wall component [Harth G. and Horwitz M.A., 1999]. The compound was also found to act synergistically with many antibiotics against MTB cultures. The bacterial growth inhibitory effect was more pronounced when L-methionine-S-sulfoxamine was combined with isoniazid and rifampicin. In both the combinations, the bacterial growth was found to be minimal signifying the effect of L-methionine-S-sulfoxamine over extracellular GS which affects the integrity of MTB cell wall thereby providing antibiotics with increased access towards the mycobacterial cytoplasm.

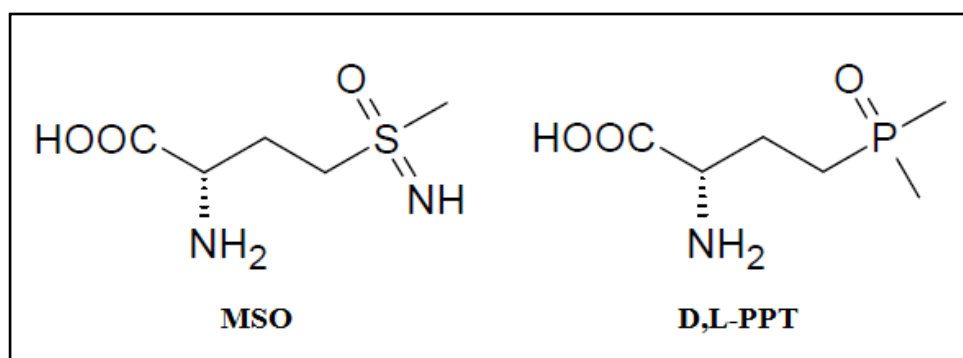


Figure 2.4: Reported MTB glutamine synthetase inhibitors targeting amino acid binding site.

Krajewski *et al.* successfully resolved the crystal structure of glutamine synthetase with ADP, magnesium ions and phosphorylated form of L-methionine-S-sulfoxamine and refined at 2.1 Å resolution (PDB ID - 2BVC) [Krajewski W.W., *et al.*, 2005]. Glutamine synthetase was found to phosphorylate L-methionine-S-sulfoxamine to yield a transition-state analogue, L-methionine-S-sulfoxamine phosphate (MSO-P). MSO-P was found to be involved in

hydrogen bonding with active site residues Glu135, Gly272, His276, Arg329, Arg368 and Arg377. Also the terminal phosphate group of MSO-P was found to interact with the three magnesium ions at the active site. Amino acid sequence analysis of MTB GS at amino acid binding site revealed the presence of amino acids that are conserved in eukaryotes which makes the amino acid site targeting a less preferable one to develop glutamine synthetase inhibitors.

2.1.3.2. ATP binding site targeting inhibitors

The high sequence similarity between the glutamine synthetase of MTB and eukaryotes made the researchers to target the ATP binding site in the process of antitubercular drug discovery. Uppasala University, Sweden in collaboration with AstraZeneca Co. identified several glutamine synthetase inhibitors belonging to different chemical classes through high throughput screening targeting its ATP site [Nilsson M.T., *et al.*, 2009]. Some of the classes are naphthyridines, aminopyrimidines, isoquinoline, diarylimidazoles, aminopurines, benzothiazoles, pyrazolopyrimidines, quinoxalines, diketopurines, imidazopyridines etc. Of these, inhibitors belonging to two chemical classes were well explored till date.

2.1.3.2a. Imidazopyridine based inhibitors

Odell *et al.* attempted to derivatize the identified imidazopyridine class of compound by substituting at various positions. Substitutions were carried out over imidazo[1,2a]pyridine ring and on 2-aryl moiety [Odell L.R., *et al.*, 2009]. These series of compounds represent the first MTB glutamine synthetase drug-like inhibitors targeting ATP binding site. **Figure 2.5(P)** shows the substitutions attempted over the identified imidazopyridine compound where R¹ corresponds to various substituents over 5th, 6th and 8th position and R² corresponds to substituents over its 2', 3' and 4' positions. A total of 33 compounds were synthesized in this series and their glutamine synthetase inhibitory activity was determined. Starting with R¹, compounds were synthesized with substituents like halogens (F, Cl, Br and I), -CF₃, -CN, -Me, -OMe at 6th position and bromine substitution at 5th and 8th positions. It was observed that compound with bromine at 6th position exhibited an IC₅₀ of 8.8 μM which was further derivatized by substituting at R² keeping bromine constant. Various aryl substitutions at R² yielded the most active compound of the series with carboxylic acid at 3' position of phenyl ring as shown in **Figure 2.5(Q)**. The IC₅₀ of this compound was found to be 0.38 μM which was more active than L-Methionine-S-sulfoximine and D,L-phosphinothricin. Exploring the

SAR for these compounds, the presence of halogen (I, Br or Cl) at the 6th position of imidazopyridine ring was found to be beneficial for MTB glutamine synthetase inhibition. Further substitution of 2-aryl group at its *meta*-position with hydrogen bond donor (-OH or -COOH) was found to be necessary for MTB GS inhibition.

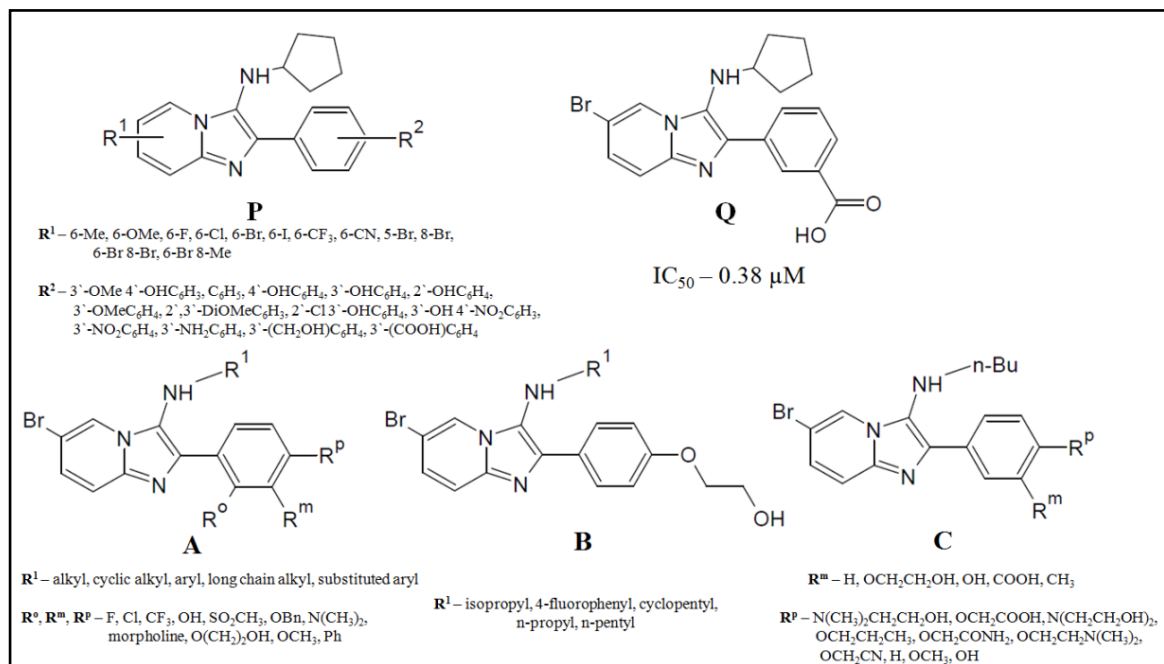


Figure 2.5: (P) SAR for imidazopyridine based inhibitors of MTB GS (Q) Most active compound of imidazopyridine series reported by Odell *et al.* (A, B, C) Generic structures of various compounds synthesized by Nordqvist *et al.*

Later, Nordqvist *et al.* from the same group further explored imidazo[1,2-a]pyridine class of compounds focusing on 2-aryl and 3-alkylamino substituted compounds targeting ATP site of GS [Nordqvist A., *et al.*, 2012]. A total of 33 compounds were synthesized in this series which were developed as three different sets. The generic structures for the three sets are shown as A, B and C in Figure 2.5. All the compounds were found to be retaining bromine at the 6th position of imidazo[1,2a]pyridine moiety. Of the compounds developed from A, compound with n-butyl chain at R¹ and 4-(2-hydroxyethoxy)phenyl group at R² was found to be active with an IC₅₀ of 3 μM which was further derivatized retaining the R² substituent and investigating R¹ with linear, branched, aromatic, larger cyclic and shorter alkyl chains (B).

The follow up series was synthesized retaining the n-butyl chain at R¹ position and substituting *meta*- and *para*-position of 2-aryl group with different substituents (shown as C

in **Figure 2.5**). Of all the compounds in the series, compound with n-butyl chain at R¹ position and carboxylic acid on the *meta*-position of the 2-phenyl ring, shown in **Figure 2.6(a)**, was found to be the most active one with 0.6 μM MTB GS inhibitory activity. In this study, MTB GS was crystallized at 2.0 \AA resolution with an inhibitor at the ATP binding site and MSO-P at the amino acid binding site (PDB ID – 4ACF). The co-crystallized inhibitor was found to be with an IC_{50} of 1.6 μM (**Figure 2.6(b)**). This crystal structure revealed the presence of a hydrogen bond between the NH of the n-butyl amino group with backbone of Lys361 and also an interaction with the water molecule which was hydrogen bonded to Ser280 as shown in **Figure 2.6(c)**. Also strong hydrophobic interactions were observed for the compound with residues Tyr129, Phe232 and Trp282.

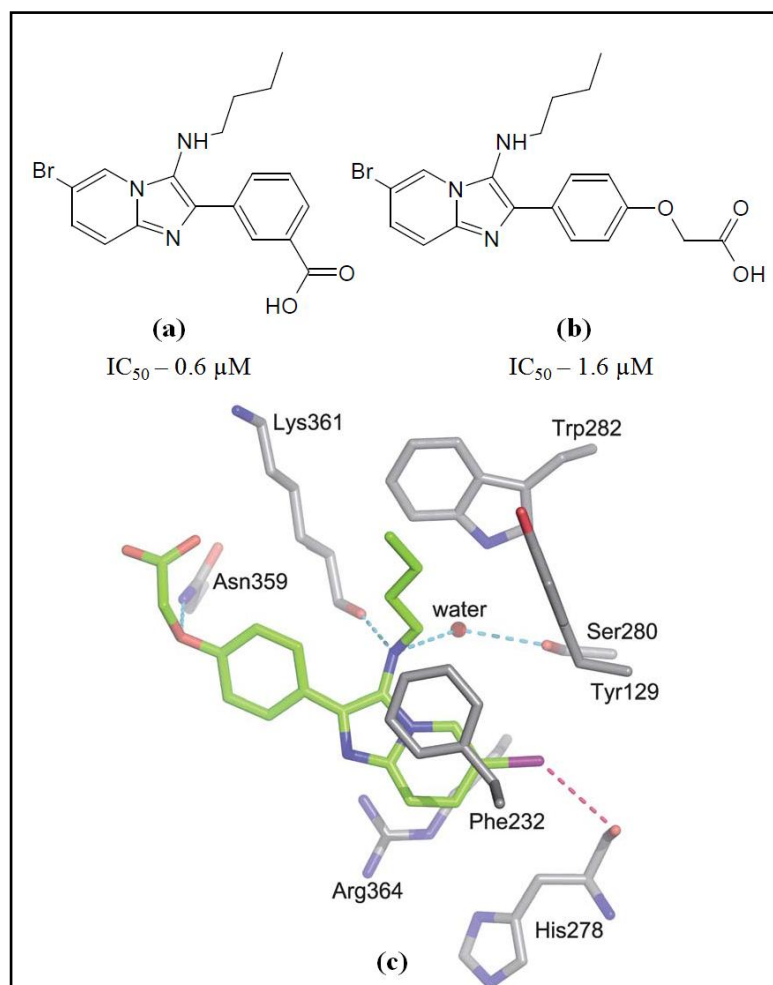


Figure 2.6: (a) Most active compound of the synthesized imidazopyridine series by Nordqvist *et al.* (b) inhibitor co-crystallized with MTB GS by Nordqvist *et al.* (c) interaction profile of inhibitor **b** at MTB GS active site as shown by Nordqvist *et al.*

2.1.3.2b. Diarylimidazole based Inhibitors

Nilsson *et al.* identified several classes of inhibitors against MTB GS through high throughput screening which were clustered based on their common structure [Nilsson M.T., *et al.*, 2009]. One of the classes of compounds identified belongs to 2-*tert*-butyl-4-aryl-5-pyridylimidazole which contained 20 compounds during the screen. Of these 20, 4-[2-*tert*-butyl-4-(6-methoxynaphthalen-2-yl)-1*H*-imidazol-5-yl]pyridine was selected and its derivatives were synthesized by Gising *et al.* for further SAR studies [Gising J., *et al.*, 2012]. A series of 17 compounds were derivatized by optimizing positions 2 and 5 containing *tert*-butyl group and 4-pyridyl group respectively. Substitutions attempted in this study are shown in **Figure 2.7(A)**.

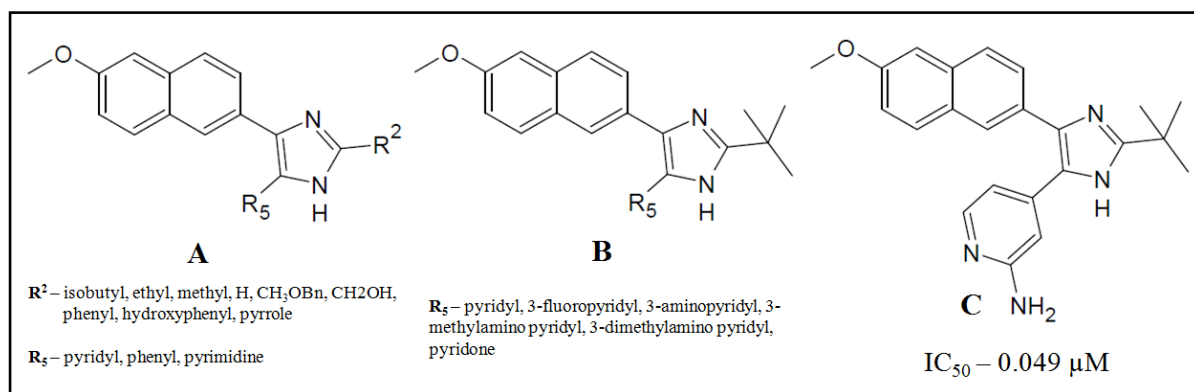


Figure 2.7: SAR for various diarylimidazole based MTB GS inhibitors reported by Nilsson *et al.*

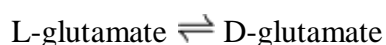
Substitution of 4-pyridyl ring with phenyl, pyrimidine rings resulted in the loss of MTB GS inhibitory activity of the compounds. Removal of two methyl groups at *tert*-butyl group resulted in compound with slight increase in activity. Further modifications like removal of third methyl group, complete removal of *tert*-butyl group, substituting with hydrogen bond donor (-OH), various phenyl derivatives resulted in loss of activity. This signified the importance of relatively bulky substituents over 2nd position of imidazole. Further, substitutions were made over 4-pyridyl ring by placing fluorine, amine, methyl amine, dimethyl amine and oxygen as shown in **Figure 2.7(B)**. The presence of fluorine and amino group were found to enhance the activity of the compound, while the compound with amino group (4-[2-*tert*-butyl-4-(6-methoxynaphthalen-2-yl)-1*H*-imidazol-5-yl]pyridine-2-amine) being the most active one with an IC_{50} of 0.049 μM and an MIC (minimum inhibitory

concentration) of 2 µg/ml (structure of compound shown in **Figure 2.7(C)**). The remaining compounds were found to be inactive suggesting the presence of a hydrogen bond donor over pyridyl ring is advantageous for MTB GS inhibitory activity.

The authors were successful in obtaining the crystal structure of MTB glutamine synthetase with the most active compound of the series (PDB ID – 3ZXV) at a resolution of 2.26 Å. The crystal structure revealed the presence of hydrogen bonds formed by nitrogen of pyridyl ring with Ser 280 and amino group over pyridyl ring with Lys 361 amino acid residue. The nitrogen of imidazole was also found to be interacting with one of the water molecule in its vicinity. The compound was found to be stabilized by hydrophobic interactions with Tyr129, Phe232, Trp282 and Ala362.

2.2. Glutamate racemase as target for potential antimycobacterial drugs

In enzymology, glutamate racemase (MurI) (EC 5.1.1.3) is an enzyme that catalyzes the chemical reaction:



Hence, this enzyme has one substrate, L-glutamate, and one product, D-glutamate. This enzyme belongs to the family of isomerases, specifically those racemases and epimerases acting on amino acids and derivatives, including proline racemase, aspartate racemase, and diaminopimelate epimerase [Kim K.H., *et al.*, 2007]. This enzyme participates in glutamate metabolism that is essential for cell wall biosynthesis in bacteria [Sengupta S., *et al.*, 2008]. Glutamate racemase performs the additional function of gyrase inhibition, preventing gyrase from binding to DNA [Reece R.J. and Maxwell A., 1991]. Glutamate racemase (MurI) serves two distinct metabolic functions: primarily, it is a critical enzyme in cell wall biosynthesis, but also plays a role in gyrase inhibition [Sengupta S., *et al.*, 2008; Reece R.J. and Maxwell A., 1991]. The ability of glutamate racemase and other proteins to serve two distinct functions is known as “moon lighting”.

2.2.1. Role in bacterial cell wall synthesis

Glutamate racemase is a bacterial enzyme that is encoded by the *murI* gene. This enzyme is most commonly known as being responsible for the synthesis of bacterial cell walls. Through experimentation it was found that this enzyme is able to construct these cell walls by synthesizing D-glutamate from L-glutamate through racemization [Hwang K.Y., *et al.*, 1999].

D-glutamate is a monomer of the peptidoglycan layer in prokaryotic cell walls. Peptidoglycan is an essential structural component of the bacterial cell wall. The peptidoglycan layer is also responsible for the rigidity of the cell wall [Schleifer K.H. and Kandler O., 1972]. This process, in which MurI helps catalyze the inter-conversion of glutamate enantiomers, like L-glutamate, into the essential D-glutamate, is also cofactor independent. As such it can proceed without needing an additional source, which would bind to an allosteric site, altering the enzyme shape to assist in catalyzing the reaction [Glavas S. and Tanner M.E., 2001]. MurI involves a two-step process to catalyze the glutamate enantiomers to D-glutamate. The first step is a deprotonation of the substrate to form an anion [Glavas S. and Tanner M.E., 2001]. Subsequently the substrate gets reprotonated. Once the glutamate is in the active site of the enzyme it undergoes a very large conformational change of its domains. Due to this main function of biosynthesis of bacterial cell walls MurI has been targeted as an antibacterial in drug discovery [Lundqvist T., *et al.*, 2007]. But in case of tuberculosis, the enzyme still remains unexplored which can be potential antimycobacterial drug target.

2.2.2. Moonlighting function of MurI

Along with its main function of cell wall biosynthesis, the moonlighting protein glutamate racemase also functions independently as a gyrase inhibitor [Sengupta S., *et al.*, 2008]. Present in certain forms of bacteria, MurI reduces the activity of DNA gyrase by preventing gyrase from binding to DNA [Sengupta S., *et al.*, 2008]. When gyrase binds to DNA, the enzyme decreases the tension in the DNA strands as they are unwound and causes the strands to become supercoiled [Sengupta S., *et al.*, 2006]. This is a critical step in DNA replication in these cells which results in the reproduction of bacterial cells [Sengupta S. and Nagaraja V., 2008]. The presence of glutamate racemase in the process inhibits gyrase from effectively binding to DNA by deforming the shape of the enzyme's active site. It essentially disallows gyrase from catalyzing the reaction that coils unwinding DNA strands [Sengupta S. and Nagaraja V., 2008].

This function of MurI was discovered experimentally. DNA gyrase was incubated with the MurI enzyme and then added to a sample of DNA; the results of this experiment showed inhibition of supercoiling activity when MurI was present. The cell wall biosynthesis function of MurI is not directly related to its moonlighting function. MurI's ability to inhibit gyrase binding can proceed independently of its main function [Sengupta S., *et al.*, 2008]. This

means that DNA gyrase, in turn, will not have any effect on MurI's racemization, which was confirmed in a study of the racemization with and without the presence of DNA gyrase. In an experimental analysis, it was determined that MurI employs the use of two different enzymatic active sites for its two functions. This was shown by the inclusion of the racemase substrate L-glutamate in an assay with the separated gyrase inhibition site. The gyrase inhibition occurs in both supercoiling and relaxing activities of the DNA gyrase, and the study concluded that the inhibition activity was able to proceed, unchanged, in the presence of the racemase substrate [Sengupta S. and Nagaraja V., 2008]. This dictates that the two functions can be carried out independently of each other, on non-overlapping sites, making MurI a true moonlighting protein. Mutant forms of MurI that are unable to exhibit their racemase function, no matter how compromised their racemase abilities were, were still proven through a study to be able to perform the DNA gyrase inhibition, with comparable results to a non-mutated form of MurI [Sengupta S. and Nagaraja V., 2008].

2.2.3. Relation between main and moonlighting functions of MurI

Glutamate racemase (MurI) provides multiple functions for bacterial cells. MurI is an enzyme which is primarily known for its role in synthesizing bacterial cell walls. While performing the function of cell wall synthesis, MurI also acts as a gyrase inhibitor, preventing gyrase from binding to DNA. The two processes have been shown to be unrelated [Sengupta S., *et al.*, 2008]. In order to ascertain the effects of gyrase inhibition on cell wall synthesis, the efficiency of the conversion of D-glutamate to L-glutamate was measured while varying the concentration of DNA gyrase. Conversely, the effects of cell wall production on gyrase inhibition were discovered by varying the concentration of the racemization substrate [Sengupta S., *et al.*, 2008]. The results of these experiments conclude that there is no significant effect of racemization on gyrase inhibition or vice versa. The two functions of MurI act independent of each other, reaffirming the fact that MurI is a moonlighting protein.

2.2.4. Structural insight of MurI

Glutamate racemase is known to use its active site to undergo racemization and participate in the cell wall biosynthesis pathway of bacteria. Till date, there is no crystal structure reported for MTB glutamate racemase. Based on homology to other racemases and epimerases, glutamate racemase is thought to employ two active site cysteine residues as acid/base catalysts [Glavas S. and Tnner M.E., 2001]. From previous studies, it is most likely that the

active site of MurI that performs racemization is not the same active site that undergoes gyrase inhibition. In order to ascertain the effects of gyrase inhibition on cell wall synthesis, the efficiency of the conversion of D-glutamate to L-glutamate was measured while varying the concentration of DNA gyrase. Conversely, the effects of cell wall production on gyrase inhibition were discovered by varying the concentration of the racemization substrate. It has been shown that the two functions are neutral to each other [Sengupta S., *et al.*, 2008]. In other words, racemization substrates are neutral to gyrase inhibition, and DNA gyrase has no effect on racemization. This explains how glutamate racemase in certain bacteria, such as Glr from *Bacillus subtilis*, do not inhibit gyrase; if one active site is involved with both functions, this independence would not be possible [Ashiuchi M., *et al.*, 2003]. Consequently, a different site of MurI, distant from its active site, is involved in interacting with gyrase [Sengupta S., *et al.*, 2008].

2.2.5. Reported glutamate racemase inhibitors

Glutamate racemase has emerged as a potential antibacterial target since the product of this enzyme, D-glutamate, is an essential component of bacterial walls. Inhibiting the enzyme will prevent bacterial wall formation and ultimately result in lysis of the bacteria cell by osmotic pressure. Furthermore glutamate racemase is not expressed nor is the product of this enzyme, D-glutamate is normally found in mammals, and hence inhibiting this enzyme should not result in toxicity to the mammalian host organism [Ruzheinikov S.N., *et al.*, 2005].

Inhibitors targeted against MurI from several bacterial species have been patented and are advocated as promising antibacterial agents. However there are no reported inhibitors against MurI of MTB, due to lack of its three dimensional crystal structure. Possible inhibitors to bacterial MurI such as *B. subtilis* includes aziridino-glutamate that would alkylate the catalytic cysteines; N-hydroxy glutamate that by mimicking Wat2 (the bound water molecule that interacts with glutamate amino group) would prevent binding of the substrate; or 4-substituted D-glutamic acid analogs bearing aryl-, heteroaryl-, cinnamyl-, or biaryl-methyl substituents that would also prevent binding of substrate [Ruzheinikov S.N., *et al.*, 2005].

2.3. Malate synthase as target for potential antimycobacterial drugs

M. tuberculosis is a pathogen capable of causing both an acute disease and an asymptomatic latent infection. In the latent infection, dormant tubercle bacilli persist for years before

reviving and resulting in reactivation of tuberculosis. Our current arsenal of drugs for treating active tuberculosis is relatively ineffective against the latent form.

In order to target the latent stage of the infection, studies have been performed to better understand the extreme intracellular conditions within host macrophages under which dormant MTB reside. Some of the identified conditions include hypoxia [James P.E., *et al.*, 1995], iron deficiency [Schnappinger D., *et al.*, 2003], low pH [Yong-jun Li., *et al.*, 2002] and a fatty acid rich carbon pool [Segal W. and Bloch H., 1956; Wheeter P.R. and Ratledge C., 1988] all contribute to the altered phenotype that MTB displays in the dormant state. With the sequencing of the MTB H37Rv genome, it has become possible to map and assign specific genes to their putative functions [Cole S.T., *et al.*, 1998]. Using microarray technology, genes that are upregulated in response to nutrient starvation [Betts J.C., *et al.*, 2002] and latency-like conditions have been identified [Sherman D.R., *et al.*, 2001; Muttucumaru D.G., *et al.*, 2004; Voskuil M.I., *et al.*, 2004; Boshoff H.I., *et al.*, 2004]. The complete genomic sequence coupled with microarray technology has been critical for the identification of metabolic pathways that are required to support the persistent state in MTB [Stewart G.R., *et al.*, 2003].

One of the changes that occur once MTB enters dormancy is activation of glyoxylate shunt within the tricarboxylic acid (TCA) cycle [Wayne L.G. and Lin K.Y., 1982; McKinney J.D., *et al.*, 2000]. This activation facilitates a metabolic shift to acetyl CoA as the primary carbon source, which is the product of the β -oxidation of fatty acids. The glyoxylate shunt consists of two enzymes, isocitrate lyase (ICL) and malate synthase (MS), which act as a bypass to the two CO₂ producing steps in the TCA cycle, thus conserving carbon (which can be used for gluconeogenesis) and replenishing TCA cycle intermediates in an anaplerotic fashion. The first enzyme in the glyoxylate shunt, ICL, catalyzes the cleavage of isocitrate to succinate and glyoxylate. In the second step, MS condenses glyoxylate and acetyl CoA to produce malate as shown in **Figure 2.8**. Since neither ICL nor MS are present in mammals, they have become attractive targets for novel antitubercular drug design [Smith C.V., *et al.*, 2004].

In MTB, the genes encoding both ICL and MS are upregulated in response to macrophage phagocytosis [Sturgill-Koszycki S., *et al.*, 1997; Honer Zu Bentrup K., *et al.*, 1999]. It has been reported that an MTB *icl* knockout strain was able to establish an acute, but not a persistent infection in mice [McKinney J.D., *et al.*, 2000]. Also, antibodies to MS have been

discovered in 90% of patients during incipient subclinical tuberculosis [Singh K.K., *et al.*, 2005]. According to Lamichhane *et al.*, the random insertion of transposons into the MTB MS gene (*glcB*, annotated Rv1837c) resulted in non-viability under normal growth conditions [Lamichhane G., *et al.*, 2003]; in contrast, Sasseti *et al.*, determined that MTB MS is not required for tuberculosis infection in mice using a similar transposon insertion method [Sasseti C.M and Rubin E.J., 2003]. However, attempts to knockout MTB *glcB* have been unsuccessful (McKinney J.D., *et al.*, personal communication). McKinney *et al.*, using *Mycobacterium smegmatis* (closely related to MTB, but nonvirulent), determined that the double knockout of *glcB* and *gcl* (glyoxylate carboligase, not present in MTB) produced an *M. smegmatis* strain that was unable to grow on acetate as the sole carbon source, which mimics the macrophage intracellular environment.

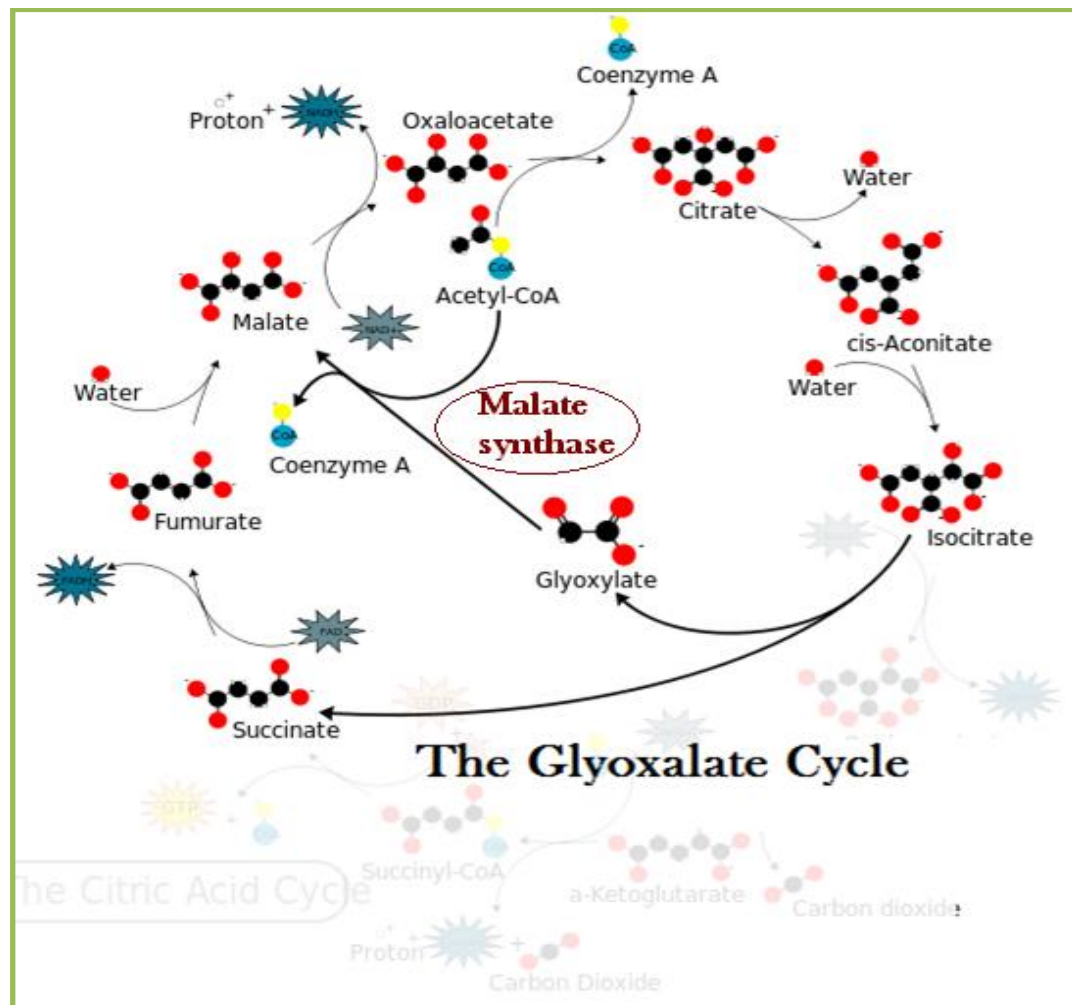


Figure 2.8: Schematic representation of glyoxylate shunt showing the reaction catalyzed by malate synthase [Myler P.J. and Stacy R. 2012].

Additionally, supplementation of MTB glcB into the double knockout *M. smegmatis* strain compensated the knockout phenotype, thus affording the complemented strain with the ability to survive on acetate as the sole carbon source (McKinney J.D., et al., personal communication).

Malate synthase can be majorly divided into two families – isoforms A and G. Malate synthase G (MSG) is an 80kDa monomer found predominantly in bacteria whereas malate synthase A (MSA) is a 65kDa oligomer found in plants and various other organisms [Anstrom D.M. and Remington S.J., 2006]. Malate synthase is considered to play multiple roles in the organism. Besides playing its traditional enzymatic role, MTB MS also takes part in the adherence of the mycobacterium to the host by binding to laminin thus proving as a virulence factor [Smith C.V., et al., 2004; Kinhikar A.G., et al., 2006]. The knockout studies of malate synthase gene from the bacterium have shown to effect its survival indicating the importance of MS [Sasseti C.M. and Rubin E.J., 2003].

Targeting malate synthase rather than ICL to disrupt the glyoxylate pathway is often a better choice due to the wide active site offered by malate synthase contrast to the small and highly polar active site of ICL [Smith C.V., et al., 2003]. Malate synthase G acts in a magnesium dependent manner and contain one Mg^{2+} at the bottom of its active site.

2.3.1. Structural information of MTB malate synthase

In 2003, Smith et al., first attempted crystallization of MTB malate synthase and succeeded in obtaining malate synthase co-crystallized with substrate glyoxylic acid, Mg^{2+} and products malate, co enzyme A and cofactor Mg^{2+} .

Structure of malate synthase complexed with the substrate glyoxylate - The structure of GlcB from *M. tuberculosis* was solved in complex with glyoxylate to 2.1 Å resolution. A Mg^{2+} ion required for activity is bound in a near perfect octahedral coordination by the carboxylate side chains of Glu434, 2.1 Å away and OD1 of Asp462 at 2.0 Å, one carboxylate oxygen (O3 2.1 Å away) and one aldehyde oxygen (O1 2.5 Å away) of the substrate glyoxylate, and two water molecules 2.1 Å and 2.2 Å away, respectively.

The interactions of glyoxylate with malate synthase are shown in **Figure 2.9**. Glyoxylate binds via the aldehyde oxygen (O1) forming a hydrogen bond to NH1 of Arg339, 3.1 Å away. O2 of glyoxylate is hydrogen bonded to the backbone NH group of 461 (2.9 Å), whereas O3

of the glyoxylate interacts with the backbone NH of residue 462 at 3.0 Å. Both Glu434 and Asp462, important in coordinating the Mg²⁺, and residue Arg339, important in binding glyoxylate, are found to be conserved in malate synthase sequences of both A and G types.

Structure of Malate Synthase Complexed with Products Malate and Coenzyme A - The overall structure of GlcB in complex with the products malate and coenzyme A (GlcB malate- CoA) was solved to 2.7 Å and is almost identical to that of GlcB-glyoxylate binary complex, with root mean square differences for C α of 0.5 Å. Interaction of acetyl Co A and malate with malate synthase are shown in **Figure 2.10**. Interaction of co A at the protein active site pocket is also shown in **Figure 2.11**. The protein ligands for Mg²⁺ in GlcB-malate-CoA are the same as in the GlcB-glyoxylate structure, with OE1 of Glu434 and OD1 of Asp-462 1.8 and 2.5 Å, respectively, away from the metal ion. There is a water involved in Mg²⁺ coordination that is 1.9 Å away from the metal ion. Malate coordinates Mg²⁺ via one carboxylate oxygen (O4) at 2.1 Å and via the hydroxyl oxygen (O3) 1.7 Å away. One of the water molecules that were seen coordinating Mg²⁺ in GlcB-glyoxylate is replaced by this hydroxyl of the malate. The backbone NH of residue 461 is 3.2 Å from O1 carboxylate of the malate forming an interaction with the product.

In 2006, Anstrom *et al.*, crystallized MTB malate synthase in ternary complex with malate, coenzyme A and magnesium ion which was deposited in protein data bank with the code 2GQ3. The protein complex was crystallized at 2.3 Å resolution. The binding site of coenzyme A and malate were revisited clearly and shown in **Figure 2.12**. The CoA binding site, as described earlier, is a pocket that is 2.3 Å deep but quite narrow, located between the TIM barrel and the C-terminal plug domains. The adenine ring binds to a hydrophobic patch, wedged between TIM barrel residues Phe126 and Pro545. The phosphate groups are partially exposed to solvent, and there is a bend in the molecule such that an intramolecular hydrogen bond forms between the N7 of the adenine ring and a hydroxyl group on the pantethenic acid portion. Malate forms hydrogen bonds to the backbone of Asp462 and Leu461, as well as two hydrogen bonds with the side chain of Arg339. Depending on the charge states, there may be an electrostatic clash between the side chain of Asp633 and the 4-carboxylic acid of malate. Malate provides two coordinating groups to the catalytic magnesium ion, one of which is an oxygen atom from the 1-carboxylic acid group, while the 2-hydroxyl group provides a second, presumably deprotonated oxygen ligand. Malate thus likely exists in the active site as a

trianion, stabilized by the +2 charge on magnesium as well as the positive charge on Arg339. Arg339 is in turn positioned to make charged hydrogen bonds with both the 2-hydroxyl oxygen and 4-carboxylic acid oxygen.

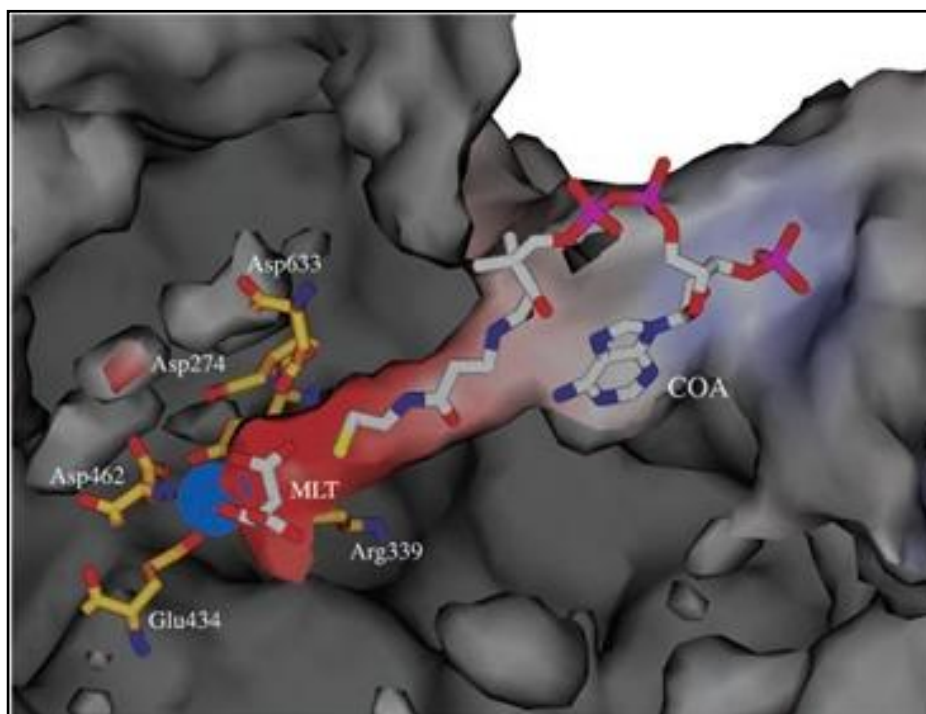


Figure 2.11: Binding of coenzyme A at active site of MS. Surfaces were made around protein atoms and colored according to the electrostatic potential, *red* for acidic, and *blue* for basic residues [Smith C.V. *et al* 2003].

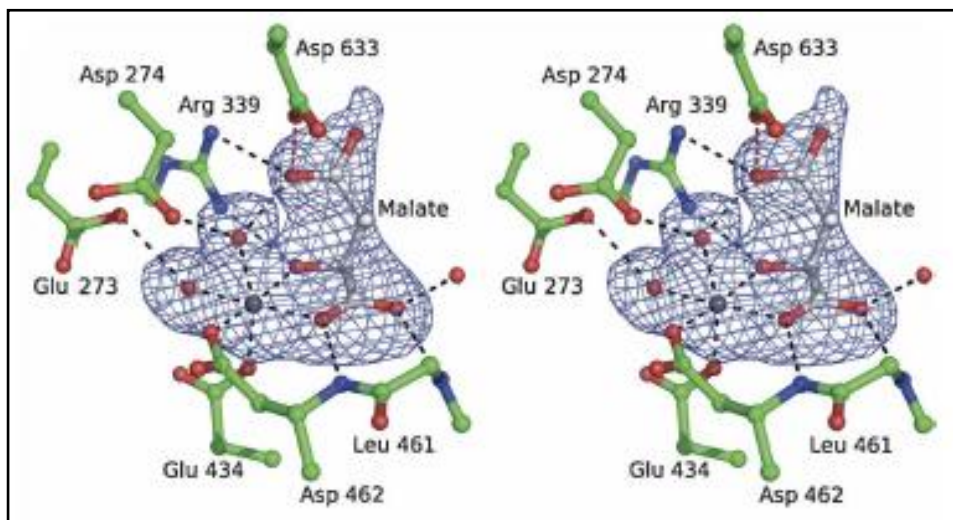


Figure 2.12: Stereo view of interaction of malate at malate synthase active site [Anstorm D.M. and Remington J., 2006].

In 2012, Krieger et al., reported phenyl diketo acid (PDKA) derivatives as potent MTB malate synthase inhibitors. The protein was crystallized along with PDKA bound at the active site. The crystal structure of GlcB complexed with PDKA was determined at 1.9 Å resolution with PDB code 3S9I, whose close examination revealed the mode of binding of the inhibitor [Krieger I.V., *et al.*, 2012].

No significant conformational changes in the protein were observed upon PDKA binding compared to structures with glyoxylate or malate and CoA bound. The backbone rmsd of the superposition between the GlcB:malate complex and the GlcB:PDKA complex is 0.32 Å over 700 Ca atoms. The interaction profile of PDKA at malate synthase binding pocket is shown in **Figure 2.13**.

The inhibitor fills two of the six octahedral coordination sites with one of the carboxylate oxygens and the adjacent ketone oxygen (2.1 Å and 2.2 Å contact distances, respectively). Carboxylate oxygens of the inhibitor hydrogen-bonded with the backbone nitrogens of Asp462 and Leu461 (dO-N = 3.0 and 3.0 Å, respectively). Both ketone oxygens also form hydrogen bonds (dO-N = 2.9 and 2.9 Å) with the Arg339 side chain, exhibiting similar contacts as the substrate and product. The catalytic Asp633 (Clark et al., 1988) side chain oxygen was within hydrogen-bonding distance (3.2 Å) to the phenyl ketone oxygen of PDKA. The aromatic ring forms multiple van der Waals interactions with the C_g of catalytic Asp633 and the side chains of Met515, Trp541, and Met631. The close contact between the Asp633 side chain and the aryl ring of the inhibitor resembles anion- π interactions.

PDKA was structurally optimized so as to identify some more potent MTB malate synthase inhibitors and some of the inhibitors were co-crystallized with the protein and deposited in PDB with codes 3S9Z, 3SAD, 3SAZ, and 3SB0. Some of these derivatives were found to be potent against both *in vitro* enzyme studies and whole cell based assays. Of these, one compound was found to be potent when tested in mouse tuberculosis model.

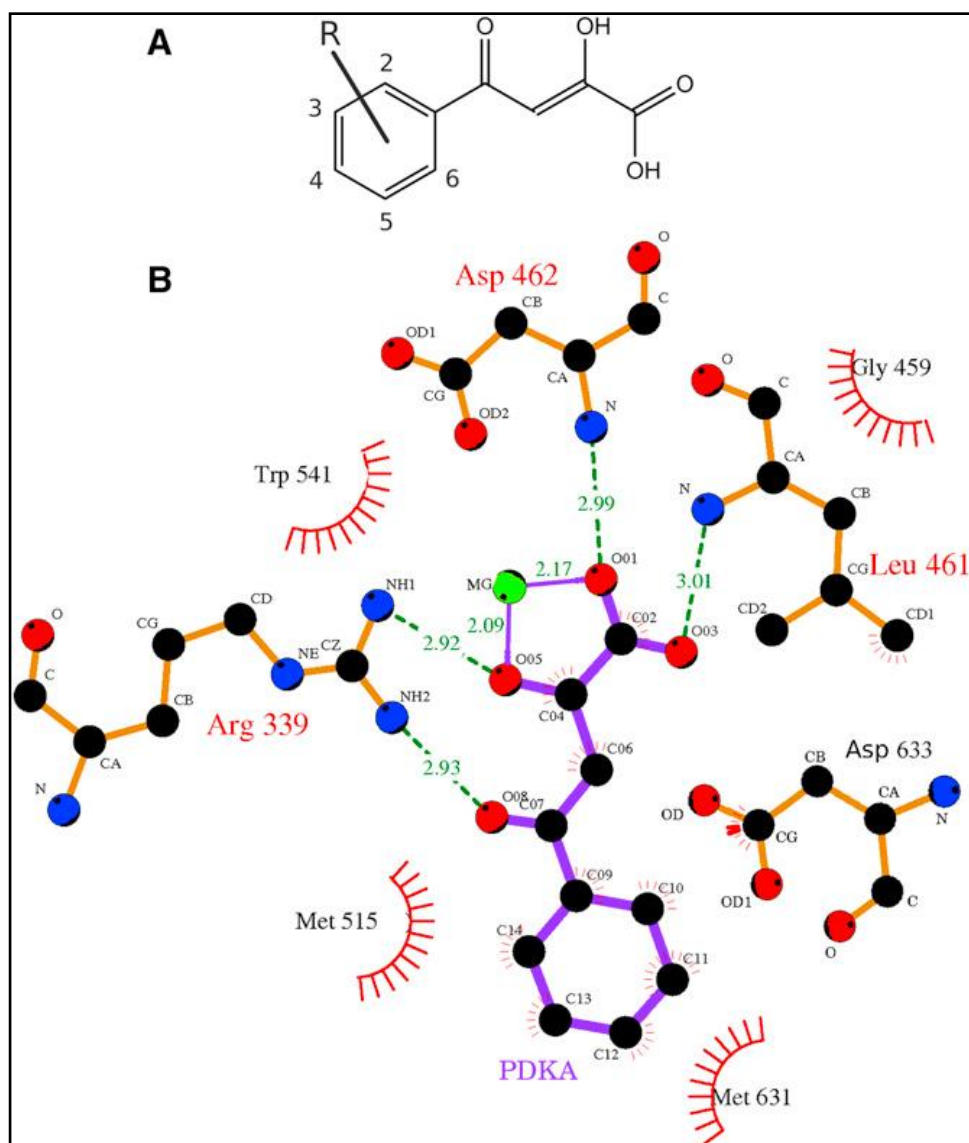


Figure 2.13: PDKA inhibitor and its contacts to MTB malate synthase. (A) PDKA chemical structure drawn here in the enol form most consistent with solution-phase ¹H and ¹³C nuclear magnetic resonance data. (B) Diagram of PDKA-GlcB interactions; hydrogen bonds are shown in green. Catalytic Asp633 contacts the face of the phenyl ring. Coordinating interactions between the Mg²⁺ ion and oxygens of the inhibitor are in purple. Atom colors: black, carbon; red, oxygen; blue, nitrogen; green, magnesium [Krieger I.V., *et al.*, 2012].

2.3.2. Mechanism of action of MTB malate synthase

Malate synthase catalyzes the Claisen condensation of glyoxylate and acetyl-CoA to form a malyl-CoA intermediate, which is subsequently hydrolyzed to release the products, malate and coenzyme A [Smith C.V., *et al.*, 2003]. The reaction can be dissected into three steps as

follows: (i) enolization, (ii) condensation, and (iii) hydrolysis (41). (i) First, an enol(ate) is formed on acetyl-CoA. Activation requires abstraction of a proton from the α -methyl group of the thioester of the acetyl-CoA by a catalytic base. The enol(ate) intermediate is stabilized by an active site general acid. Formation of an enolic intermediate is believed to facilitate the removal of the α -proton of a carbon acid by overcoming the high pK_a (~20–30) of the α -proton (54). (ii) The electrophilic substrate, glyoxylate, is polarized for nucleophilic attack, a step in which magnesium is essential, leading to the formation of the malyl-CoA intermediate. In this condensation step another general acid is required for the protonation of the carbonyl group of the glyoxylate. (iii) Finally, an activated water molecule hydrolyzes the thioester of the malyl-CoA, leading to the formation of malate and coenzyme A. Enolization is believed to be the rate-limiting step in the reaction mechanism.

Comparison of the active sites in the GlcB-glyoxylate structure and of GlcB-malate-CoA helps clarify our understanding of the catalytic mechanism of malate synthase. OD1 of the carboxylate side chain of the proposed catalytic base, Asp633, is 3.0 Å away from S1 of the coenzyme A. The enol(ate) intermediate of the acetyl-CoA is then most likely stabilized by the guanidinium group of Arg339. Another possibility discussed by Howard *et al.* (41) is that the Mg²⁺ may stabilize the enol(ate). Though this is unlikely based on current structural information, which shows that the Mg²⁺ is more than 6 Å away from S1 of the coenzyme A, it cannot currently be ruled out using glyoxylate-bound and product-bound structures. Mg²⁺ is, however, essential in the polarization of the glyoxylate for nucleophilic attack. In the GlcB-glyoxylate structure the Mg²⁺ is positioned by the strictly conserved residues, Glu-434 and Asp-462, as well as via waters to other conserved residues (Glu-273 and Asp-274) and to the carboxylate oxygen (O3) and aldehyde oxygen (O1) of the substrate. The importance of Mg²⁺ in developing the positive charge on the C2 of the carbonyl group and in positioning the glyoxylate in a suitable orientation for reaction have been discussed in the case of malate synthase G from *E. coli* (41). As in *E. coli* an Arg, in this case Arg339, hydrogen bonded to the aldehyde oxygen of glyoxylate, also important in stabilizing the enol(ate), facilitates orientating the two substrates for condensation, stabilizing the oxyanion and yielding a malyl-CoA intermediate.

Hydrolysis of the thioester bond is the next step of the reaction. In the product-bound structure, the hydroxyl of malate replaces one of the waters involved in coordinating the

Mg²⁺ in the glyoxylate-bound structure (Fig. 3). OD1 of Asp- 274 is 2.6 Å, and OE1 of Glu273 is 3.8 Å away from this water. We propose that one or both of these residues are involved in activation of this water toward hydrolysis of the malyl-CoA intermediate. Glu273 is totally conserved in all malate synthases including members of both the MSA and MSG families. Asp274 is also highly conserved, being substituted by a Glu in the sequence of only one malate synthase from *Streptomyces arenae* (55).

2.3.3. Reported inhibitors of MTB malate synthase

2.3.3.1. Phenyl-diketo acid derivatives

As discussed in the earlier section, Krieger *et al.*, identified phenyl diketo acids derivatives as potent malate synthase inhibitors.

A focused library of 35 small molecules with a glyoxylate-like substructure was assayed against GlcB and ICL at a single concentration point of 40 mg/ml. Of these, 19 showed activity against GlcB. All of the GlcB active compounds were phenyldiketo acids (PDKAs) derivatives. The parent PDKA exhibited an IC₅₀ of 2.0 mM against GlcB and was inactive against ICL. Based on these initial findings, approximately 100 PDKA analogs were synthesized. A series of compounds was selected that demonstrated a good balance of enzyme inhibition and whole-cell activity. Aryl diketo acids have also been identified in drug discovery projects for other Mg²⁺-dependent enzymes. These include HIV-1 integrase and hepatitis C virus-polymerase, where the keto acid moiety was found to coordinate the catalytic divalent metal cation. These compounds had IC₅₀s against GlcB ranging from 20 nM to >100 mM. However, the minimal inhibitory concentrations (MICs) against cultured mycobacteria were, in certain cases, in disagreement with the enzyme inhibition level and had poor reproducibility.

Several replacements for the phenyl ring in PDKA were prepared, including aliphatic moieties, exemplified by cyclohexyl and adamantyl cores. But these were found to be inactive against GlcB, suggesting a strong requirement for an aromatic moiety. Naphthyl-, indole-, pyrrole-, and thiophene-based diketo acids were active against the enzyme with IC₅₀s ranging from 20 nM to 5 mM. However, the first three did not exhibit adequate whole-cell activity, and thiophenes had only low whole-cell activity (≥50 mM). Furan-, quinoline-, benzodioxole-, and benzothiazole-based PDKAs exhibited low enzyme inhibition activity (IC₅₀s ranging

from 30 to 100 mM). Thiazole-, pyridine and pyrimidine-based PDKAs were inactive against the enzyme.

The crystal structure of the complex with PDKA was analyzed, and contacts at lateral positions around the phenyl ring were identified. The distances from phenyl carbons to closest protein contacts are 3.7-4.4 Å. Substituents at the five positions on the ring that could potentially enhance the interaction with each contact were then synthesized and tested, individually or in combination (**Figure 2.14**). At R1, halogens (F, Cl, Br) were tested, along with alkyl groups of varying size (Me, Et, iPr, MeF₃), OH and OMe. At R2, halogens, Me and OH, along with large substituents were tested, including thiophene, phenyl, benzyl, OMe. At R3, a series of alkyl chains were tested, from C1 to C6, along with halogens, benzyl and OH. At R4 and R5, halogens, Me, and OH were tested (though these were always in combination with a substitution at R1, since a single ortho-substitution always rotated toward Val118).

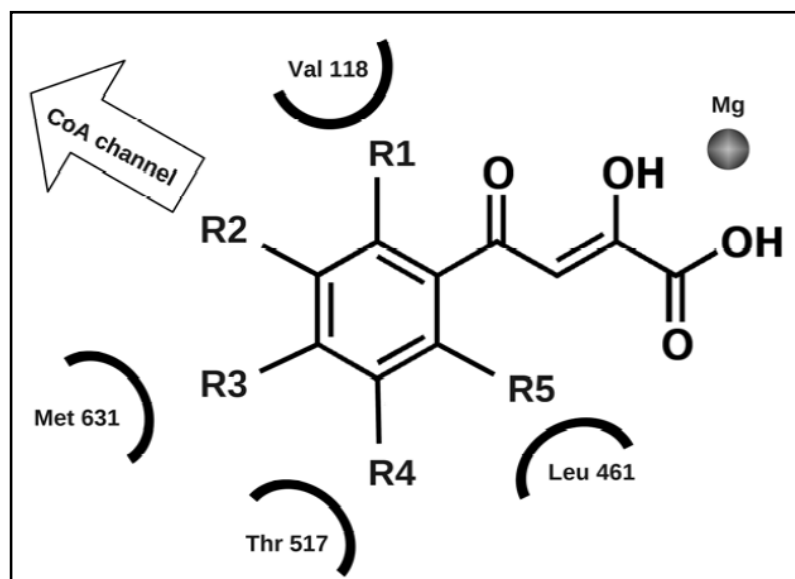


Figure 2.14: Schematic representation of the substitutions attempted over phenyl-diketo acid. The active site residues of malate synthase interacting with PDKA are shown [Krieger I.V., *et al.*, 2012]

Krieger et al., in 2012 determined crystal structures of complexes of GlcB with 20 of the synthesized PDKA analogs at resolutions ranging from 1.8 to 2.2 Å to evaluate their binding modes. The crystal structure of GlcB in complex with 2-Br-PDKA (**4**) showed that the Br oriented toward the Val118 side chain (**Figure 2.15A**). The potency of the ortho-substituted

analogues was improved compared to unsubstituted PDKA (2.0 mM). The most potent were those with halogens, with a preference for smaller groups: 2-F (0.24 mM) < 2-Cl (0.5 mM) < 2-Br (0.6 mM) < 2-Me (1.1 mM) (**Table 2.1**). This was presumably due to the increase of steric clashes with the Val118 side chain (3.2 Å from Br to the closest C γ of Val118). There is little space available to accommodate a larger group. Indeed, *o*-Et-PDKA showed an IC₅₀ of only 35 mM.

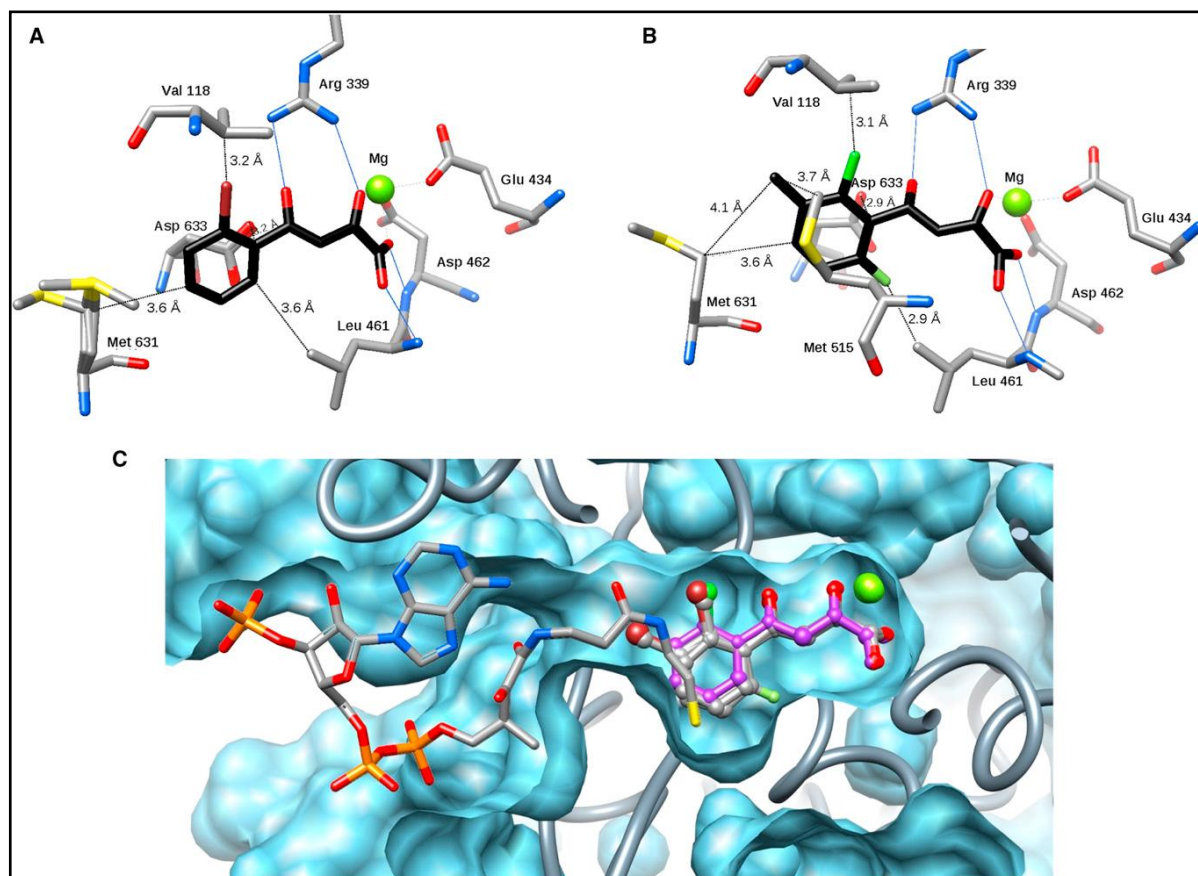


Figure 2.15: Comparing binding of PDKA analogs to GlcB

(A and B) Binding of GlcB to inhibitor **4** (A) and inhibitor **11** (B) colored by element, with C_{protein} in gray and C_{ligand} in black. Hydrogen bonds are indicated by solid blue lines, and distances from key positions on the phenyl ring to protein residues are marked as dashed lines. (C) Crystal structure overlay of malate synthase complexed with PDKA (in magenta); **1**, **4**, **7**, and **11**, represented by ball-and-stick, and CoA, represented by a stick model (colored by element), with the Mg atom in green. The CoA model and protein surface were made from chain A of the 2GQ3 model [Krieger I.V., *et al.*, 2012].

Crystal structures of ortho-substituted PDKA complexes with malate synthase indicated that all the ortho substituents orient in the same direction i.e., none are rotated to position 6 (**Figure 2.13A**), regardless of their size or nature. The ring of the ortho-substituted PDKA does not overlap exactly with the position of the parent PDKA ring (**Figure 2.15**). For all of 2-substituted inhibitors, it is moved about 0.7 Å away from Val118 to accommodate the group at the 2 position.

Table 2.1: Synthesized PDKA derivatives with their MTB malate synthase inhibitory profile

Compound	R (substituent)	IC ₅₀ (μM)
PDKA	Ph	2.0
1	2-MePh	1.1
2	2-FPh	0.24
3	2-ClPh	0.5
4	2-BrPh	0.6
5	3-MePh	0.18
6	3-ClPh	0.17
7	7-BrPh	0.8
8	4-MePh	6.0
9	4-BrPh	5.7
10	2-Cl-6-FPh	2.7
11	2-Cl-6-F-3MePh	5.5

The methyl ester of compound **11**, considered as compound **12** was later synthesized and observed to show the best combination of potency with *in vitro* pharmacokinetic properties among the PDKA analogs tested and therefore was selected for further *in vivo* pharmacokinetic, pharmacodynamic and toxicity studies. Compound **12** was tested in a murine model of acute TB infection (Rullas et al., 2010). Several dosing strategies from 300

to 600 mg/kg were tested to determine the best compound exposure above the MIC at or below the MTD (maximum tolerated dose) established. Treatment with moxifloxacin (30 mg/kg), which is used in the treatment of multidrug-resistant tuberculosis (Cox et al., 2011), was used for comparison.

Compound **12** exhibited a statistically significant reduction (p values < 0.0001) in the MTB bacterial load compared to the control by over 100-fold. Thus, inhibition of GlcB resulted in impairment of the ability to establish an acute infection in mice making compound **12** as an effective malate synthase inhibitor.

Chapter 3

OBJECTIVES AND PLAN OF WORK

3.1. Objectives

Despite the discovery and availability of cheap and effective methods of treatment, tuberculosis still remains to be a global threat accounting for high mortality rate with millions of active TB cases reporting every year. Due to the emergence of MDR-TB, high incidence of HIV/TB co-infection and lack of new antitubercular drugs, TB has declared a global health emergency. The increasing rate of mortality and the emergence of newer resistant MTB strains, stress out the importance of discovery of newer, more effective and safer mode of treatment for TB. The current available drug regimen against TB is no more effective in cases of MDR and XDR TB which prove the emergency need of new antitubercular agents. *Mycobacterium tuberculosis* (MTB), being a tricky bacteria with high rate of mutations, should be targeted by choosing some underexplored targets which can effectively kill the pathogen. A thorough review over various available literatures highlighted the importance of *M. tuberculosis* glutamine synthetase in active form of TB. Glutamate racemase is one of the least explored crucial enzymes which in turn have the capacity to regulate DNA gyrase, one of the important antitubercular targets. The final target, malate synthase, is a well proven effective target of choice for the treatment of dormant form of TB. All these enzymes play a crucial role in the synthesis of MTB cell wall, the major limiting factor in the tuberculosis treatment.

The main objective of the proposed work was:

1. Design and identification of novel *M. tuberculosis* glutamine synthetase, glutamate racemase and malate synthase inhibitors using structure based drug design. The lack of crystal structure for MTB glutamate racemase, being one of the limiting factors in structure based drug design, provoked the development of 3D protein model using homology modeling protocol.

- a. Evaluation of inhibitory potency of identified MTB glutamine synthetase hits by glutamine synthetase enzymatic assay.
- b. Evaluation of inhibitory potency of identified MTB glutamate racemase hits by glutamate racemase enzymatic assay.
- c. Evaluation of inhibitory potency of identified MTB malate synthase hits by malate synthase enzymatic assay.
2. Optimization studies of selected hits, synthesis and characterization of derivative compounds.
3. Evaluation of binding affinity of the identified active inhibitor (based on enzymatic assay results) towards its corresponding protein target using biophysical characterization techniques.
4. *In vitro* antimycobacterial screening of the synthesized compounds using MABA assay.
5. *In vitro* cytotoxicity studies for all the synthesized compounds using MTT assay.
6. Computational evaluation of protein-inhibitor binding stability using molecular dynamics simulation studies.
7. Determination of free energy of solvation for the identified active inhibitors against their respective targets using *in silico* free energy perturbation studies.

3.2. Plan of work

The plan of work was classified into the following categories.

3.2.1. Designing of MTB glutamine synthetase and malate synthase inhibitors

We have utilized two strategies for designing the inhibitors.

3.2.1a. Structure based drug design approach

The available crystal structures of mycobacterial glutamine synthetase and malate synthase proteins bound to inhibitor were utilized as a structural framework for virtual screening of a commercially available database (asinex) and BITS *in house* compounds collection to identify new leads.

3.2.1b. Development of homology model for MTB glutamate racemase

The amino acid sequence for MTB glutamate racemase was retrieved from UniProt and protein BLAST was run for this sequence so as to identify suitable template to build the model. The model was built using Prime v3.1 of Schrödinger 2012 molecular modeling

package. The developed model was further evaluated using ramachandran plot generated using PROCHECK. The developed model was also evaluated for its structural stability using molecular dynamic simulation studies. Later the active site analysis was carried out for the developed model so as to

identify the binding site of the protein based on the sequence alignment over the template.

3.2.2. Cloning, expression and purification of MTB GS, MurI and MS

3.2.2a: Cloning, expression and purification of MTB glutamine synthetase protein

The *glnA1* gene was amplified from *M. tuberculosis* H37Rv genomic DNA by standard PCR techniques. Clones were screened by restriction digestion and the resulting construct was transformed in to expression vector pQE2 (Qiagen) with a 6-His-tagged cloned vector and was then transformed into BL21 (DE3) cells.

3.2.2b: Cloning, expression and purification of MTB glutamate racemase protein

MurI gene (Rv2780) was amplified from *M. tuberculosis* H37Rv genomic DNA by standard PCR techniques and was transformed into BL21 (DE3) cells. The crude obtained after the cell lysis was purified and the protein obtained was further tested for its activity.

3.2.2c: Cloning, expression and purification of MTB malate synthase protein

The *glcB* gene was amplified from *M. tuberculosis* H37Rv genomic DNA by standard PCR techniques. Clones were screened by restriction digestion and the resulting construct was transformed in to expression vector pQE2 (Qiagen) with a 6-His-tagged cloned vector and was then transformed into BL21 (DE3) cells.

3.2.3. Biological inhibitory assessment of designed hits against protein targets

3.2.3a. *In vitro* MTB glutamine synthetase enzyme inhibition assay

The identified MTB glutamine synthetase hits were further evaluated for their glutamine synthetase inhibitory potency employing an assay based on the spectrophotometric determination of inorganic phosphate released during the reaction catalyzed by glutamine synthetase. The assay is carried out in 96-well plate.

3.2.3b. *In vitro* MTB glutamate racemase enzyme inhibition assay

The identified *M. tuberculosis* glutamate racemase analogues will be further evaluated for their MTB MurI inhibitory potency using an assay based on the spectrophotometric

determination of the racemization of D-glutamate to L-glutamate adapted to 96-well plate format.

3.2.3c. *In vitro* MTB malate synthase enzyme inhibition assay

The identified *M. tuberculosis* malate synthase analogues will be further evaluated for their MTB

MTB MS inhibitory potency using an assay based on the spectrophotometric determination of Coenzyme A released during the reaction catalyzed by malate synthase.

3.2.4. Synthesis and characterization

Optimization studies for identified potential hits were carried out and were further derivatized in our laboratory utilizing novel/previously reported methodologies available in literature for structurally related compounds. All reactions were monitored using thin layer chromatography and LCMS. Elemental analysis for the synthesized compounds was carried out. ¹H-NMR and ¹³C NMR for the synthesized compounds were recorded and analyzed to confirm the structure of the compounds.

3.2.5. Evaluation of protein-inhibitor binding affinity using biophysical technique

Binding affinity of potent inhibitors against corresponding targeted proteins was evaluated by differential scanning fluorimetry experiments using real time PCR.

3.2.6. *In vitro* M. tuberculosis screening by MABA assay

All molecules were further screened for their *in vitro* antimycobacterial activity against *M. tuberculosis* H37Rv by microplate alamar blue assay (MABA) method.

3.2.7. *In vitro* cytotoxicity screening by MTT assay

All the compounds were also tested for *in vitro* cytotoxicity against RAW 264.7 cells at 50 μ M concentration using MTT assay to evaluate their selectivity index and toxicity profiles.

3.2.8. Molecular dynamics simulation studies

Binding stability of identified potential inhibitors with their respective protein targets was evaluated using *in silico* molecular dynamics simulation studies. The simulation studies were carried out employing Desmond Molecular Dynamics System, v3.1, D. E. Shaw Research, NY, 2012. Stability of protein-ligand complex was evaluated by root mean square deviation (RMSD) analysis, root mean square fluctuation (RMSF) analysis. Simulation interaction

studies considering various types of interactions, radius of gyration analysis, molecular surface area and solvent accessible surface area (SASA) analysis and torsion potential studies were also carried out for the complex simulation trajectory.

3.2.9. Free energy perturbation studies

The solvation energies of the most active inhibitors were calculated by employing free energy perturbation (FEP) studies. The absolute free energies of the compounds were determined using Desmond v3.1, D. E. Shaw Research, NY, 2012 employing the total free energy calculation using FEP.

Chapter 4

MATERIALS AND METHODS

4.1. Identification of novel inhibitors targeting MTB acting through the inhibition of glutamine synthetase, glutamate racemase and malate synthase

4.1.1. Design of novel inhibitors for MTB glutamine synthetase, glutamate racemase and malate synthase

In the case of mycobacterial glutamine synthetase and malate synthase proteins, we utilized structure based design (e-pharmacophore) strategy for developing novel inhibitors, as described below. The absence of crystal structure for glutamate racemase provoked the development of tertiary protein structure for this protein employing homology modeling studies. The model was further used in the structure based virtual screening for the identification of potential hits against the protein.

4.1.1.1. Structure based drug design approach

In the case of mycobacterial glutamine synthetase and malate synthase, we describe here a novel protocol for generating energy-optimized pharmacophore (e-pharmacophore) based on mapping of the energetic terms from the Glide XP scoring function onto atom centers. Beginning with a ligand-receptor complex we refined the ligand pose, computed the Glide XP scoring terms, and mapped the energies onto atoms. Then, pharmacophore sites were generated, and the Glide XP energies from the atoms that comprised each pharmacophore site were summed. The sites are then ranked based on these energies, and the most favorable sites were selected for the pharmacophore hypothesis [Salam N.K., *et al.*, 2009]. Finally, these e-pharmacophores were used as queries for virtual screening.

4.1.1.1a. Protein targets for MTB GS and MS

In the present study, crystal structures of *M. tuberculosis* glutamine synthetase in complex with imidazopyridine inhibitor (PDB code: 4ACF) and malate synthase in complex with

dioxobutanoic acid inhibitor (PDB code: 3S9Z) were retrieved from protein data bank (PDB) and were utilized for structure-based drug design [Nordqvist A., *et al.*, 2012; Krieger I.V., *et al.*, 2012]. Hydrogen atoms, bond orders and formal charges were added using the protein preparation wizard of the maestro software package. Water molecules were removed from the atomic co-ordinates, except which were found to be involved in water mediated hydrogen bonding interactions between the protein and ligand, thus while preparation of protein, these water molecules were retained. The resulting structure was energy minimized using OPLS_2005 force field [Banks J.L., *et al.*, 2005]. Interactions of the ligand with the protein residues in the active site were visualized using ligand interaction diagram in Schrödinger 9.3.

4.1.1.1b. Protein and ligand preparation

The protein files were prepared using protein preparation wizard and impact energy minimization was performed using 500 cycles of steepest descent (SD) and 5000 cycles of conjugate gradient (CG) methods. OPLS_2005 (optimized potential for liquid simulations) force field was attained. The active site of the proteins was defined and grid files were generated using receptor grid generation panel. The reference ligand structure of both the proteins were downloaded from PDB and minimized using impact energy minimization with 100 cycles of SD and 500 cycles of CG. The three dimensional structure of the compounds were retrieved from Asinex and *in house* database were employed for the virtual screening. Database compounds were energy minimized using LigPrep v2.2, Schrödinger 2012) module.

4.1.1.1c. Glide XP (Extra-Precision) docking

Generated grid files from the prepared proteins were used for Glide XP docking calculations. The minimized conjugate gradient output of the reference ligand was used. “Write XP descriptor information” option and “Compute RMSD” option were enabled and the settings were kept default for rest of the parameters. XP Glide scoring function was used to order best ranked compounds and the specific interactions like π -cation and π - π stacking were analyzed using XP visualizer in Glide module. The input RMSD of the ligand was also ascertained.

4.1.1.1d. E-pharmacophore generation

The pharmacophore hypotheses were created for the reference ligands of both proteins by using the XP descriptor file of the Glide XP output in the docking post processing tool of the scripts module by using default settings for refinement and scoring. Starting with the refined

crystal ligands, pharmacophore sites were automatically generated with Phase using the default set of six chemical features: hydrogen bond acceptor (A), hydrogen bond donor (D), hydrophobic (H), negative ionizable (N), positive ionizable (P), and aromatic ring (R). Hydrogen bond acceptor sites were represented as vectors along the hydrogen bond axis in accordance with the hybridization of the acceptor atom. Hydrogen bond donors were represented as projected points, located at the corresponding hydrogen bond acceptor positions in the binding site. Projected points allowed the possibility for structurally dissimilar active compounds to form hydrogen bonds at the same location, regardless of their point of origin and directionality [Singh K.D., *et al.*, 2012]. The reference ligands were docked with Glide module of Schrödinger 9.3 in extra precision mode (XP) and the docked pose was refined and the Glide XP scoring terms were computed to map energies onto the atoms [Friesner R.A., *et al.*, 2006]. The pharmacophore sites were generated, and the Glide XP energies from the atoms that comprised each pharmacophore sites were summed up. These sites were then ranked based on the individual energies, and the most favorable sites were selected for the pharmacophore hypotheses.

4.1.1.1e. Development of tertiary model for MTB glutamate racemase using homology modeling protocol

The amino acid sequence for MTB glutamate racemase was retrieved from UniProt (accession id - P9WPW9) [Cole S., *et al.*, 1998]. Protein BLAST was run for this sequence against non-redundant database (Protein Data Bank (PDB)) to identify the most suitable template [Johnson M., *et al.*, 2008]. Template selection was based on the percentage identity and the extent to which the query was covered during alignment. Prime v3.1 of Schrödinger 2012 molecular modeling package was employed in the development of MurI model [Andrec M., *et al.*, 2002]. Energy based model generation was opted in the present study due to its accuracy and for this OPLS_2005 force field was employed. The generated model was checked for any ramachandran plot violations, based on which the model was subjected to loop refinement and side chain corrections. The final model was energy minimized operating OPLS_2005. Ramachandran plot was generated using PROCHECK, whose analysis gives the stereo chemical quality of the built model [Laskowski R.A., *et al.*, 1993]. The active site analysis for the model was carried out in order to identify the binding site of model based on the sequence alignment over template. The developed glutamate racemase model was further validated for

its structural stability using molecular dynamics simulation studies, methodology followed for this is given in the upcoming sections. The RMSD and RMSF of the protein during the simulation were analyzed. The protein was further utilized in high throughput virtual screening (HTVS) against commercial asinex database and BITS in house database in order to identify some potential hits against glutamate racemase. The virtual screening methodology operated is given in the upcoming sections.

4.1.1.1f. Preparation of commercial database

Asinex database containing 5,00,000 unique structures and BITS in-house database of 1700 compounds were used in this study [Asinex, ASINECorp, USA]. Database molecules were prepared using LigPrep and Epik to expand protonation and tautomeric states at pH 7.0 [Shelly J.C., *et al.*, 2007]. Conformational sampling was performed for all molecules using the ConfGen search algorithm. We employed ConfGen with the OPLS_2005 force field and a duplicate pose elimination criterion of 1.0 Å RMSD to remove redundant conformers. A distance-dependent dielectric solvation treatment was used to screen electrostatic interactions. A maximum relative energy difference of 10.0 kcal.mol⁻¹ was chosen to exclude high energy structures. Using Phase, the database was indexed with the automatic creation of pharmacophore sites for each conformer to allow rapid database alignments and screening.

4.1.1.1g. Molecular docking studies – Virtual screening workflow

For the e-pharmacophore approach, explicit matching was required for the most energetically favourable site (scoring better than 1.0 kcal.mol⁻¹) that finds matching pharmacophores in the ligands. For filtering the database molecules, a minimum of 4-5 sites were required to match for hypotheses with 5-7 sites. The above criterion was followed in the present work to screen the Asinex database. In order of their fitness score, database hits were ranked to measure how well the aligned ligand conformer matched the hypothesis based on RMSD, site matching, vector alignments and volume terms. Database ligands after e-pharmacophore filter were docked into the binding sites of the protein utilizing high-throughput virtual screening (HTVS) scoring function to estimate protein-ligand binding affinities. Ligands filtered from HTVS were subjected to Glide SP (standard precision) docking. The centre of the Glide grid was defined by the position of the co-crystallized ligand. Default settings were used for both the grid generation and docking. Post docking minimization was implemented to optimize the

ligand geometries. Compounds with best docking and Glide scores were then subjected to Glide XP (extra precision) docking. Final short listing of possible hit compounds was based on visual inspection of the important amino acid residues in the active site cleft involved in binding and the hydrophobic interactions.

4.1.1.1h. Molecular docking using GOLD

In order to check the accuracy and validity of the ligand-based and structure-based approaches, the molecular docking studies were carried out to understand the binding modes of inhibitors using the Genetic Optimization for Ligand Docking (GOLD v5.2) software on a Windows-based PC, which allowed partial flexibility of the protein and full flexibility of the ligand [Jones G., *et al.*, 1995]. The reported crystal structures of MTB GS and MS (PDB ID: 4ACF and 3S9Z) were downloaded from the PDB. Initially, the protein was considered without the ligand for the purpose of docking studies. The proteins were minimized up to a gradient of 0.01 kcal/mol and hydrogen were added using the CHARMM force field available in the Discovery studio 3.5 software. The energy-minimized structure was used for further docking analysis. In the GOLD docking software, the default parameters were: population size (100); selection-pressure (1.1); number of operations (10,000); number of islands (1); niche size (2); and operator weights for migrate (0), mutate (100) and crossover (100) were applied. The active site was defined within 10Å and the ligand-binding interactions were analyzed using scoring functions: Goldscore (GS) and Chemscore (CS).

4.1.1.1i. Binding Energy calculations

Binding free energies for selected compounds were calculated using Prime MM-GBSA methods. This approach is well established for predicting the theoretical binding free energy of ligand molecules which are bound to protein [Beard H., *et al.*, 2013]. For these calculations, docked poses of ligand and protein complexes were energy minimized and free energies were calculated using OPLS_2005 force field employing the generalized-Born (GB)/surface area (SA) continuum model for water as solvent. Equation 1 was used for computation of free energy of binding ($\Delta G_{\text{Binding}}$) for ligand as

$$\Delta G_{\text{Binding}} = \Delta E + \Delta G_{\text{Solv}} + \Delta G_{\text{SA}} \quad \text{Equation 1}$$

$$\text{Where } \Delta E = E_{\text{Complex}} - (E_{\text{Protein}} + E_{\text{Ligand}}) \quad \text{Equation 2}$$

$$\Delta G_{Solv} = \Delta G_{Solv\ Complex} - (\Delta G_{Solv\ Protein} + \Delta G_{Solv\ Lig}) \quad \text{Equation 3}$$

$$\Delta G_{SA} = \Delta G_{SA\ Complex} - (\Delta G_{SA\ Protein} + \Delta G_{SA\ Ligand}) \quad \text{Equation 4}$$

As for description of above terms used in the equations, **E** represents the energy minimized states of protein-ligand used in the calculations, **Solv** and **SA** represents the solvation energy and surface area associated energy respectively. All the intrinsic simulations were carried out employing GB/SA continuum model in Prime v3.1 of Schrödinger 9.3. It is noteworthy to mention that for the computation carried out employing GB model, we used Gaussian surface instead of van der Waals surface scaling. The reason for above is that Gaussian surface represents better the solvent-accessible surface area (SASA) compared to that of van der Waals scaling [Lyne P.D., *et al.*, 2006].

4.1.1.1j. QikProp analysis

The selected compounds after virtual screening were further selected for in-silico prediction of absorption, distribution, metabolism, excretion and toxicity using QikProp module [QikProp, v3.5, Schrödinger 2012]. QikProp efficiently evaluated pharmaceutically relevant properties for over half a million compounds per hour, making it an indispensable lead generation and lead optimization tool. Accurate prediction of absorption, distribution, metabolism, elimination (ADME) properties prior to expensive experimental procedures, such as HTS, could eliminate unnecessary testing on compounds that would ultimately fail; ADME prediction can also be used to focus lead optimization efforts to enhance the desired properties of a given compound. The ADME properties of the synthesized compounds were also predicted using QikProp. The compounds prepared were subjected to druglikeness filter. The criteria of the filter included molecular weight 160-480, number of heavy atoms 20-70, lipophilicity 40-130, number of hydrogen bond donors 4-7, number of hydrogen bond acceptors 8-12, percentage of human oral absorption, solubility, cell permeability etc.

4.1.2. Synthesis and characterization

The top active lead compound identified by the above mentioned strategies were taken up for further lead optimization through synthesis. Hit expansion of the various lead identified were achieved using the following synthetic protocols.

4.1.2.1. Synthetic protocol adopted for hit expansion of the lead against MTB glutamine synthetase obtained from e-pharmacophore based virtual screening

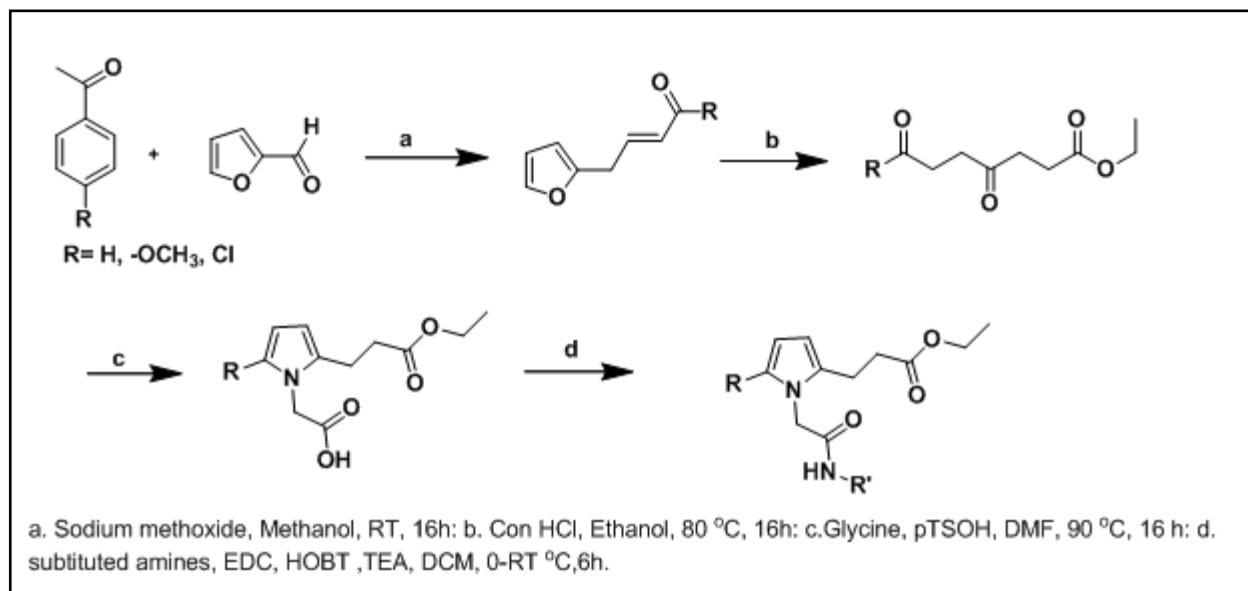


Figure 4.1: Synthetic protocol operated for development of glutamine synthetase inhibitors

4.1.2.2. Synthetic protocol adopted for hit expansion of the lead against MTB glutamate racemase obtained from structure based virtual screening

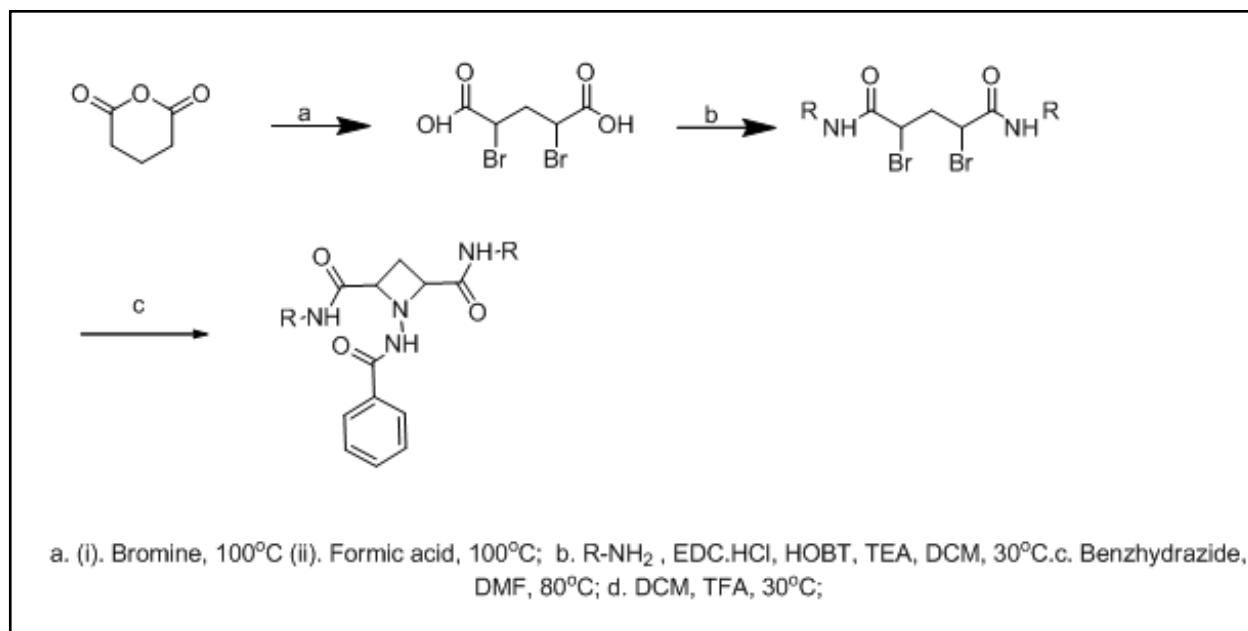


Figure 4.2: Synthetic protocol operated for development of glutamate racemase inhibitors

4.1.2.3. Synthetic protocol adopted for hit expansion of the lead against MTB malate synthase obtained from e-pharmacophore based virtual screening

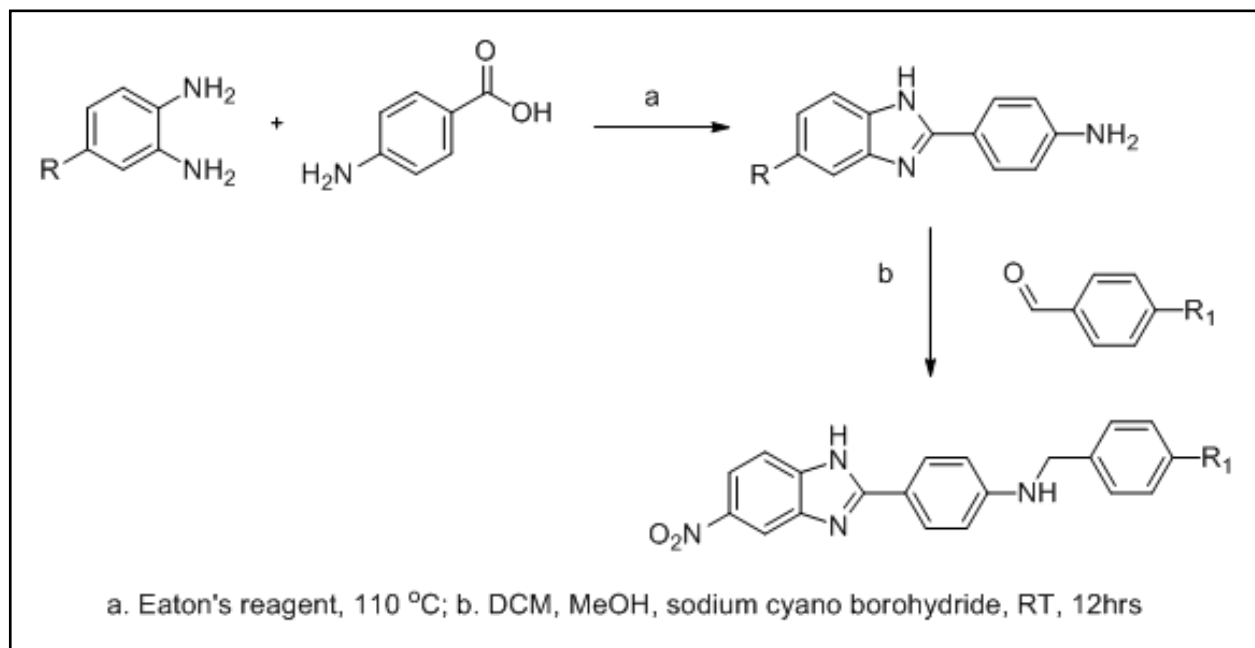


Figure 4.3: Synthetic protocol operated for development of glutamate racemase inhibitors

All commercially available chemicals and solvents were used without further purification. TLC experiments were performed on alumina-backed silica gel 40 F254 plates (Merck, Darmstadt, Germany). The homogeneity of the compounds was monitored by thin layer chromatography (TLC) on silica gel 40 F254 coated on aluminum plates, visualized by UV light and KMnO_4 treatment. Purifications were done on Biotage Isolera purification system on silica gel (MPLC grade) by using either hexane: ethylacetate or dichloromethane: methanol as eluent. All ^1H and ^{13}C NMR spectra were recorded on a Bruker AM-300 (300.12 MHz, 75.12 MHz) NMR spectrometer, BrukerBioSpin Corp. Germany. Chemical shifts are reported in ppm (δ) with reference to the internal standard TMS. The signals were designated as follows: s, singlet; d, doublet; dd, doublet of doublets; t, triplet; m, multiplet. Molecular weights of the synthesized compounds were checked by LCMS 6100B series Agilent Technology. Elemental analyses were carried out on an automatic Flash EA 1112 Series, CHN Analyzer (Thermo). The purity of the final compounds was examined by elemental analysis.

4.1.3. *In vitro* biological assay and biophysical evaluation

4.1.3.1. Cloning, expression and purification of the target proteins

4.1.3.1a. Cloning, expression and purification of MTB glutamine synthetase

glnA1, gene encoding *M. tuberculosis*, was amplified from H37Rv genomic DNA using forward primer 5' CACCCATATGGTGACGGAAAAGACGCCCGA3' and reverse primer 5' AGCTAAGCTTTTAAACGTCGTAGTACAGCG3' with MTB genomic DNA. Pfu Phusion (New England Biolabs) was used for this. Further PCR products were digested with NdeI and HindIII. Similarly, vector pQE2 (Qiagen) was also digested with NdeI and HindIII. Further digested vector and insert were ligated with T4 DNA ligase. Finally sequencing confirmation was done to verify the clones. This pQE2-MTB *glnA1* construct was transformed into *E. coli* BL21(DE3) cells. The transformed cells were later grown at 37 °C in Luria-Bertani (LB) broth containing 100 µg/ml ampicillin to an optical density of 0.6 at 600 nm. Later the transformed bacterial cells were induced for protein expression in presence of 0.2 mM isopropyl-β-D-thiogalactopyranoside (IPTG). The bacterial cells were allowed to grow for 12 h at 20 °C. Cell pellets were collected and were re-suspended in lysis buffer containing 50 mM TrisHCl, pH 7.5, 300 mM NaCl, and 10% glycerol. Later after re-suspension, PMSF (Phenyl methane sulphonyl fluoride), a protease inhibitor was added to inhibit protease activity. Later, cells were lysed by sonication after which the lysate was centrifuged at 10,000 rpm for 30 min at 4 °C to remove the cell debris. The lysate was applied to Ni-NTA column (Bio-Rad) and equilibrated for 3 hrs. The column was then washed with wash buffer (50 mM TrisHCl, pH 7.5, 300 mM NaCl, and 10% glycerol) to remove unbound protein molecules. Later, the desired protein MTBGS was eluted with elution buffer (50 mM TrisHCl, pH 7.5, 300 mM NaCl, 10% glycerol) with various concentration of imidazole ranging from 100 mM to 300 mM respectively. Fractions containing desired MTBGS protein were identified using sodium dodecyl sulphate polyacrylamide gel electrophoresis (SDS-PAGE). The purified protein was stored at -80 °C for the enzymatic studies.

4.1.3.1b. Cloning, expression and purification of MTB glutamate racemase

The *MurI* gene encoding glutamate racemase was transformed and expressed in *E. coli* BL21DE3 cells. The cells were grown in LB (Luria Broth) media with ampicillin (100 µg/ml) at 37 °C and induced with 0.5 mM IPTG (isopropyl β-D-1-thiogalactopyranoside) when the optical density reached 0.6 read at 600 nm. The induction with IPTG was done for 12 hrs at

25 °C. The cells were harvested and the pellet was lysed using lysis buffer (50 mM Tris, 400 mM NaCl, 5% Glycerol and 0.5 mM PMSF (phenylmethanesulfonyl fluoride)). Later, the cells were sonicated using ultra sonication. The lysate was centrifuged at 10,000 rpm, 4 °C for 1 hr. The clear lysate was equilibrated with Ni-NTA beads for 3hrs. The equilibrated cell lysate was then poured in to Ni-NTA column (Bio-Rad); the column was then washed using wash buffer (50 mM TBG, pH 8) to remove unbound protein and other debris. The target protein of interest was eluted with elution buffer with different concentrations of imidazole ranging from 100 mM to 300 mM. The eluted samples containing malate synthase were identified using sodium dodecyl sulfate polyacrylamide gel electrophoresis (SDS-PAGE). The purified protein was pooled and stored at -80 °C for enzyme inhibition studies.

4.1.3.1c. Cloning, expression and purification of MTB malate synthase

glcB was PCR amplified using *M. tuberculosis* genomic DNA and pfu polymerase. Forward primer (5' CACCCATATGACAGATCGCGTGTCTCGGT3') was containing NdeI restriction site while reverse primer (5' AGCTAAGCTTCTAGCGGGCCGCATCGTCAC 3') was with HindIII site. Final PCR product and pQE2 vector were digested with NdeI and HindIII restriction enzymes. Further digested PCR products and vector were ligated with the help of T4 DNA ligase at 25 °C for 2 hrs. Final clones were confirmed with the help of sequencing. The *glcB* gene encoding malate synthase (MS) was transformed and expressed in *E. coli* BL21DE3 cells. The cells were grown in LB (Luria Broth) media with ampicillin (100 µg/ml) at 37 °C and induced with 0.5 mM IPTG (isopropyl β-D-1-thiogalactopyranoside) when the optical density reached 0.6 read at 600 nm. The induction with IPTG was done for 12 hrs at 25 °C. The cells were harvested and the pellet was lysed using lysis buffer (50 mM Tris, 400 mM NaCl, 5% Glycerol and 0.5 mM PMSF (phenylmethanesulfonyl fluoride)). Later, the cells were sonicated using ultra sonication. The lysate was centrifuged at 10,000 rpm, 4 °C for 1 hr. The clear lysate was equilibrated with Ni-NTA beads for 3hrs. The equilibrated cell lysate was then poured in to Ni-NTA column (Bio-Rad); the column was then washed using wash buffer (50 mM TBG, pH 8) to remove unbound protein and other debris. The target protein of interest was eluted with elution buffer with different concentrations of imidazole ranging from 100 mM to 300 mM. The eluted samples containing malate synthase were identified using sodium dodecyl sulfate polyacrylamide gel electrophoresis (SDS-PAGE). The purified protein was pooled and stored at -80 °C for enzyme inhibition studies.

4.1.3.2. Enzyme kinetic studies

During glutamine synthetase assay, concentration of enzyme was determined based on the range finding experiments. In order to determine the kinetic parameters K_m and V_{max} , L-glutamate was varied keeping the substrate concentration from 10 mM to 250 mM respectively. The reactions were performed according to the enzymatic assay described in **section 4.13.3.3a** and the K_m and V_{max} were analyzed using non-linear regression analysis using GraphPad prism software.

In case of glutamate racemase assay, the concentration of the purified enzyme was estimated based on the range finding experiment. The kinetic parameters for D-glutamate were estimated by varying the concentration of D-glutamate from 1 mM to 100 mM. The assay was carried out according the methodology given in the proceeding section and the parameters were calculated using GraphPad prism software.

In case of malate synthase assay, the kinetic parameters were determined for glyoxylate and acetyl CoA by varying different concentrations of glyoxylate from 3.5 mM to 1 μ M; acetyl-CoA was varied from 10 mM to 1 μ M respectively. Concentration of malate synthase enzyme used for the enzymatic reactions was determined based on the range finding experiments. The end product 5,5'-dithiobis-(2-nitrobenzoic acid) (DTNB)-Co-A adduct formed was measured at 412 nm.

4.1.3.3. *In vitro* enzyme assays for target proteins

4.1.3.3a. *In vitro* glutamine synthetase inhibition assay

MTB glutamine synthetase enzymatic assay was performed with assay buffer (50 mM of HEPES pH 6.8) was added to the reaction mixture, 150 mM glutamate, 7.5 mM of ammonium chloride (NH_4Cl) and 32.5 mM of magnesium chloride (MgCl_2) in a reaction volume of 60 μ l. The reaction was initiated by varying enzyme (12 μ M to 0.1 μ M) and 7.6 mM of ATP. The reaction was allowed to proceed for 2 h at 25 °C. Later, half of the reaction mixture was taken (to avoid excess of inorganic phosphate production after hydrolysis of ATP) and added to the 96 well flat bottom microtiter plates. In-order to stop the reaction, 12% w/v of L-ascorbic acid (Hi-media) in 1N HCl and 2% ammonium molybdate in distilled water were mixed in 2:1 proportion and 90 μ l was added to 30 μ l of reaction mixture. The reaction mixture was mixed well in order to develop blue color immediately. Later it was incubated for 7 min and after

that 90 μ l of 2% sodium citrate tribasic hydrate in 2% acetic acid was added to the reaction mixture to stop the further development of color due to production of inorganic phosphates. The inorganic phosphate released during the reaction was measured at 635 nm in microtitre plate reader Spectramax M4, Molecular Devices, Sunnyvale, USA.

In order to determine the inhibitory capacity of the identified hits against the selected three protein targets, initial screening at 25 μ M inhibitor concentration was carried out. Later, the compounds with better percentage inhibition were carried for further screening at concentrations varying from 10 μ M to 1 μ M to calculate the compound IC₅₀s.

4.1.3.3b. *In vitro* glutamate racemase inhibition assay

The racemization activity of the purified glutamate racemase was assessed as described earlier [Sengupta S., *et al.*, 2006]. Purified MurI samples were incubated in presence of D-glutamate and then rapidly heated to inactivate the enzyme and assayed for L-glutamate using NAD⁺/L-glutamate dehydrogenase (GDH). 16.4 picomoles of MurI was incubated with 10 mM D-glutamate in a buffer containing 100 mM Tris-HCl pH 8.0, 2 mM DTT at 37 °C for 30 min. Samples were then heated at 95 °C for 15 min. Denatured protein was removed by centrifugation for 10 min at 14 000 rpm. The L-glutamate formed was then measured by adding 5 mM of NAD⁺ and 10 U of GDH. Increase in absorbance at 340 nm was monitored for 6 min at 25 °C using UV/vis spectrophotometer. Varying concentrations of the identified hits were tested using the assay in order to analyze their MurI inhibitory activity.

4.1.3.3c. *In vitro* malate synthase inhibition assay

The malate synthase inhibition studies were performed similar to that in the reported literature [Freundlich J.S., *et al.*, 2014]. The assay buffer (20 mM Tris pH-7.5 and 5 mM MgCl₂) was incubated with 10.1 picomoles of enzyme and the designed compounds (dissolved in 100% DMSO) were added such that the final concentration in the reaction was <5% and incubated for 20min at room temperature. Later, 0.1 mM of acetyl CoA was added and the enzymatic reaction was initiated by the addition of 1.12 mM of glyoxylate. The reaction was terminated by adding 2 mM of DTNB after addition of glyoxylate to measure the free thiol groups formed in the enzymatic reaction. The absorbance was finally measured at 412 nm in order to estimate the formed 5,5'-dithiobis-(2-nitrobenzoic acid) (DTNB)-CoA adduct. The complete reaction with 100% DMSO solution in place of inhibitor with and without enzyme was taken

as control and blank respectively. The percentage inhibition of MTB malate synthase by a compound was calculated using the formula:

$$\% \text{ Inhibition} = 100 * \left\{ \frac{\text{Total enzyme reaction} - \text{Inhibitor absorbance}}{\text{Total enzyme reaction}} \right\} \quad \text{Equation 5}$$

4.1.3.4. Biophysical characterization using DSF

The stabilization of top active leads when bound to protein was evaluated by thermal shift assay, where the recombinant protein and protein-ligand complexes were subjected to gradual temperature rise in the presence of fluorescent dye Sypro Orange (Sigma Aldrich). The fluorescence emitted from the dye is a measure of protein denaturation, where the hydrophobic residues are exposed [Niesen F.H., *et al.*, 2007]. In case of glutamine synthetase, the target protein MTB GS (5 μ L of protein (0.96 mg/ml) + 10.4 μ L of buffer (100 mM HEPES-NaOH, pH-7.8)) and different concentration of inhibitors were subjected to stepwise heating in real time PCR instrument (Bio-Rad iCycler-5) from 25 $^{\circ}$ C to 95 $^{\circ}$ C with an increase in 0.1 $^{\circ}$ C/min in the presence of dye. As the temperature increases, the stability of the protein decreases and becomes zero at equilibrium where the concentrations of folded and unfolded protein are equal and this temperature is defined as melting temperature (T_m). The shifts in the melting temperature of protein in presence of inhibitors were observed was observed. In case of MurI, the experiment was optimized by 10 μ L of MurI protein, 6 μ L of dye (SyproOrange, 1:100), and 4 μ L of buffer (100 mM HEPES-NaOH, pH-7.8). In case of malate synthase, the experiment was optimized by 10 μ L of MS protein, 4 μ L of dye (SyproOrange, 1:100), and 6 μ L of buffer (100 mM HEPES-NaOH, pH-7.8). Different concentrations of inhibitor were used in order to qualitatively estimate their binding affinity with the protein targets.

4.1.3.5. *In vitro* antitubercular screening using MABA assay

In this technique, the minimal inhibitory concentration (MIC) value of all the identified compounds against *M. tuberculosis* H37Rv in 90% was determined using alamar blue as a fluorescent vital dye. In brief, the inoculum was prepared from fresh LJ medium re-suspended in 7H9-S medium (7H9 broth, 0.1% casitone, 0.5% glycerol, supplemented oleic acid, albumin, dextrose, and catalase [OADC]), adjusted to a McFarland tube No. 1, and diluted 1:20; 100 μ l was used as inoculum. Each drug stock solution was thawed and diluted in 7H9-S at four-fold the final highest concentration tested. Serial two-fold dilutions of each drug

were prepared directly in a sterile 96-well microtiter plate using 100 µl 7H9-S. A growth control containing no antibiotic and a sterile control were also prepared on each plate. Sterile water was added to all perimeter wells to avoid evaporation during the incubation. The plate was covered, sealed in plastic bags and incubated at 37°C in normal atmosphere. After 7 days incubation, 30 mL of alamar blue solution was added to each well, and the plate was re-incubated overnight. A change in colour from blue (oxidised state) to pink (reduced) indicated the growth of bacteria, and the MIC was defined as the lowest concentration of drug that prevented this change in colour [Sriram D., *et al.*, 2005].

4.1.3.6. *In vitro* cytotoxicity screening

The compounds displaying good *in vitro* potency in enzymatic assays were further examined for toxicity in mouse macrophage RAW 264.7 cell line at 50 µM concentration. After 48 h of exposure, viability was assessed on the basis of cellular conversion of MTT into a formazan product using the Promega Cell Titer 96 non-radioactive cell proliferation assay. Mouse macrophages cell lines (RAW 264.7) were grown in RPMI medium supplemented with 10% foetal bovine serum (FBS), 10,000 units penicillin and 10 mg streptomycin per mL in T25 flasks to attain 80-90% confluency. Cells were scraped and seeded into wells i.e., 5,000 cells per well in poly-L-lysine coated plates. The microtiter plates were incubated at 37 °C, 5% CO₂, 95% air and 100 % relative humidity for 24 h prior to addition of experimental drugs. The test compounds at 50 µM concentrations were then added to cells and incubated at 37 °C for 48 h. Later 10 µL of 10 mg/mL concentration of MTT was added and incubated for 3 h at 37 °C. At the end of incubation period formazon crystals were formed, the plates were then centrifuged and the media from microtiter plates were removed. Later, plates were air dried. The bound crystals were subsequently dissolved by adding 100 µL DMSO. The absorbance was then read on ELISA plate reader at a wavelength of 595 nm. Relative to the control wells the percent growth was calculated for each well. The percentage of cells killed was obtained from the formula [Sriram D., *et al.*, 2005].

$$\text{Percentage of cells killed} = \left(\frac{100 - \text{mean OD sample}}{\text{mean OD day 0}} \right) \quad \text{Equation 6}$$

4.1.4. Molecular dynamics simulation

Molecular dynamics (MD) simulation was performed for a time scale ranging 10-20 ns for the

top active inhibitors against respective target proteins in order to analyze the consistency of molecular interactions between ligand and receptor employing Newton's Laws of Motions. All the MD simulations and calculations were done using Desmond employing OPLS-AA force field [Jorgenson W.L., *et al.*, 1996; Desmond v3.1, D.E. Shaw Research, NY 2012]. The prime objective of this MD study is to understand the macroscopic properties like temperature, pressure in presence of solvent system based on its microscopic properties (bonded and non-bonded properties). For comparison studies, a 10 ns MD was also run for crystal structure of MTB glutamine synthetase without ligand in its ATP site (PDB ID – 4ACF (ligand was removed)). TIP3P water model was used to setup the solvent system in orthorhombic solvent box, keeping a cut-off of 10 Å from any solute atom in all directions [Jorgenson W.L., *et al.*, 1983]. Counter ions were added to neutralize the system. A cut-off of 14 Å was maintained for calculating the non-bonded interactions.

Initially, the system was minimized maintaining the convergence threshold criteria of 1 kcal.mol⁻¹.Å⁻¹. Further, system was minimized using Berendsen thermostat applying with and without restraints on solute atoms at 10 K temperature for a time period of 12 ps. The temperature of the system was further raised to 300 K for 24 ps at a pressure of 1 atm. M-SHAKE algorithm was used with an integration time step of 2 fs for rearranging the hydrogen bonds in the simulation [Kräutler V., *et al.*, 2001]. The MD simulation was run for 10 ns recording the trajectory frames at an interval of every 4.8 ps.

4.1.4.1. RMSD analysis

The root mean square deviation (RMSD) is used to measure the average change in displacement of a selection of atoms for a particular frame with respect to a reference frame. It is calculated for all frames in the trajectory. The RMSD for frame x is:

$$RMSD_x = \sqrt{\frac{1}{N} \sum_{i=1}^N (r'_i(t_x) - r_i(t_{ref}))^2} \quad \text{Equation 7}$$

where N is the number of atoms in the atom selection; t_{ref} is the reference time, (typically the first frame is used as the reference and it is regarded as time $t=0$); and r' is the position of the selected atoms in frame x after superimposing on the reference frame, where frame x is recorded at time t_x . The procedure is repeated for every frame in the simulation trajectory.

Protein RMSD plot shows the RMSD evolution of a protein (left Y-axis). All protein frames

are first aligned on the reference frame backbone, and then the RMSD is calculated based on the atom selection. Monitoring the RMSD of the protein can give insights into its structural conformation throughout the simulation. RMSD analysis can indicate if the simulation has equilibrated – its fluctuations towards the end of the simulation are around some thermal average structure. Changes of the order of 1-3 Å are perfectly acceptable for small, globular proteins. Changes much larger than that, however, indicate that the protein is undergoing a large conformational change during the simulation.

Ligand RMSD indicates how stable the ligand is with respect to protein and its binding pocket. RMSD plot for ligand shows the RMSD of ligand that is aligned and measured just on its reference conformation. This RMSD value measures internal fluctuations of ligand atoms.

4.1.4.2. RMSF analysis

The Root Mean Square Fluctuation (RMSF) is useful for characterizing local changes along the protein chain. The RMSF for residue i is:

$$RMSF_i = \sqrt{\frac{1}{T} \sum_{t=1}^T \langle (r'_i(t) - r_i(t_{ref}))^2 \rangle} \quad \text{Equation 8}$$

where T is the trajectory time over which the RMSF is calculated, t_{ref} is the reference time, r_i is the position of residue I ; r' is the position of atoms in residue I after superposition on the reference, and the angle brackets indicate the average of the square distance is taken over the selection of atoms in the residue. In the RMSF plot, peaks indicate areas of the protein that fluctuate the most during the simulation.

The ligand root mean square fluctuation (L-RMSF) is useful for characterizing changes in the ligand atom positions. The RMSF for atom a is:

$$RMSF_a = \sqrt{\frac{1}{T} \sum_{t=1}^T \langle (r'_a(t) - r_a(t_{ref}))^2 \rangle} \quad \text{Equation 9}$$

Where T is trajectory time over which RMSF is calculated, t_{ref} is reference time (usually for the first frame, and is regarded as the zero of time); r is the position of atom i in the reference at time t_{ref} , and r' is the position of atom i at time t after superposition on the reference frame.

Ligand RMSF shows the ligand's fluctuations broken down by atom, corresponding to the 2D structure in the top panel. The ligand RMSF may give the insights on how ligand fragments interact with the protein and their entropic role in the binding event.

4.1.4.3. Simulation interaction analysis

Protein interactions with the ligand can be monitored throughout the simulation. These interactions can be categorized by type and summarized below. Protein-ligand interactions (or 'contacts') are categorized into four types: Hydrogen Bonds, Hydrophobic, Ionic and Water Bridges. The stacked bar charts are normalized over the course of the trajectory: for example, a value of 0.7 suggests that 70% of the simulation time the specific interaction is maintained. Values over 1.0 are possible as some protein residue may make multiple contacts of same subtype with the ligand.

Hydrogen bonds – (H-bonds) play a significant role in ligand binding. Consideration of hydrogen-bonding properties in drug design is important because of their strong influence on drug specificity, metabolization and adsorption. Hydrogen bonds between a protein and a ligand can be further broken down into four subtypes: backbone acceptor; backbone donor; side-chain acceptor; side-chain donor.

The current geometric criteria for protein-ligand H-bond is: distance of 2.5 Å between the donor and acceptor atoms (D—H···A); a donor angle of $\geq 120^\circ$ between the donor-hydrogen-acceptor atoms (D—H···A); and an acceptor angle of $\geq 90^\circ$ between the hydrogen-acceptor-bonded_atom atoms (H···A—X).

Hydrophobic contacts - fall into three subtypes: π -cation; π - π ; and other, non-specific interactions. Generally these types of interactions involve a hydrophobic amino acid and an aromatic or aliphatic group on ligand, but we have extended this category to also include π -cation interactions.

Current geometric criteria for hydrophobic interactions are: π -cation- Aromatic and charged groups within 4.5 Å; π - π - Two aromatic groups stacked face-to-face or face-to-edge; other-non-specific hydrophobic side chain within 3.6 Å of ligand's aromatic or aliphatic carbons.

Ionic interactions - or polar interactions, are between two oppositely charged atoms that are within 3.7 Å of each other and do not involve a hydrogen bond. We also monitor Protein-Metal-Ligand interactions, which are defined by a metal ion coordinated within 3.4 Å of protein's and ligand's heavy atoms (except carbon). All ionic interactions are broken down into two subtypes: those mediated by a protein backbone or side chains.

Water bridges - are hydrogen-bonded protein-ligand interactions mediated by a water molecule. Hydrogen-bond geometry is slightly relaxed from the standard H-bond definition.

The current geometric criteria for a protein-water or water-ligand H-bond are: a distance of 2.7 Å between the donor and acceptor atoms (D—H···A); a donor angle of 110° between the donor-hydrogen-acceptor atoms (D—H···A); and an acceptor angle of 80° between the hydrogen-acceptor-bonded atoms (H···A—X).

4.1.5. Free energy calculations

Prediction of accurate free energies of compounds is one of the major and useful concepts in computational field [Jorgenson W.L., 2004]. The solvation energies can be calculated by employing free energy perturbations (FEP) and thermodynamic integrations (TI) coupled with molecular dynamics (MD) and monte carlo (MC) simulations [Kollman P., 1993]. This was proved successfully for the first time by Jorgensen et al who computationally derived the difference between methanol and ethane which was totally in agreement with the experimental observations [Jorgensen W.L. and Ravimohan C., 1985]. This was identified by using MC simulations. Though the macroscopic properties of a system like temperature, pressure, number of particles in the system and free energy of binding of a compound can be derived using MD simulation, the microscopic properties like atomic positions (r) and momenta (p) cannot be derived from MD [Kirkwood, J.K., 1935]. For this purpose, the concept of free energy perturbation was developed. Zwanzig's equation is the main basis for the determination of energy difference between the two states A and B [Kar, R.K., 2013].

$$\Delta V = V_B - V_A = -\beta^{-1} \ln[\exp(-\beta\Delta V)]_A \quad \text{Equation 10}$$

where $\beta = 1/kT$ (k is Boltzmann constant and T is temperature, $\Delta V = V_A - V_B$ where V_A and V_B are the potential energies of A and B states. $[\dots]_A$ denotes an ensemble average of state A generated by MD or MC simulations.

The absolute free energies of the compounds were determined using Desmond employing the total free energy calculation using FEP. The top active compounds against their respective targets were annihilated separately for 10 ns using TIP3P water model. The solvation energies of compounds were obtained along with their absolute free energies.

Chapter 5

RESULTS AND DISCUSSION FOR DEVELOPMENT OF MTB GLUTAMINE SYNTHETASE INHIBITORS

5.1. Design and development of MTB glutamine synthetase inhibitors

Glutamine synthetase (GS), being one of the crucial enzymes which are involved in various major activities of MTB, was selected for the development of its inhibitors. Glutamine synthetase catalyses the formation of glutamine in which glutamate and ammonia act as substrates. The extracellular synthesis of glutamate is an important step involved in the formation of cell wall. The synthesized glutamine is involved in the formation of a crucial cell wall component, poly L-glutamic acid/glutamine. Targeting glutamine synthetase in the design of antitubercular agents is an excellent opportunity to disrupt the cell wall of MTB which in turn destroy the bacteria.

In the present study, we employed the e-pharmacophore based screening approach in the identification of novel MTB GS inhibitors which were subjected to molecular docking studies. The identified hits were checked for their binding energies, ADME properties and subjected to *in vitro* studies based on which further optimizations were carried out. One of the lead compounds was selected and optimized and derivatized to develop a series of 40 compounds which were further evaluated by both *in silico* and *in vitro* studies for their GS inhibitory studies.

5.1.1. Design of glutamine synthetase inhibitors using structure based drug design

5.1.1.1. Selection of glutamine synthetase crystal structure and its binding site analysis

Till date, a number of crystal structures of glutamine synthetase are available co-crystallized with substrates and inhibitors. Among them, crystal structure of glutamine synthetase co-

crystallized with {4-[6-bromo-3-(butylamino)imidazo[1,2-a]pyridin-2-yl]phenoxy}acetic acid with PDB code 4ACF was utilized in the present study for the development of e-pharmacophore. The crystal structure was found with 2.0 Å resolution and the IC₅₀ of the ligand was reported to be 1600 nM. The binding site analysis of glutamine synthetase crystal structure revealed the presence of a large druggable cavity which accommodates glutamate and ATP endogenously. The surface of the active site is highly hydrophilic due to its presence towards the solvent and residues Gln231, Thr356, Asn359, Lys361, Lys363 and Arg364 form the solvent accessible surface of glutamine synthetase active site. The active site pocket was observed to be spacious and highly hydrophobic as it is lined by residues Ala128, Tyr129, Phe130, Tyr230, Phe232, Cys277, Leu281, Trp282, Pro287, Pro360 and Leu365. The crystal ligand was found to be involved in hydrogen bonding with residues Asn359 and Lys361 and also in strong hydrophobic interactions with other active site residues as shown in **Figure 5.1**. Hence, targeting glutamine synthetase would be much appreciative using compounds with greater hydrophobic component which in turn can result in strong non-polar interactions.

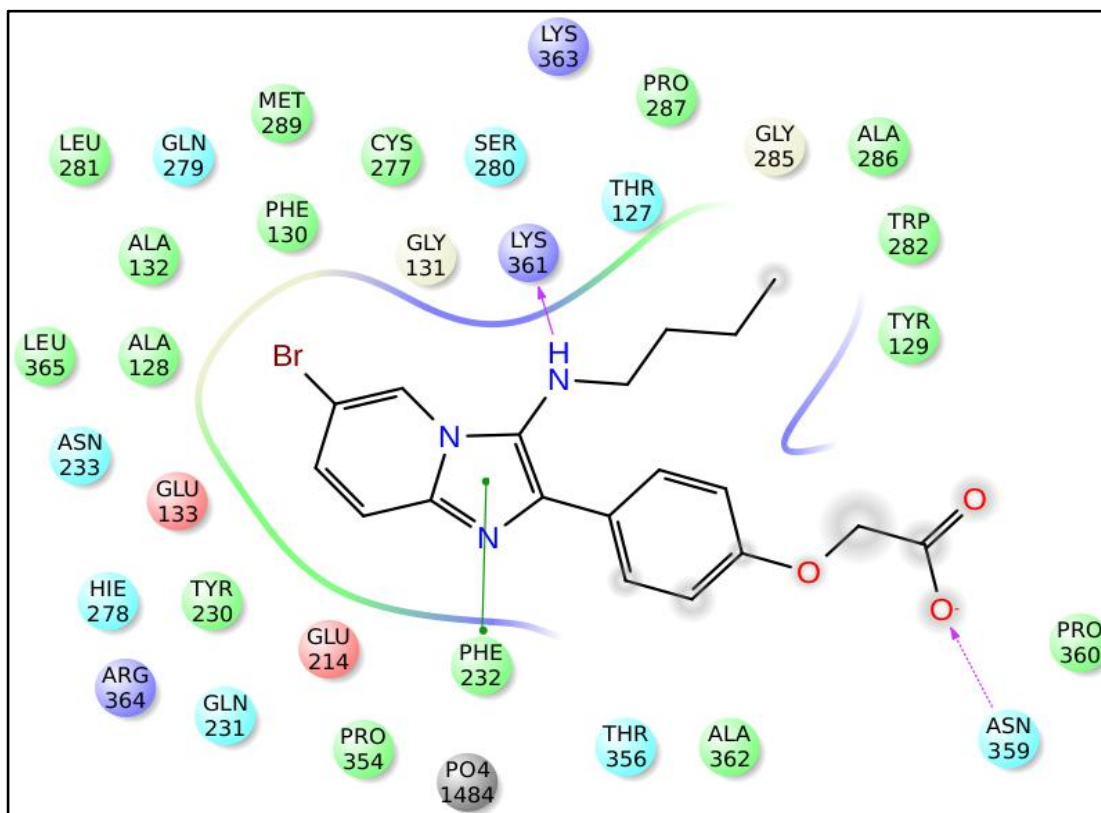


Figure 5.1: Interaction profile of the crystal ligand at the active site of glutamine synthetase (PDB code – 4ACF).

5.1.1.2. Protein active site validation and e-pharmacophore generation

In order to validate the docking program utilized for e-pharmacophore generation, the crystal ligand from 4ACF was prepared and redocked on to the grid of the active site using extra precision (XP) docking of Glide v5.7. The docked confirmation of the ligand was found to be similar to that in the crystal structure with an RMSD of 0.04 Å. The ligand was found to retain the active site interactions as of in the crystal structure with XP glide score of -7.24 kcal.mol⁻¹.

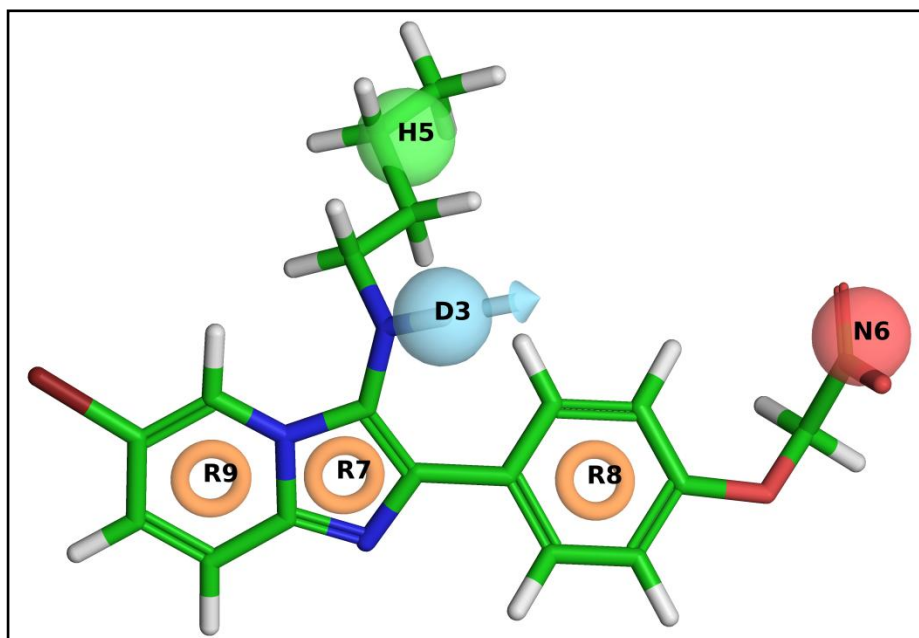


Figure 5.2: e-Pharmacophore generated for the crystal ligand from MTB glutamine synthetase crystal structure (PDB code – 4ACF).

Pharmacophore hypothesis was generated using the Glide descriptors which consist of polar, non-polar, van der Waals and electrostatic binding energies of the ligand with the protein which were mapped for the identification of pharmacophoric features. The pharmacophore generation protocol applied for the crystal ligand yielded a hypothesis with six features as shown in **Figure 5.2**. Each feature was assigned a score which accounts for the energy contribution of that particular site interacting at the binding pocket of protein which is given in **Table 5.1**. The six features of the generated hypothesis were one hydrogen bond donor (D3), one hydrophobic feature (H5), three aromatic ring features (R7, R8 and R9) and one negative-ionizable feature (N6). The D3 feature corresponds to the secondary amine of ligand which was found to be involved in H-bond with Lys361. H5 corresponds to aliphatic butyl

chain of ligand involved in hydrophobic interactions with Tyr129 and Trp282. N6 was mapped to the carboxylic acid terminal of ligand. The three aromatic ring features (R7, R8 and R9) were mapped to the three aromatic rings in ligand which were mainly involved in interactions with Phe232 and Ala362.

Table 5.1: Energy scores of each feature in the generated e-pharmacophore.

Rank	Feature Label	Score	Type
1	R9	-1.14	Aromatic Ring
2	D3	-0.7	H-bond donor
3	R7	-0.58	Aromatic Ring
4	R8	-0.57	Aromatic Ring
5	H5	-0.45	Hydrophobic
6	N6	-0.35	Negative ionisable

5.1.1.3. E-pharmacophore based screening of chemical databases

The six-point e-pharmacophore was employed for screening asinex database (a commercial database) in search of compounds with similar pharmacophore features. The search criterion was put to match at least 4 of 6 features of the pharmacophore. The aim of virtual screening workflow operated in this work is to reduce the enormous chemical library into a manageable number of compounds which would be comfortable for identification of inhibitors thereby increasing the chances of identification of drug candidate. The pharmacophore based screening of asinex database resulted in compounds with significant fitness value, which acts as a measure of how well the compound fits the pharmacophore. In the present study, 1038 compounds with fitness above 1.00 were selected and carried forward for virtual screening.

5.1.2. Molecular docking studies of the selected compounds

The virtual screening workflow involved high throughput virtual screening (HTVS), standard precision and extra precision docking. A cut-off of $-6.0 \text{ kcal.mol}^{-1}$ docking score was defined for the compounds to be selected from HTVS which resulted in 359 compounds which were further subjected to SP and XP docking. The final selection of compounds was done based on the XP glide score and glide energy. Further selection process of compounds fitting in the above range was done using fitness value (above 1) and their interactions at GS active site.

A total of 102 compounds were selected after SP docking with the docking scores ranging

between $-9.6 \text{ kcal.mol}^{-1}$ and $-6.0 \text{ kcal.mol}^{-1}$. These compounds were further subjected to XP docking and GOLD docking and were selected considering XP glide score (above $-6.0 \text{ kcal.mol}^{-1}$), glide energy (above $-35.00 \text{ kcal.mol}^{-1}$), GOLD score (greater than $50.00 \text{ kcal.mol}^{-1}$) and their binding pattern at the active site.

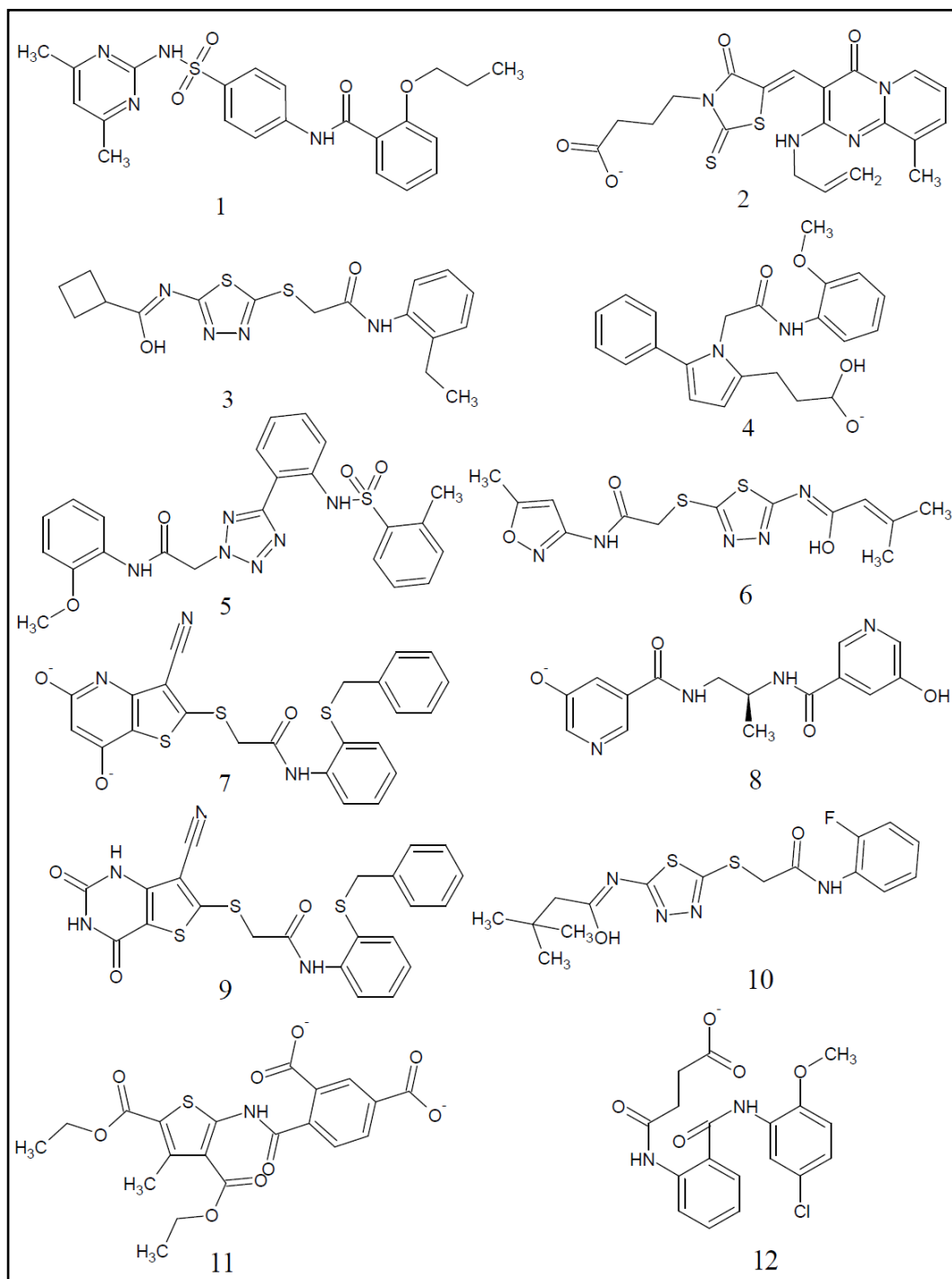


Figure 5.3: Structures of 12 compounds selected from asinex against MTB GS.

Another important criterion considered in selection of compounds was their hydrophobic nature as the active site was found to be dominated with aromatic residues Tyr129, Phe232 and Trp282. These residues were found to be involved in π - π stacking interactions with the active site ligand in the crystal structure. Hence, the compounds selection also involved consideration of their aromatic nature which can serve as better MTB GS inhibitors. These selection criteria resulted in finalization of 12 compounds and further subjected to *in vitro* MTB GS enzymatic assay. The chemical structures of the selected 12 compounds are shown in **Figure 5.3**. All 12 compounds were found to retain key interactions at the active site - hydrogen bonding with Glu214, Asn359, Lys361, Arg364 and hydrophobic interactions with residues Tyr129, Phe232, Trp282 and Ala362. Glide scores and glide energies for selected compounds are given in **Table 5.2**.

Table 5.2: Glide score, glide energy, fitness and GOLD score for the selected 12 compounds

Compound	Glide XP gscore	Glide Energy	Fitness	GOLD Score
X-ray ligand	-7.25	-46.94	3.00	54.94
1	-6.99	-45.67	1.22	74.38
2	-6.31	-45.46	1.67	59.72
3	-7.95	-47.97	1.57	51.77
4	-9.23	-38.72	1.65	54.27
5	-7.49	-46.43	1.50	70.72
6	-7.25	-46.96	1.41	65.99
7	-9.64	-47.39	1.14	81.06
8	-8.87	-38.22	1.41	58.61
9	-8.24	-50.21	1.14	80.71
10	-7.62	-45.27	1.54	64.66
11	-6.52	-43.61	1.38	66.35
12	-8.07	-46.36	1.47	67.62

XP glide score of the selected compounds ranged between $-6.3 \text{ kcal.mol}^{-1}$ and $-9.6 \text{ kcal.mol}^{-1}$ and their GOLD score between 51 and 81. The selected 12 compounds fit best at the binding pocket of MTB GS. The interactions of these compounds with the active site residues are given in **Table 5.3**.

Table 5.3: Interactions of the selected 12 compounds at MTB glutamine synthetase ATP site

Compound	H-bond Interactions	Cation- π Interactions	Anion- π Interactions	Hydrophobic Interactions
X-ray ligand	Asn359, Lys361	Phe232, Tyr129	--	Ala362
1	Glu214, Arg364	Tyr129, Phe232	Arg364	Trp282, Ala362
2	Asn359, Lys361	--	--	Tyr129, Ala362
3	Phe232, Lys361	Tyr129, Trp282	--	Phe232, Ala362
4	Lys361, Arg364	Tyr129, Phe232, Trp282	Arg364	Ala362
5	Asn359, Lys361, Arg364	--	--	Tyr129, Phe232
6	Glu214, Phe232, Lys361	Tyr129, Trp282	--	Phe232, Ala362
7	Asn359, Lys361, Arg364	Tyr129, Phe232, Trp282	--	Phe232, Ala362
8	Tyr129, Glu214, Lys361	Tyr129, His278, Trp282	Arg364	Phe232, Ala362
9	Asn359, Lys361, Arg364	Tyr129, Phe232, Trp282	--	Glu214, Ala362
10	Glu214, Phe232, Lys361	Tyr129, Trp282	--	Phe232, Ala362
11	Trp282, Asn359, Lys361	Phe232	--	Tyr129, Phe232, Ala362
12	Asn359, Lys361	Phe232, Trp282	--	Tyr129, Phe232, Ala362

The 12 compounds selected from the molecular docking studies were observed with different scaffolds such as thiophene, thiazole, thiadiazole, tetrazole and pyrimidine which offer a diverse set of compounds to study. Three compounds were selected with thiadiazole scaffold (compound **3**, **6** and **10**) with differences in their terminal groups so as to observe the effect of

each group on the activity profile of compounds. Compound **7** (cyanothieno pyridine scaffold) and **9** (cyanothieno pyrimidine scaffold) were also selected with similar basis. The main implication of selection of compounds with diverse structural features is to evaluate their MTB glutamine synthetase inhibitory activity and further structural optimization of the active compounds based on their synthetic feasibility. The binding energies of the selected 12 compounds towards MTB glutamine synthetase were also determined in order to assess their binding capacity towards the protein.

5.1.3. ADMET analysis of the selected compounds

Pharmacokinetic properties analysis helps us to identify suitable compounds with pharmaceutical importance which can be further developed in to a drug candidate. All the selected compounds were subjected to *in silico* ADMET analysis using QikProp module of Schrödinger 2012. All the compounds were found to be in accordance with Lipinski's rule of Five which is the basic criteria for a compound's drug-likeness. Various properties like SASA (Predicted Solvent Accessible Surface Area in Å²), QPlogBB (Predicted brain/blood partition coefficient), QPlogHERG (Predicted IC₅₀ value for HERG K⁺ channels), QPPCaco (Predicted apparent Caco-2 cell permeability in nm/s) were determined for the compounds and were checked for any deviations.

All the properties determined are listed out in **Table 5.4**. The compounds are found to be with least blood brain barrier permeability which indicates the compounds to be CNS (Central Nervous System) inactive. All the 12 compounds were found to obey Lipinski rule of Five, showing good percentage oral absorption, solubility, good permeability thereby reflecting the drug-likeness of the compounds.

Table 5.4: *In silico* pharmacokinetic profile for the selected 12 compounds

Comp.	SASA	QPlogBB	QPlogHERG	QPPCaco	QPPMDCK	% Human Oral Absorption	QPlogKp
1	768.87	-1.66	-6.58	312.25	142.72	89.17	-2.58
2	702.64	-1.78	-3.46	33.95	38.79	72.74	-3.72
3	692.18	-1.23	-3.97	128.43	156.46	89.90	-2.69
4	714.09	-1.10	-5.52	211.52	117.38	100.00	-1.29

5	744.48	-1.38	-6.88	334.12	235.67	87.88	-2.13
6	660.57	-1.64	-5.52	211.16	254.14	82.30	-3.66
7	775.65	-2.33	-7.20	72.70	76.93	85.40	-3.19
8	602.35	-2.31	-5.79	51.30	19.96	58.09	-4.42
9	755.33	-2.53	-6.77	34.40	34.30	72.67	-4.23
10	675.11	-1.05	-3.88	140.44	274.45	91.15	-2.53
11	692.94	-3.29	-1.22	0.38	0.20	31.09	-6.78
12	625.64	-1.11	-3.60	98.30	126.14	82.79	-2.70

Properties and Ranges: **SASA** – Predicted Solvent Accessible Surface Area in Å²(300-1000). **QPlogBB** – Predicted brain/blood partition coefficient (-3.000 to 1.200). **QPlogHERG** – Predicted IC₅₀ value for HERG K⁺ channels (concern below -5). **QPPCaco** – Predicted apparent Caco-2 cell (model for gut-blood barrier) permeability in nm/s (<25 – poor, >500 – great). **QPPMDCK** - Predicted apparent MDCK cell (model for blood-brain barrier) permeability in nm/s (<25 – poor, >500 – great). **QPlogKp** – Predicted skin permeability (-8.000 to -1.000).

5.1.4. Binding energy calculations

The relative binding affinities of the selected 12 compounds towards MTB glutamine synthetase protein were calculated using MM-GBSA calculations. Prime MM-GBSA calculation was used to evaluate/rescore the docked compounds and further their binding energies were determined. The compounds were analyzed for their total binding energies, coulomb interaction energies and also van der Waal interaction energies which are listed out in **Table 5.5**.

As observed from the table, compound **4** was found with highest binding energy (-25.79 kcal.mol⁻¹) towards MTB glutamine synthetase. Compounds **8**, **1** and **6** were also found with high binding energies predicting them to be active towards GS. Also the compounds were predicted to possess considerable coulombic and van der Waal energies. As observed from the results in **Table 5.5**, majority of the compound's binding energy was contributed by the generalized born electrostatic salvation energy ($\Delta G_{\text{bind Solv GB}}$). These compounds were procured from asinex database for further *in vitro* studies.

Table 5.5: Binding energies of 12 compounds calculated using Prime MM-GBSA protocol

Compound	ΔG bind	ΔG bind Coulomb	ΔG bind vdW	ΔG bind Solv GB
1	-46.84	14.57	-47.03	2.69
2	-85.69	-37.83	-45.71	36.86
3	-79.15	-19.56	-52.53	23.52
4	-25.79	6.190	-45.12	36.00
5	-57.68	15.95	-43.94	-9.15
6	-47.81	-22.71	-40.59	35.28
7	-67.96	-42.10	-38.66	48.40
8	-40.22	54.75	-32.93	-39.85
9	-65.14	-9.10	-40.27	19.09
10	-83.53	-31.71	-37.91	28.41
11	-80.86	-71.80	-55.12	71.30
12	-58.25	-13.56	-42.59	22.45

5.1.5. *In vitro* enzyme inhibition studies

glnA1 gene was successfully cloned, transformed, expressed and purified using Ni-affinity chromatography. Detailed procedure for these studies is given under section 4.1.3.1.a in materials and methods chapter. MTB glutamine synthetase was eluted at 150 mM imidazole and confirmed with SDS-PAGE. Kinetic parameters were determined for L-glutamate.

5.1.5.1. Enzyme kinetics of MTB glutamine synthetase

The activity of enzyme concentration followed first order kinetics. At constant enzyme concentration of 0.258 $\mu\text{g}/\mu\text{L}$, the substrate L-glutamic acid was varied from 10 mM to 400 mM respectively. The K_m and V_{max} for glutamate are **151.9** mM and **1.919** absorbance units respectively which were determined using GraphPad Prism 6 and shown in **Figure 5.4**.

5.1.5.2. *In vitro* glutamine synthetase assay for selected compounds

Procured 12 compounds from asinex database were evaluated for their MTB glutamine synthase inhibitory activity. Detailed enzymatic assay procedure is discussed in the section 4.1.3.3a of materials and methods chapter. In the initial screening at 25 μM , 12 compounds

showed >50% inhibition towards the protein which were further screened at lower concentrations. In order to calculate the compound IC₅₀s, the compound concentrations had been varied from 10 μM to 1 μM. The IC₅₀ values for 12 active compounds were calculated using GraphPad Prism 6 and given in **Table 5.6**.

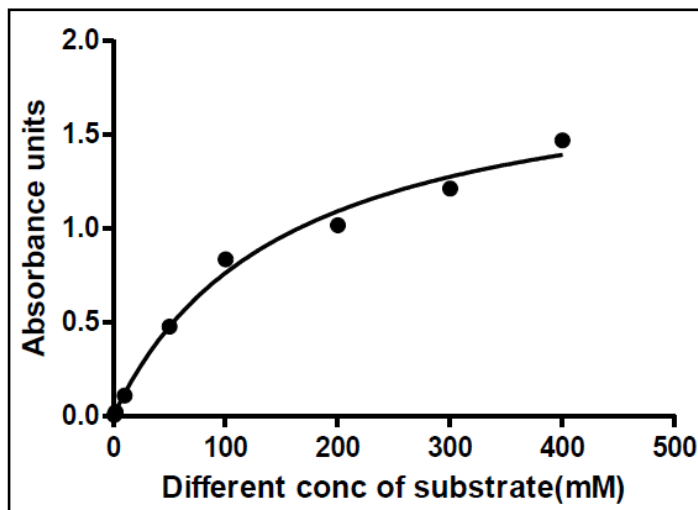


Figure 5.4: Enzyme kinetics plot for L-glutamate.

Table 5.6: Activity table showing the IC₅₀ values for the selected 12 compounds

Compound	IC ₅₀ * (in μM)
1	3.81±0.08
2	6.00±0.01
3	25.28±0.04
4	10.31±0.06
5	7.60±0.02
6	2.12±0.03
7	6.32±0.01
8	9.81±0.01
9	10.06±0.07
10	6.98±0.02
11	10.60±0.01
12	5.24±0.03

*IC₅₀ values calculated using GraphPad Prism version 6 (mean±SEM)

Compounds **6**, **1** and **12** were found with MTB glutamine synthetase inhibitory activity below 5 μM . Compound **6** was found to be top active with an IC_{50} of 2.12 μM . Dose response curves for compounds **6**, **1** and **12** are shown in **Figure 5.5**.

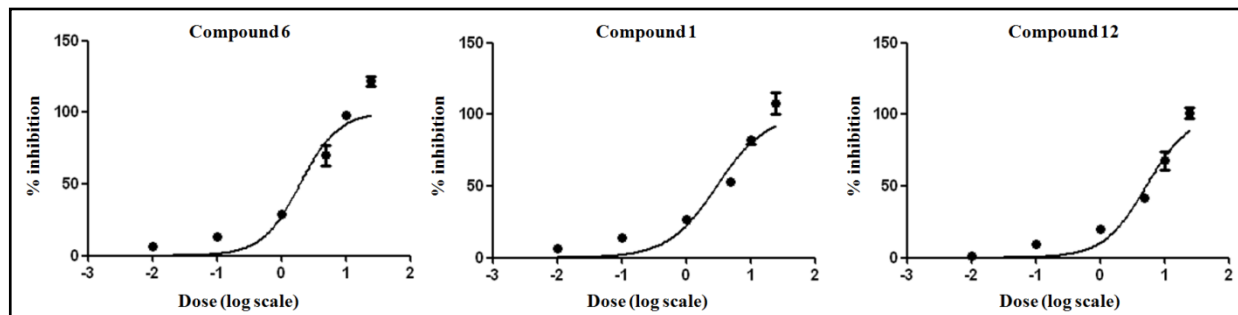


Figure 5.5: Dose response curves for compounds **6**, **1** and **12**.

Compounds **3**, **6** and **10** which contain identical scaffold (thiadiazole) vary in their activity profile as observed from **Table 5.6**. Of the three, compound **3** was found to be least active with 25 μM activity. The interaction profile of this compound is given in **Figure 5.6**. The figure shows that the three compounds retain the similar active site interactions except the compound **3** which excludes the interaction with Glu214. This can be explained by the presence of terminal cyclobutane whose orientation pulled back the hydroxyl group thereby losing the interaction. Compounds **6** and **10** (shown in **Figure 5.6**) were found with almost identical interactions and orientation at the active site supporting their activity. Similarly, compounds **7** and **9** retained the similar active site interactions which are shown in **Figure 5.7**. The three most active compounds (**6**, **1** and **12**) were selected for further hit qualification studies which include their biophysical characterization studies, *in silico* molecular simulations and free energy calculation studies.

The interaction pattern of top 3 actives (compound **6**, **1** and **12**) is shown in **Figure 5.8**. The compounds were found to be interacting strongly at the active site forming hydrogen bonding with residues majorly Glu214, Asn359, Lys361 and Agr364. Also, the compounds possess strapping hydrophobic interactions including cation- π and π - π contacts with residues Tyr129, Phe232, Ser280, Trp282 and Ala362. These top 3 active ligands in complex with protein were subjected to a 10 ns simulation in order to study the protein-ligand interaction stability in dynamic conditions and to generate further theoretical information to support their activity.

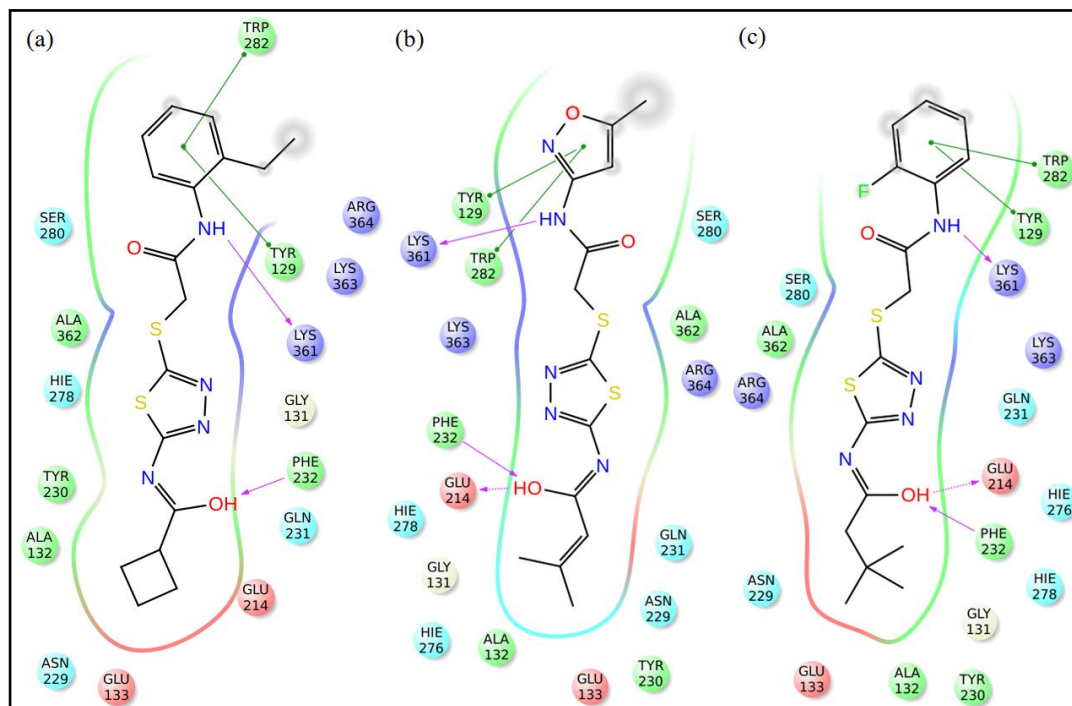


Figure 5.6: Interaction profile of (a) compound 3, (b) compound 6 and (c) compound 10.

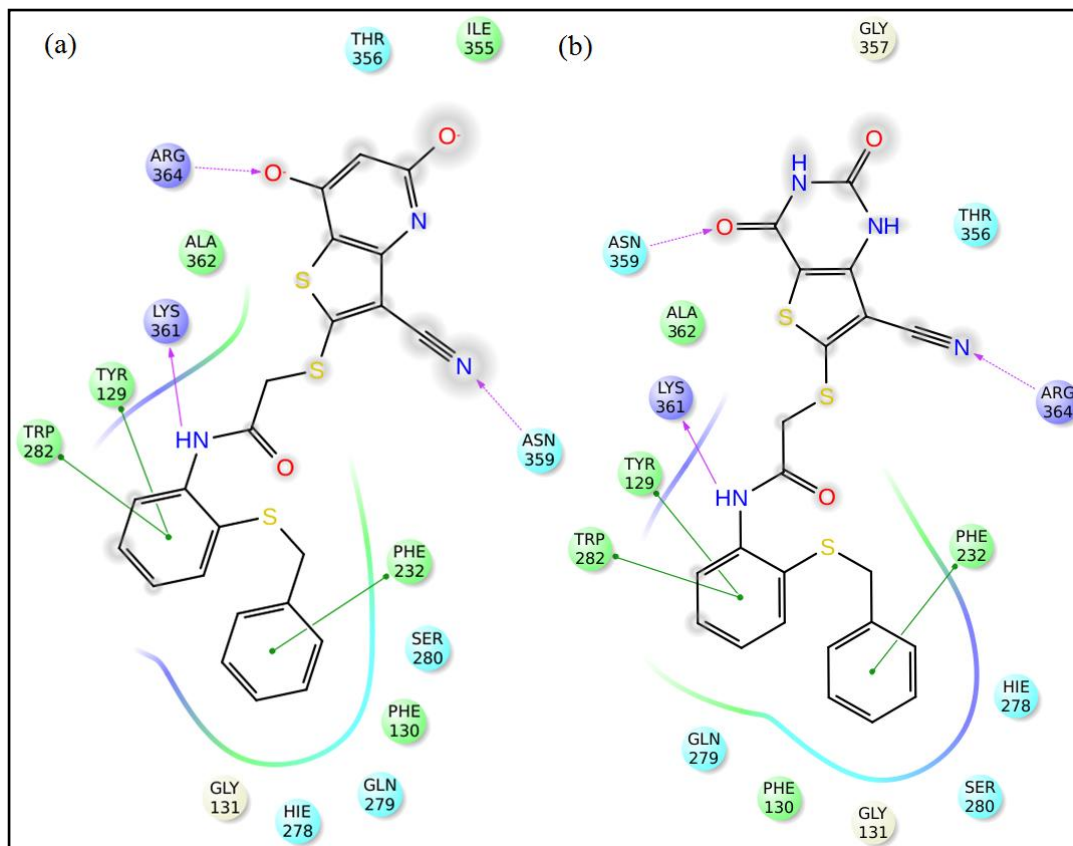


Figure 5.7: Interaction profile of (a) compound 7 and (b) compound 9.

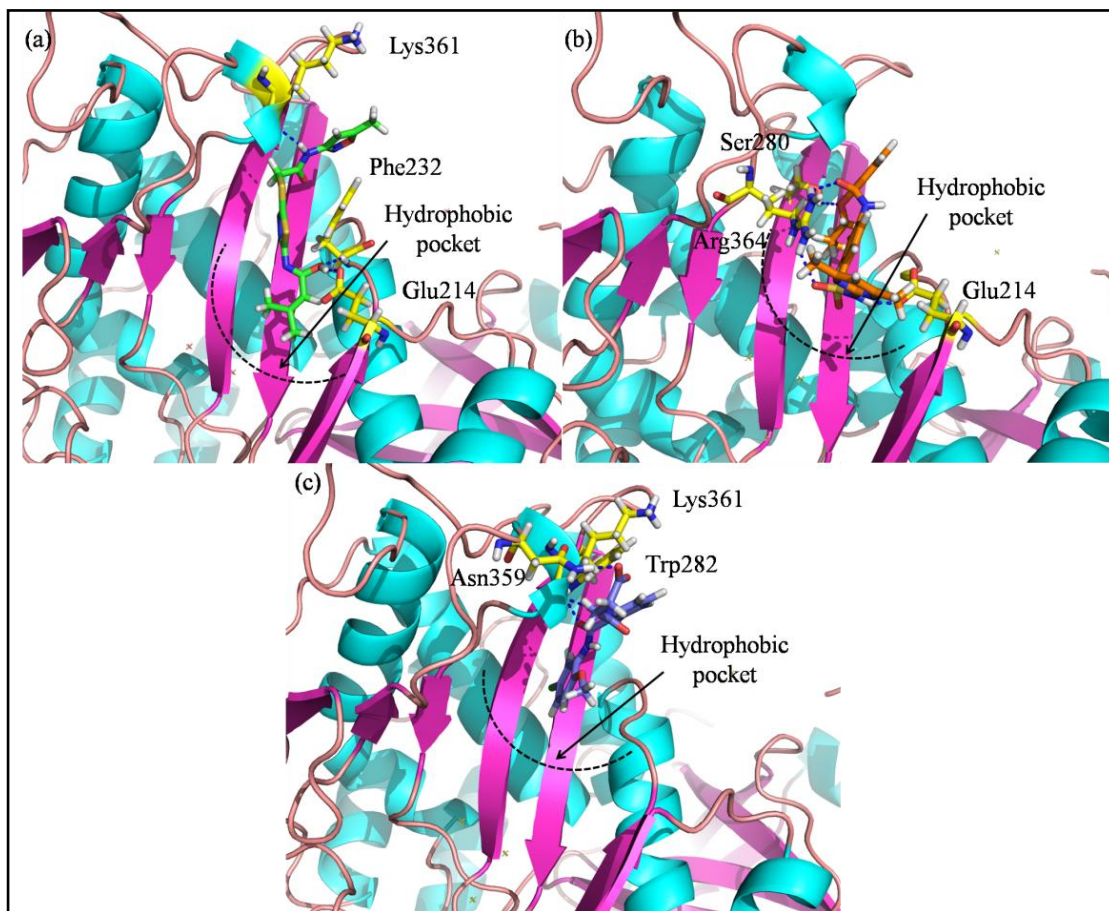


Figure 5.8: Interaction profile of the top 3 active compounds: (a) compound 6 (green), (b) compound 1 (orange) and (c) compound 12 (purple) at the MTB glutamine synthetase active site. Active site residues shown in yellow, blue dashed lines represent hydrogen bonds.

5.1.6. Molecular dynamics simulations

The ligand bound protein complexes of top 3 active compounds were simulated explicitly using OPLS_AA force field in Desmond v3.1. A free state of GS protein (no bound ligand) was also run as a reference so as to analyze the effect of identified compounds on protein stability.

Root mean square deviation (RMSD) analysis for all the three trajectories has been carried out so as to measure the distance between atoms during the simulation. The RMSD (in Å) plots for all the three ligand bound protein complexes are shown in **Figure 5.9(a)**. Considering all the residues of protein, ligand bound protein complexes show lesser rms deviation when compared to that of protein in free state. All the three RMSD plots were found to be stable

showing minimal deviations. This signifies the stabilization effect of all the three ligands over the protein by binding tightly at the active site. The free state of protein as shown in **Figure 5.9(b)** exhibited rms deviations which show the lack of ligand strain over the protein. An initial jump in RMSD of free state and ligand bound states of protein during initial few ps when compared to the original starting frame during simulation can be attributed to the relaxation of model in solvent system. Standard deviations of all atoms in ligand bound state were ~ 0.322 Å, ~ 0.305 Å and ~ 0.297 Å for compound **6**, **1** and **12** respectively and ~ 0.421 Å for protein in free state.

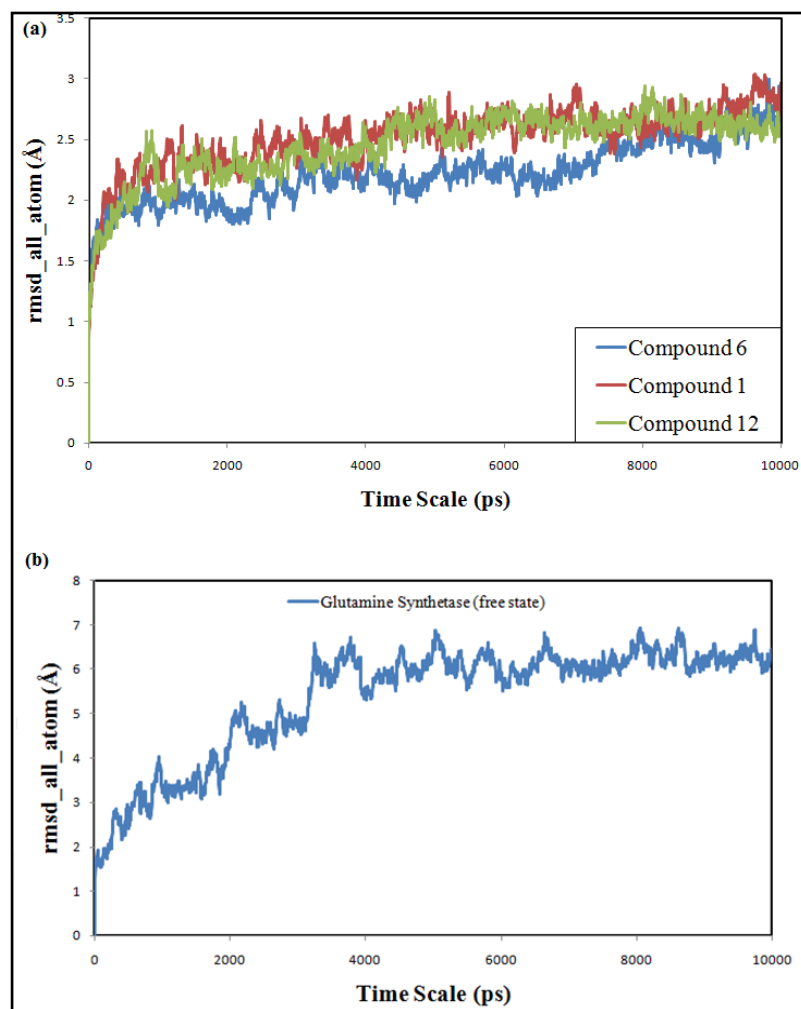


Figure 5.9: (a) RMSD plot of glutamine synthetase in bound states with compounds **6**, **1** and **12** as a function of time. (b) RMSD plot of glutamine synthetase in its free state.

The root mean square fluctuation (RMSF) analysis of a simulation trajectory shows the fluctuation range undergone by each residue in the protein during simulation. The RMSF of

crystal structure of glutamine synthetase was plotted as a function of residue number which is shown in **Figure 5.10(a)**. The crystallographic B factor of residues in crystal structure of glutamine synthetase was also plotted across the residue number so as to compare and correlate the results of both theoretical and experimental studies. The highly flexible region of the protein can be pointed out at residues approximately between 150-180 and 410-430 as shown both in crystallographic and simulation data (**Figure 5.10(b)**). Also the C- and N-terminal regions of protein were found to be highly flexible accounting for their terminal free residues. It was found that the RMSF analysis of residues from simulation data was in complete accordance with the crystallographic B-factor of the residues validating the computational studies. RMSF plots for all atoms of the top 3 ligand-protein complexes are shown in **Figure 5.11**. The figure displays least fluctuations of binding site such as residues at position 129 (Tyr), 232 (Phe), 282 (Trp) and 361 (Lys) attributing to the efficient binding of all the three compounds at the active site of MTB GS.

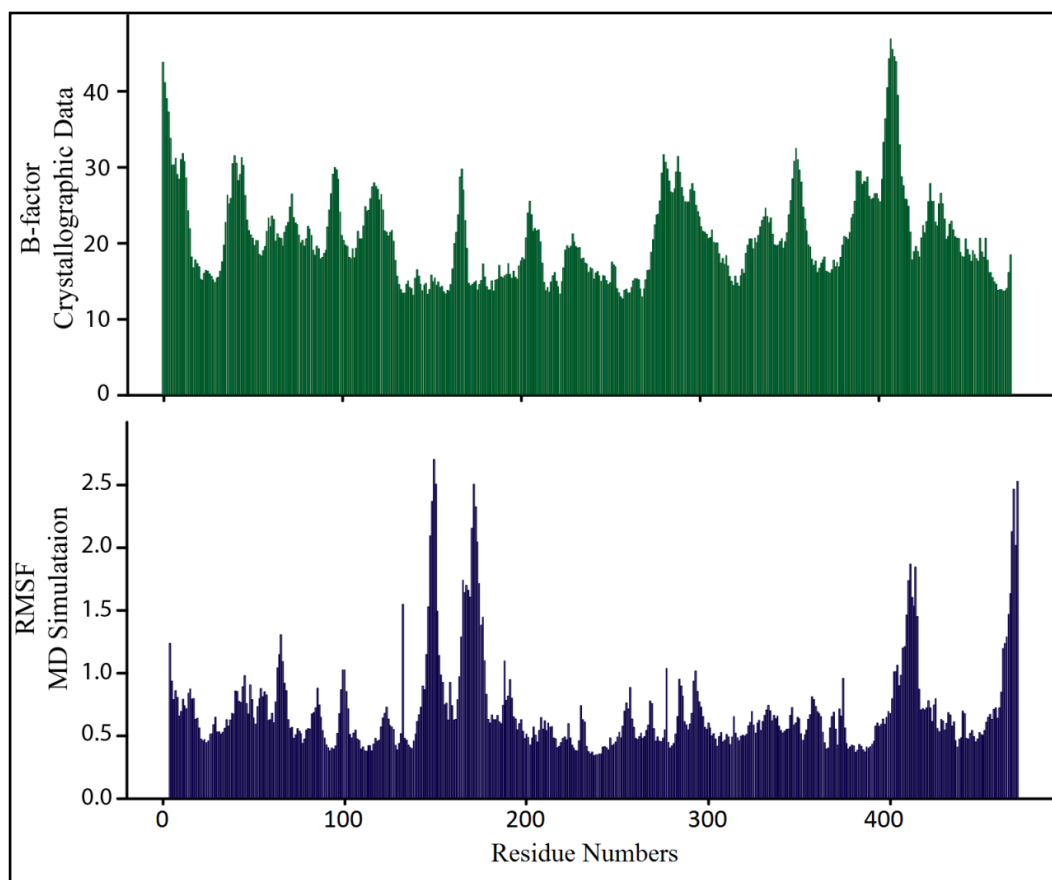


Figure 5.10: RMSF plot for all atoms of glutamine synthetase in its free state resulted from 10 ns simulation trajectory plotted in comparison with that of the crystallographic B factor.

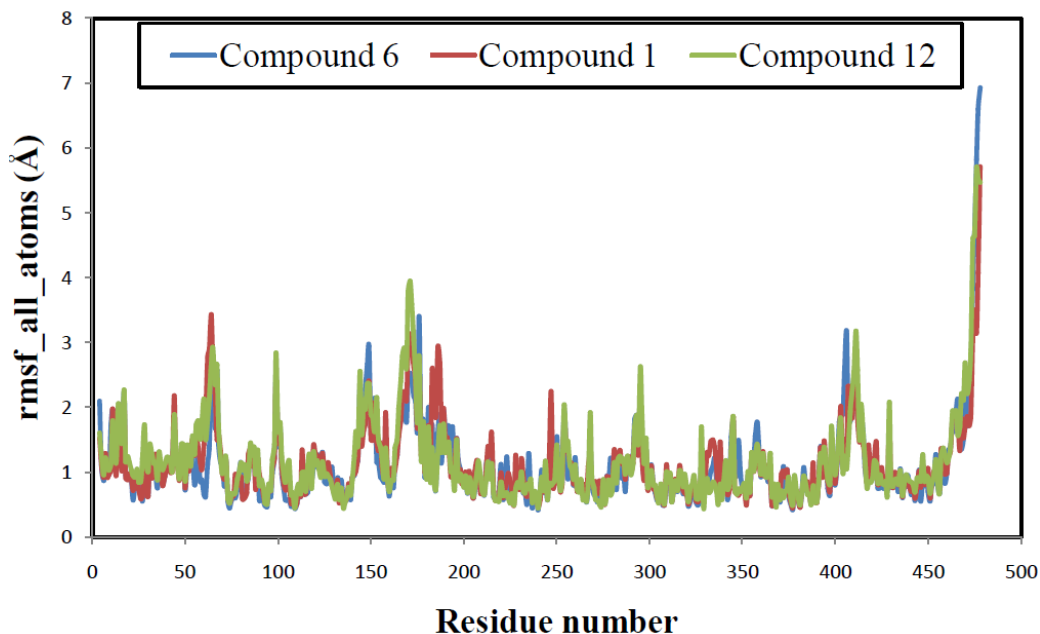


Figure 5.11: rmsf plot of glutamine synthetase in bound states with compound **6**, **1** and **12**.

5.1.6.1. Hydrogen bond analysis

For any molecule to bind at the active site of protein, hydrogen bonding is one of the crucial interactions required to hold the molecule tightly with the protein. The more the hydrogen bonding between ligand and protein, higher the stable is the complex. The hydrogen bond analysis of the top 3 active compounds (compound 1, 6 and 12) has been carried out in order to study their hydrogen bond network at the active site which can indeed correlated with their MTB GS inhibitory activity. The most active ligand, compound **6**, was found to possess hydrogen bonding with residues Glu214, Phe232 and Lys361. The bonds were found between secondary amine of ligand and carboxyl group of Lys361, hydroxyl group of ligand and amine of Phe232 and the same hydroxyl group from ligand were also involved in hydrogen bonding with carboxylic terminal of Glu214. The inter-atomic distance fluctuation of hydrogen bonding atoms was plotted over the simulation time period and is shown in **Figure 5.12(a)**. It can be observed from the plot that the hydrogen bonding of ligand with Lys361 is more stable when compared over other two interactions. The residues Glu214 and Phe232 were found to be fluctuating in the terms of distance from ligand; particularly Glu214 was found with more fluctuations. This can also be confirmed from the crystallographic B factor of Glu214 whose average B factor was found to be ~27, which shows the flexible nature of the residue.

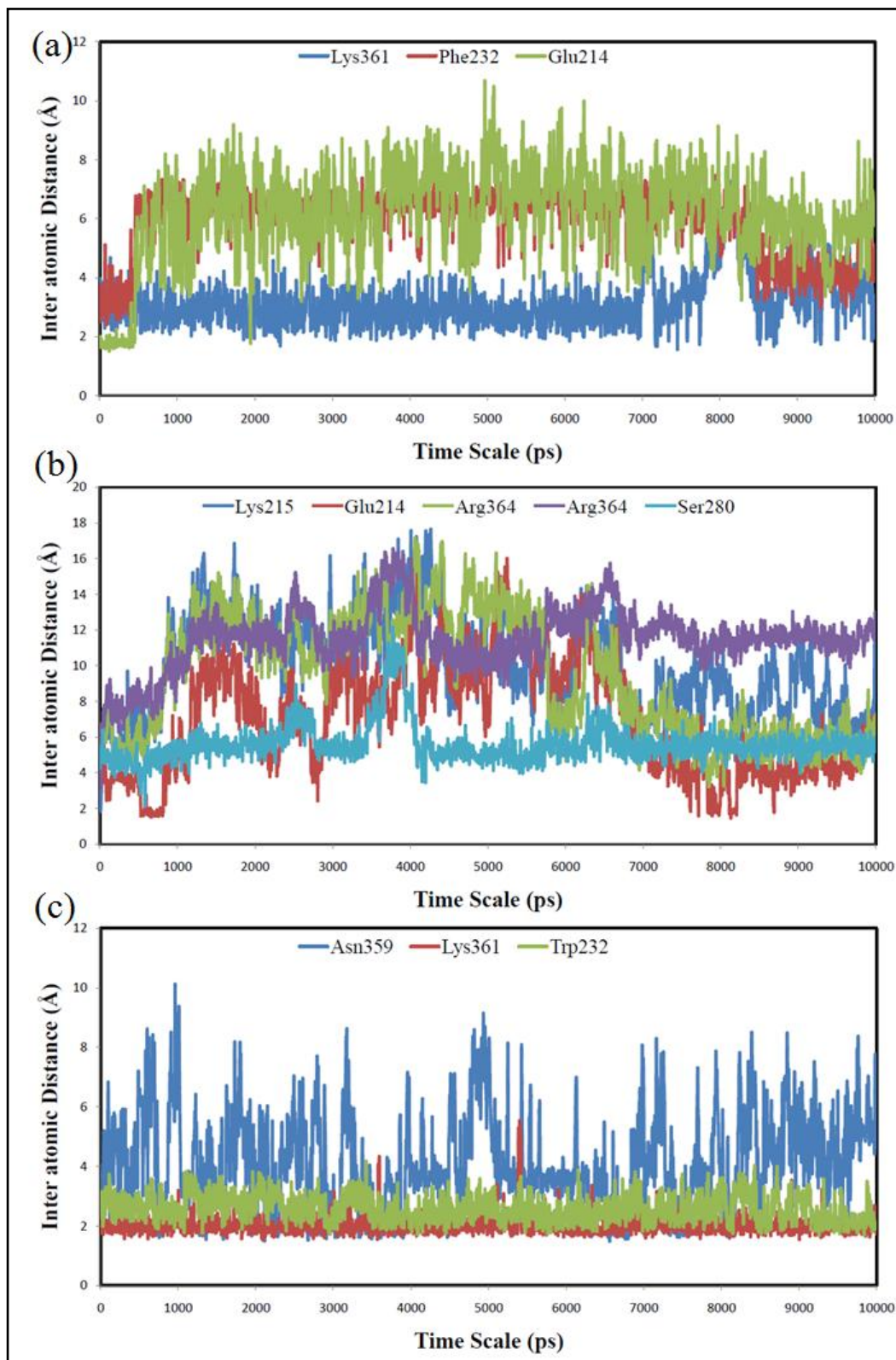


Figure 5.12: Hydrogen bonding analysis for glutamine synthetase bound states with ligands (a) compound **6**, (b) compound **1** and (c) compound **12** plotted as a function of time.

The next active ligand, compound **1** was found to have hydrogen bond interactions with residues Lys215, Glu214 and two interactions with Arg364. The inter-atomic distance fluctuations of hydrogen bonding atoms of ligand and protein over simulation time period is shown in **Figure 5.12(b)**. It can be analyzed from the graph that the interactions of compound 1 with Ser280 and Arg364 are stable when compared to other residues. The residues Glu214, Lys215 were found to be fluctuating which can be attributed to the instability of hydrogen bonds with these residues.

Compound **12** had been in hydrogen bonding with residues Trp282, Asn359 and Lys361. The inter-atomic distance fluctuations of hydrogen bonding atoms over simulation time period is shown in **Figure 5.12(c)**. The plot shows highly stable bonding network of ligand with residues Trp282 and Lys361 whereas the interaction with residue Asn359 was highly deviating. The B factor of Asn359 was found ~ 31.5 which shows the high flexible nature of residue. Hence the tight binding of compound 12 may be attributed to strong interactions with residues Trp282 and Lys361.

5.1.7. Free energy perturbation (FEP) analysis

Free energy perturbation (FEP) studies have been revolutionized the process of computational drug discovery by offering a high degree of reliability for further studies. Hence, in the present study we employed FEP calculations for the top 3 active compounds to determine their free energies so as to correlate the results with their *in vitro* activity. The solvation free energies for the top 3 compounds were determined in pure solvent conditions. The resulting energetic parameters for all the 3 compounds are shown in **Table 5.7**.

Table 5.7: Solvation free energies calculated for the top 3 active compounds using FEP.

Parameters	Compound 6	Compound 1	Compound 12
Absolute Free Energy	-2.19	-4.27	-3.62
ΔG FEP Solvation	-563.25 \pm 6.62	-19.92 \pm 0.11	-82.63 \pm 0.24
ΔG FEP Coulomb	-562.11 \pm 6.62	-18.74 \pm 0.04	-80.15 \pm 0.23
ΔG van der Waal	2.952 \pm 0.081	04.99 \pm 0.10	03.06 \pm 0.07
ΔG Solvent transfer	-561.34 \pm 6.62	-18.01 \pm 0.11	-80.72 \pm 0.24

The annihilation of compounds resulted in solvation energies of $-563.25 \text{ kcal.mol}^{-1}$, $-19.92 \text{ kcal.mol}^{-1}$ and $-82.63 \text{ kcal.mol}^{-1}$ for compounds **6**, **1** and **12** respectively. This indicates that the compound **1** is more solvated when compared to the other ones. This can also be supported by high solvent accessible surface area (SASA) value of compound **1** given in **Table 5.7**.

The annihilation of compounds also resulted in absolute free energies of $-2.19 \text{ kcal.mol}^{-1}$, $-4.27 \text{ kcal.mol}^{-1}$ and $-3.62 \text{ kcal.mol}^{-1}$ for compounds **6**, compound **1** and compound **12** respectively. The absolute free energies obtained from the FEP calculations indicate the readiness of the compound to bind to the target. All the three compounds were found to possess nearly similar free energies with compound **6** having greater free energy which can readily bind to the protein tightly. Also the ΔG energies for solvation, coulomb, van der Waal support the inhibitory activity of the three compounds studied. These observations, supported by high IC_{50} value of the compound **6** ($2.12 \mu\text{M}$), prove the accuracy and reliability of theoretical simulations which play a major role in the drug development process.

Also the free energy perturbations of the 3 compounds gave the non-bonded interaction energies, coulomb and van der Waal energies, showing the contribution of each type of interaction in the binding of ligand to the protein. Considering the resulting values for these interactions, it can be concluded that not only the bonding energies, but also the non-bonding energies play a significant role in ligand-protein binding.

5.1.8. Lead expansion and optimization studies for the most active compound obtained from virtual screening

Most of the selected compounds were found to be with better MTB GS inhibitory profile. Though compounds **1**, **6** and **12** were found to be active ones out of the selected 12, compound **4** (3-(-(2-methoxyphenyl)amino)-2-oxoethyl)-5-phenyl-1H-pyrrol-2-yl)propanoic acid) was selected for further structural optimization and derivatization studies. Binding energy calculations from Prime-MMGBSA studies showed compound **4** as the one with highest binding energy. The interaction profile of compound **4** (as shown in **Figure 5.13**) revealed the presence of three hydrogen bonds; two between oxygen atoms of terminal carboxylate group and Arg364 and one between secondary amine and Lys361. π - π stacking interactions were found with residues Tyr129, Phe232 and Trp282. Also the compound was found involved in cation- π interaction with Arg364. This compound was selected on the grounds of its binding

energy (theoretical data), interaction profile at glutamine synthetase active site, its synthetic feasibility and activity ($IC_{50} = 10.31 \mu M$) which was aimed to improve based on some structural modification.

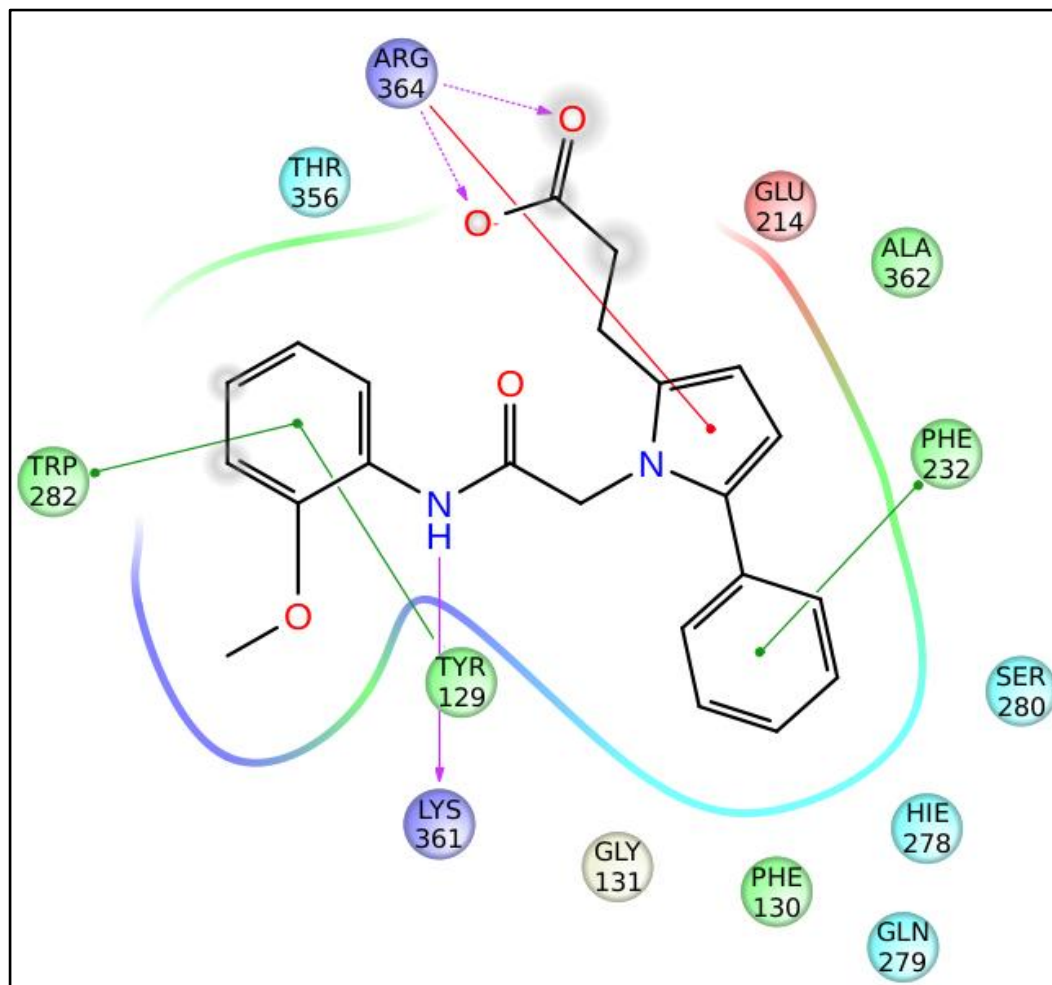


Figure 5.13: Interaction profile of compound 4 considered for lead optimization studies

The propanoic acid chain of the compound was retained due to its interactions at the active site. One of the two substitutions attempted over the compound was the modification over phenyl group attached to the amide side chain with *para* substituted phenyl moieties and some other aromatic groups like thiazole and benzothiazole. These substitutions were attempted so as to observe the effect of various hydrophilic and hydrophobic moieties over the glutamine synthetase inhibitory activity of the compound. The second modification was attempted on the *para* position of the phenyl group attached to the pyrrole moiety. The phenyl group was found

to be involved in hydrophobic interactions which made us to retain the aromatic group but to substitute with various hydrophobic moieties. The substitutions attempted were hydrogen, chlorine, methyl and methoxy groups.

5.1.8.1. Development of 3-[1-(2-amino-2-oxoethyl)-5-phenyl-1H-pyrrol-2-yl]propanoic acid derivatives as potential *M. tuberculosis* glutamine synthetase inhibitors

A series of 40 compounds, 3-[1-(2-amino-2-oxoethyl)-5-phenyl-1H-pyrrol-2-yl]propanoic acid derivatives, were synthesized by following a four-step synthesis protocol as given in **Figure 4.1** in materials and methods under **section 4.1.2.1**. The first step involved the condensation of 2-furaldehyde and substituted acetophenone in the presence of methanol, sodium methoxide at room temperature which was allowed for stirring for about 16 h. The resultant mixtures were diluted and extracted with ethyl acetate. The product, substituted (E)-4-(furan-2-yl)-1-phenylbut-2-en-1-one was obtained by drying the combined organic layers over anhydrous sodium sulphate and the solvent was removed *in vacuo*. The later step involved the synthesis of substituted ethyl-4,7-dioxo-7-phenylheptanoate which involved the heating and reflux of substituted (E)-4-(furan-2-yl)-1-phenylbut-2-en-1-one in the presence of conc. HCl for 16 h. The reaction was concentrated and diluted with dichloromethane and washed with water. The resultant organic layer was dried similar to the previous step over anhydrous sodium sulphate and solvent was removed *in vacuo* to obtain the resultant mixture.

Glycine was added to the synthesized substituted ethyl-4,7-dioxo-7-phenylheptanoate in ethanol followed by the addition of *p*-toulene sulfonic acid monohydrate. The reaction mixture was heated under reflux for 16 h and the solvent was removed *in vacuo* to obtain a crude product. This crude product upon purification by silica gel flash chromatography resulted in substituted 2-(2-(3-ethoxy-3-oxopropyl)-5-phenyl-1H-pyrrol-1-yl)acetic acid.

The substituted 2-(2-(3-ethoxy-3-oxopropyl)-5-phenyl-1H-pyrrol-1-yl)acetic acid was dissolved in dry dichloromethane and cooled to 0 °C. To this reaction mixture, triethyl amine was added drop wise under cool condition. Then EDC HCl and HOBT were added followed by substituted amines and reaction mixture was cooled to room temperature and stirred for 6 h. The reaction mixture was washed with water and after phase separation, the organic layer was dried over anhydrous Na₂SO₄ and the solvent removed *in vacuo* to obtain the crude

mixture, which was purified by silica gel flash chromatography to obtain substituted ethyl 3-(1-(2-oxo-2-(phenylamino)ethyl)-5-phenyl-1H-pyrrol-2-yl)propanoate in good yields. The general procedure followed for the synthesis of 40 compounds is given in **Annexure-I**.

5.1.8.2. Molecular docking analysis of the synthesized compounds

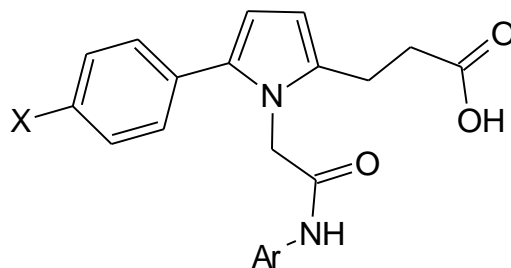
The synthesized 40 compounds were subjected to molecular docking studies with the glutamine synthetase protein using extra precision mode of Glide v5.7. Most of the compounds were found to be possessing better interaction profile when compared to the lead compound identified. The common residues involved in hydrogen bonding with most of the compounds were found to be Lys361 and Arg364. Based on interaction profile analysis for all the compounds, it was understood that it is the hydrophobic interactions which make protein-ligand complex stabilized thereby adding up to the binding affinity of ligand. The most common residues involved in hydrophobic interactions with the compound were found to be Tyr129, Phe130, Tyr230, Phe232, Trp282, Pro287, Met289, and Leu365. The compounds were further subjected to *in vitro* glutamine synthetase inhibition studies to study their inhibitory potency.

5.1.8.3. *In vitro* glutamine synthetase inhibition assay, antimycobacterial potency and cytotoxicity studies for the synthesized compounds

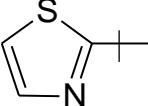
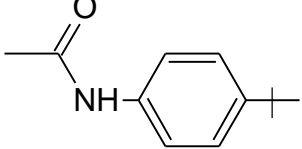
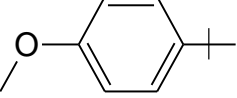
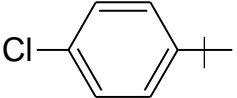
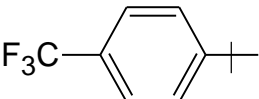
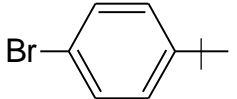
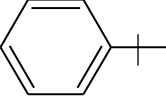
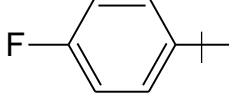
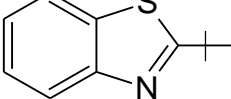
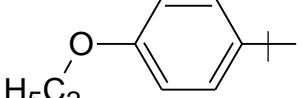
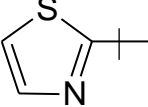
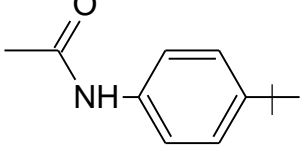
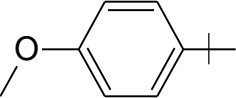
5.1.8.3a. *In vitro* glutamine synthetase inhibition assay

The glutamine synthetase enzyme inhibition assay was carried out for the synthesized 40 compounds. As described in the previous sections, various concentrations of the compounds starting from 25 μM , 10 μM , 5 μM , 1 μM and 0.5 μM were tested against glutamine synthetase to understand the inhibitory capacity of the compounds. The IC_{50} s for all the compounds were calculated using Graph Pad Prism and are given in the **Table 5.8**. The activity range of the synthesized compounds was found to be 1.34 - >25 μM . Of all the compounds, compound **PSC10** was found to be the most active one with an IC_{50} of **1.34 μM** . Dose response curve for compound PSC10 is shown in **Figure 5.14**. The next active compounds of the series were found to be compounds PSOM10 (IC_{50} – 3.12 μM) and PSC05 (IC_{50} – 3.34 μM). Total six compounds were found with IC_{50} less than 5 μM and 20 compounds were found with activity between 5 – 10 μM range. The remaining compounds were found to be moderately active and some of which were completely inactive.

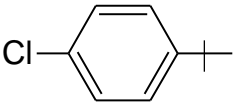
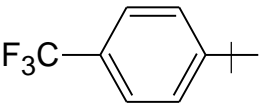
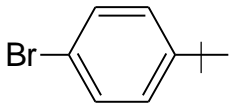
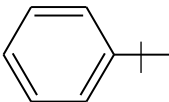
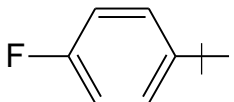
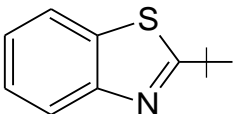
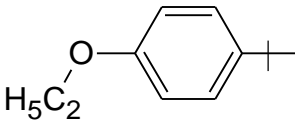
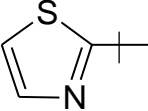
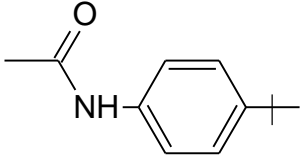
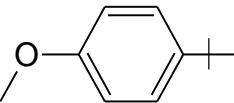
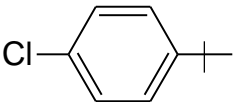
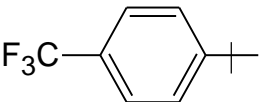
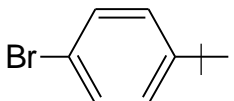
Table 5.8: *In vitro* inhibitory activities of the synthesized analogues

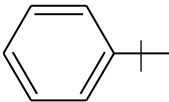
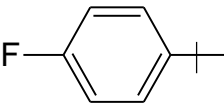
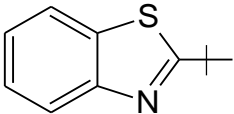
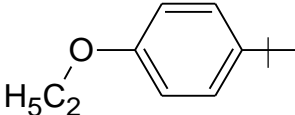
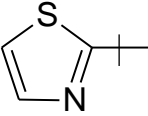
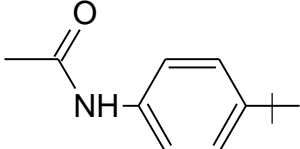


Code	Ar	X	IC ₅₀ (μM)
Lead		-H	10.31±1.56
PS01		-H	7.16±0.98
PS02		-H	7.93±0.47
PS03		-H	>25
PS04		-H	8.64±2.13
PS05		-H	6.55±0.71
PS06		-H	8.11±0.04
PS07		-H	9.66±1.24
PS08		-H	9.96±2.13

PS09		-H	18.69±1.17
PS10		-H	5.27±1.44
PSC01		-Cl	7.03±0.63
PSC02		-Cl	8.16±0.57
PSC03		-Cl	16.71±2.96
PSC04		-Cl	12.12±1.32
PSC05		-Cl	3.34±1.85
PSC06		-Cl	9.41±0.72
PSC07		-Cl	6.91±1.21
PSC08		-Cl	16.17±1.63
PSC09		-Cl	22.49±0.52
PSC10		-Cl	1.34±0.81
PSM01		-CH ₃	9.64±0.09

Inhibitors against MTB Glutamine Synthetase

PSM02		-CH ₃	10.51±0.54
PSM03		-CH ₃	17.66±1.47
PSM04		-CH ₃	16.83±1.29
PSM05		-CH ₃	5.61±0.56
PSM06		-CH ₃	7.12±0.98
PSM07		-CH ₃	9.02±0.42
PSM08		-CH ₃	18.41±1.27
PSM09		-CH ₃	>25
PSM10		-CH ₃	4.15±0.78
PSOM01		-OCH ₃	8.31±1.24
PSOM02		-OCH ₃	7.14±2.75
PSOM03		-OCH ₃	15.63±0.48
PSOM04		-OCH ₃	6.29±0.74

PSOM05		-OCH ₃	4.41±0.36
PSOM06		-OCH ₃	6.24±0.48
PSOM07		-OCH ₃	3.92±1.25
PSOM08		-OCH ₃	11.61±1.97
PSOM09		-OCH ₃	11.24±1.17
PSOM10		-OCH ₃	3.12±0.67

* IC₅₀ calculated using GraphPad Prism 6 (mean±SEM).

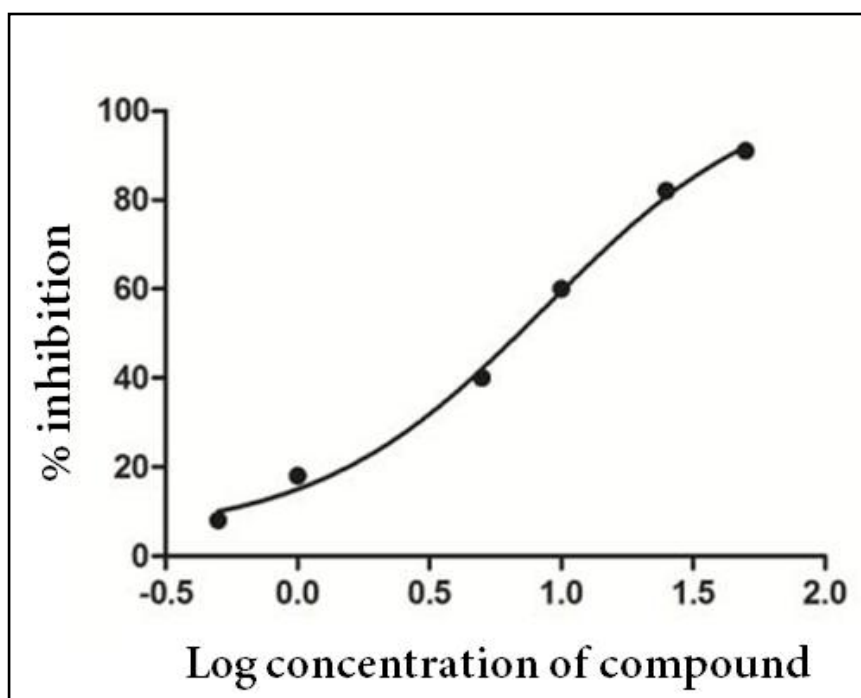


Figure 5.14: Dose response curve for compound PSC10.

5.1.8.3b. *In vitro* antimycobacterial screening for the synthesized compounds

The synthesized compounds were tested for their *in vitro* antimycobacterial activity using MABA assay. All compounds were found to be inactive with MIC more than 25 μ M. This could be probably due to the lesser hydrophobic nature of the compounds which restricted them to pass through the mycobacterial cell wall which is highly hydrophobic. Presence of propanoic acid may have imparted the hydrophilicity to the compounds which supported the lesser activity of compounds. The compounds were not tested for their cytotoxicity profiles.

5.1.9. Molecular dynamics simulation analysis

The most active compound, PSC10, complexed with glutamine synthetase was analyzed for its interaction pattern at the active site. Interaction profile of the most active compound PSC10 is shown in **Figure 5.15**. PSC10 was found to be involved in hydrogen bonding with residues Lys361 and Arg364. A cation- π interaction was observed between the residue Arg364 and pyrrole group of the compound. Three π - π stacking interactions were observed between the compound and residues Tyr129, Phe232 and Trp282. This PSC10-glutamine synthetase complex was subjected to 20 ns simulation in order to study the protein-ligand interaction stability in dynamic conditions (simulating body conditions) and to generate further theoretical information to support its activity. This ligand-protein complex was simulated explicitly using OPLS_2005 force field in Desmond v3.1.

RMSD analysis for the obtained trajectory has been carried out to analyze the stability of protein and ligand in complex during simulation. **Figure 5.16** shows RMSD for C α atomic positions and heavy atoms for glutamine synthetase-PSC10 complex throughout the simulation. An initial jump in RMSD of complex during initial few pico seconds when compared to the original starting frame during simulation may be attributed to the relaxation of model in solvent system. It was observed from the plot that both the C-alpha atoms and heavy atoms of the complex were found to be behaving in similar fashion during simulation with minimal fluctuations and were found to be stable. From the plot, it was inferred that the protein was found to fluctuate with lesser deviations in structure up to a time period of 10 ns after which RMSD for the protein was found to be highly stable. The plot indicated the stabilizing nature of PSC10 over protein. Root mean square deviation for compound PSC10 was analyzed throughout the simulation time period and shown in **Figure 5.17**.

The plot illustrated behaviour of PSC10 in the complex under dynamic conditions. The compound was initially found to be fluctuating until a time period of 10 ns after which it was found equilibrated. Fluctuations till 10 ns may be correlated to RMSD of protein till the same time point (**Figure 5.16**). It was observed that complex had undergone some fluctuations till a particular time period after which it was found to be highly stabilized proving binding affinity of compound PSC10 towards glutamine synthetase and their binding stability.

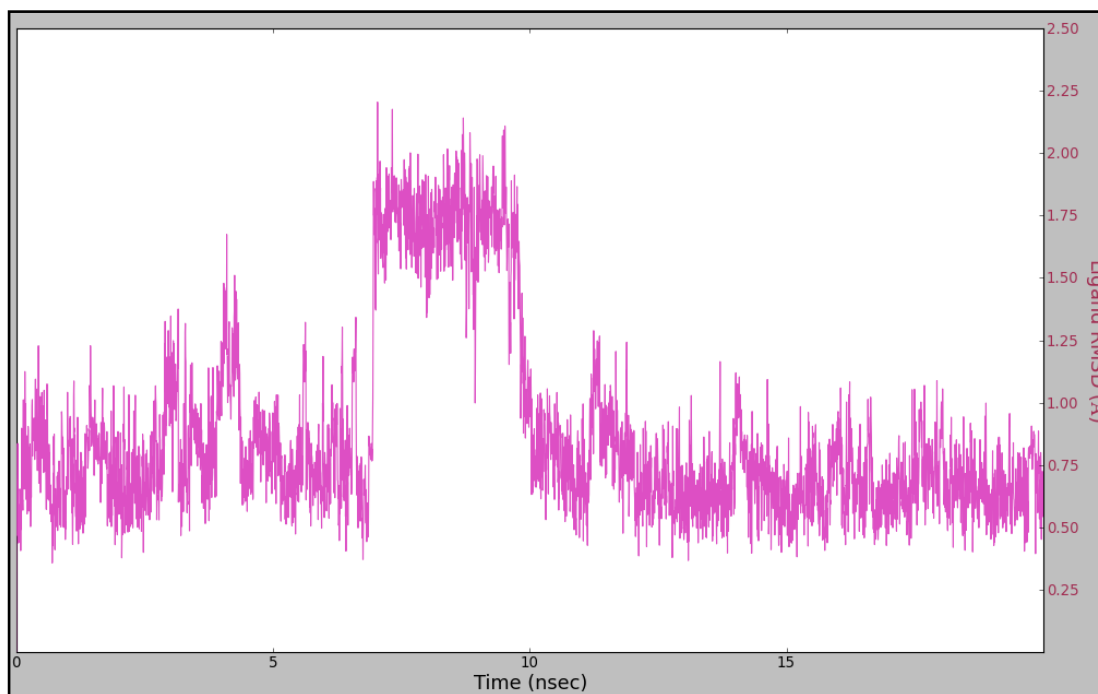


Figure 5.17: RMSD plot of compound **PSC10** plotted in complex with glutamine synthetase

Root mean square fluctuation (RMSF) of protein was analyzed for characterizing local changes along the protein chain during simulation. **Figure 5.18** portrays RMSF plot for C-alpha of the protein with respect to their residue index. The plot also contains B-factor information for the residues of protein. On this plot, peaks indicate areas of the protein that fluctuate the most during simulation. Typically, it was observed from the plot that N- and C-terminals fluctuate more than any other part of the protein. Secondary structure elements like alpha helices and beta strands are usually more rigid than the unstructured part of the protein, and thus fluctuate less than the loop regions. Protein residues that interact with the ligand are marked with green colored vertical bars. From the plot, it was observed that most of the active site residues were stable with lesser fluctuations. The major peaks showing fluctuating residues fall into the loop region which was found to be away from the active site.

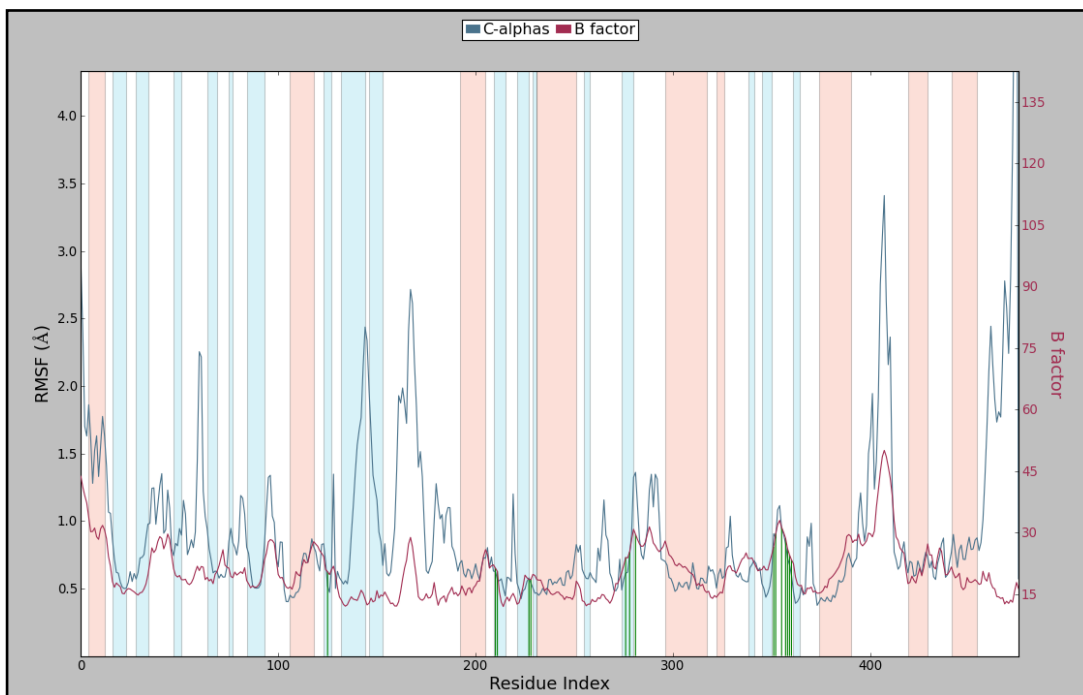


Figure 5.18: RMSF plot for C-alpha atoms of glutamine synthetase-PSC10 complex. Green lines indicate the residues interacting with compound PSC10.

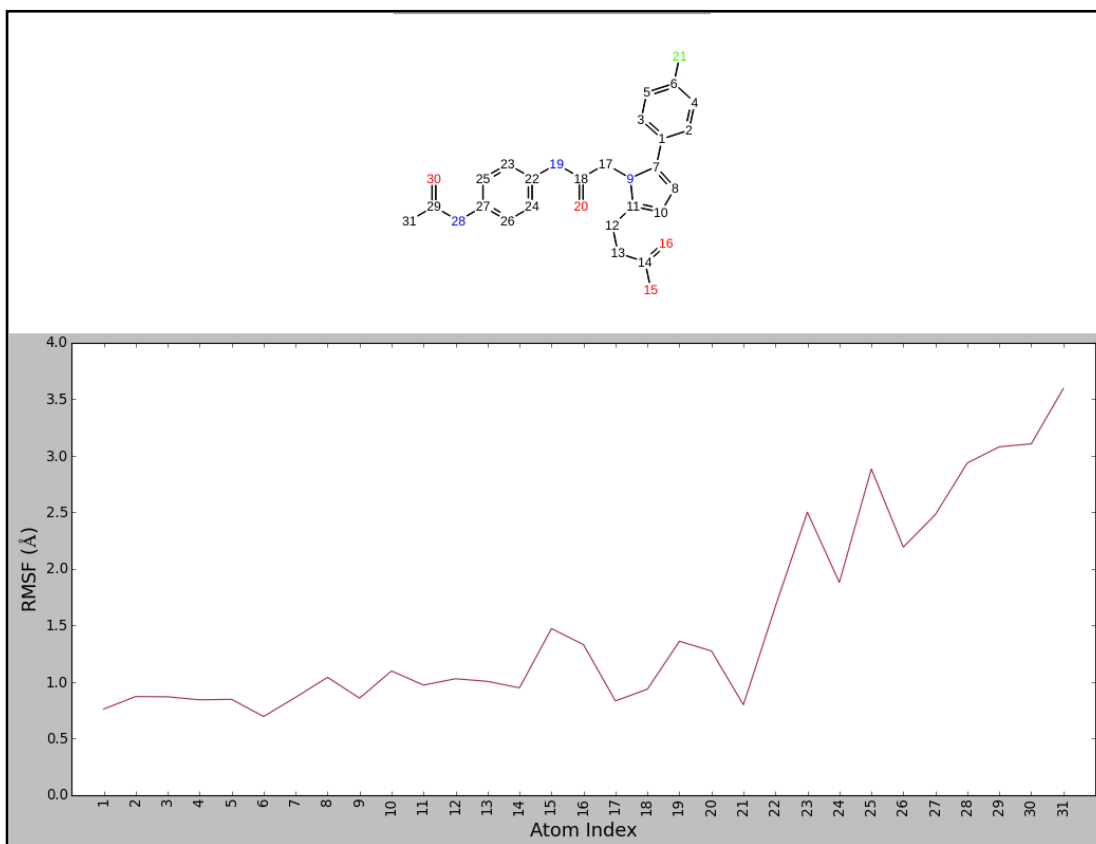


Figure 5.19: RMSF plot for PSC10 with respect to its each atom during simulation

Considering RMSF for compound PSC10 during simulation, a plot was plotted for each atom of the ligand with respect to their fluctuation considered throughout the simulation time period and shown in **Figure 5.19**. It was seen that all atoms from PSC10, except those in the terminal N-phenyl acetamide moiety, were found to be highly stable. Terminal N-phenyl acetamide part of PSC10 was found to be with greater fluctuations as this region of ligand were found to be oriented towards solvent in the active site. This part of the compound was found to interact with residues Tyr129 and Trp282 lining the opening of active site.

Torsion angle analysis of compound PSC10 during the simulation time period was carried out to understand the torsional stress undergone by each rotatable bond at glutamine synthetase active site. The ligand torsions plot summarizes the conformational evolution of every rotatable bond (RB) in the ligand throughout the simulation trajectory (0.00 through 20.00 nsec). **Figure 5.20** shows the 2D schematic of a ligand with color-coded rotatable bonds. Torsion plot for each bond is represented by a dial plot and bar plots of the same color. Dial (or radial) plots portray the conformation of the torsion throughout the course of the simulation. The centre of the radial plot was found to be beginning of the simulation which with time evolution is plotted radially outwards.

The bar plots summarize the data on the dial plots, by showing the probability density of the torsion (**Figure 5.20**). With the available torsional potential information, the plot also shows the potential of the rotatable bond (by summing the potential of the related torsions). The values of the potential are on the left Y-axis of the chart, and are expressed in kcal.mol⁻¹. Looking at the histogram and torsion potential relationships give the insights into the conformational strain the ligand undergoes to maintain a protein-bound conformation.

From the **Figure 5.20**, it was observed that both the bonds between the secondary amine and the phenyl group undergo maximum torsional stress with highly fluctuating torsion potentials. These fluctuating torsion potentials were not observed with any other bonds of the compound. This high fluctuation in the potentials of these bonds may be attributed to the presence of the N-phenyl acetamide towards the solvent which was found to be highly fluctuating. This was also supported by ligand RMSF data from **Figure 5.19** which displays high fluctuation of atoms 22-31. This can also be supported in terms of available space at the entry of GS active

site because of which much torsion stress was observed over the bonds to maintain the orientation of ligand at active site.

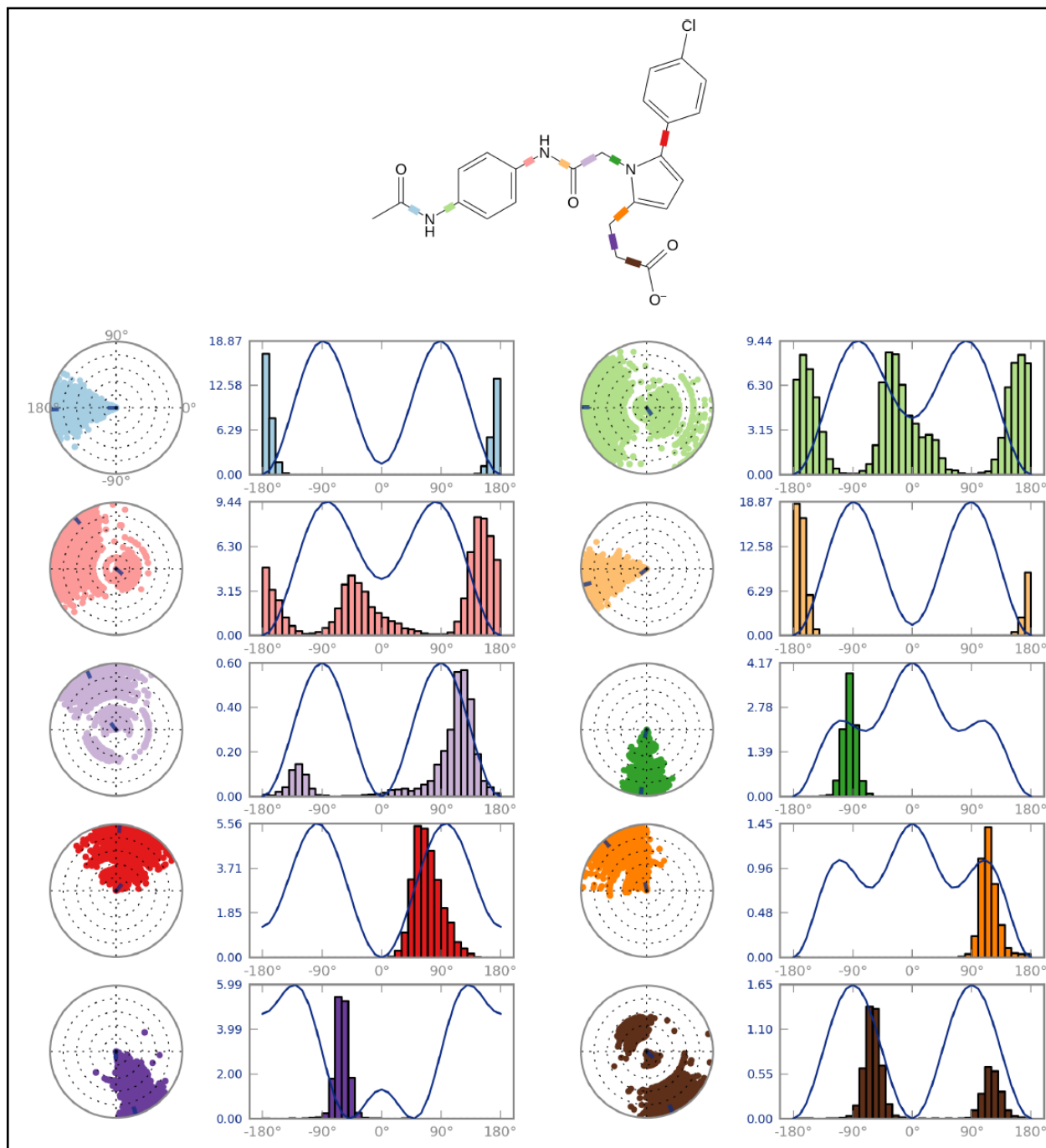


Figure 5.20: 2D representation of compound PSC10 shows its rotatable bonds with different color scheme. Torsion angle and torsion potential plotted for each rotatable bond of compound PSC10 are shown in radial and bar plot respectively.

5.1.9.1. Simulation interaction analyses

Interaction profile of the compound PSC10 at the active site of glutamine synthetase is shown in **Figure 5.21** with the percentage strength of each interaction. It was found that Arg364 was the main residue interacting with over 95% with PSC10. The compound was also found to be involved in water mediated hydrogen bonding with residues Lys361 and Lys363.

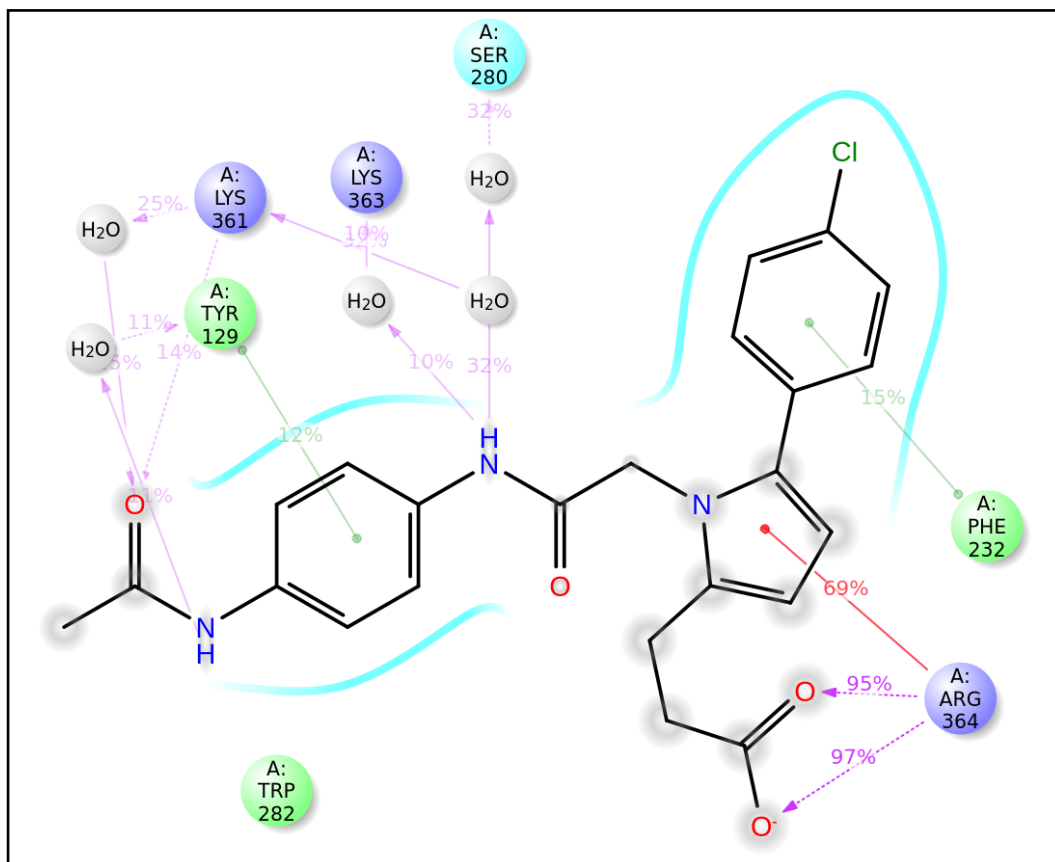


Figure 5.21: Interaction profile of the compound PSC10 with glutamine synthetase showing the strength of each interaction.

Top panel of **Figure 5.22** represents total number of specific contacts the protein makes with the ligand over the course of the trajectory. The contacts here are categorized into four types: hydrogen bonds, hydrophobic, ionic and water bridges. It was seen that compound PSC10 was found to be interacting with glutamine synthetase with at least 2-4 interactions throughout the simulation which altered at some particular simulation time points. Bottom panel shows the residues which interact with the ligand during a particular time frame. Some residues make more than one specific contact with the ligand, which is represented by a darker shade of orange, according to the scale to the right side of plot. From the bottom panel of **Figure**

5.22, it was seen that residues Tyr129, Asn359, Lys361 and Arg364 were constantly interacting with PSC10 with more than one contact throughout the simulation.

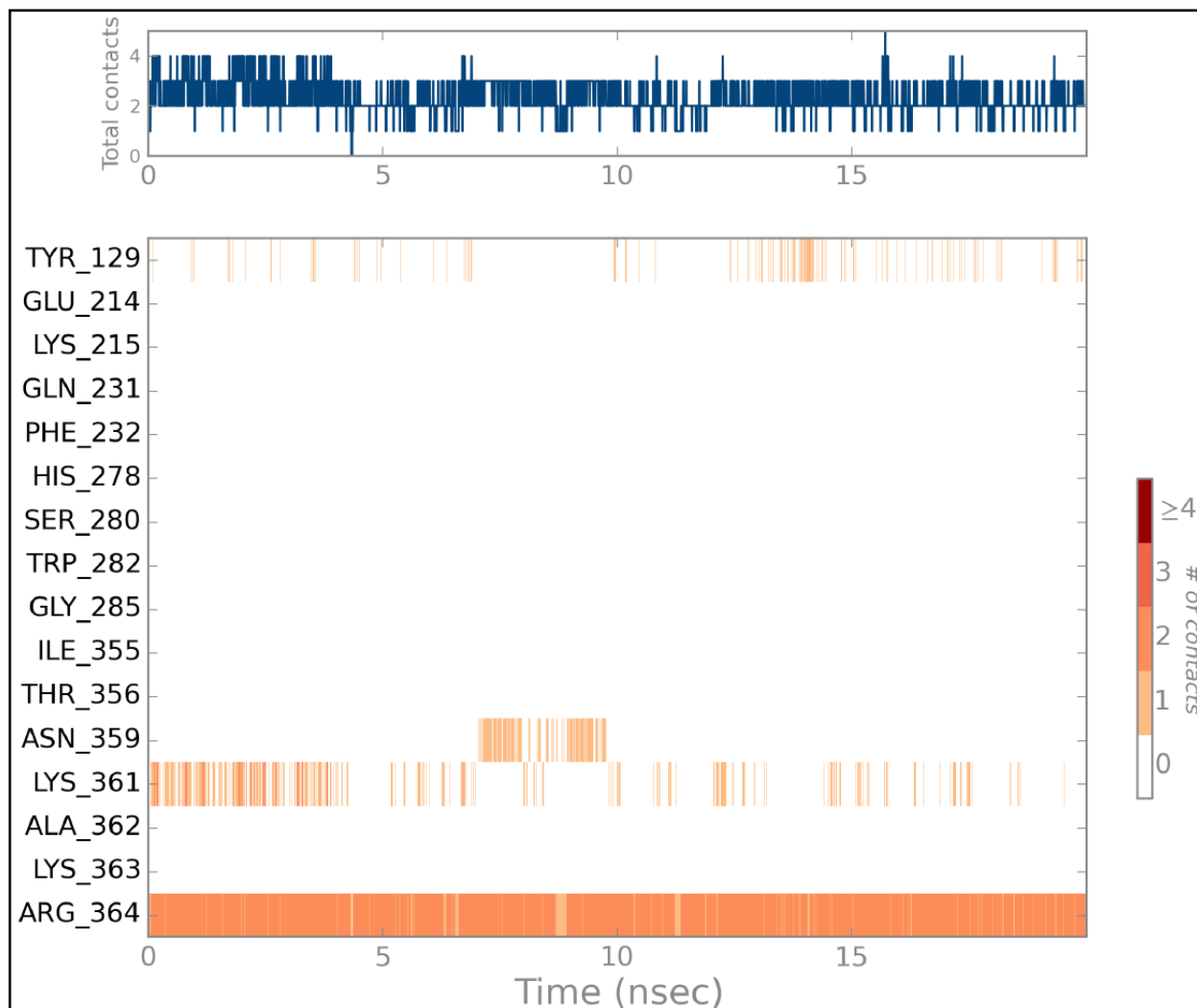


Figure 5.22: Timeline representation of the interactions and contacts (**H-bonds, Hydrophobic, Ionic, Water bridges**) between the compound PSC10 and glutamine synthetase. The top panel shows the total number of specific contacts between MTB GS with compound PSC10 over the course of the trajectory. The bottom panel shows residues interacting with the ligand in each frame.

Hydrogen bond analysis of glutamine synthetase-PSC10 complex revealed the presence of hydrogen bond between residue Arg364 and PSC10. From bar plot of **Figure 5.23**, it was understood the strength of Arg364 was nearly 200% accounting to the presence of two hydrogen bonds, each with terminal oxygens of propanoic acid of the compound. Hydrogen

from amine group of arginine side chain was involved in hydrogen bonding with the compound. In the bottom plot of **Figure 5.23**, hydrogen bonding of residues with PSC10 in each trajectory was plotted. Hydrogen bonding with Arg364 was observed to be strong enough to hold the compound at glutamine synthetase active site throughout the simulation.

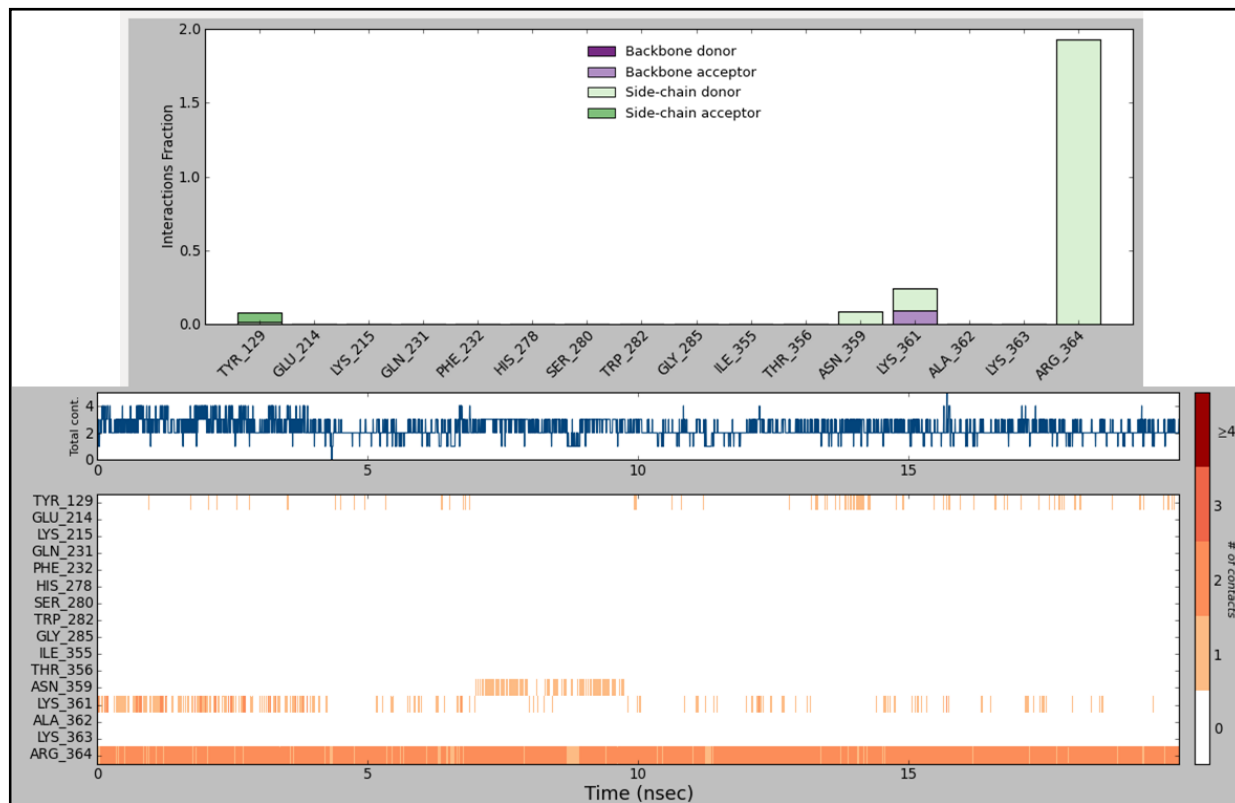


Figure 5.23: Top panel of the figure shows the residues of glutamine synthetase involved in hydrogen bonding with compound PSC10. Stacked bar plots indicate the strength of the bond during simulation time period. Bottom panel shows hydrogen bonding residues interacting with the ligand in each frame.

Hydrophobic interactions were found to be one of the key interactions at glutamine synthetase active site with PSC10. Hydrophobic interaction analysis for the complex is given in **Figure 5.24**. From the figure, it was found that Phe232 was found to be involved in hydrophobic interactions with the compound during the simulation with interaction strength of 138%. The strength of this interaction reveals the presence of more than one interaction of the compound with the residue Phe232. Also, it was found that PSC10 possessed strong hydrophobic interaction with residues Trp282 and Arg364 with almost 83% and 76% respectively. These

interactions were found to be observed throughout the simulation accounting for stable glutamine synthetase-PSC10 complex.

Simulation interaction analysis of protein-ligand complex revealed the presence of an ionic interaction in the complex. The interaction was found between secondary amine of the compound linking the phenyl group with pyrrole moiety and residue Lys361. From the **Figure 5.25**, it was observed that the side chain of Lys361 was involved in ionic interaction with the compound and was found to be stable at each trajectory frame of the simulation. Though the strength of the interaction was observed to be less, this weak interaction also contributed to the binding affinity of compound PSC10 towards glutamine synthetase.

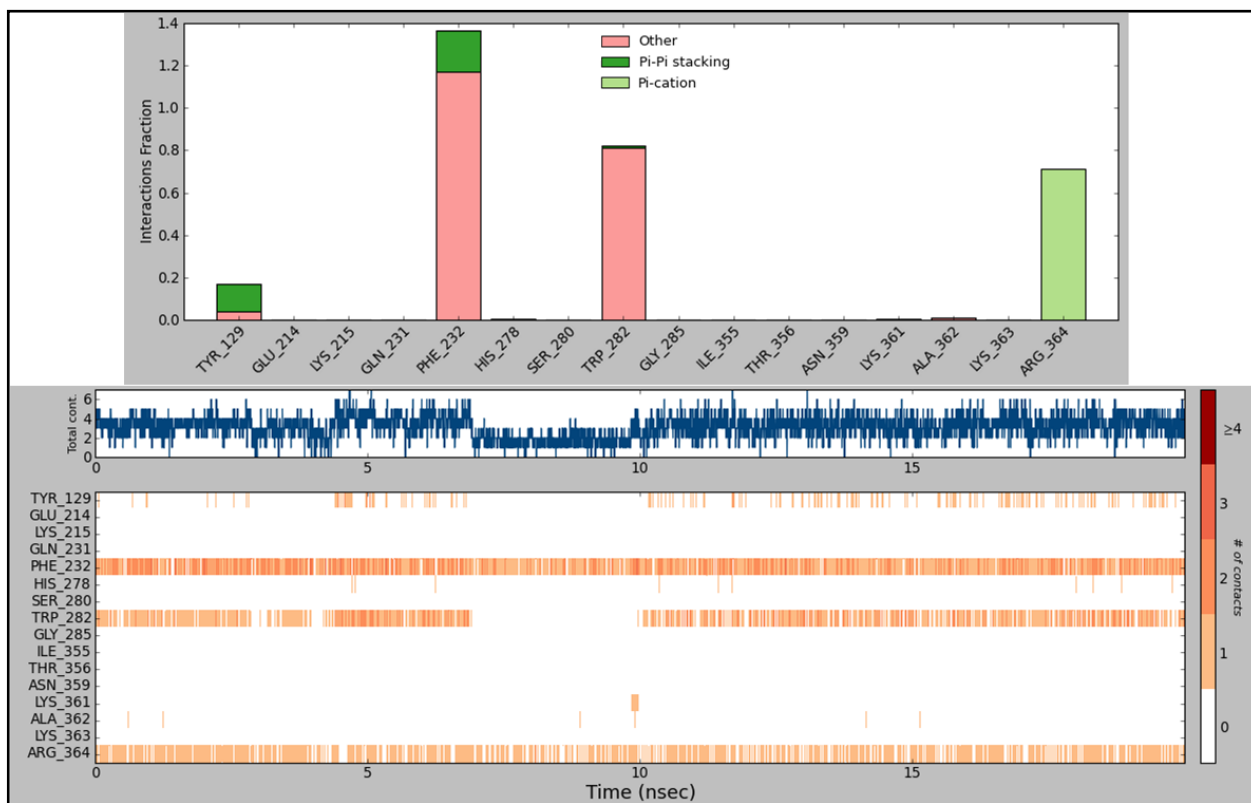


Figure 5.24: Top panel of the figure shows the residues of glutamine synthetase involved in hydrophobic interactions with compound PSC10. Stacked bar plots indicate strength of the bond during the simulation time period. Bottom panel shows residues interacting with the ligand in each frame.

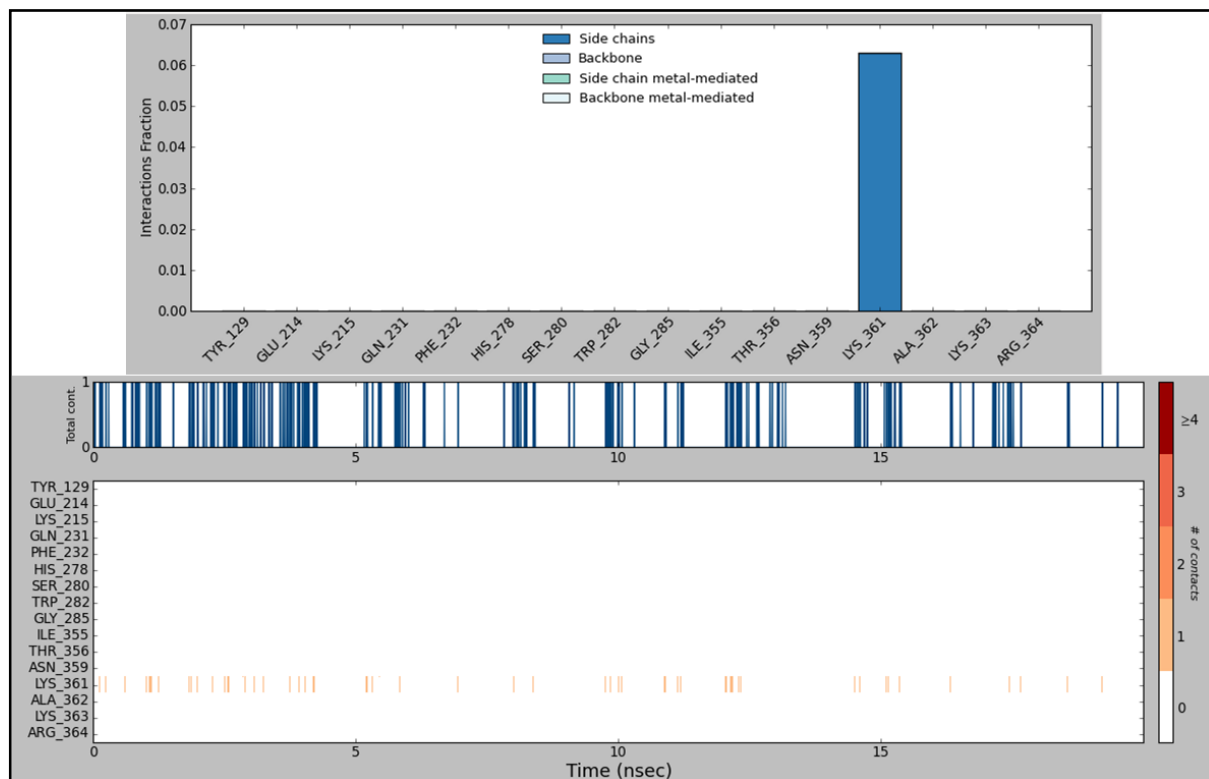


Figure 5.25: Top panel of the figure shows the residues of glutamine synthetase involved in ionic bonds with compound PSC10. The stacked bar plot indicate the strength of the ionic bond during the simulation time period. The bottom panel shows the residue interacting via ionic bond with the ligand in each frame.

Water mediated hydrogen bonding between the active site residues of glutamine synthetase and the compound PSC10 was analyzed and given in **Figure 5.26**. The interactions were majorly found to be observed between the compound PSC10 and residues Ser280 and Lys 361 accounting to strength of 34% and 64% respectively. Other weak strength interactions were found with residues Tyr129, Gln231, Gly285, Ile355, Thr356, Asn359, Lys363 and Arg364. Many of these interactions were found to be present between the glutamine synthetase and compound PSC10 at each frame of the trajectory.

Various other components of the protein-ligand interactions were also analyzed during the simulation time period. The ligand, compound PSC10, was found to be stable at the glutamine synthetase active site during the simulation highlighting its binding affinity towards the protein. The compound was found to fluctuating at a time period of 6-10 ns after which the compound was completely stable.

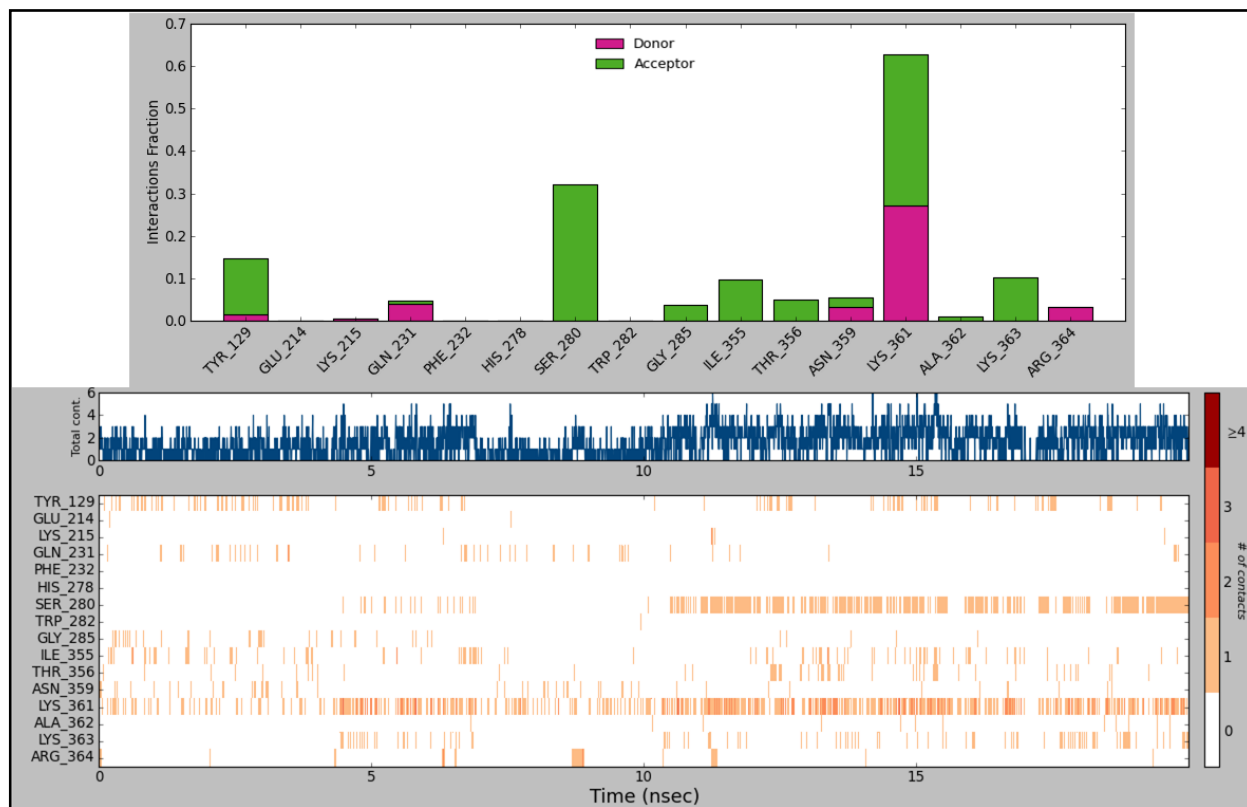


Figure 5.26: Top panel of the figure shows the residues of glutamine synthetase involved in water mediated hydrogen bonding with compound PSC10. The stacked bar plots indicate the strength of the bond during the simulation time period. The bottom panel shows residues interacting via water bridge interactions with the ligand in each frame.

From **Figure 5.27**, the mean RMSD of the compound PSC10 was found to be 0.8 Å which shows the stability of the ligand. The radius of gyration of the ligand was analyzed throughout the simulation and is given in plot **5.27**. The radius of gyration refers to the distribution of the components of an object around an axis. The lesser the radius of gyration, the more compact is the protein structure and vice versa. From the plot, it was inferred that the ligand structure remained stable without much fluctuations. Similar to RMSD, the compound radius of gyration was found to be fluctuating at 6-10 simulation time period. Later the compound was found to be equilibrated from 10 – 20 ns. This observation can in turn be explained by the stabilization effect of the compound PSC10 over glutamine synthetase and its strong binding interactions with the protein which made the ligand stable. The mean radius of gyration for the compound PSC10 calculated over the 20 ns simulation time period was found to be 4.9 Å.

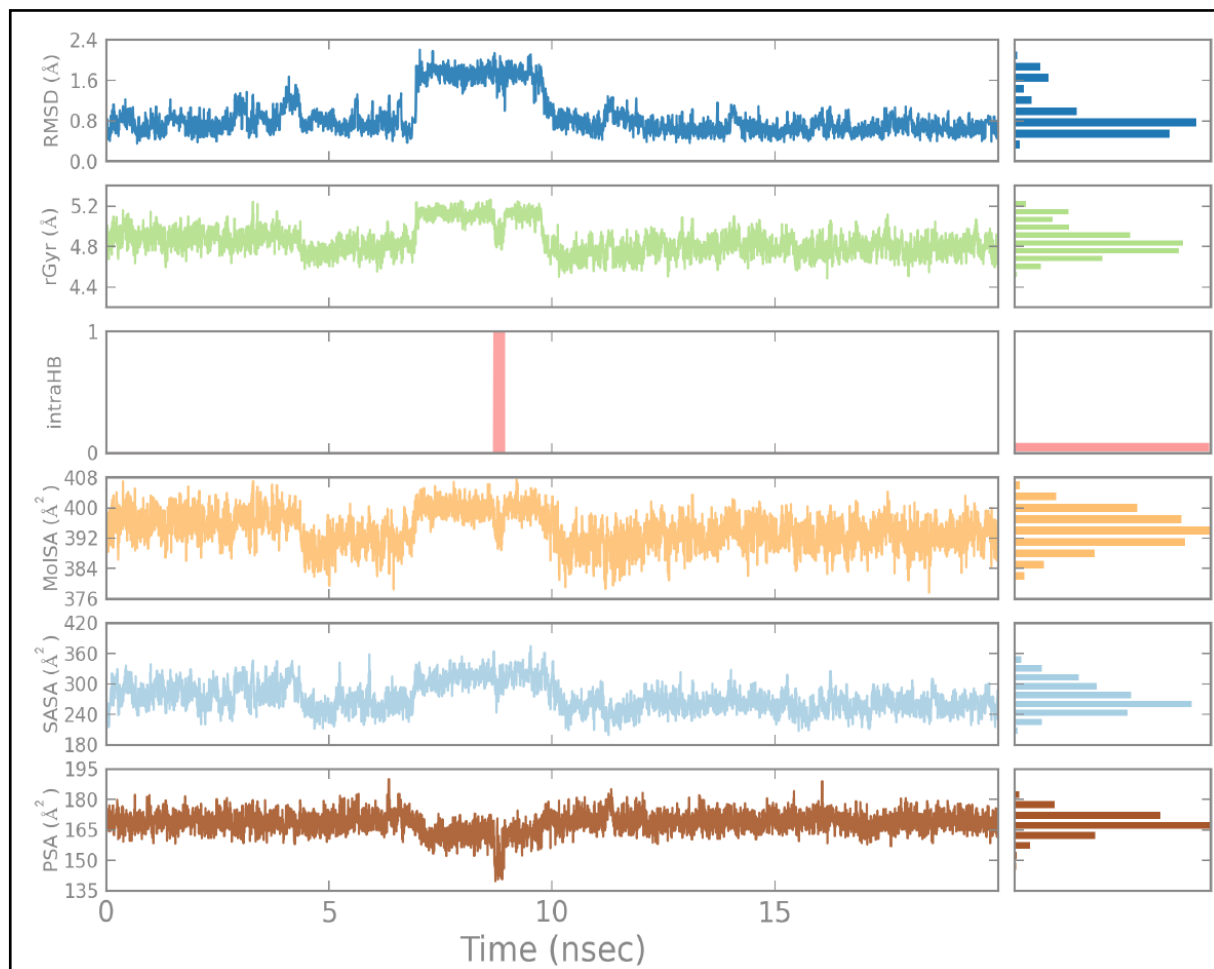


Figure 5.27: Plot representing various ligand properties analyzed during the simulation of glutamine synthetase-compound PSC10 complex.

No intramolecular hydrogen bonding was found with the compound during the simulation. The molecular surface area of the compound PSC10 was analyzed throughout the simulation time period so as to observe any fluctuations in it. The molecular surface area was calculated with a 1.4 Å radius probe. From the **Figure 5.27**, it was observed that some fluctuations in the molecular surface area were observed till 10 ns simulation time period. After 10 ns, the molecular surface area of the compound was found to be equilibrated highlighting the stable nature of the compound. The mean molecular surface area for the compound PSC10 calculated over the simulation time period was found to be 395 Å². Another property of the ligand analyzed during the simulation was solvent accessible surface area (SASA). The SASA is the surface area of a molecule is the surface which is accessible to the solvent and can be typically considered as a reverse of molecular surface area. SASA for the compound PSC10

was analyzed during the simulation and given in **Figure 5.27**. The SASA for the compound was found to be varying with respect to the simulation time period in similar fashion to that of molecular surface area. It was observed that the SASA of the compound PSC10 fluctuated till a time period of 10 ns and later was found to be slightly reduced at the end of the simulation. It was understood based on the above pattern that glutamine synthetase had undergone conformational changes upon the compound PSC10 binding and the binding site was found to be fluctuating which altered the SASA of the compound. The mean SAS for the compound Rv1 was found to be 260 Å during the simulation. Also the polar surface area (PSA) for the compound PSC10 which was contributed only by oxygen and nitrogen was analyzed and plotted with respect to time period (**Figure 5.27**). The polar surface area can be considered as the area available of the ligand available for hydrogen bonding at the active site of protein. Hence this analysis can be a measure of the hydrogen bonding stability between the ligand and the protein. The polar surface area was found to be stable throughout the simulation with slight fluctuations between a time periods of 7-10 ns which inferred that the compound polar region was involved in a stable hydrogen bonding network with the protein glutamine synthetase. The mean polar surface area of the compound PSC10 was found to be 167 Å.

5.1.10. Free energy perturbation studies

In the present study, we employed FEP calculations for the top active compound, **PSC10**, to determine its free energy that is readily available for the compound for binding to its target. The binding free energy for the crystal ligand ($IC_{50} = 1.6 \mu M$) from glutamine synthetase crystal structure (4ACF) was also calculated. The solvation free energies for both compounds were determined in pure solvent conditions. The resulting energetic parameters for both compounds are shown in **Table 5.9**. Annihilation of compounds resulted in solvation energies of $-741.38 \text{ kcal.mol}^{-1}$ and $-108.64 \text{ kcal.mol}^{-1}$ for crystal ligand and PSC10 respectively. This indicated PSC10 was more solvated when compared to the other one.

The annihilation of compounds also resulted in absolute free energies of $-1.07 \text{ kcal.mol}^{-1}$ and $-0.83 \text{ kcal.mol}^{-1}$ for crystal ligand and PSC10 respectively. The absolute free energy for compound PSC10, obtained from the FEP calculations, indicate the readiness of the compound to bind to glutamine synthetase. Also, ΔG energies for solvation, coulomb, van der Waal support the better inhibitory activity of PSC10 compared to that of crystal ligand. These

observations, supported by high IC₅₀ value of compound **PSC10** (1.34 μM), prove the accuracy and reliability of theoretical simulations which play a major role in the drug development process.

Free energy perturbation results for compound PSC10 proved the significant role of non-bonding interactions in the binding of compound at glutamine synthetase active site.

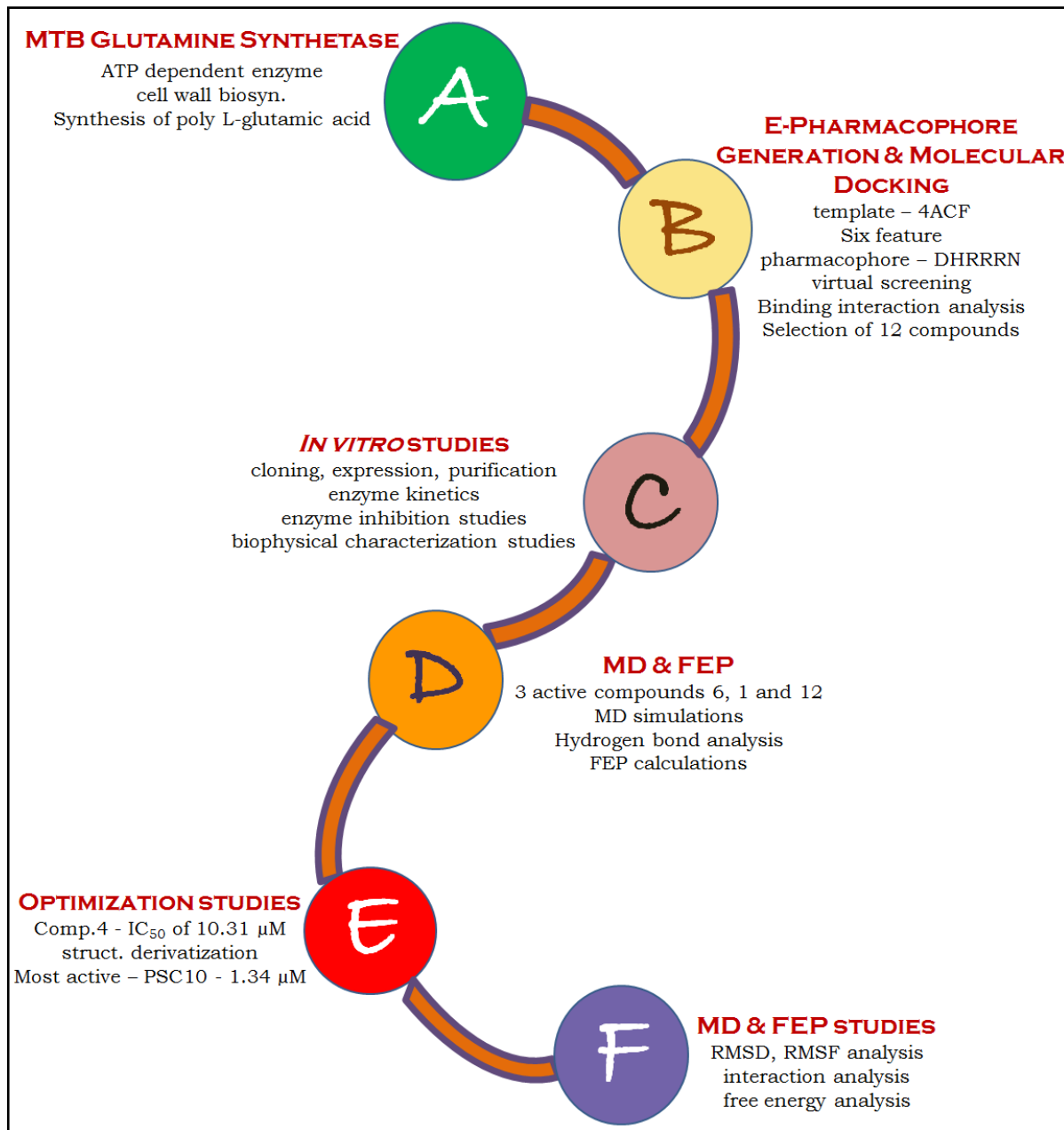
Table 5.9: Solvation free energies calculated for crystal ligand and PSC10 using FEP

Parameters	Crystal ligand	PSC10
Absolute Free Energy	-1.06	-0.83
ΔG FEP Solvation	-741.38±4.87	-108.63±6.79
ΔG FEP Coulomb	-726.21±5.22	-98.74±3.22
ΔG van der Waal	1.81±0.98	1.13±0.74
ΔG Solvent transfer	-729.14±4.98	-99.12±4.56

5.1.10. Highlights of the study

In the present study, energy optimized pharmacophore was developed based on crystal ligand, {4-[6-bromo-3-(butylamino)imidazo[1,2-a]pyridine-2-yl]phenoxy}acetic acid, co-crystallized with glutamine synthetase. This model consisting of six chemical features i.e. one hydrophobic group (H5), one hydrogen bond donor (D3), one negative potential (N6) and three ring features (R7, R8 and R9) was used as query for screening asinex database which led to the selection of twelve compounds as potent *M. tuberculosis* hits based on the glide score, fitness and interaction profile. Furthermore, *in vitro* enzymatic inhibition studies were performed for these twelve hits of which compound **6** was found to be top active with 2.12 μM inhibitory activity. Of the 12 compounds, 3-(1-{2-[(2-methoxyphenyl)amino]-2-oxoethyl}-5-phenyl-1*H*-pyrrol-2-yl)propanoic acid was identified and optimized to generate a chemical library of 40 compounds. Of these 40, compound **PSC10** was identified as the most active glutamine synthetase inhibitor with IC₅₀ of 1.34 μM. The behavior of glutamine synthetase-PSC10 complex under dynamic conditions was analyzed using molecular dynamics studies which provided many insights into the ligand binding stability over protein. Thus, the overall analysis suggested that the structure based e-pharmacophore model may provided useful information required for proper understanding of the important structural and physicochemical features for designing novel *M. tuberculosis* glutamine synthetase inhibitors.

Overview of glutamine synthetase work



Chapter 6

RESULTS AND DISCUSSION FOR DEVELOPMENT OF MTB GLUTAMATE RACEMASE INHIBITORS

6.1. Design of MTB glutamate racemase inhibitors

Glutamate racemase (MurI), one of the crucial enzymes involved in cell wall synthesis of MTB, is targeted in the present study. MTB glutamate racemase remains to be an unexplored target with none of its inhibitors reported till date. The major limitation in this aspect may be the absence of any reported crystal structure of MTB MurI. Hence, in the present study we aimed at design of MurI inhibitors based on its predicted three dimensional protein model developed using homology modeling protocol.

6.1.1. Development of 3D glutamate racemase model using homology modeling

6.1.1.1. Template search using BLASTp and sequence alignment

The amino acid sequence for MTB glutamate racemase was retrieved from Swiss prot with accession id P9WPW9. This sequence containing 271 amino acids was used as a query while running protein BLAST (BLASTp) in search of proteins with similarity. The BLAST run was set such that the similarity search was carried against protein data bank (PDB) to identify the crystal structure of the protein identical to the query. BLASTp resulted in a series of crystal structures with their corresponding percentage similarities and gaps. The top five leads resulted from protein BLAST are given in **Table 6.1**.

In the present study, crystal structure of glutamate racemase from *Listeria monocytogenes* (3HFR), with an identity of 42% and 0% gaps, was chosen as template due to its better identity with the query sequence and absence of any gaps when compared to other identified protein leads. The sequence alignment of both the query and template is shown in **Figure 6.1**.

3HFR refers to the crystal structure of glutamate racemase from *Listeria monocytogenes* deposited in PDB containing 269 amino acid residues with 2.3 Å resolution. This protein structure was found to contain predominantly alpha helices with beta sheets and loop regions. Due to absence of ligand in 3HFR, glutamate from 2GZM (crystal structure of glutamate racemase from *Bacillus anthracis*) was exported into the 3HFR while its usage as template during generation of homology model.

Table 6.1: Top 5 crystal structures identical to MTB MurI obtained from BLAST

PDB	Identity	Positives	Gaps
3HFR	42%	57%	0%
3IST	42%	57%	0%
2GZM	38%	60%	0%
1ZUW	42%	59%	1%
2VVT	40%	58%	0%

```

Query  2  NSPLAPVGVFDSGVGGLTVARAIIDQLPDEDIVYVGDGTGNGPYGPLTIPEIRAHALAIGD
      N+   +G DSGVGGTLV R ++ QLP E + Y+GDT PYGP E+   +
Sbjct  2  NAXKQAIGFIDSGVGGTLVVREVLKQLPHEQVYYLGD TARCPYGP RDKEEVAKFTWEXTN

Query  62 DLVGRGVKALVIACNSASSACL RDARERYQVPVVEVILPAVRRRAVAATRNGRIGVIGTRA
      LV RG+K LVIACN+A++A L D RE+ +PV+ VI P R A+ ATRN +IGV+GT
Sbjct  62 FLVDRGIKXLVIACNTATAAALYDIREKLDIPVIGVIQPGSRAALKATRNNKIGVLTGLG

Query  122 TITSHAYQDAFAA-ARDTEITAVACPRFVDFVERGVTSGRQVLGLAQGYLEPLQRAEVD
      T+ S AY A R E+ ++ACP+FV VE G + L PL+ ++DT
Sbjct  122 TVESXAYPTALKGLNRRVEVDSLACPKFVSVVESGEYKSAIAKKVVAESLLPLKSTKIDT

Query  181 LVLGCTHYPLLSGLIQLAMGENVTLVSSAEETAKEVVRVLTEIDLRLPHDAPPATRIFEA
      ++LGCTHYPLL +I+ G+ V +++S EETA EV +L +LL D R F
Sbjct  182 VILGCTHYPLLKPIIENFXGDGVAVINSGEETASEVSALLDYHNLDDATDEEIEHRFF-T

Query  241 TGDPEAFTKLAARFLG
      TG + F +A +L
Sbjct  241 TGSTQIFKDIAKDWLN
    
```

Figure 6.1: Sequence alignment of MTB MurI (Query) over the selected template (Sbjct).

The RMSD of 5HFR when aligned over 2GZM was found to be 1.19 Å. The imported ligand, glutamate, retained its conformation as of in 2GZM and was found to be interacting by hydrogen bonding with Asp6, Ser7 and Thr181 residues of 3HFR. Residues Pro37, Tyr38, Val144 and His182 of 3HFR were involved in hydrophobic interactions with glutamate. The

template structure was initially processed for its missing loops and side chains which were added based upon its sequence using Prime v3.1 of Schrödinger 2012. For this purpose, the amino acid sequence of 3HFR was used based on which the missing loops of the crystal structure were added. This processed structure of 3HFR was employed in 3D model generation of MurI.

6.1.1.2. Generation of 3D MurI model using homology modeling

Prime v3.1 of Schrödinger 2012 was employed for generation of MurI protein model. MurI sequence was loaded as a query for which the processed 3HFR was utilized as the template. The query sequence was aligned over the template structure which was used in identification of identical residues. Based on this alignment, the protein model for query was generated. Energy based model for MurI was generated for which OPLS_2005 force field was utilized. The ligand, glutamate, from 3HFR was incorporated in the model during homology modeling. Loops in generated model were found with residues falling in the generously allowed and disallowed regions of ramachandran plot which were refined by loop refinement. The final protein model was energy minimized and its quality was finally evaluated using ramachandran plot.

The developed glutamate racemase model for MTB was found to be similar to that of template used, with alpha helices found predominantly in the model. Glutamate racemase protein with D-glutamate at its active site is shown in **Figure 6.2(a)**. RMSD of the developed protein model when aligned over the template, 3HFR, was found to be 1.06 Å. Glutamate at the active site of MTB glutamate racemase was observed to be involved in polar interactions with residues Asp3, Ser4 and Thr178 as shown in **Figure 6.2(b)**. The hydrophobic interactions were found with residues Val6, Pro34, Tyr35, Ala65, Cys66 and Cys177. Electrostatic analysis of the protein model revealed the nature of active site which was found to be hydrophilic over the surface of active site and a mixture of hydrophilic and hydrophobic nature at the active site. The theoretical behavior of protein model was studied further using molecular dynamics simulations.

6.1.1.3. Validation of generated MurI homology model

RMSD of 1.06 Å upon alignment of the model and template shows minimum deviations among the model developed. A good structural overlapping was noticed between the model

and template especially in alpha helices and β -sheets region. The conservation of sequence and the structural superimposition suggested that MurI model was robust and accurate. Integrity of generated model was validated using ramachandran plot. Loops with residues falling in the disallowed regions were corrected employing loop refinement for the developed model. The side chain residues were corrected and the final model was energy minimized. The model built was analyzed for its structural integrity by ramachandran plot using PROCHECK analysis.

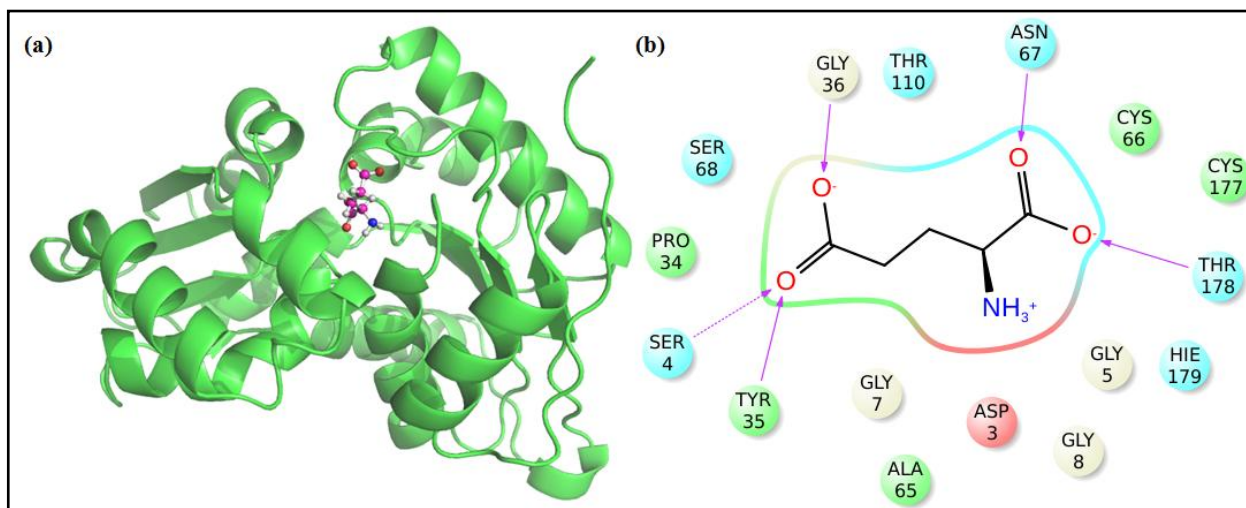


Figure 6.2: (a) Three dimensional structure of glutamate racemase developed with D-glutamate at its active site; (b) interaction profile of D-glutamate at the active site. Pink lines indicate the hydrogen bonds.

The ramachandran plot for the final energy minimized glutamate racemase model is given in **Figure 6.3**. Upon calculation of Φ/Ψ distribution for backbone conformation, the model revealed the percentage of residues falling into various plot regions. About 90.9% of residues were found to be in most favored region, 8.6% in additional allowed region, 0.5% in generously allowed region and none of the residues were found in disallowed region, showing the structural integrity of the protein model. Ser259 residue was found to be the only one falling into generously allowed region of ramachandran plot.

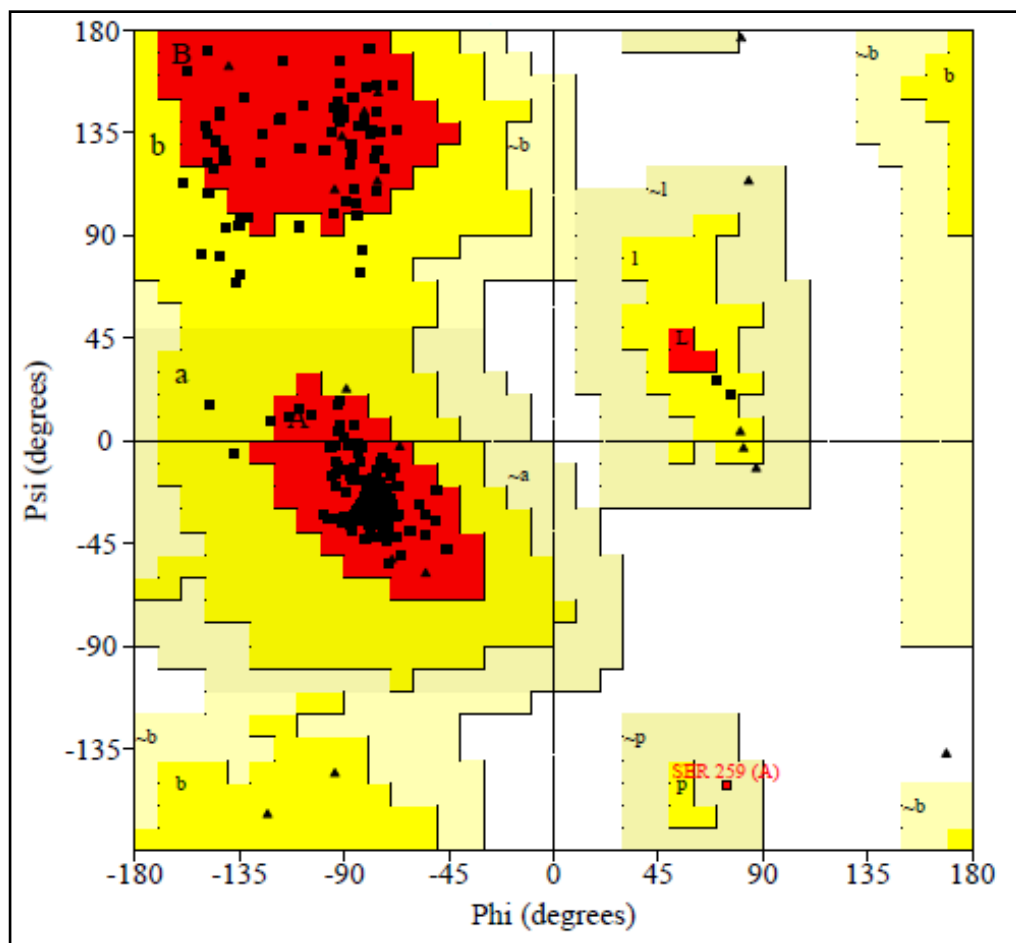


Figure 6.3: Ramachandran plot for the developed glutamate racemase protein model.

6.1.1.4. Molecular dynamics simulations analysis for MurI model

Molecular dynamics simulation is one of the well-known theoretical techniques, popularly used for assessing stability of any predicted three dimensional protein model. An MD simulation for a period of 20 ns was carried out for the model generated to evaluate its behaviors such as stability during dynamic conditions and structural flexibility. Simulation of protein model was carried out in explicit solvent conditions using TIP3P water model under OPLS_2005 force field. Root mean square deviation analysis of model was carried out and was plotted as a function of time. RMSD for C-alpha atoms, all residues and backbone atoms of the protein are shown in **Figure 6.4**.

From the plot, it was well observed that the model was stable with least deviations at few time periods displaying its stability even under dynamic environment. Depicted from the **Figure 6.4**, RMSD for both C-alpha atoms and all atoms were overlapped displaying similar

deviations. Considering the backbone atoms of protein, the RMSD was found to vary slightly when compared to the other two but with similar deviations. For a comparative study, simulation of the template was also carried out for a period of 10 ns (data not included). RMSD analysis of the template was compared with that of the model, which revealed almost identical deviations in both the proteins. Overall MD simulation analysis portrays the protein model to be highly stable even under dynamic conditions with a few deviations proving its consistency. These simulation studies thereby strongly support the quality and stability of the model developed which can further be employed for molecular docking studies.

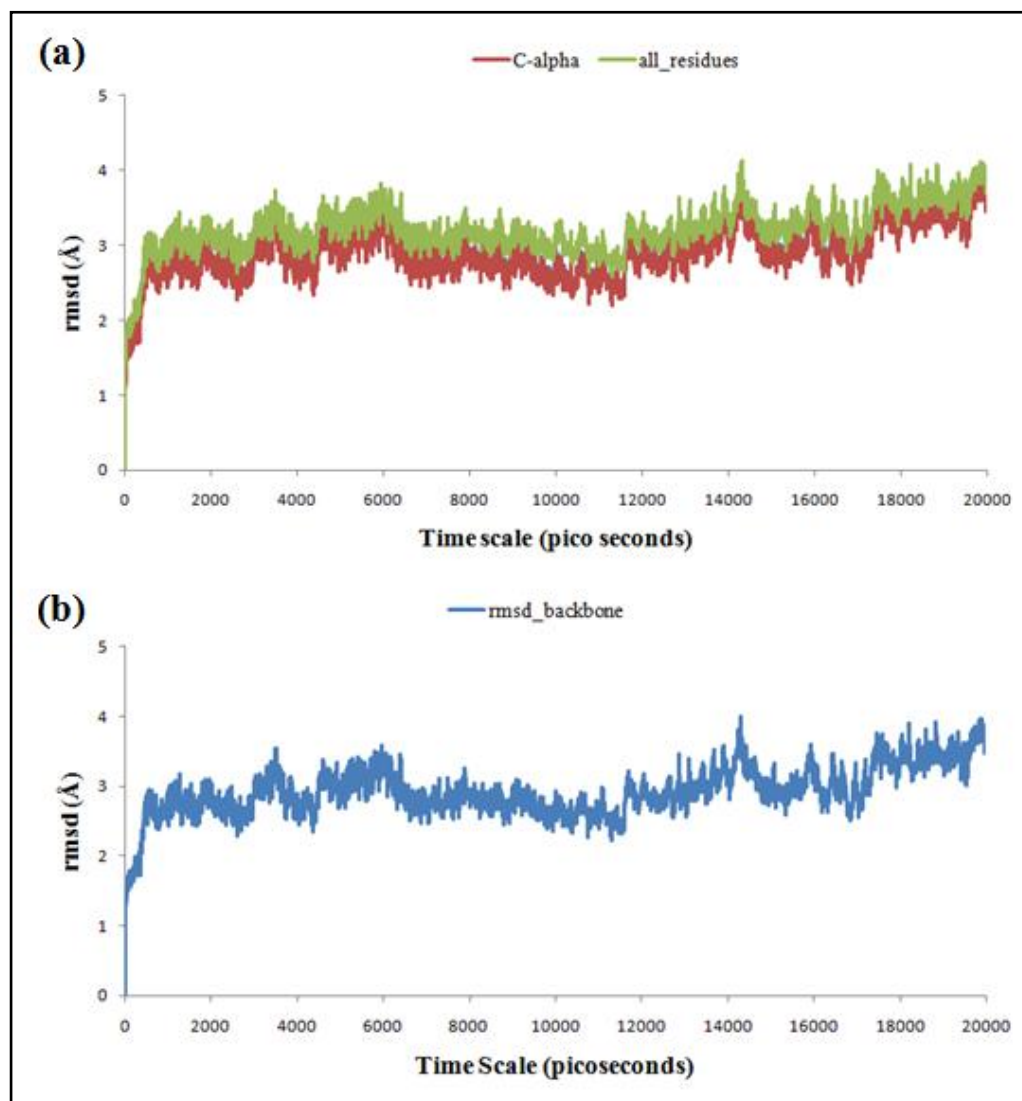


Figure 6.4: RMSD plot for MTB glutamate racemase showing for (a) C-alpha atoms and all residues of the protein and (b) backbone atoms of the protein.

6.1.2. Molecular docking studies using virtual screening

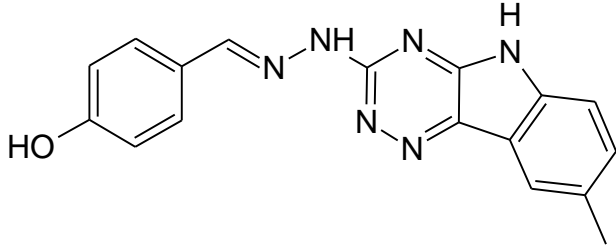
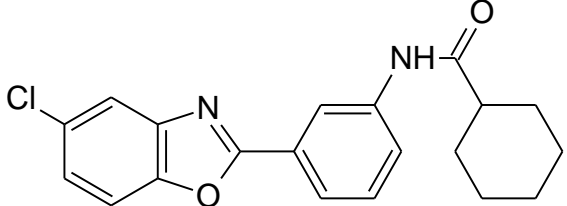
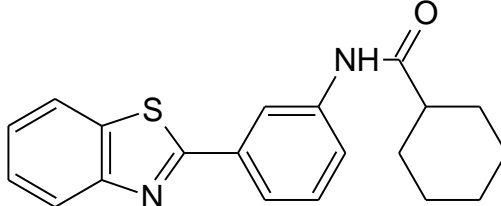
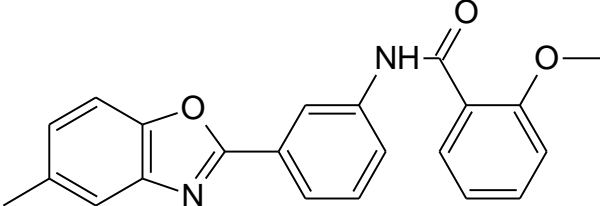
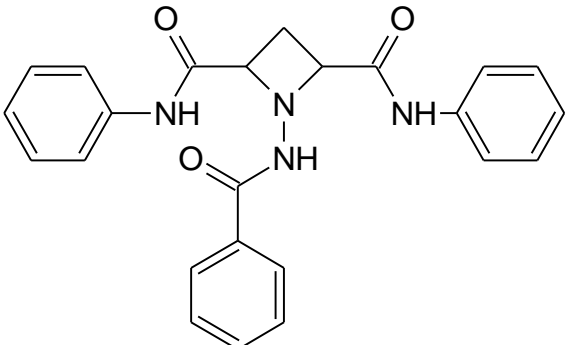
One of the crucial steps involved in structure based drug design using the predicted model is identification of active site of the protein model developed. The active site should be carefully identified and well validated as it is not similar to that of in crystal structure, in which a prominent well identified active site is reported. Active site of the model was identified by overlapping the template protein (crystal structure of *L. monocytogenes* glutamate racemase) over that of query and identifying the amino acids conserved in both the proteins. Active site of the template was compared to the corresponding region of the model and was checked for any conserved residues. The sequence alignment of glutamate racemase of both *M. tuberculosis* and *L. monocytogenes* is shown in **Figure 6.1**. Almost 80% of the active site residues were found to be conserved in MTB glutamate racemase compared to that of template. The probable binding pocket of the model was also identified using SiteMap v2.6 of Schrödinger 2012, which also resulted in identification of same pocket as that from structural alignment. Residues Asp3, Ser4, Gly7, Gly8, Pro34, Tyr35, Cys66, Asn67, Thr110, Val141, Cys177, Thr178, His179 and Tyr180 were found to be lining the wall of active site.

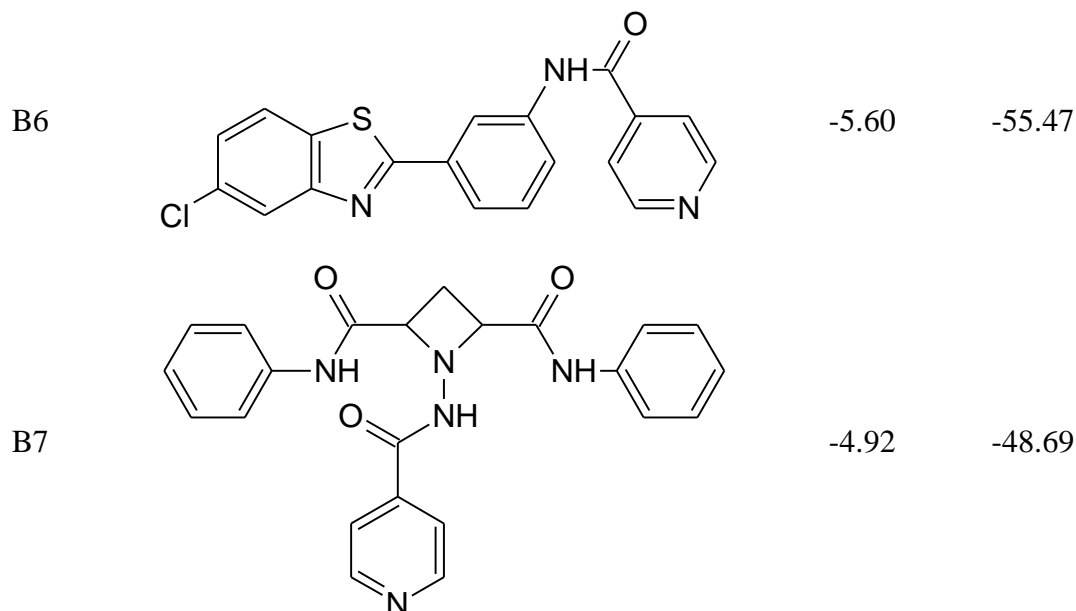
The protein model was used for generation of grid at its identified active site which was further employed for molecular docking studies. The methodology followed for docking studies is given in detail in materials and methods chapter. Virtual screening workflow (VSW) was operated against BITS in-house compound database so as to identify some potential leads which can serve as MTB glutamate racemase inhibitors. The selection of compounds was carried out based on their interaction pattern at the active site, docking scores and orientation of compound at the binding site. These selected compounds were further subjected to *in vitro* enzyme inhibition studies so as to study their inhibitory potential.

The virtual screening workflow involved screening of the compounds using HTVS, SP and XP docking. The high throughput virtual screening (HTVS) of the BITS database resulted in 219 compounds with glide score above $-4.5 \text{ kcal.mol}^{-1}$, which were proceeded for SP docking. Standard precision mode of docking resulted in 127 compounds above $-4.5 \text{ kcal.mol}^{-1}$ glide score which were further subjected to extra precision docking. XP docking resulted in 23 compounds with glide scores above $-4.5 \text{ kcal.mol}^{-1}$. Of these 23 compounds, seven compounds were selected based on their glide score, interaction pattern at the active site and compound availability and are given in **Table 6.2** along with their glide scores and glide

energies. The selected compounds were further subjected to *in vitro* glutamate racemase inhibition studies so as to analyze the inhibitory profile of the compounds.

Table 6.2: Structures of selected seven compounds with their glide scores and glide energies

Comp. code	Structure	Glide score	Glide energy
B1		-5.01	-48.21
B2		-4.96	-46.80
B3		-4.91	-43.12
B4		-5.42	-48.47
B5		-4.67	-52.44



6.1.3. *In vitro* enzyme inhibition studies

6.1.3.1. Enzyme kinetics of glutamate racemase activity

Initially, the rate at which the *M. tuberculosis* glutamate racemase enzyme works was measured. The racemization activity of enzyme generally followed first-order kinetics. At constant enzyme concentration, the substrate D-glutamate was varied from 1 mM to 100 mM concentration. The K_m for glutamate was found to be 10.08 mM which was determined using GraphPad Prism 6 (GraphPad Prism software, San Diego, CA) and shown in **Figure 6.5**.

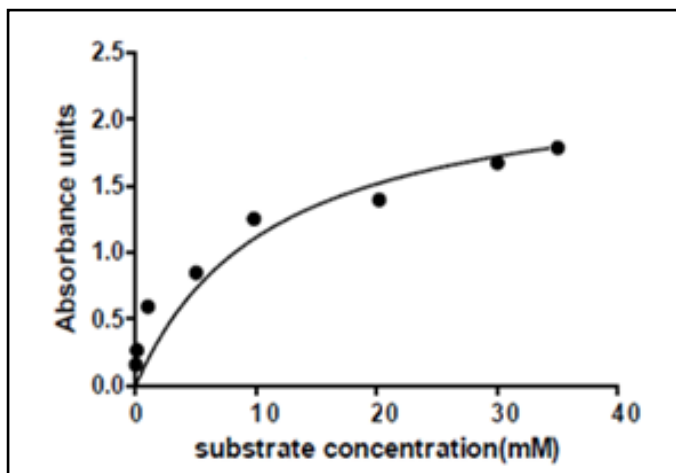


Figure 6.5: Enzyme kinetics plot for D-glutamate, plotted using GraphPad Prism 6.

6.1.3.2. *In vitro* enzymatic assay for the selected compounds

The selected compounds were subjected to *in vitro* glutamate racemase inhibition assay so as

to study their inhibitory profile over the enzyme. The compounds were initially tested at 25 μM concentration against the enzyme. At this concentration, all the compounds, except compound **B5**, were found to be inhibiting the enzyme about less than 50%. The compound **B5** was further tested at different concentrations - 10 μM , 5 μM and 1 μM and the IC_{50} of the compound was determined using GraphPad Prism 6 software. The compound **B5** was found to be inhibiting the enzyme with an IC_{50} of 5.97 μM . This lead compound, **B5**, was considered for further chemical derivatization studies

6.1.4. Lead expansion and optimization of the most active compound

6.1.4.1. Development of azetidine derivatives as potential MTB MurI inhibitors

Confident by the promising result of lead B5 from BITS in-house database, we designed a compound library with the goal of obtaining a lead series with tractable SAR and potencies better than the identified lead. Interaction profile of compound B5 was obtained from docking studies and was analyzed for suitable molecular substitutions. Compound B5 interaction pattern at glutamate racemase active site is shown in **Figure 6.6**. B5 was observed to be in hydrogen bonding with residues Ser4, Tyr35 and Glu145. The compound was also involved in hydrophobic interactions with Pro34, Pro37, Ala65, Cys66, Val141 and Cys177.

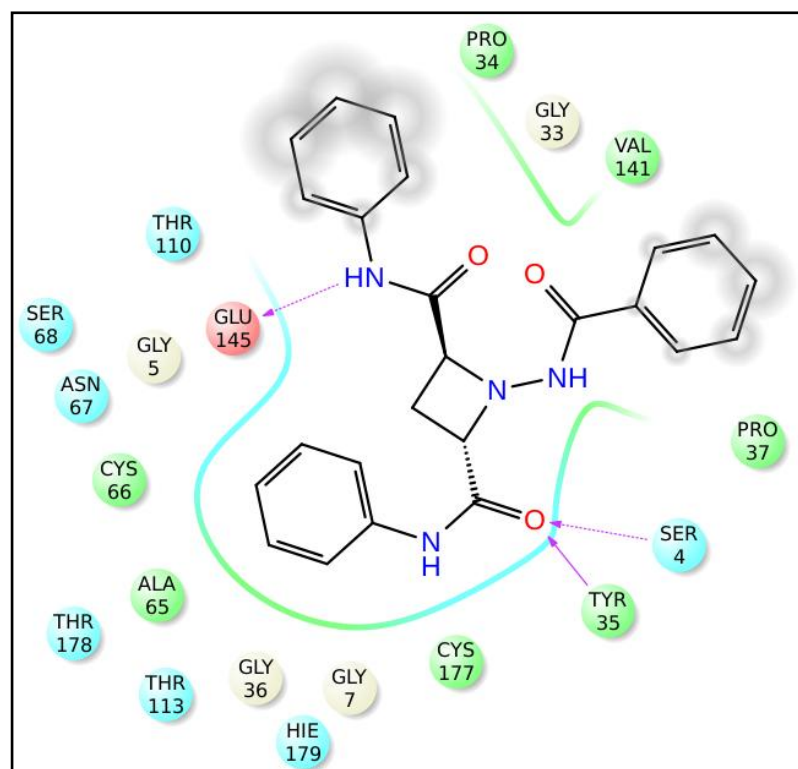


Figure 6.6: Interaction profile of compound **B5** at glutamate racemase active site.

It was decided to retain the carbonyl chain attached to the nitrogen of azetidine. The substitutions were mainly aimed over the phenyl groups on the 2nd and 4th positions of azetidine. The main substitutions targeted were methyl, ethyl, dimethyl, methoxy, halogens like chloro and bromo and hetero aryl groups such as pyridine and benzthiazole.

A library of eleven compounds which are azetidine derivatives were synthesized by following 3 step synthetic protocols as shown in **Figure 4.1** in material and methods chapter under **section 4.1.2.2**. In the first step, dihydro-2*H*-pyran-2,6(3*H*)-dione (compound **I**) on reaction with bromine at 100 °C produced 2,4-dibromopentanedioic acid (compound **II**). Reactions of compound **II** with various amines at 0 °C under nitrogen atmosphere resulted in corresponding 2,4-dibromo-N,N`-disubstituted pentanediamides (compound **III**). In the last step of synthetic route, amides (compound **III**) were reacted benzohydrazide in dry dimethylformamide (DMF) and heated to 80 °C for 2 hr. The reaction mixture was concentrated to remove DMF and the residue was dissolved in dichloromethane. The organic layer was washed with saturated aq. NaHCO₃ solution, water, brine, dried over sodium sulfate (Na₂SO₄) and concentrated. The crude product was purified by column chromatography to afford the final product (RV 1-11).

6.1.4.2. Molecular docking analysis of synthesized compounds

The synthesized 11 compounds were subjected to molecular docking studies with glutamate racemase protein model. Most of the compounds were observed possessing better interaction profile as of the lead compound identified. The polar and non-polar interactions of the synthesized compounds are given in **Table 6.3** along with their glide XP score. The common residues involved in hydrogen bonding with most of the compounds were found to be Ser4 and Tyr35. Analyzing the interaction profiles of all compounds, it was understood that it is the hydrophobic interactions which mainly contribute to protein-ligand interaction, thereby contributing to the binding affinity of ligand.

Table 6.3: Glide scores and MurI active site interactions of synthesized azetidine derivatives.

Compound	Glide score	H-bond interactions	Hydrophobic interactions
B5	-4.668	Ser4, Tyr35, Glu145	Pro34, Tyr35, Pro37, Ala65, Cys66, Cys177

Inhibitors against MTB Glutamate Racemase

RV1	-5.233	Ser4, Glu145	Val6, Pro34, Tyr35, Ala65, Cys66, Val141, Cys177, Ala237
RV2	-5.343	Glu145	Val6, Pro34, Pro138, Val141, His179, Ala237
RV3	-5.127	Glu145	Pro34, Pro37, Cys66, Val141, Cys177, His179
RV4	-5.215	Ser4, Tyr35	Val6, Pro34, Tyr35, Pro37, Ala65, Cys66, Val141, Cys177, His179
RV5	-5.417	Ser4, Tyr35, Glu145	Val6, Pro34, Tyr35, Pro37, Ala65, Cys66, Val141, Cys177
RV6	-4.981	Glu145	Val6, Tyr35, Pro37, Ala65, Cys66, Val141, Cys177
RV7	-5.014	Ser4, Tyr35, Glu145	Pro34, Tyr35, Ala65, Cys66, Val141, Cys177, His179
RV8	-5.266	Ser4, Tyr35	Val6, Pro34, Tyr35, Pro37, Ala65, Cys66, Val141, Cys177, His179
RV9	-4.785	Ser4	Val6, Pro34, Tyr35, Cys66, Pro138, Val141, Cys177, His179
RV10	4.826	---	Pro34, Tyr35, Pro37, Ala65, Cys66, Ala112, Val141, His179
RV11	-5.332	Ser4, Glu145	Val6, Pro34, Tyr35, Pro37, Ala65, Cys66, Ala112, Cys177

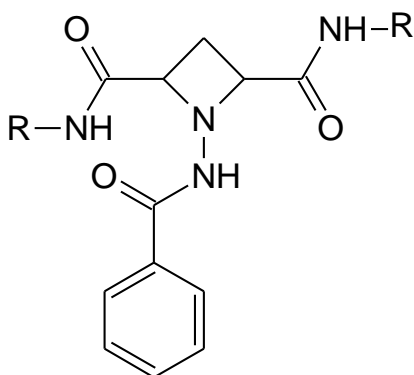
6.1.4.3. *In vitro* glutamate racemase inhibition assay, antimicrobial potency and cytotoxicity studies for the synthesized compounds

6.1.4.3a. *In vitro* glutamate racemase inhibition assay

Glutamate racemase enzyme inhibition assay was carried out for the synthesized 11 compounds. As described in the previous sections, various concentrations of the compounds starting from 25 μ M, 10 μ M, 5 μ M, 1 μ M and 0.5 μ M were tested to determine the inhibitory capacity of the compounds. IC₅₀s for all the compounds were calculated using GraphPad

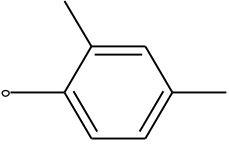
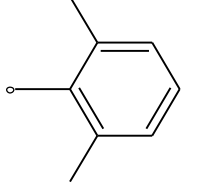
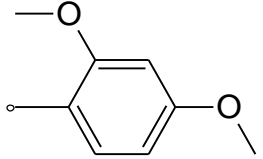
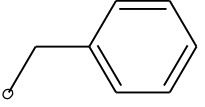
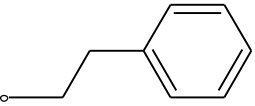
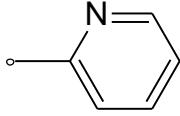
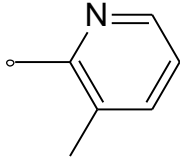
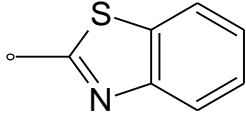
Prism 6 and are given in **Table 6.4**. Of all, compounds **RV4** and **RV8** were found to be the most active ones from the series with IC_{50} s 1.01 μ M and 1.02 μ M respectively. Compounds RV3, RV9 and RV10 were found to be least active ones of the series with activity greater than 25 μ M. The remaining compounds were found to be moderately active with IC_{50} ranging between 3.04 – 9.81 μ M. The dose response curve for compound RV4 is shown in **Figure 6.7** plotted using GraphPad Prism 6.

Table 6.4: *In vitro* inhibitory activities of the synthesized analogues



Comp. code	R	IC_{50} (in μ M)*	MTB MIC (in μ M)	Cytotoxicity at 50 μ M
B5		5.97±0.46	25	17.65
RV1		8.35±0.24	12.5	34.0
RV 2		9.81±0.41	12.5	24.56
RV3		28.68±0.33	25	18.89

Inhibitors against MTB Glutamate Racemase

RV4		1.01±0.12	1.56	24.78
RV5		4.98±0.17	25	15.63
RV6		7.00±0.36	12.5	21.56
RV7		3.04±0.52	3.125	31.54
RV8		1.02±0.34	1.56	28.54
RV9		38.95±0.12	>25	24.08
RV10		25.18±0.48	>25	16.34
RV11		5.98±0.79	3.125	32.12

* IC₅₀ calculated using GraphPad Prism 6 (mean±SEM).

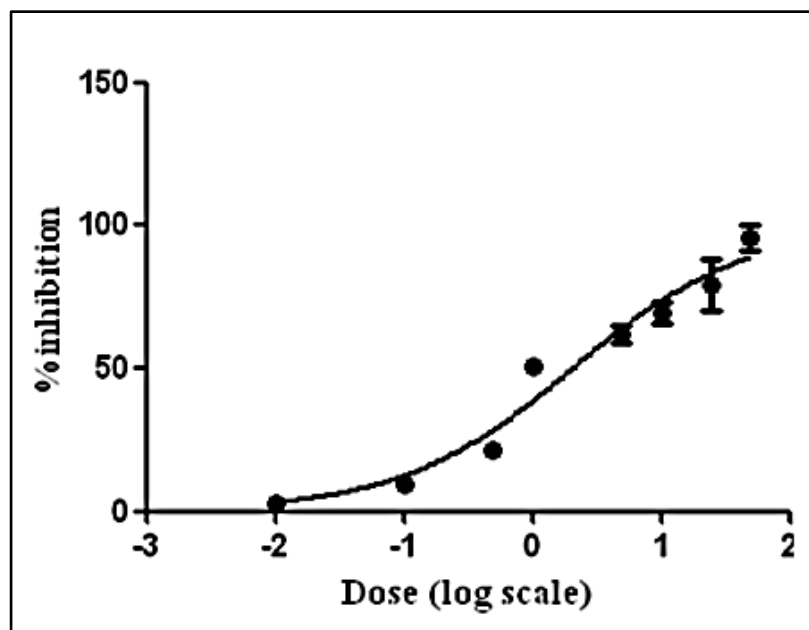


Figure 6.7: Dose response curve for compound **RV4** (IC₅₀ - 1.014 μM).

6.1.4.3b. Structure activity relationship (SAR) of the synthesized compounds

The synthesized 11 compounds were studied for their structure activity relationship with respect to their MurI inhibitory activity. A valid SAR was developed relating the activity of the compounds to their *in silico* interactions at MurI active site analyzed from molecular docking studies. The lead compound **B5**, with activity of 5.97 μM, was found to be interacting at the active site with oxygen from benzamide involving in polar contact with Ser4. The compound was found to be involved in hydrophobic interactions with residues Pro34, Tyr35, Pro37, Ala65, Cys66 and Val141. Substitution of chlorine over *para* position of phenyl ring at both 2nd and 4th position of azetidine, compound **RV1**, resulted in moderate decrease in activity with IC₅₀ of 8.35 μM. This decrease in activity of the compound may be attributed to the high electron affinity nature of chlorine. The presence of chlorine over phenyl ring tends to the electron accepting nature which results in the distortion of π electron cloud over the ring, thus contributing to the loss of aromaticity. This loss of aromaticity tends to loss of hydrophobic interactions, one of the crucial interactions necessary for the activity. Presence of second chlorine over *meta* position of both the phenyl rings, in compound **RV2**, contributed to the further loss in activity. Further, substitution of bromine over *para* positions of phenyl ring (compound **RV3**) resulted in complete loss of activity (IC₅₀ – 28.68 μM). The docking analysis of the compound showed completely different orientation of compound

benzamide and bromophenyl moieties towards solvent. This can be explained in terms of steric hindrance offered by bromine. Bromine, being a big atom in size, cannot adjust the compound inside the active site thus resulting in different orientation of the compound, making the compound unavailable for interactions.

The most active compound of the series, **RV4**, was yielded by the substitution of methyl group over both the phenyl rings at *ortho* and *para* positions resulting in compound with activity 1.014 μM . The interaction analysis of the compound revealed the presence of two polar contacts with residues Ser4 and Tyr35. The compound was also found to be involved in pi-pi stacking interactions with His179. Also the compound was found to be stabilized by strong hydrophobic interactions with residues Val6, Pro34, Pro37, Ala65, Cys66, Ala112, Val141, Cys177 and Phe238. The methyl substituents were also found to be involved in these hydrophobic interactions adding up to the binding affinity of the compound. Substitution of methyl groups at both the *ortho* positions of both the phenyl rings yielded compound **RV5** with moderate activity (4.98 μM). The compound exhibited lesser activity when compared to **RV4**, proving the suitability of *para* position for the substitution of methyl group. The compound also exhibited similar interactions as that of RV4. Methoxy substitutions over the phenyl rings resulted in compound **RV6** with moderate activity of 7 μM suggesting unsuitability of methoxy group for MurI activity. This decrease can be attributed to high electron affinity nature of oxygen.

Further modifications were made at the linker point of carboxamide with phenyl moiety. Incorporation of methyl group as linker on both the carboxamide side chains yielded in compound **RV7** with 3.04 μM activity. The compound was found to be more active than the lead one there by showcasing the suitability of incorporation of a linker methyl group. The compound was found to be interacting with residues Ser4, Tyr35 and Glu145. Also π - π stacking interactions were observed between phenyl ring of the compound and imidazole of His179. Further attempts were made to study the effect of chain length of the linker over MurI activity of the compounds. Increase in the chain length from methyl to ethyl yielded a highly active compound **RV8** with IC_{50} of 1.017 μM . The compound was equipotent as of compound RV4. Interaction analysis of the compound revealed orientation of the compound similar to that of RV4 with polar contacts with Ser4 and Tyr35. Hydrophobic interactions were found to be similar as that of RV4.

Attempts were made to study the effect of replacement of phenyl groups at 2nd and 4th positions of azetidine with various other hetero aromatic moieties. The first substitution was carried out by the replacement of both the phenyl rings with pyridine which resulted in compound **RV9**. The compound was found with complete loss of activity ($IC_{50} = 38.95 \mu M$). This loss can be attributed to the less aromaticity of pyridine in comparison to that of benzene. Non-polar interactions, being one of the crucial components in determining the activity, were found to destabilize by the substitution of phenyl ring with pyridine. The interaction analysis of the compound shows the complete exposure of one of the pyridine towards the solvent making it unavailable for non-polar interactions. The substitution of methyl group over both the pyridine rings was found to enhance the activity resulting in compound **RV10** IC_{50} of $25.18 \mu M$. This increase in activity can be explained by the hydrophobicity imparted by methyl moiety. The final substitution attempted was the substitution of phenyl rings with benzothiazole moieties yielding compound **RV11**. This substitution over the lead compound did not show any effect over the activity. This can be explained by the similar level of aromaticity offered by benzothiazole as that of benzene. The compound was found to be interacting with residues Ser4 and Glu145 and also was involved in strong hydrophobic interactions.

6.1.4.3c. *In vitro* antimycobacterial screening for the synthesized compounds

The compounds were further screened for their *in vitro* antimycobacterial activity against *M. tuberculosis* H37Rv by the MABA method as described in **section 4.1.3.5** of materials and methods. The MICs of the synthesized compounds are given in **Table 6.4**. A good correlation had been observed between the glutamate racemase inhibition assay and the *in vitro* MTB minimum inhibitory concentration (MIC). However, a few compounds exhibited slightly lesser MICs than their MurI inhibitory potential, which may be because of the compounds inability to penetrate the cell wall of the organism or the compounds inefficiency to interfere with the organism's vitality. Compounds **RV4**, **RV7**, **RV8** and **RV11** were promising analogues, with MICs in the lower micromolar range. These compounds were found to be more active than the first-line antitubercular drug ethambutol ($MIC = 15.31 \mu M$) but were less active compared with isoniazid ($MIC = 0.66 \mu M$) and rifampicin ($MIC = 0.23 \mu M$). The compounds were further tested for their cytotoxic profile.

6.1.4.3d. *In vitro* cytotoxicity studies for the synthesized compounds

Safety profile for all the synthesized compounds was assessed by testing their *in vitro* cytotoxicity effect on RAW 264.7 cells at 50 μ M concentration using MTT assay. The methodology for this study is given under **section 4.1.3.6** of materials and methods chapter. Cytotoxicity results for all the compounds are given in **Table 6.4**. Almost all the tested compounds demonstrated a good safety profile with very low inhibitory potential. Compounds were found to inhibit cells within a range of 15.63 - 34.0%. Furthermore, the most active compound **RV4** exhibited 24.78% inhibition when tested at 50 μ M concentration, reflecting its safety profile in eukaryotes.

6.1.5. ADMET analysis of the synthesized compounds

All the selected compounds were subjected to *in silico* ADMET analysis using QikProp v3.5 module of Schrödinger 2012. All compounds were found to be in accordance with Lipinski's rule of Five which is the basic criteria of drug-likeness. Various properties like SASA (Predicted Solvent Accessible Surface Area in \AA^2), QPlogBB (Predicted brain/blood partition coefficient), QPlogHERG (Predicted IC₅₀ value for HERG K⁺ channels), QPPCaco (Predicted apparent Caco-2 cell permeability in nm/s) were determined for the compounds and were checked for any deviations. All the properties determined are listed out in **Table 6.5**. The compounds are found to be with least blood brain barrier permeability which indicates the compounds to be CNS (Central Nervous System) inactive. All the 12 compounds (including **B5**) were found to obey Lipinski rule of Five, showing good percentage oral absorption thereby reflecting the drug likeliness of compounds.

Table 6.5: *In silico* pharmacokinetic profile for the synthesized compounds

Comp	SASA	QPlogBB	QPlogHERG	QPPCaco	QPPMDCK	% Human Oral Absorption	QPlogKp
B5	747.80	-0.83	-7.78	1244.00	626.38	100	-0.67
RV1	795.03	-0.52	-7.57	1255.29	3856.03	100	-1.00
RV2	835.88	-0.26	-7.35	1256.33	1000.00	95.13	-1.27
RV3	804.63	-0.51	-7.61	1255.79	4459.88	89.25	-1.01

RV4	798.00	-0.70	-6.52	2171.11	1143.57	100	-0.95
RV5	781.74	-0.49	-6.61	2489.06	1325.61	100	-0.72
RV6	827.44	-1.04	-6.02	1163.97	582.94	82.41	-1.28
RV7	804.32	-0.94	-5.15	563.48	701.89	100	-0.47
RV8	871.41	-1.22	-5.56	509.95	666.90	100	-0.38
RV9	748.76	-1.26	-7.36	573.63	271.30	100	-1.66
RV10	733.69	-1.07	-6.57	616.69	293.38	100	-1.75
RV11	859.13	-1.22	-8.30	623.95	763.40	92.66	-1.42

Properties and Ranges: **SASA** – Predicted Solvent Accessible Surface Area in Å²(300-1000). **QPlogBB** – Predicted brain/blood partition coefficient (-3.000 to 1.200). **QPlogHERG** – Predicted IC₅₀ value for HERG K⁺ channels (concern below -5). **QPPCaco** – Predicted apparent Caco-2 cell (model for gut-blood barrier) permeability in nm/s (<25 – poor, >500 – great). **QPPMDCK** - Predicted apparent MDCK cell (model for blood-brain barrier) permeability in nm/s (<25 – poor, >500 – great). **QPlogKp** – Predicted skin permeability (-8.000 to -1.000).

6.1.6. Biophysical characterization studies for MurI-RV4 complex

Binding affinity of a compound towards its target is one of the major points to be considered during the aspect of drug design. Hence, in the present study differential scanning fluorimetry experiments were performed to evaluate the binding affinity and stabilization effect of active compound towards MTB glutamate racemase. This was measured by comparing the thermal stability of native protein (MurI) with that of the protein-ligand mixture. The enzyme and dye concentrations required for the experiment were optimized by varying the concentrations of both. Further, the experiment was carried out in presence of compound **RV4**.

Figure 6.8 depicts the curve obtained from DSF experiments for protein complex with comp.RV4. The positive shift in melting temperature (T_m) for protein-ligand complex when compared to that of native protein indicates the stability of the complex. The native protein was observed with T_m of **47.2 °C**. Compound **RV4** was observed with T_m of **51.03 °C** with a positive shift of **3.83 °C** when compared to that of T_m of native protein. Compound **RV4** was found with characteristic binding affinity towards glutamate racemase thereby correlating with its MurI inhibitory activity.

hydrophobic interactions including π - π contacts with residues Val6, Pro34, Tyr35, Pro37, Ala65, Cys66, Ala112, Val141, Val144 and His179. The top active ligand (**RV4**) in complex with MurI was subjected to 20 ns simulation in order to study the protein-ligand interaction stability in dynamic conditions (simulating body conditions) and to generate further theoretical information to support its activity. This protein-ligand complex was simulated under explicit solvent conditions using OPLS_2005 force field in Desmond v3.1.

RMSD analysis of the obtained trajectory was carried to analyze the stability of protein and ligand in the complex during simulation. **Figure 6.10** shows RMSD of C α atomic positions and heavy atoms for MurI-RV4 complex throughout the simulation. An initial jump in RMSD of protein-ligand complex during initial few pico seconds when compared to the original starting frame during simulation can be attributed to the relaxation of model in solvent system. From the plot, it was observed both C-alpha atoms and heavy atoms of the complex were found to be behaving in similar fashion during simulation. The complex was found to be stable with minimal fluctuations.

Figure 6.11 shows the RMSD fluctuation of both C-alpha and heavy atoms with respect to frame count of the trajectory. This plot showcases the stability of the complex throughout the simulation proving the stabilizing effect of the ligand over protein. The plot also represents the behaviour of ligand during simulation. It displays the highly stable nature of ligand thereby owing to its binding affinity towards MurI.

Analyzing the behaviour of ligand during the simulation, from **Figure 6.12**, it was observed the ligand was stable after a period of 5 ns. This observation was also supported by **Figure 6.11** where the ligand was found to be stabilized after 1000 frame. These observations prove the highly stable nature of the MurI-RV4 complex throughout the simulation supporting the binding affinity of compound RV4 towards MTB glutamate racemase.

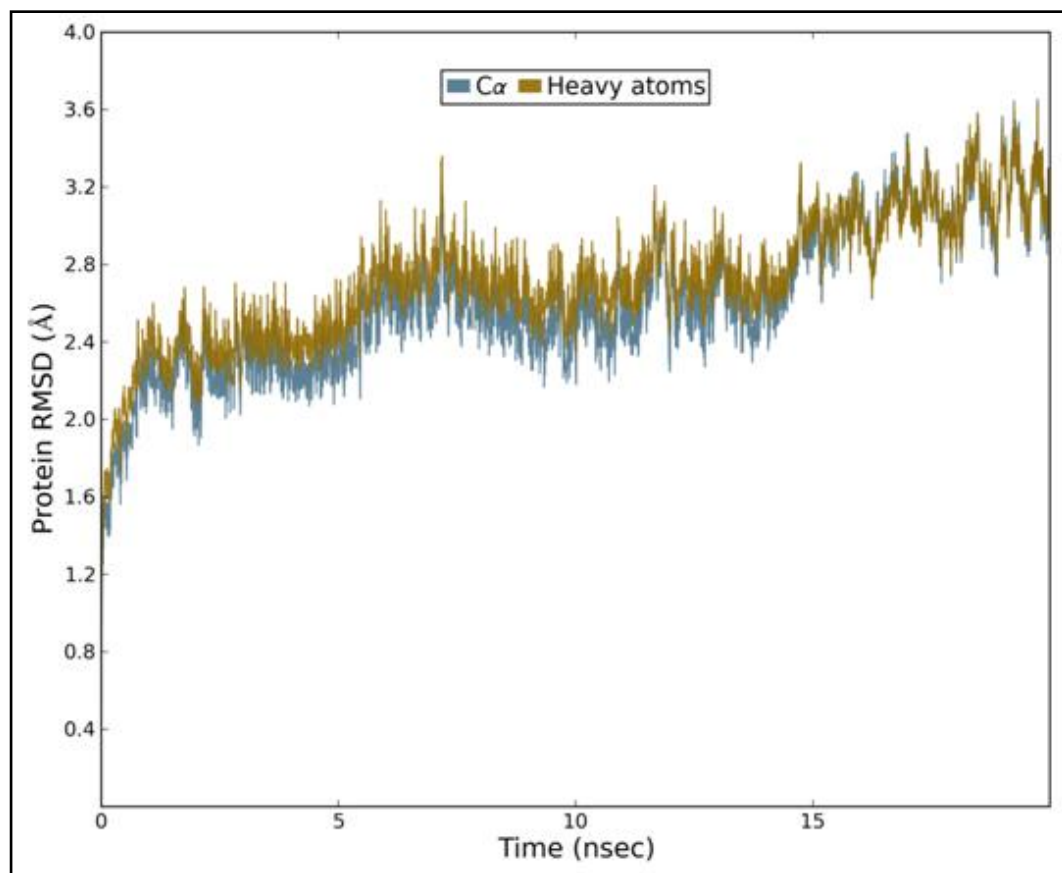


Figure 6.10: RMSD plot of glutamate racemase in bound state with compound **RV4**.

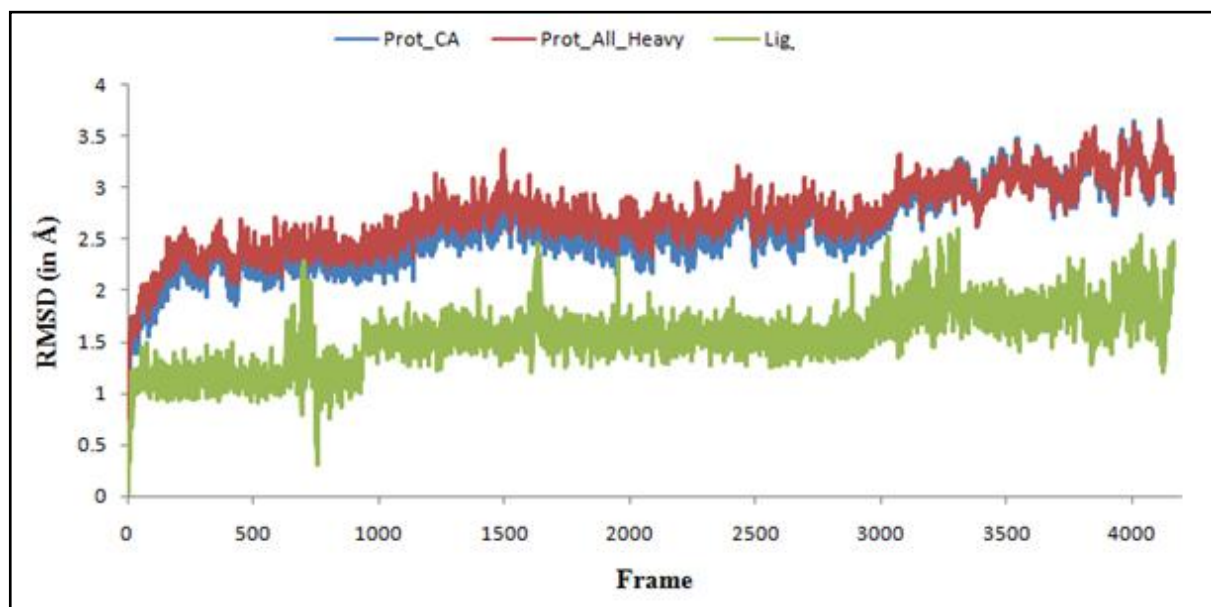


Figure 6.11: RMSD plot of glutamate racemase in bound state with compound **RV4** with respect to the simulation trajectory frame.

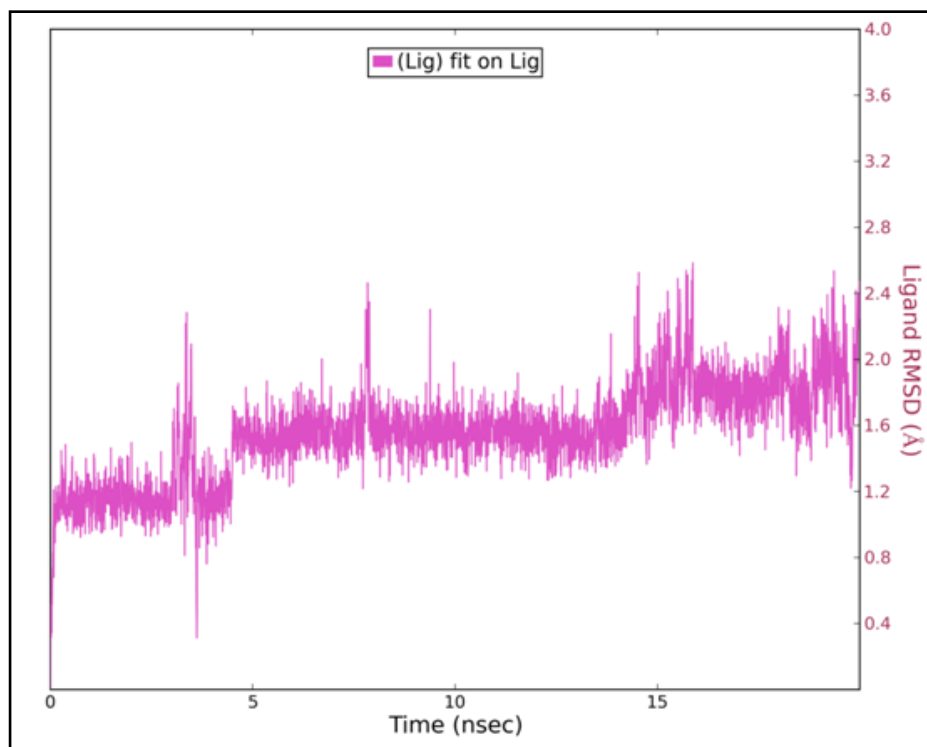


Figure 6.12: RMSD plot of compound **RV4** plotted in complex with glutamate racemase.

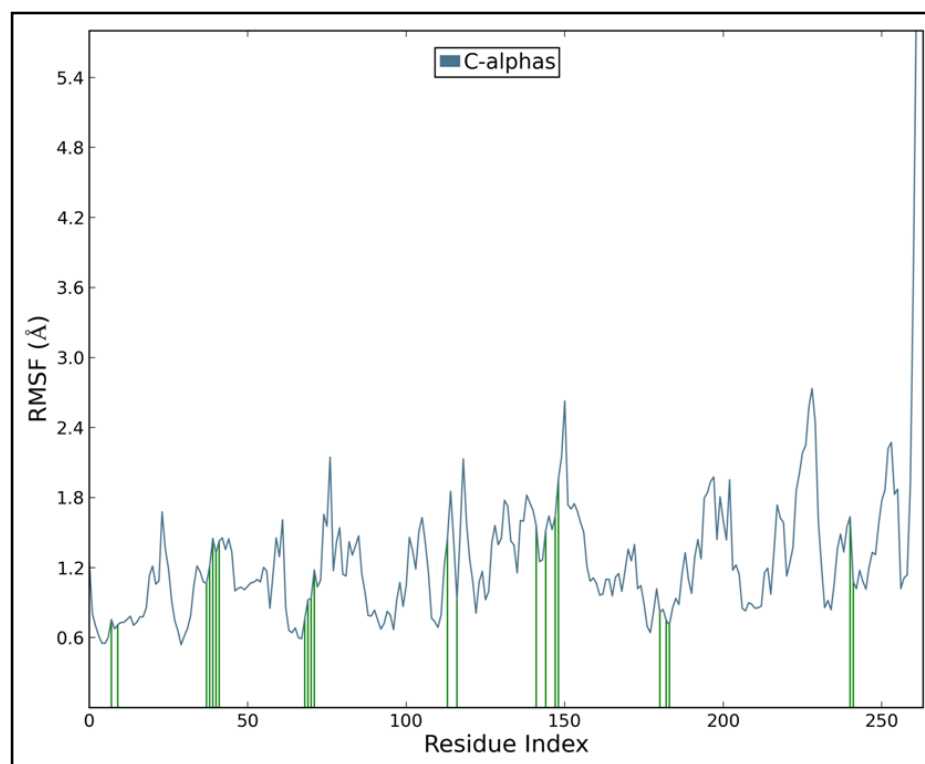


Figure 6.13: RMSF plot for C-alpha atoms of glutamate racemase-RV4 complex. Green lines indicate the residues interacting with compound **RV4**.

Root mean square fluctuation (RMSF) of MurI was analyzed for studying the local changes along the protein chain during simulation. **Figure 6.13** portrays the RMSF plot for total protein with respect to their residues. In this plot, peaks indicate areas of the protein that fluctuate the most during the simulation. Typically, it was observed from the plot that the N- and C- terminals fluctuate more than any other part of the protein. Secondary structure elements like alpha helices and beta strands are usually more rigid than the unstructured part of the protein, and thus fluctuate less when compared to that of loop regions. From the plot, it was observed that most of the residues were stable with lesser fluctuations. Protein residues that interact with the ligand are marked with green colored vertical bars. From the plot, it was observed that the active site residues interacting with compound RV4 were stable. The two major peaks observed in the plot correspond to residues Gly147 and Pro225 which were found to be highly flexible but do not fall into active site region.

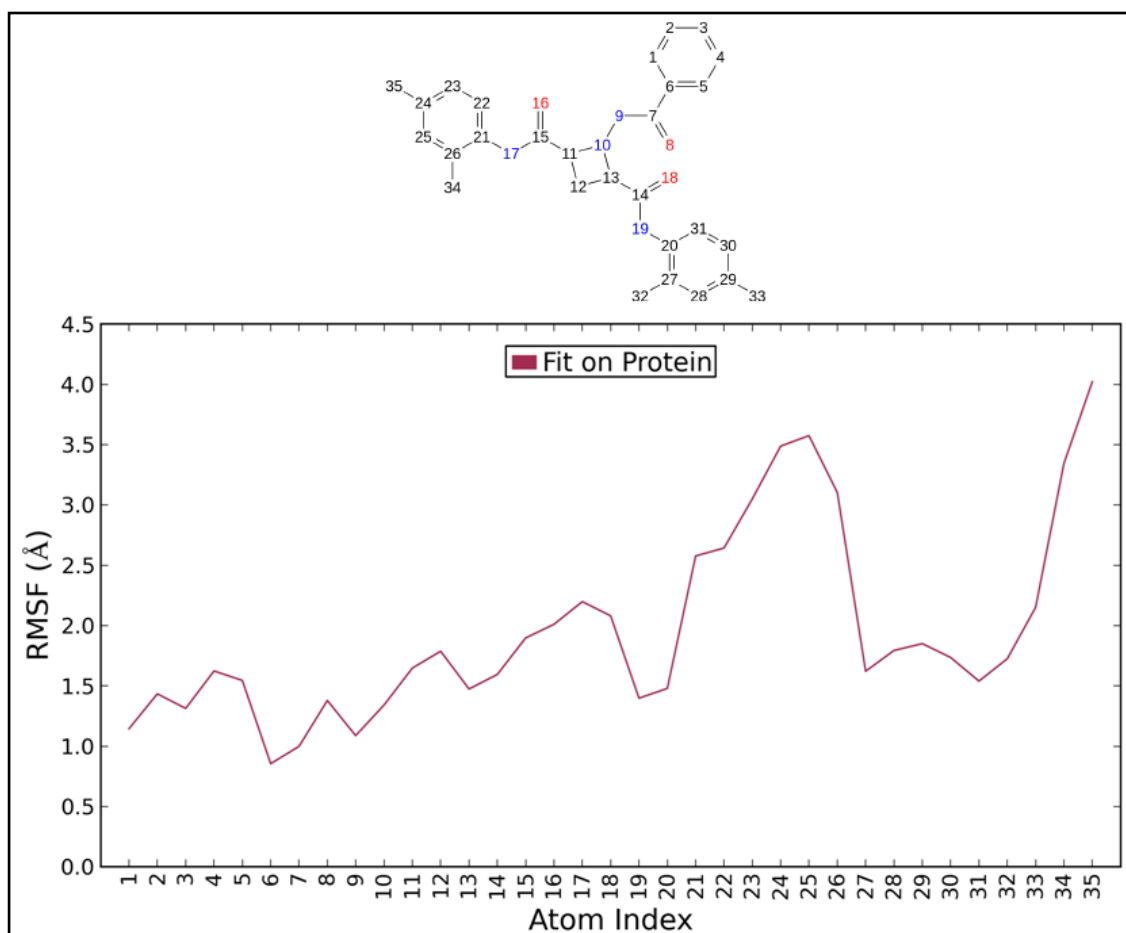


Figure 6.14: RMSF plot for the compound RV4 with respect to its each atom during simulation.

Ligand root mean square fluctuation (L-RMSF) was also analyzed to observe changes in ligand atom positions during simulation. From the **Figure 6.14**, it was observed that the ligand atoms were stable with minimal changes except for the atoms 21-26, 34 and 35 which correspond to the dimethyl benzene ring exposed to the solvent upon ligand binding to MurI. This fluctuation shows highly flexible nature of dimethyl benzene which was observed to be least involved in interactions with the protein. The remaining atoms of the compound RV4 were found to be stable with lesser fluctuations owing to the interaction of this part of ligand with protein.

The torsion angle analysis of the compound RV4 during the simulation time period was carried out to understand the torsional stress undergone by each rotatable bond of ligand at the glutamate racemase active site. The ligand torsions plot summarizes the conformational evolution of every rotatable bond (RB) in the ligand throughout the simulation trajectory (0.00 through 20.00 nsec).

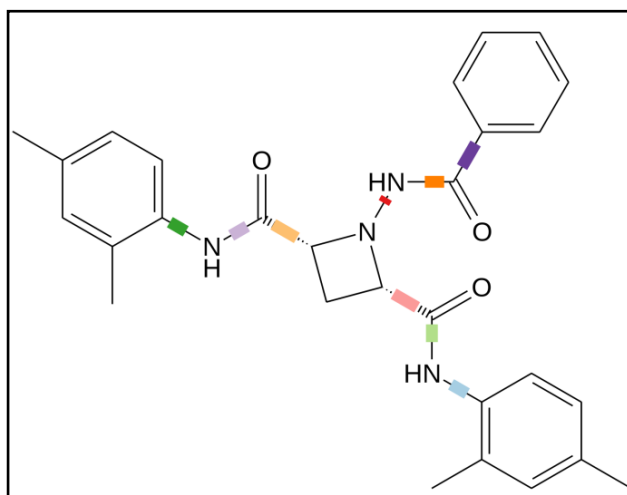


Figure 6.15: Representation of rotatable bonds of compound RV4 with different color scheme.

Figure 6.15 shows the 2D schematic representation of ligand, RV4, with color-coded rotatable bonds. Torsion plot for each bond is represented by a dial plot and bar plots with the same color. Dial (or radial) plots portray the conformation of the torsion throughout the course of the simulation. The centre of the radial plot was found to be beginning of the simulation which with time evolution was plotted radially outwards. The bar plots summarize the data on the dial plots, by showing the probability density of the torsion (**Figure 6.16**).

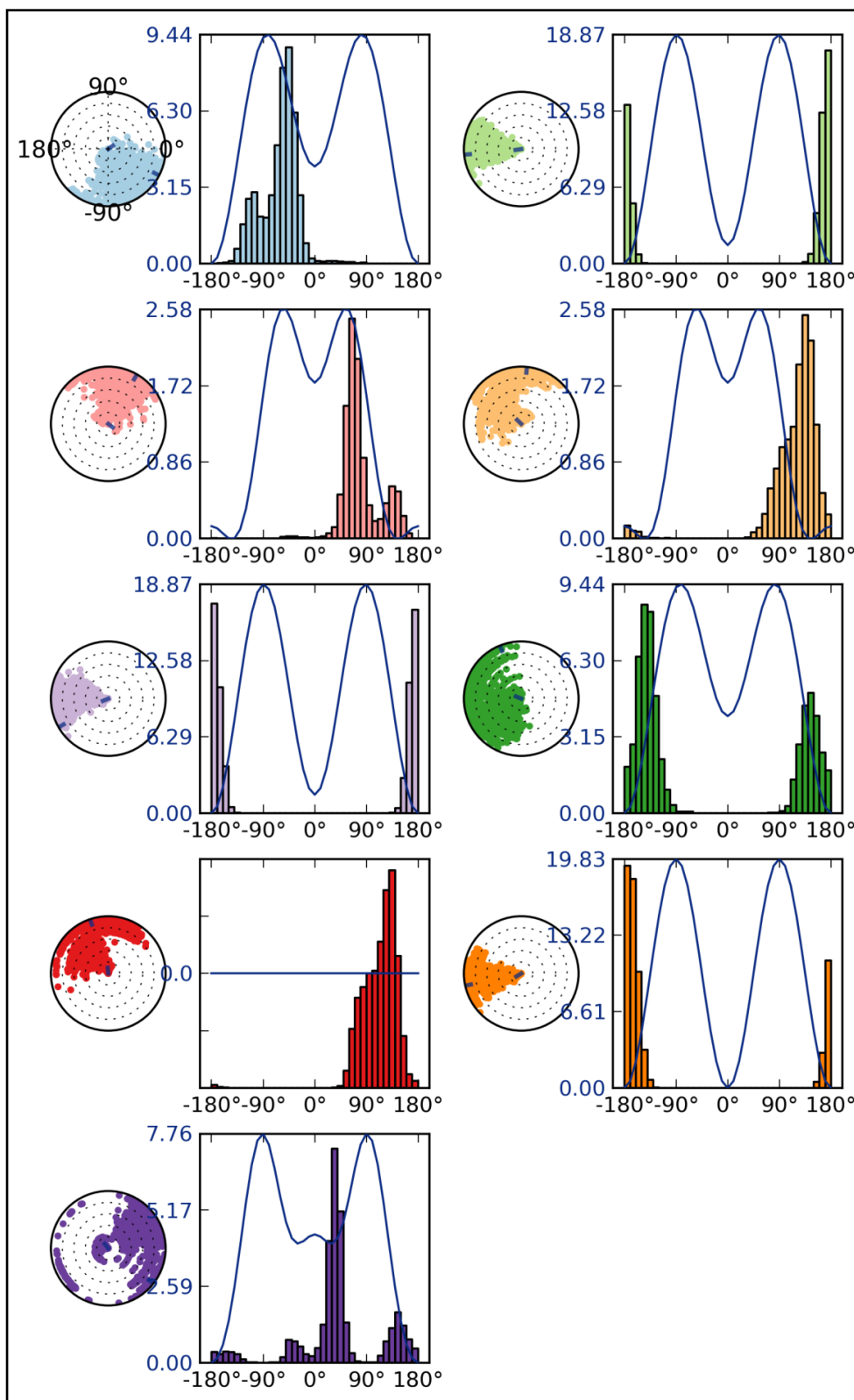


Figure 6.16: Torsion angle and torsion potential plotted for each rotatable bond of compound RV4.

With the available torsional potential information, the plot also shows the potential of the rotatable bond (by summing the potential of the related torsions). The values of the potential are on the left *Y*-axis of the chart, and are expressed in kcal.mol⁻¹. The histogram and torsion potential relationships give the insights into the conformational strain the ligand undergoes to maintain a protein-bound conformation.

From **Figure 6.16**, it was observed that the three bonds connecting the amines with the three phenyl moieties undergone high torsional stress when compared to other rotatable bonds. The dark green and sky blue colored bonds represent the bonds between dimethyl benzene and amine group. These two bonds were observed to undergo similar torsional stress, of which green colored bond was observed to undergo the maximum. This was probably due to the orientation of RV4 at MurI active site with dimethyl benzene oriented towards the opening of active site. From the analyses, the high torsional stress of this rotatable bond might be due to the availability of wider space at the entry of active site when compared to the pocket inside. This intern was supported by the ligand RMSF data from simulation. From **Figure 6.14**, the atoms with number 21-26, 34 and 35 (corresponding to dimethyl benzene) were highly flexible and fluctuating when compared to remaining atoms. On the whole, it might be concluded that absence of interactions of dimethyl benzene moiety at glutamate racemase active site and its location at the wider side of pocket accounted to its high fluctuations and greater torsional stress.

6.1.7.1. Simulation interaction analyses

Intermolecular forces majorly contribute to binding of ligand at protein active site in any protein-ligand association. These forces include hydrogen bonds, ionic bonds and van der Waals forces. The docking association is usually reversible. Actual irreversible covalent bonding between the ligand and its target molecule is rare in biological systems. The simulation interaction diagram analysis of the protein-ligand trajectory provides insights over the interactions of RV4 at the binding site of MurI throughout the simulation. **Figure 6.17** represents interaction strengths of each bond between compound RV4 and MurI.

The top panel of **Figure 6.18** shows the total number of specific contacts between RV4 with MurI over the course of simulation. The contacts here are categorized into four types: hydrogen bonds, hydrophobic, ionic and water bridges.

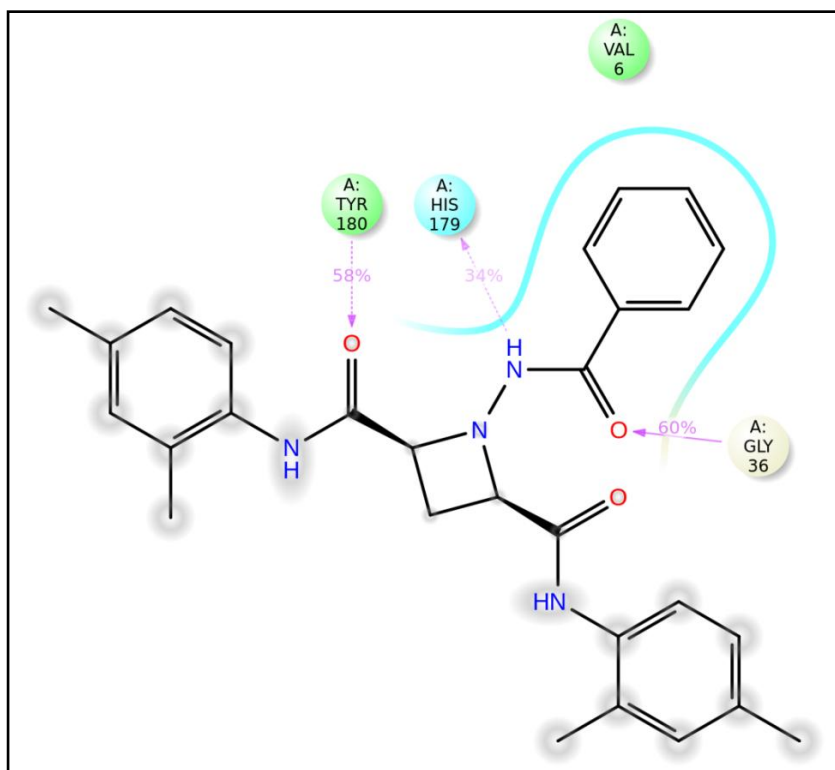


Figure 6.17: Interaction profile of the compound RV4 with glutamate racemase showing the strength of each interaction.

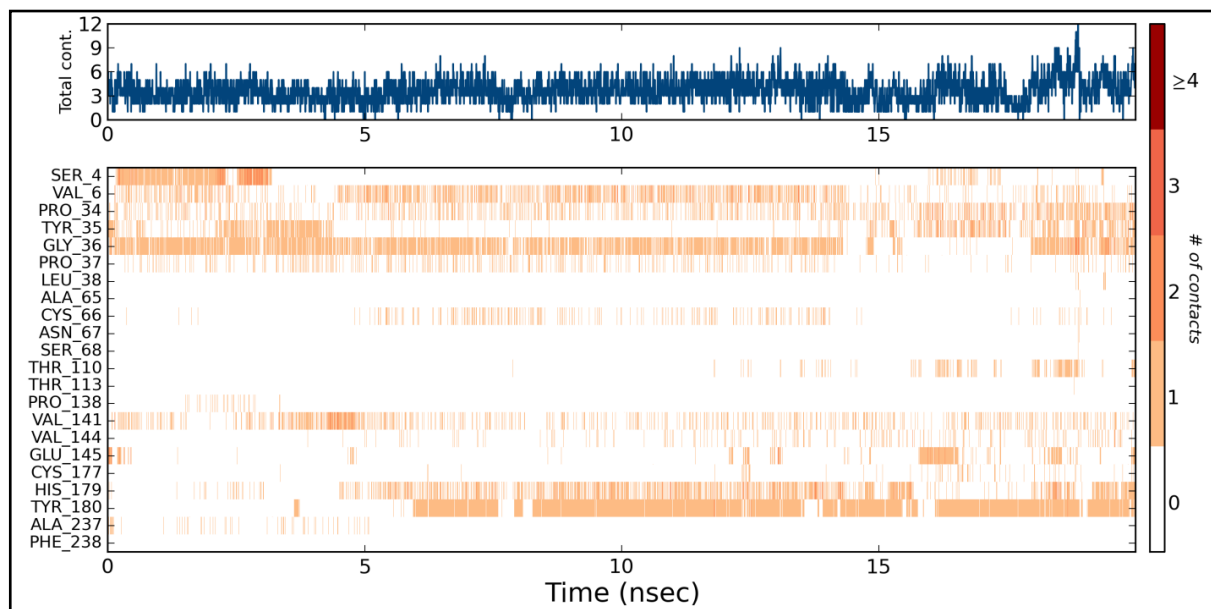


Figure 6.18: Timeline representation of interactions and contacts (**H-bonds, Hydrophobic, Ionic, Water bridges**) between the compound RV4 and glutamate racemase. The top panel shows the total number of specific contacts between MurI with compound RV4 over the course of trajectory. Bottom panel shows residues interacting with ligand in each frame.

It was seen compound RV4 interacting with MurI with at least 3-5 interactions throughout the simulation which altered to even 7 to 12 contacts at particular simulation time points. Bottom panel represents the residues which interact with ligand during a particular time frame. Some residues were involved in more than one specific contact with the ligand, which is represented by a darker shade of orange, according to the scale on right side of the plot. From the bottom panel of **Figure 6.18**, it was observed that residues Val6, Pro34, Gly36, His179 and Tyr180 were constantly interacting with RV4 with more than one contact throughout the simulation.

Analyzing each of the interaction separately allows studying the residues majorly participating in the protein-ligand interaction stability. This data can be further useful in identifying the crucial amino acids for the particular enzyme using *in vitro* mutational studies.

The hydrogen bond analysis of MurI-RV4 trajectory helped us to identify residues involved in hydrogen bonding with compound RV4. The analysis also helped in identification of residues acting as acceptor/donor using its atoms from backbone/side-chain of the residue. From the bar plot of **Figure 6.19**, it was observed Gly36 and Tyr180 are the two main residues involved in strong hydrogen bonding with compound RV4. Both Gly36 and Tyr180 residues were observed acting as hydrogen bond donors, involving their backbone and side-chain respectively. Gly36 and Tyr180, from the **Figure 6.19**, were seen interacting with RV4 with about 62% and 58% during the simulation. Hydrogen from amine group of Gly36 was found to be interacting with carbonyl oxygen of compound RV4. In a similar fashion, hydrogen from amine group of Tyr180 was found to be interacting with carbonyl oxygen of RV4. Hydrogen bond analysis of MurI-RV4 complex also revealed presence of lesser strength hydrogen bond interactions at MurI active site with residues His179 (34%), Ser4 (13%), Tyr35 (12.8%) and Glu145 (3.6%). Interaction pattern of residues involved in hydrogen bonding with RV4 is shown in the bottom panel of figure 6.15. The higher interaction strength with residues Gly36 and Tyr180 was understood from the figure which displays the interaction pattern for these residues with ligand. It was observed Gly36 and Tyr180 were bonding with RV4 throughout the simulation except for a few nanoseconds time scale. Also, it was observed His179 interacting with RV4 in a similar fashion. From the contacts plot, it was studied that on average the compound was involved in 2-3 hydrogen bonds with glutamate racemase throughout the simulation time period with Gly36, His179 and Tyr180 playing a major role in hydrogen bonding.

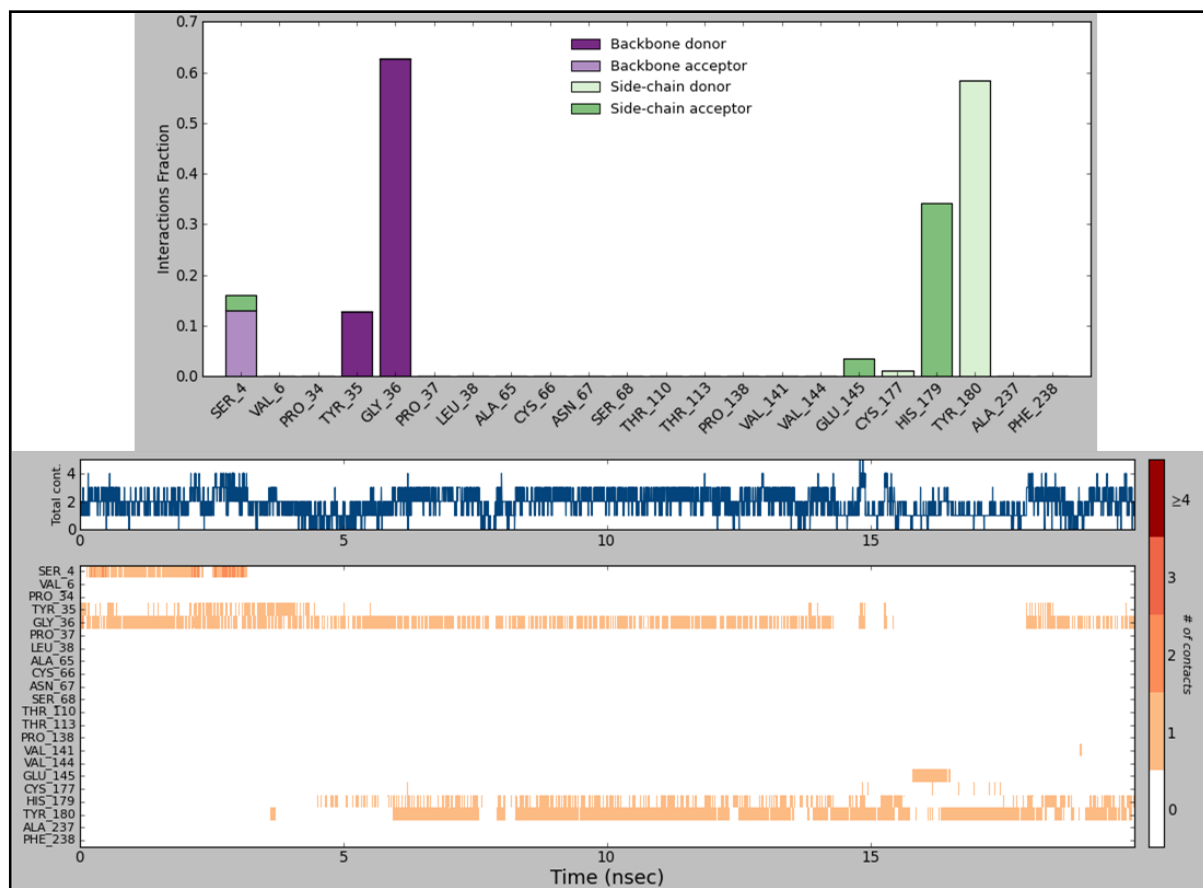


Figure 6.19: Top panel shows the residues of MurI involved in hydrogen bonding with RV4. The stacked bar plots indicate the strength of the bond during the simulation time period. The bottom panel shows hydrogen bonding residues interacting with the ligand in each frame.

Weak intermolecular interactions such as hydrogen bonding and hydrophobic interactions are key players in stabilizing energetically-favored ligands, in an open conformational environment of protein structures. The active site of glutamate racemase, as observed from the model constructed, was found to be both hydrophilic and hydrophobic in nature at its active site. Analysis of hydrophobic interactions of RV4 at glutamate racemase active site revealed non-polar interactions with various residues such as Val6 (39.3%), Pro34 (32.7%) and Val141 (22.9%) as shown in **Figure 6.20**. Some other residues were also involved in hydrophobic interactions, but with lesser strength, with the compound. They were found to be Tyr35, Pro37, Cys66, Pro138, Val144, His 179 and Ala237. Tyr35 and His179 were found to be involved in π - π stacking interactions with the compound involving their phenyl and imidazole rings respectively. From the analysis, it was observed hydrophobic interactions playing a key role in binding of RV4 to MurI, supporting the inhibitory capability of RV4.

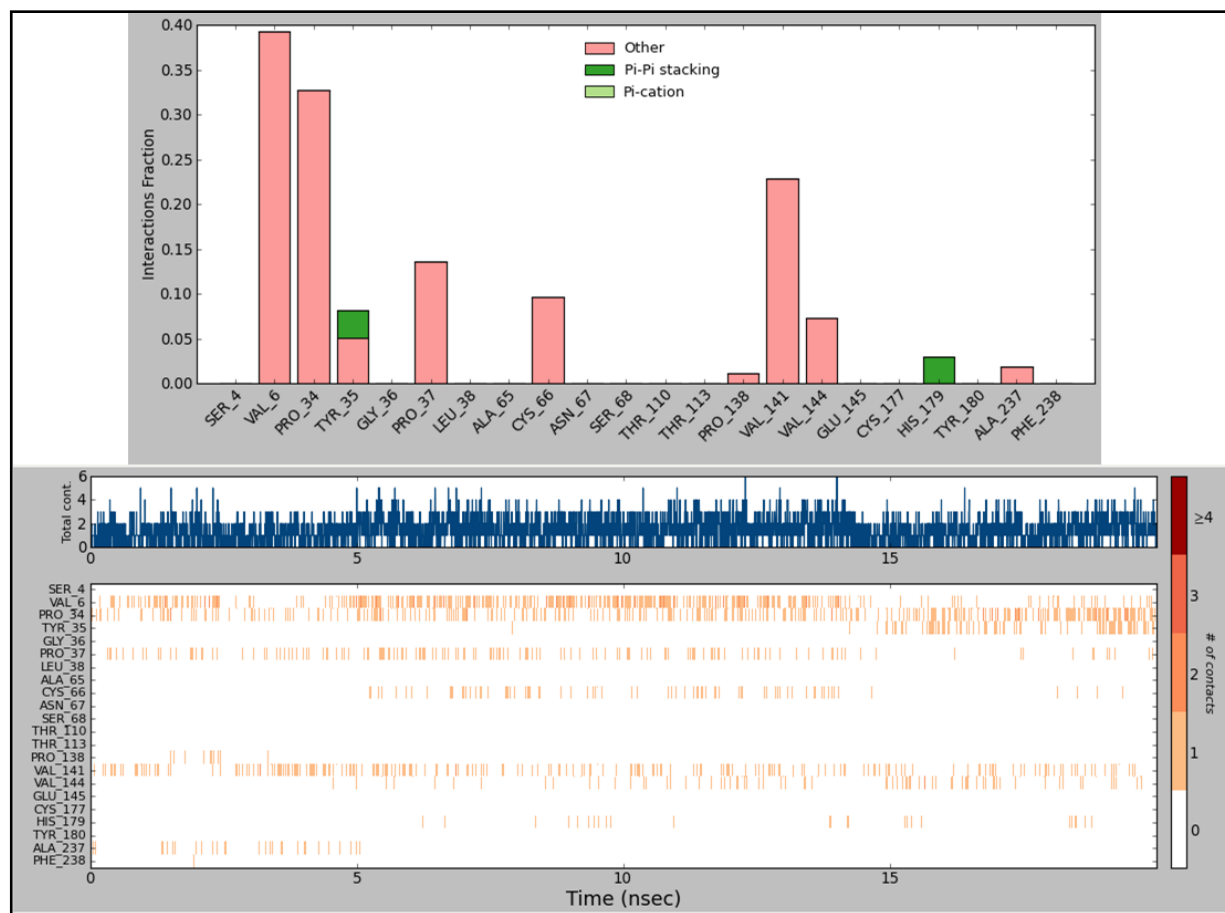


Figure 6.20: Top panel of the figure shows the residues of glutamate racemase involved in hydrophobic interactions with compound RV4. The stacked bar plots indicate the strength of the bond during the simulation time period. The bottom panel shows residues interacting with the ligand in each frame.

Another crucial type of interaction involved in the protein-ligand binding is water bridge interaction which involves the hydrogen bonding between protein and the ligand mediated by water. Though weaker in strength, this type of interaction plays a major role in the specificity of ligand towards a particular protein. Hence, in the present study, the analysis of water bridge interaction was also carried out. As observed from **Figure 6.21**, many active site residues of glutamate racemase were involved in water bridge interactions with compound RV4. The green and pink bars from the plot distinguish the residues acting as hydrogen bond acceptor and donor respectively. Glu145 and Thr110 were found to be effectively involved in these interactions with strength of 6.5% and 6.2% respectively. Glu145 was found to be acting as hydrogen bond acceptor and Thr110 was found to be shuffling its role as both hydrogen bond

acceptor and donor. Other residues involved in water mediated interactions were Ser4, Tyr35, Gly6, Val141, Cys177, His179 and Tyr180. Residues such as Ser4, Val141, His179 and Tyr180 were found to be the key residues involved in water mediated binding with RV4 as these interactions were involved in more than one interactions (as observed from the bottom panel of **Figure 6.21**).

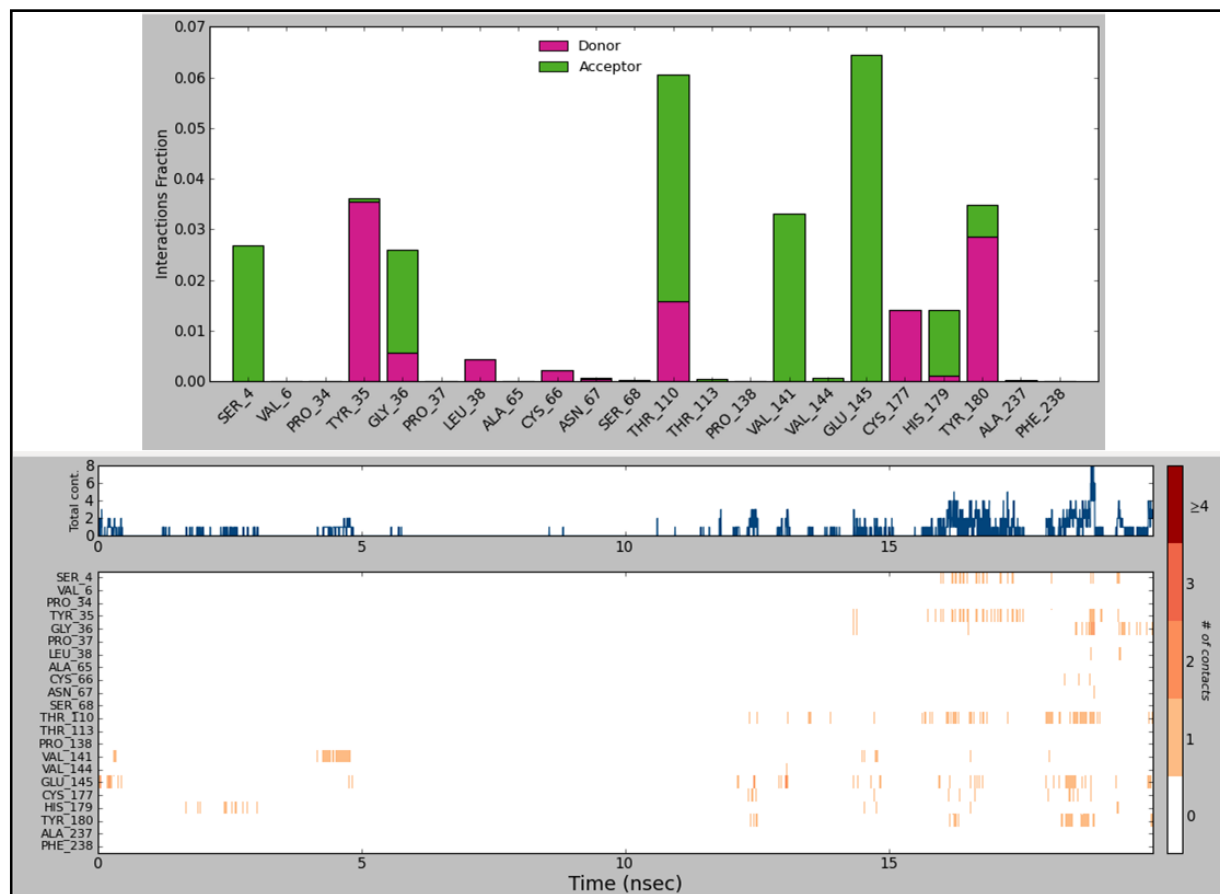


Figure 6.21: Top panel of the figure shows the residues of glutamate racemase involved in water mediated hydrogen bonding with compound RV4. The stacked bar plots indicate the strength of the bond during the simulation time period. The bottom panel shows residues interacting via water bridge interactions with the ligand in each frame.

Various other components of the protein-ligand interactions were also analyzed during the simulation time period. The ligand, compound RV4, was found to be highly stable at the glutamate racemase active site during the simulation highlighting its binding affinity towards the protein. From **Figure 6.22**, the mean RMSD of the compound RV4 was found to be 1.61

Å which shows its stability during simulation. The radius of gyration of the ligand was analyzed throughout the simulation and is given in **Figure 6.22**. The radius of gyration refers to the distribution of the components of an object around an axis. The lesser the radius of gyration, the more compact is the protein structure and vice versa. From the plot, it was inferred that the ligand structure remained stable without much fluctuations. This observation can in turn be explained by the stabilization effect of compound RV4 over glutamate racemase and its strong binding interactions with MurI. The mean radius of gyration for the compound RV4 calculated over 20 ns simulation time period was found to be 4.85 Å.

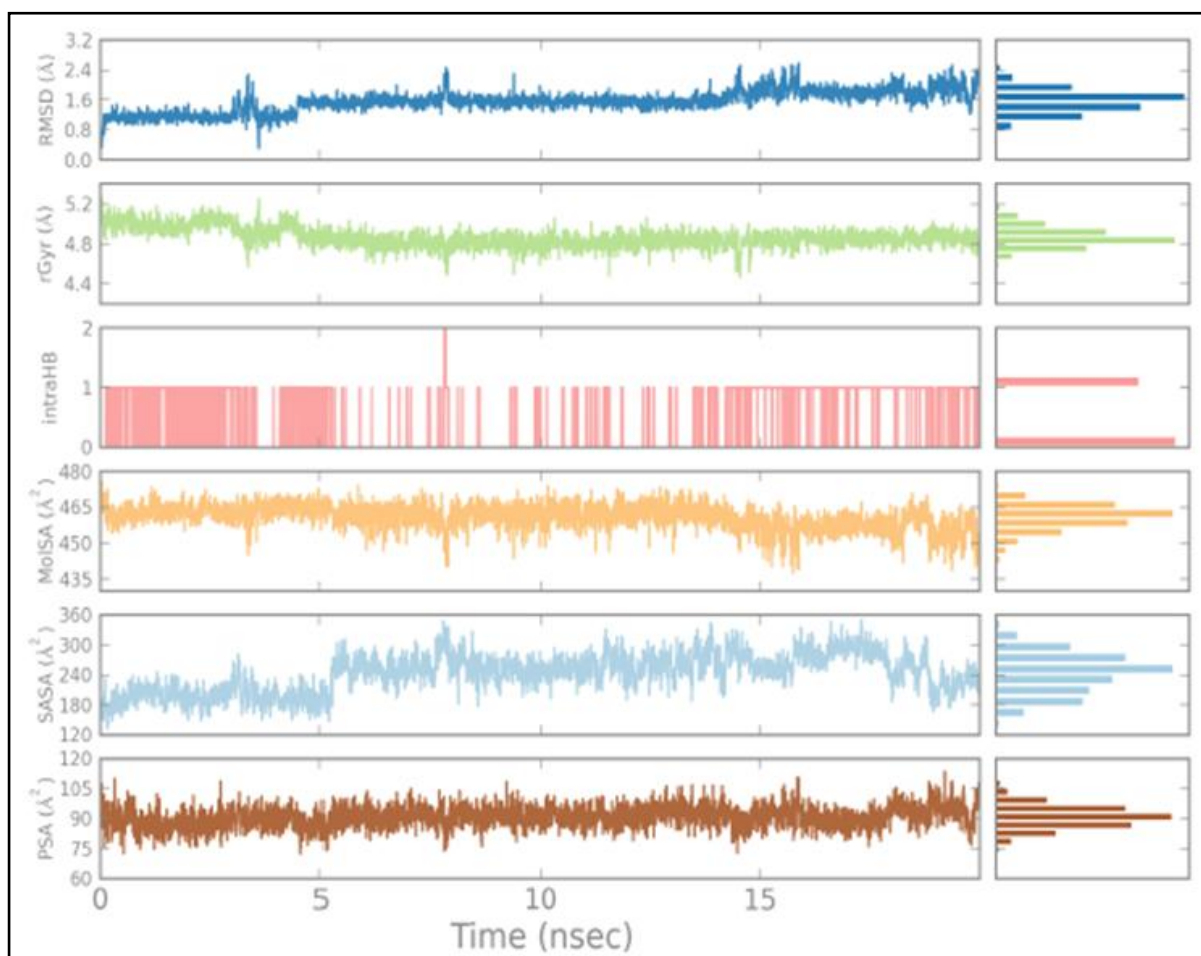


Figure 6.22: Plot representing various ligand properties analyzed during the simulation of glutamate racemase-compound RV4 complex.

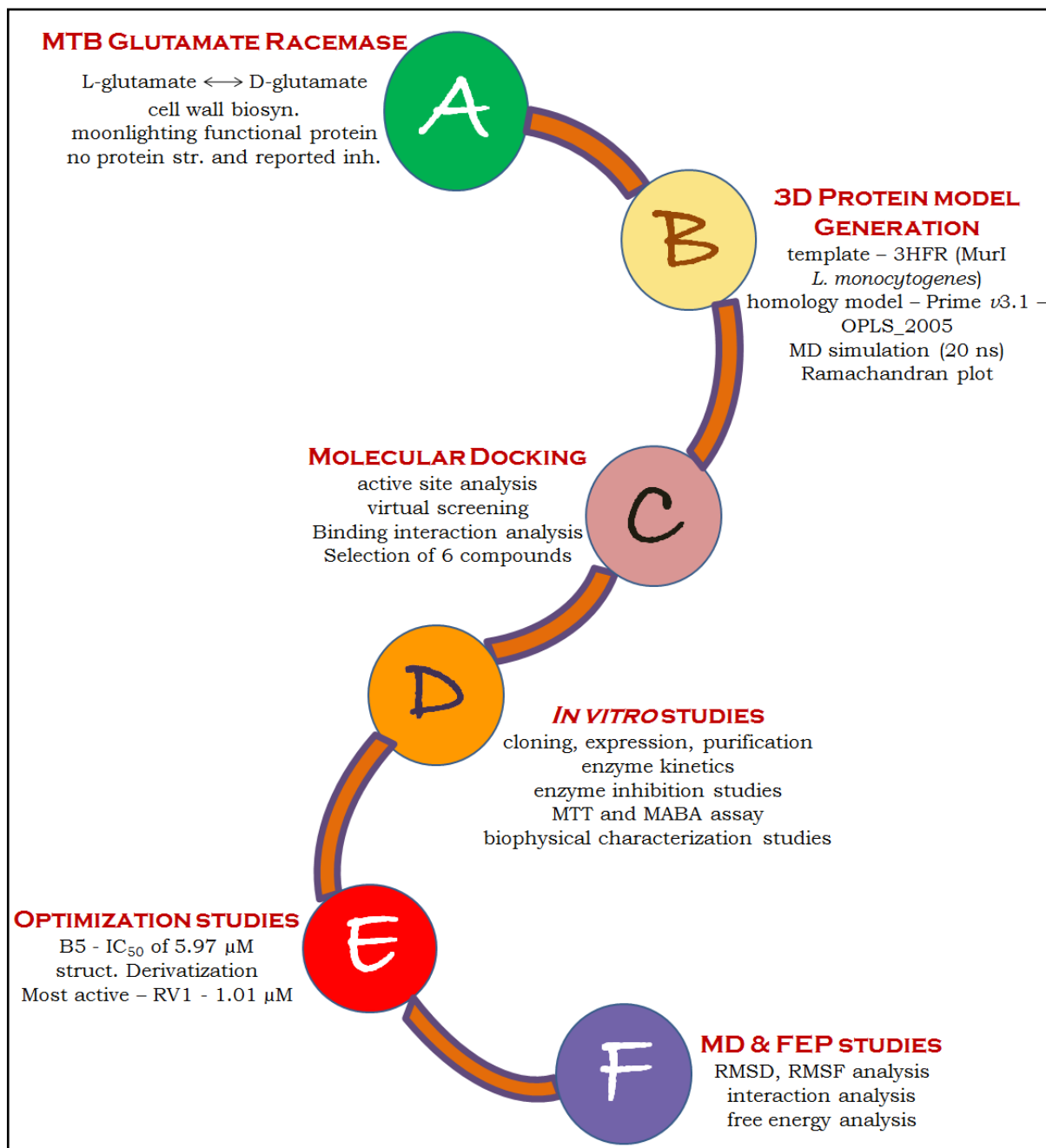
The compound was observed to involve in intramolecular hydrogen bonding during the simulation period. The compound was found with one internal hydrogen bond which was

observed between amine attached to dimethyl phenyl group and carbonyl oxygen linking amine group to phenyl moiety. Second internal hydrogen bond was also found until a particular simulation time point but later was disconnected. The molecular surface area of the compound RV4 was analyzed throughout the simulation time period so as to observe any fluctuations in it. The molecular surface area was calculated with a 1.4 Å radius probe. From the plot **6.22**, it was observed that no major fluctuations in the molecular surface area were observed with respect to simulation time period. Fewer minor fluctuations were observed at the end of simulation ignoring which highlighted the stable nature of the compound. The mean molecular surface area for RV4 calculated over the simulation time period was found to be 463 Å.

6.1.8. Highlights of the study

In the present study, the 3D protein structure for MTB glutamate racemase was developed using homology modeling methodology. The developed model was validated for its stereochemical quality and was validated using molecular dynamics simulations. The developed model was subjected to *in silico* virtual screening which identified 1-(benzamido)-N²,N⁴-diphenylazetidine-2,4-dicarboxamide as lead molecule in further drug design studies. The structural optimization of the identified compound resulted in synthesis of eleven compounds, of which compound RV4 was found to be the most active compound with activity of 1.014 μM. The binding affinity of the compound was reascertained by DSF studies and supported by molecular dynamics simulations. The studies reveal structure based design as a powerful tool in the identification of novel MTB glutamate racemase inhibitors.

Overview of glutamate racemase work



Chapter 7

RESULTS AND DISCUSSION FOR DEVELOPMENT OF MTB MALATE SYNTHASE INHIBITORS

7.1. Design and development of MTB malate synthase inhibitors

Activation of glyoxylate shunt within the tricarboxylic acid (TCA) cycle is one of the characteristic metabolic changes observed in MTB during dormant conditions. This is to conserve the carbon resources by utilizing acetyl Co A from β -oxidation and replenishing TCA cycle intermediates in an anaplerotic fashion. Malate synthase, being one of the crucial enzymes involved in glyoxylate pathway, was targeted in the present study to design and develop inhibitors against it. Absence of malate synthase in human makes it an attractive target for developing antitubercular drug candidates.

7.1.1. Design of malate synthase inhibitors using structure based drug design

7.1.1.1. Selection of malate synthase crystal structure and its binding site analysis

Many crystal structures of malate synthase are available till date co-crystallized with substrates and inhibitors. Among them, crystal structure of malate synthase co-crystallized with 4-(2-bromophenyl)-2,4-dioxobutanoic acid with PDB code 3S9Z was utilized in the present study for the development of e-pharmacophore. The structure was found with 1.79 Å resolution and the IC_{50} of the ligand was reported to be 600 nM. The binding site analysis of malate synthase crystal structure revealed the presence of a large druggable cavity which endogenously in organism accommodates the pantothenate part of acetyl Co A. The surface of the active site is highly hydrophilic due to its presence towards the solvent and residues Phe126, Ser544, Pro545 and Met631 form the solvent accessible surface of malate synthase active site. The active site pocket was observed to be long and highly hydrophobic as it is lined by residues Leu117, Val118, Val119, Pro120, Phe126, Ala130, Leu461, Met515,

Trp541, Pro545, Ala619, Asp633 and Ala635. Hence, targeting malate synthase would be much appreciative with compounds which are hydrophobic and which in turn result in strong non-polar interactions. Also, a catalytic Mg^{2+} ion is present at the bottom of active site. Design of malate synthase inhibitors can be more valid if the compounds can interact with the Mg^{2+} ion thereby making it unavailable for catalysis.

7.1.1.2. Protein active site validation and e-pharmacophore generation

Ligand-based pharmacophore studies have been found to be one of the most valid and efficient methods due to their enhanced output over only ligand based approach. This approach was found to incorporate the ligand-protein interaction data when compared to the conventional ligand based pharmacophore studies. The crystal ligand was docked to the prepared malate synthase protein using extra precision (XP) mode of Glide docking. The ligand was found to interact at the malate synthase active site by forming four hydrogen bonds with an XP glide score of -8.479. The RMSD of the docking pose with that of the crystal structure was found to be 0.92 Å. Interaction profile of the crystal ligand at malate synthase active site is shown in **Figure 7.1**.

The terminal two oxygen atoms of carboxylate moiety were found to form hydrogen bonds with Leu461 and Asp462 one with each residue. The other two oxygen atoms between the phenyl ring and carboxylic acid terminal were found to interact with Arg339 by two hydrogen bonds. One of the carboxylate oxygens and the adjacent ketone oxygen were found to be involved in coordinate covalent bonding with Mg^{2+} ion (Mg802). The crystal ligand was also found to be stabilized by strong hydrophobic interactions with residues like Trp541, Pro543, Ala619, Asp633 and Ala635.

The protein-ligand docking pose generated using Glide XP docking was considered for e-pharmacophore generation using Phase v3.4 of Schrödinger 9.3. The Glide XP descriptor file containing information regarding hydrophobic, electrostatic, π - π , cation- π , anion- π interactions of crystal ligand-protein dock pose was used to assign the energetic values of each pharmacophore site generated for the ligand. A four feature pharmacophore hypothesis was generated for the crystal ligand-protein docked complex. The features generated were – one ring feature, two hydrogen bond acceptors and one negative-ionizable. These features correspond to the phenyl ring (R5), two ketonic oxygens adjacent to phenyl ring acting as two

hydrogen bond acceptors (A1, A2) and terminal carboxylate ion (N4). The generated e-pharmacophore is shown in **Figure 7.2** and energy scores of pharmacophore features along with their ranking are given in **Table 7.1**.

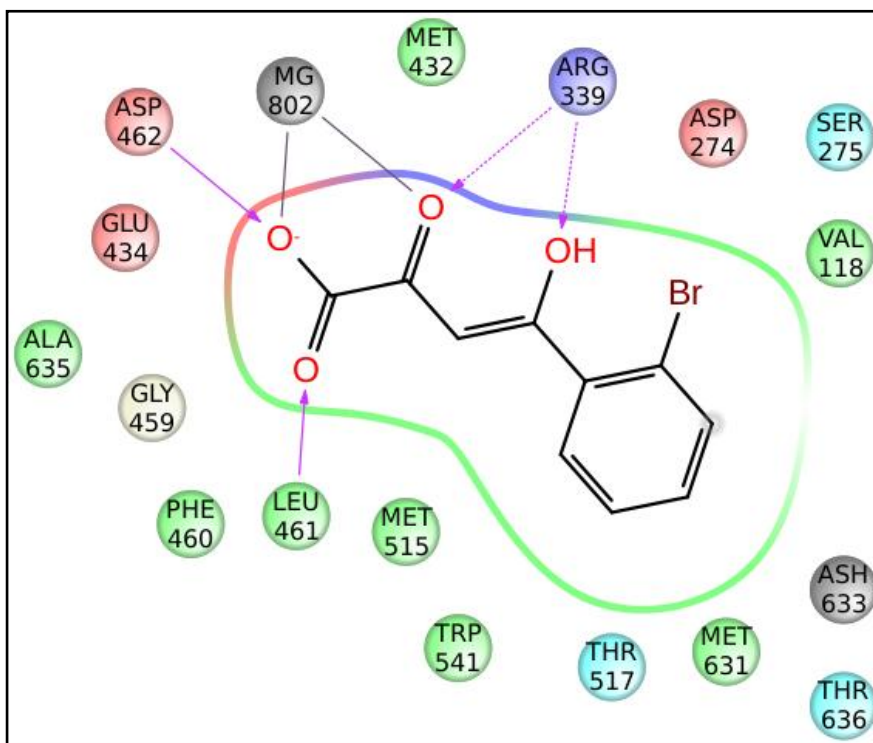


Figure 7.1: Interaction profile of crystal ligand at malate synthase active site (PDB - 3S9Z)

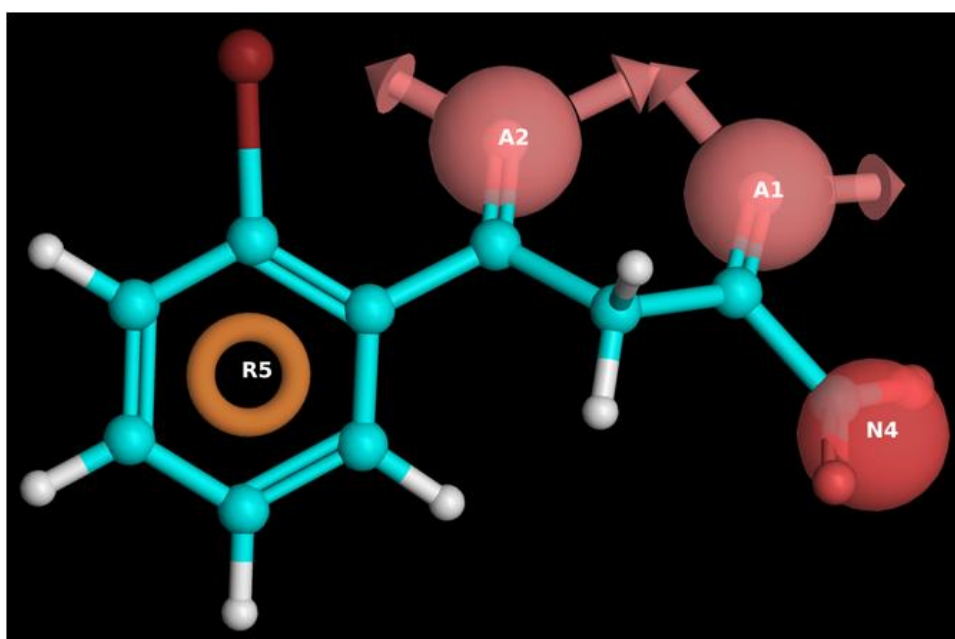


Figure 7.2: e-Pharmacophore generated for crystal ligand of malate synthase (PDB - 3S9Z).

Table 7.1: Scores of each feature in the generated e-pharmacophore.

Rank	Feature Label	Score	Type
1	R5	-1.13	Aromatic Ring
2	A1	-0.35	H-bond acceptor
3	A2	-0.23	H-bond acceptor
4	N4	-0.23	Negative ionizable

7.1.1.3. E-pharmacophore based screening of chemical databases

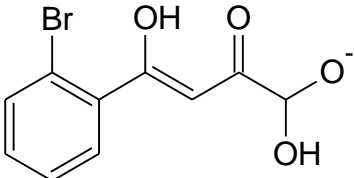
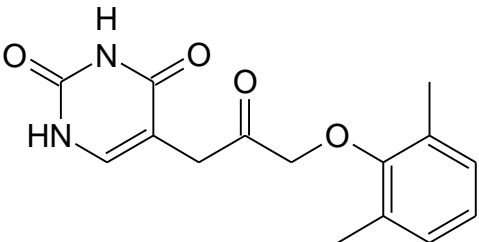
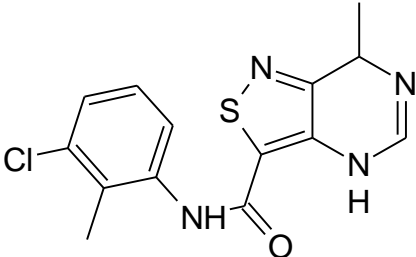
The generated pharmacophore was employed as a query in search of potential MTB malate synthase inhibitors. Asinex database, a commercially available chemical library containing novel scaffolds, and BITS in-house database were screened for the identification of malate synthase inhibitors. Criterion for compounds screening was set to match at least three features out of four. A total of 3,257 hits were retrieved as a result of screening methodology. The fitness of the compounds was found to be in the range of 0.5 – 1.9. The obtained hits were subjected to molecular docking studies to study their interaction pattern at malate synthase active site.

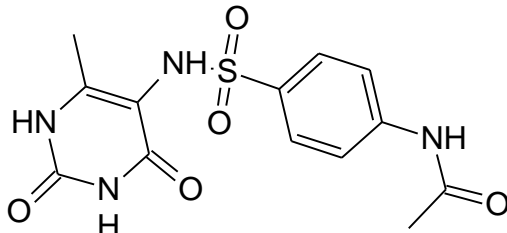
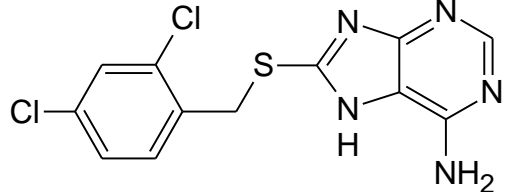
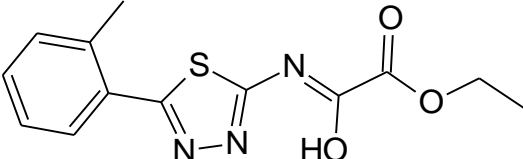
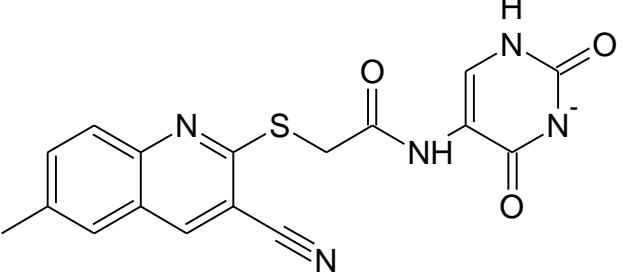
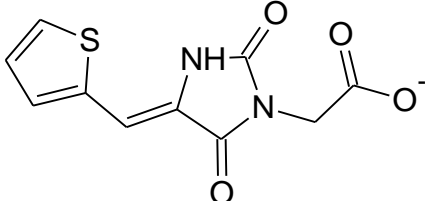
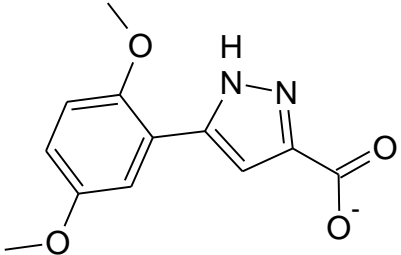
7.1.2. Molecular docking studies of the retrieved hits

Structure based virtual screening results in the identification of newer chemical entities against the target based on the interaction information of previously reported inhibitors against the target. In the present study, virtual screening workflow was operated by employing Glide v5.8 of Schrödinger suite 2012. Virtual screening workflow was carried out while operating docking protocol to cut short the number of hits at each step based on their docking scores. Hits retrieved from e-pharmacophore based screening of asinex and BITS in-house database were subjected to virtual screening which involves high throughput virtual screening (HTVS), standard precision (SP) and extra precision (XP) mode of docking using Glide v5.8. Compounds from HTVS with docking score above $-7.5 \text{ kcal.mol}^{-1}$ were selected and subjected to standard precision (SP) of docking. Standard precision mode of docking offers a more reliable mode of docking with high accuracy. The compounds from SP docking with docking score above $-7.5 \text{ kcal.mol}^{-1}$ were further carried forward to extra precision (XP)

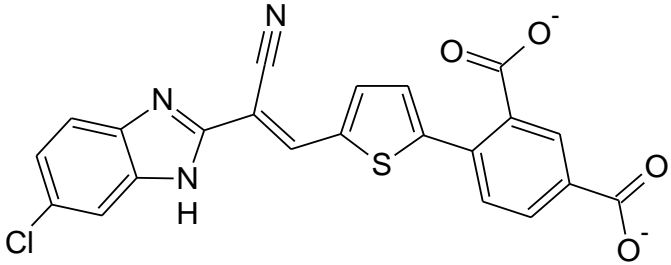
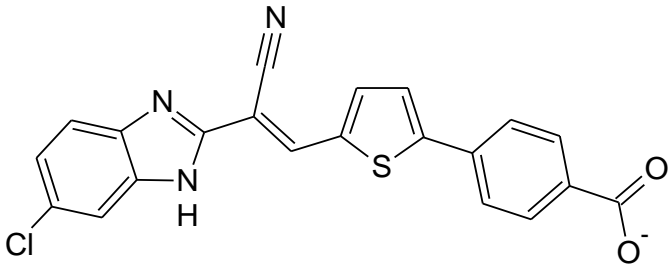
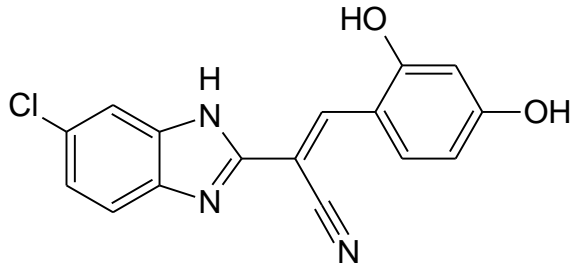
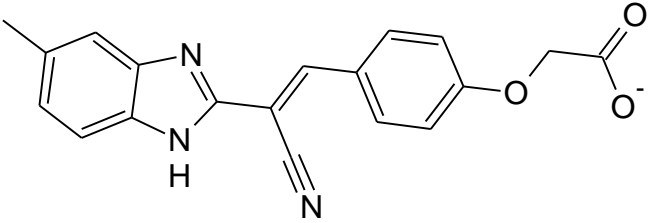
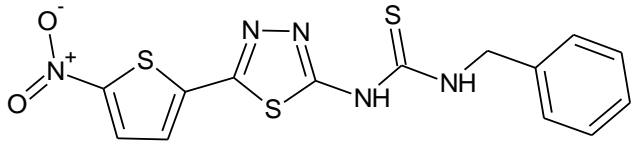
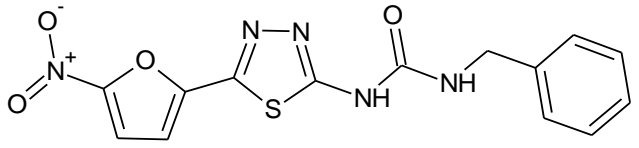
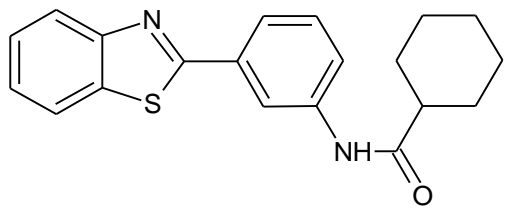
docking. Extra precision docking results in the elimination of false positives employing extensive sampling and advanced scoring methods with higher enrichment. Compounds with XP glide score above $-7.5 \text{ kcal.mol}^{-1}$ retaining crucial active site interactions with malate synthase were considered during the final selection of compounds. A total of 21 compounds, 8 from asinex and 13 from BITS in-house database, with diverse scaffolds were selected based on their binding interactions at the malate synthase active site, glide scores and orientation at the pocket. The glide score, energy and fitness for these compounds are given in **Table 7.2**. The compounds from asinex database were purchased and total 21 compounds were subjected to *in vitro* enzyme inhibition studies.

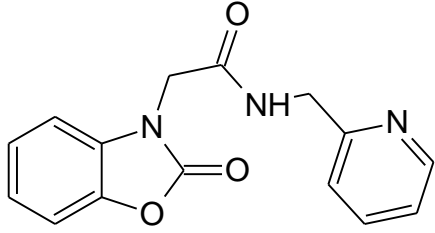
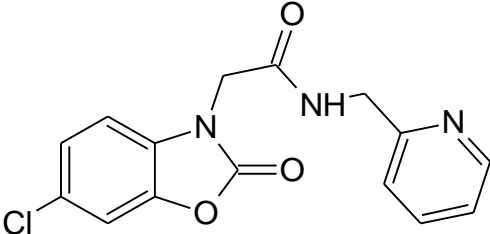
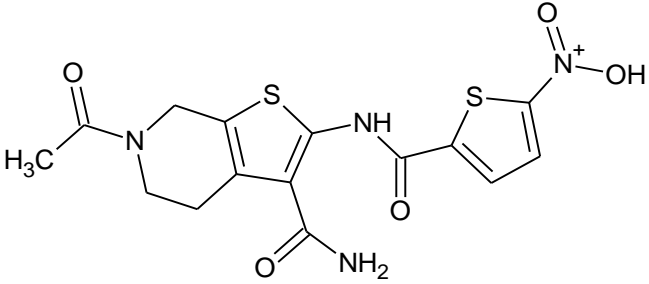
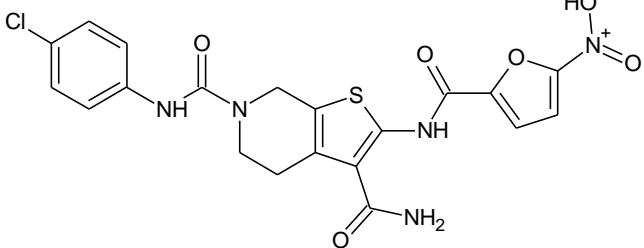
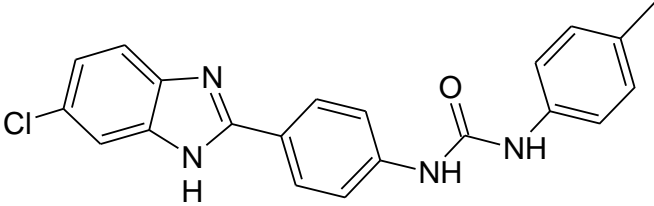
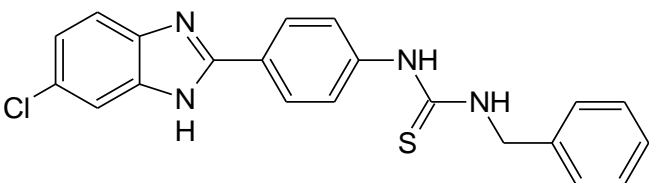
Table 7.2: Glide scores, glide energy and fitness for selected 21 compounds against MTB MS.

Comp	Structure	Glide XP gscore	Glide Energy	Fitness
Crystal ligand		-8.50	-53.90	3
Asinex Database				
Am1		-11.13	-55.76	1.98
Am2		-10.33	-47.19	1.87

Am3		-10.11	-48.81	1.97
Am4		-10.05	-48.34	1.99
Am5		-9.51	-56.08	2.05
Am6		-8.87	-53.32	1.79
Am7		-8.57	-35.55	1.81
Am8		-8.07	-54.81	2.03

BITS in-house database

Bm1		-8.29	-58.47	1.75
Bm2		-9.93	-61.95	1.61
Bm3		-8.29	-44.85	1.27
Bm4		-9.28	-55.05	1.68
Bm5		-9.17	-86.95	-1.16
Bm6		-8.91	-87.86	-1.07
Bm7		-8.26	-54.63	-1.00

Bm8		-8.53	-46.07	1.49
Bm9		-8.52	-45.52	1.50
Bm10		-8.86	-59.07	1.06
Bm11		-7.90	-83.38	-1.01
Bm12		-7.13	-50.44	0.29
Bm13		-8.54	-49.45	0.29

7.1.3. *In vitro* enzyme inhibition studies

The *glcB* gene was successfully cloned and transformed. This clone was expressed and purified using Ni-affinity chromatography. The target protein MTB malate synthase was eluted at 200 mM imidazole and confirmed with SDS-PAGE. The kinetic parameters were determined for glyoxylate and acetyl CoA.

7.1.3.1. Enzyme kinetics of MTB malate synthase

The enzyme concentration activity followed first order kinetics. At constant enzyme concentration of 0.258 $\mu\text{g}/\mu\text{L}$, the substrates glyoxylate and acetyl Co A were varied from 3.5 mM to 1 μM and 10 mM to 1 μM respectively. The K_m for glyoxylate and acetyl Co A were found to be 1.123 mM and 0.1434 mM respectively which were determined using GraphPad Prism 6 (GraphPad Prism software, San Diego, CA) and shown in **Figure 7.3**.

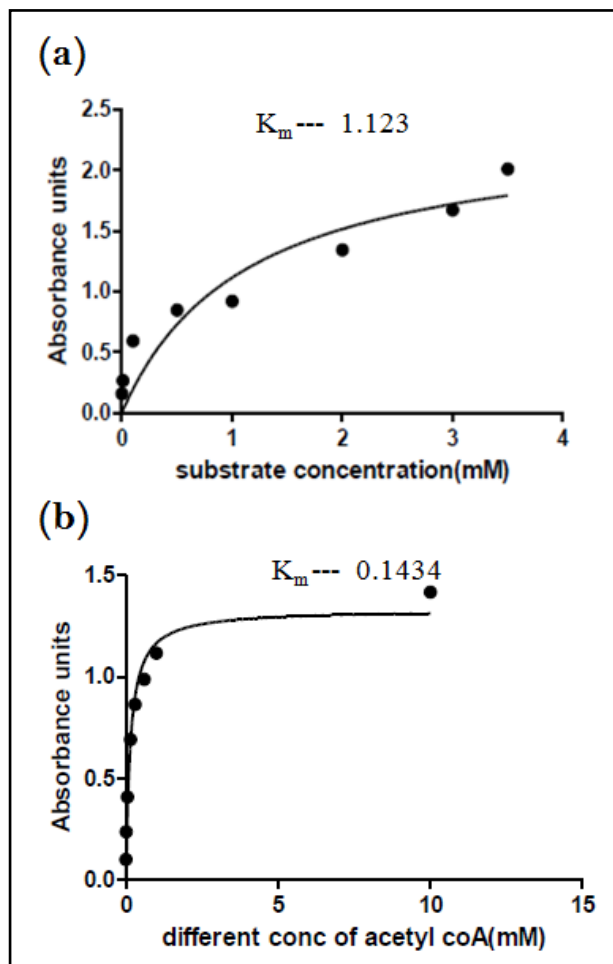


Figure 7.3: Enzyme kinetics plot for (a) glyoxylate and (b) acetyl Co A.

7.1.3.2. *In vitro* malate synthase assay for the selected compounds

The selected 21 compounds were retrieved and evaluated for malate synthase inhibition assay. The procedure was discussed in the experimental section. Initially, all the compounds were screened at their 25 μM concentration at which compounds showed varying percentage inhibition of MTB MS. The eight compounds procured from asinex (**Am1-8**) and compounds **Bm5-11** from BITS in-house database did not show any considerable MS inhibition which were eliminated for further screening. The remaining six compounds were screened at 10 μM and further lower concentrations of 5 μM , 1 μM and 0.1 μM and their IC_{50} s were calculated using GraphPad. The IC_{50} s for the six in-house database compounds are given in **Table 7.3**. All the six compounds were found to be with considerable malate synthase inhibitory activity ranging 3-13 μM with five compounds activity less than 10 μM . Compounds **Bm13** and **Bm1** were observed to be the top active ones with 3.09 μM and 3.63 μM activity. The interactions of the active six compounds at the malate synthase active site are given in **Table 7.4**.

Table 7.3: Activity profile of the selected 6 benzimidazole derivatives against MS

Compound	IC_{50} (in μM)*
Bm1	3.64 \pm 0.04
Bm2	9.03 \pm 0.02
Bm3	13.66 \pm 0.04
Bm4	9.49 \pm 0.04
Bm12	5.41 \pm 1.01
Bm13	3.09 \pm 0.02

* IC_{50} calculated using GraphPad Prism 6 (mean \pm SEM).

Table 7.4: Interactions of active 6 compounds at MTB malate synthase active site.

Compound	H-bond interactions	π - π stacking interactions	Hydrophobic interactions	Mg^{2+} bonds*
X-ray ligand	Arg339, Leu461, Asp462	Phe126, Trp541	Leu117, Val118, Met432, Phe460, Met515, Trp541, Pro543, Ala619, Met631,	Mg802

		Ala635		
Bm1	Val118, Arg339	Phe126	Leu117, Val119, Pro120, Ala130, Met432, Met515, Trp541, Pro543, Pro545, Met631, Ala635	Mg802
Bm2	Val118, Arg339	Phe126	Leu117, Val119, Pro120, Ala130, Met432, Trp541, Pro543, Pro545, Met631, Ala635	Mg802
Bm3	Val118, Arg339	Phe126	Leu117, Val119, Pro120, Ala130, Met432, Trp541, Pro543, Pro545, Ala635	Mg802
Bm4	Val118, Arg339	Phe126	Leu117, Val119, Pro120, Ala130, Met432, Leu461, Trp541, Pro543, Pro545, Met631, Ala635	Mg802
Bm12	Val118, Asp633	Phe126, Trp541	Leu117, Val119, Pro120, Ala130, Met432, Phe460, Leu461, Pro543, Pro545, Met631, Ala635	--
Bm13	Val118, Asp633	Phe126, Phe541	Leu117, Val119, Pro120, Ala130, Met432, Phe460, Leu461, Met515, Pro543, Pro545, Ala635	--

* Residues interacting with Mg²⁺ with coordinate covalent bonding.

7.1.4. ADMET analysis

Pharmacokinetic properties analysis helps to identify suitable compounds with pharmaceutical importance which can be developed into a drug candidate. Selected compounds were subjected to *in silico* ADMET analysis using QikProp. All the compounds were found to be in accordance with Lipinski's rule of Five which is the basic criteria of drug-likeness. Various properties like SASA (Predicted Solvent Accessible Surface Area in Å²), QPlogBB (Predicted brain/blood partition coefficient), QPlogHERG (Predicted IC₅₀ value for HERG K⁺ channels), QPPCaco (Predicted apparent Caco-2 cell permeability in nm/s) were determined for the compounds and were checked for any deviations.

All the properties determined are listed out in **Table 7.5**. Compounds were found with least blood brain barrier permeability indicating compounds to be CNS (Central Nervous System) inactive. All the compounds were observed with better oral absorption.

Table 7.5: *In silico* ADME properties for the selected 6 benzimidazole inhibitors of MTBMS.

Comp	SASA	QPlogBB	QPlogHERG	QPPCaco	QPPMDCK	% Oral Absorption	QPlogKp
Bm1	755.33	-2.53	-6.77	034.40	034.30	072.67	-4.22
Bm2	675.12	-1.05	-3.88	140.44	274.45	091.15	-2.53
Bm3	692.94	-3.29	-1.22	000.38	000.20	081.09	-6.78
Bm4	625.64	-1.11	-3.60	098.30	126.14	082.79	-2.70
Bm12	775.66	-2.33	-7.20	072.70	076.93	085.40	-3.18
Bm13	602.35	-2.31	-5.79	051.30	019.96	058.09	-4.42

Properties and Ranges: **SASA** – Predicted Solvent Accessible Surface Area in Å²(300-1000). **QPlogBB**– Predicted brain/blood partition coefficient (-3.000 to 1.200). **QPlogHERG**– Predicted IC50 value for HERG K⁺ channels (concern below -5). **QPPCaco**– Predicted apparent Caco-2 cell (model for gut-blood barrier) permeability in nm/s (<25 – poor, >500 – great). **QPPMDCK** - Predicted apparent MDCK cell (model for blood-brain barrier) permeability in nm/s (<25 – poor, >500 – great). **QPlogKp**– Predicted skin permeability (-8.000 to -1.000).

7.1.5. Hit expansion and optimization of the most active compound from virtual screening

7.1.5.1. Development of 4-(1*H*-benzimidazol-2-yl)-*N*-benzylaniline derivatives as potential *M. tuberculosis* malate synthase inhibitors

The identified hits and their *in vitro* enzyme inhibition studies showcase the better activity profile of benzimidazole derivatives as MTB malate synthase inhibitors (as seen in compounds Bm1-4, Bm12 and Bm13). The interaction pattern of the two top active compounds is shown in **Figure 7.4**. Both the compounds were found to bind to the active site in almost similar pattern with strong hydrophobic interactions. **Figure 7.5** shows the electrostatic surface of malate synthase with both the compounds **Bm13** and **Bm1** at the active site.

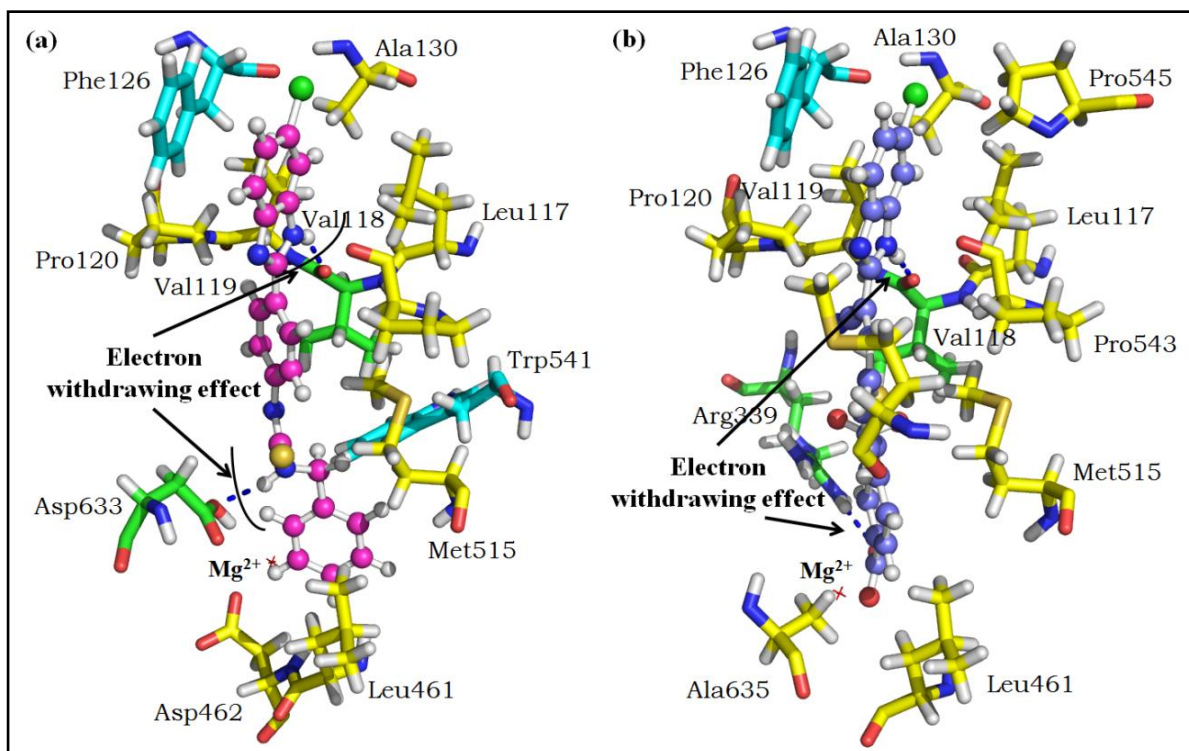


Figure 7.4: Interaction profile of top two active compounds (a) compound **Bm13** (pink) and (b) compound **Bm1** (purple) at the active site of MTB malate synthase. Green sticks indicate residues involved in hydrogen bonding, blue residues involved in π - π stacking interactions, yellow residues involved in hydrophobic interactions. Blue dashed lines indicate H-bonds.

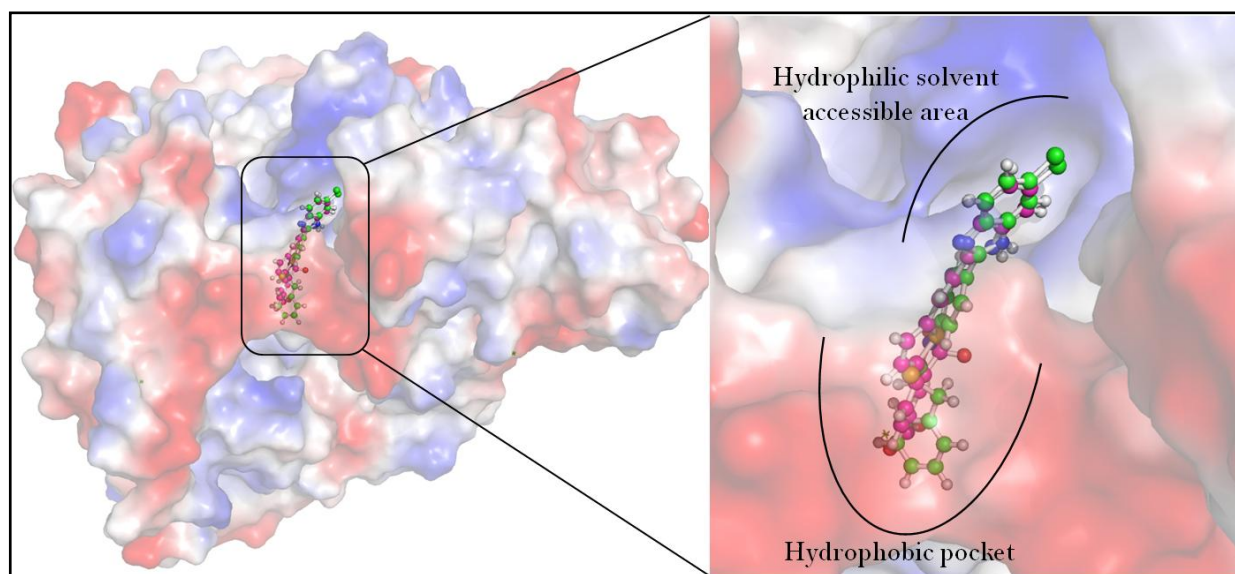


Figure 7.5: Electrostatic surface view of MTB malate synthase with compounds **Bm1** (pink) and **Bm13** (green) at its active site.

From the figure it can be understood that the binding pocket of MTB malate synthase is highly non-polar, a key point to be remembered while designing inhibitors towards MTB malate synthase. Analyzing the binding pattern of these six benzimidazole derivatives, it was observed that the benzimidazole moiety retain towards solvent accessible are of the protein. Though the active site of malate synthase is highly hydrophobic, its inability to accommodate this huge moiety may be the reason for benzimidazole to remain outside the pocket.

The other terminal of the compounds was observed to be buried into the pocket. Benzimidazole scaffold was found to be stabilized by hydrophobic interactions with Leu117, Val118, Pro120, Phe126, Ala130, Pro545, Pro543 and Ala619. All the compounds were seen to be involved in hydrogen bonding with Val118 with one of the –NH of the imidazole ring. The terminal aromatic rings of all the 6 inhibitors were also involved in hydrophobic interactions with Met432, Leu461, Asp462, Met515, Trp541, Met631, Asp633 and Ala635. One of the crucial interactions to be considered is the co-ordinate covalent bonding with Mg²⁺ (Mg802). These interactions were seen among compounds Bm1-4 at the active site. Interesting point is that these four compounds possess terminal oxygen (either –COOH/-OH) which interact with Mg²⁺.

Summarizing these points, we tried to further optimize these inhibitors to end up in designing a lead which can be further derivatized for studying the *in vitro* MTB MS inhibitory activity. The benzimidazole scaffold was thought to be retained in the lead structure because of its interactions (both polar and non-polar) at the active site. In case of compounds Bm1-4, the linker between benzimidazole and aromatic ring (phenyl/thiophene) was found to be neutral without much participation in any interactions. The linker was found to be absent in case of compounds Bm12 and Bm13, in spite of which the compounds possess better activity profile. Hence this linker was deleted while designing the lead. The phenyl ring was retained next to benzimidazole due to its higher aromaticity. In compounds Bm12 and Bm13, a urea/thiourea linker was observed (but absent in compounds Bm1-4). This linker was found to be involved in H-bonding particularly one amine group, the second being uninvolved. This linker was replaced by methanamine (-NH-CH₂-) retaining amine for H-bonding. The oxygen/sulfur was replaced by methyl so as to decrease the steric clashes at the pocket. The terminal phenyl ring was retained for hydrophobic interactions.

On the whole, the designed lead was 4-(1*H*-benzimidazol-2-yl)-*N*-benzylaniline, which is given in the **Figure 7.6(a)**. Two modifications were thought to be attempted, one over the benzimidazole ring (R^1) with some halogens, nitro and methoxy groups and the second at the *para* position of phenyl ring (R^2) with some halogens, nitro and hydroxyl groups. Docking studies of this lead revealed the hydrogen bonding of the compound with residues Val118 and Asp 633 retaining all the hydrophobic interactions. The interaction pattern of the lead is shown in **Figure 7.6(b)**.

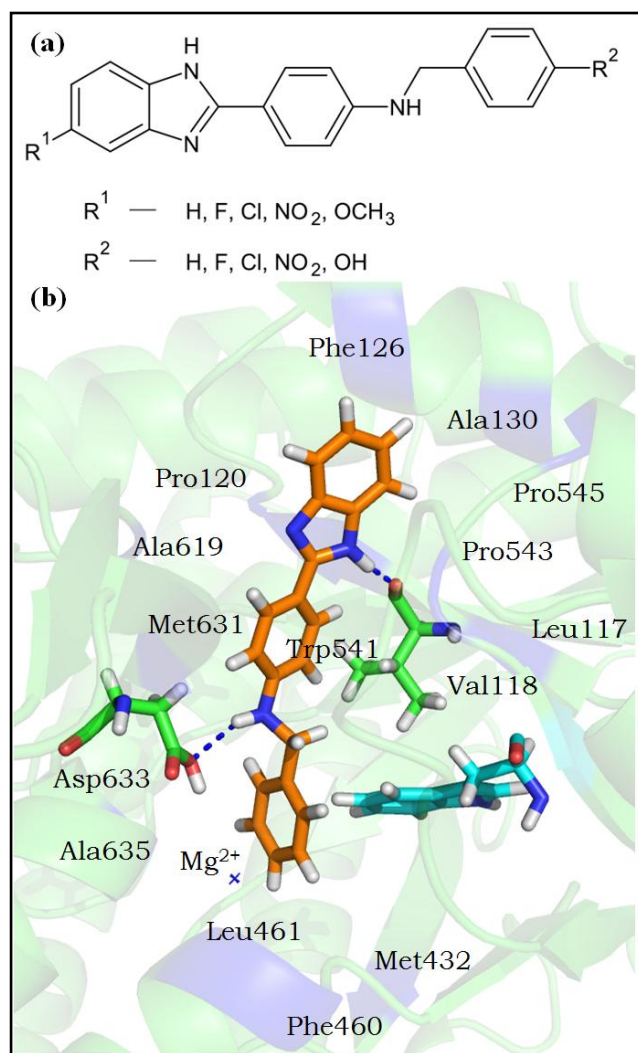


Figure 7.6: (a) Structure of the designed lead with substituents. (b) Interaction profile of lead at the MTB malate synthase active site. Orange indicate lead compound, green indicate H-bond residues, and blue shaded ribbon areas are residues involved in hydrophobic interactions labeled. Blue dashed lines indicate H-bonds.

A library of 25 compounds which are 4-(1*H*-benzimidazol-2-yl)-*N*-benzylaniline derivatives were synthesized by following a 2 step synthesis protocol as shown in **Figure 4.3** in material and methods **section 4.1.2.3**.

The first step aimed at the synthesis of substituted 4-(1*H*-benzo[*d*]imidazole-2-yl)aniline. Eaton's reagent (10 vol; wt/vol) was added drop wise to a well pulverised mixture of the corresponding 1,2-phenylenediamine (1 equiv) and 4-amino benzoic acid (1 equiv) at 0°C. The reaction mixture was then heated at 130 °C for 10 - 12 h (monitored by TLC and LCMS for completion). The reaction mixture was cooled and neutralised with 10% sodium hydroxide solution to pH of 6-7, the precipitate formed was filtered and washed repeatedly with water and dried. The solid obtained was re-crystallized from ethanol to afford the desired product in good yield.

To solution of 4-(1*H*-benzo[*d*]imidazole-2-yl)aniline, (1 mmol) in 10% methanol DCM, corresponding aldehyde (1.1 mmol) , molecular sieves and catalytic amount of acetic acid were added and stirred for 8 hrs. The reaction mixture was then filtered through celite bed and the filtrate was concentrated under argon atmosphere. The resulting residue was dissolved in methanol and cooled to 0 °C followed by the addition of sodium cyanoborohydride (1.5 mmol) portion wise. The resultant solution was allowed to attain room temperature and stirred for 4 hrs (monitored by TLC and LCMS for completion). The solvent was evaporated under reduced pressure and the residue was dissolved in ethyl acetate. The organic layer was washed with water followed by brine solution and evaporated in vacuum. The resulting residue was purified by column chromatography using hexane, ethyl acetate as eluent to afford pure product.

The general procedure followed for the synthesis of series of 25 compounds is given in **Annexure-III**.

7.1.5.2. Molecular docking analysis for the synthesized compounds

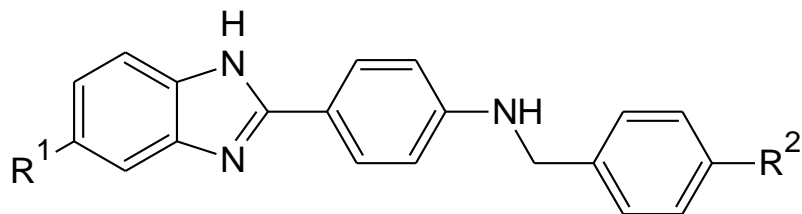
The synthesized 25 compounds were subjected to molecular docking studies with the malate synthase protein using extra precision mode of Glide. Most of the compounds were found to be possessing better interaction profile when compared to the lead compound identified. The common residues involved in hydrogen bonding with most of the compounds were found to be Val118 and Arg339. Analysis of the interaction profiles of all the compounds, it can be

understood that it is the hydrophobic interactions which make the protein-ligand interactions much stabilized thereby adding up to the binding affinity of the ligand. The most common residues involved in hydrophobic interactions with the compound were found to be Val119, Pro120, Phe126, Ala130, Leu461, Met515, Pro543 and Met631. The compounds were further subjected to *in vitro* malate synthase inhibition studies to study their inhibitory potency.

7.1.5.3. *In vitro* malate synthase inhibition assay for the synthesized compounds

The malate synthase enzyme inhibition assay was carried out for the synthesized 25 compounds. As described in the previous sections, various concentrations of the compounds starting from 25 μM , 10 μM , 5 μM , 1 μM and 0.1 μM were tested so as to understand the inhibitory capacity of the compounds. The IC_{50} s for all the compounds were calculated using GraphPad Prism 6 and are given in **Table 7.6**. The activity range of the synthesized compounds was found to be 1.09 – 8.97 μM . Of all the compounds, compound **RP07** was found to be the most active one with an IC_{50} of **1.09 μM** . Dose response curve of compound RP07 is given in **Figure 7.7**. The next active compounds of the series were found to be compounds RP15 (IC_{50} – 1.17 μM) and RP08 (IC_{50} – 1.22 μM). Total sixteen compounds were found with IC_{50} less than 5 μM the remaining nine compounds fall in to the activity range of 5.0 – 9 μM . The compounds were analyzed for their structure activity relationship and structural features important for malate synthase inhibitory activity were identified.

Table 7.6: *In vitro* inhibitory activities of the synthesized analogues



Compound code	R ¹	R ²	IC ₅₀ (μM)*
RP01	-H	-H	8.97±2.05
RP02	-H	-F	5.32±0.86
RP03	-H	-Cl	8.05±1.24

Inhibitors against MTB Malate Synthase

RP04	-H	-OH	5.01±0.91
RP05	-H	-NO ₂	3.87±0.08
RP06	-F	-H	2.14±2.28
RP07	-F	-F	1.09±0.77
RP08	-F	-Cl	1.22±0.16
RP09	-F	-OH	6.56±1.47
RP10	-F	-NO ₂	7.10±1.92
RP11	-Cl	-H	1.82±0.14
RP12	-Cl	-F	7.05±0.21
RP13	-Cl	-Cl	2.60±0.34
RP14	-Cl	-OH	2.71±1.27
RP15	-Cl	-NO ₂	1.17±0.82
RP16	-NO ₂	-H	1.77±0.09
RP17	-NO ₂	-F	4.28±1.06
RP18	-NO ₂	-Cl	2.12±1.33
RP19	-NO ₂	-OH	2.81±0.67
RP20	-NO ₂	-NO ₂	4.96±2.68
RP21	-OCH ₃	-H	2.15±2.44

RP22	-OCH ₃	-F	5.41±1.62
RP23	-OCH ₃	-Cl	4.89±0.46
RP24	-OCH ₃	-OH	5.32±0.93
RP25	-OCH ₃	-NO ₂	1.67±1.06

* IC₅₀ calculated using GraphPad Prism 6 (mean±SEM).

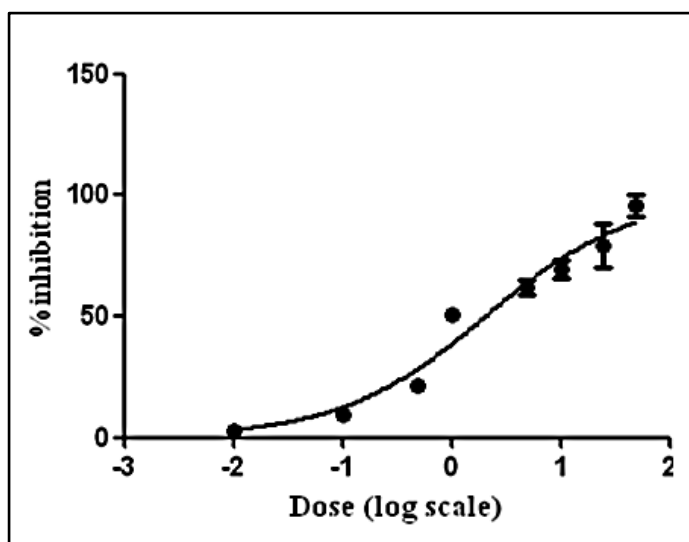


Figure 7.7: Dose response curve for compound **RP07** (IC₅₀ - 1.09 μM).

7.1.5.3a. Structure activity relationship (SAR) for the synthesized compounds

The synthesized 25 compounds were studied for their structure activity relationship with respect to their malate synthase inhibitory activity. A valid SAR was developed relating the activity of the compounds to their *in silico* interactions at malate synthase active site analyzed from molecular docking studies. The modifications attempted at R¹ were -H, -F, -Cl, -NO₂ and -OCH₃ and at R² were -H, -F, -Cl, -OH and -NO₂.

Here in the SAR, the total analysis can be considered into five groups according to the modifications attempted at R¹ position. The first group of compounds was **RP1-5** with hydrogen at R¹. These groups of compounds were found with activity in the range of 3.8-8.9 μM being the least active group of the series. The less activity of the compounds when compared to other compounds may be attributed to the unavailability of the substituents over

the benzimidazole ring to interact with the active site residues of malate synthase. Of these five compounds, RP05 was found to be the most active of this subgroup with activity 3.87 μM . This may be attributed to the presence of nitro substitution at the R² position which was found to be interacting with Arg339 and also involved in co-ordinate covalent bonding with Mg802.

The later substitution attempted was fluorine at R¹ which resulted in compounds **RP6-10**. This subgroup of the series was found with activity ranging 1.09-7.1 μM . RP07 was found to be the most active compound of the series with activity 1.09 μM . The compound was found to be interacting with residues Val118, Phe126 and Trp541. Presence of fluoro group in compounds RP06 and RP08 resulted in compounds with better activity profile when compared to their corresponding hydrogen substituted ones (RP01 and RP03). But the fluoro substitution was found to be unfavorable for compounds with nitro and hydroxyl substitutions as the compounds were found to be orienting in different manner.

Chlorine was the second choice of substitution among halogens at R¹ resulting in compounds **RP11-15**. The compounds were found with good inhibitory activity ranging 1.17-7.05 μM . Compound RP15 was found to be the second most active compound of the series with activity 1.17 μM . The compound was found to be interacting with Val118 and Phe126. Oxygen from nitro group was found to be interacting with Arg339 and Mg802. Substitution of chlorine can be considered as a favorable one due to the better activity profile of the compounds in the subgroup with an exception of RP12.

Later substitutions attempted were nitro and methoxy moieties over R¹ position which resulted in compounds **RP16-25** with active to moderately active range. Compounds were found with activity in the range of 1.67-5.3 μM . Compound RP25 was found to be the most active compound of the subgroup accounting to hydrophobic interactions imparted by methoxy group and polar interactions involving nitro group with the active site residues. Also nitro group was found to be a suitable substitution as seen in the compounds RP16, 18 and 19. Interaction analysis of these compounds revealed completely opposite orientation of compounds with benzimidazole aligned into the active site. Nitro group of these compounds was found to be interacting with Arg339 and Mg802 with more than one co-ordinate covalent bond attributing to their malate synthase inhibitory activity.

7.1.6. Biophysical characterization analysis

The binding affinity of a compound towards the target is one of the major points to be considered in the aspect of drug design. Hence, in the present study differential scanning fluorimetry experiments have been performed so as to check the binding affinity and stabilization effect of active compounds towards MTB malate synthase. This was measured by comparing the thermal stability of native protein (malate synthase) with that of the protein-ligand mixture. The enzyme and dye concentrations required for the experiment were optimized by varying the concentrations of both. Further, the experiment was carried out in the presence of compound **RP07**.

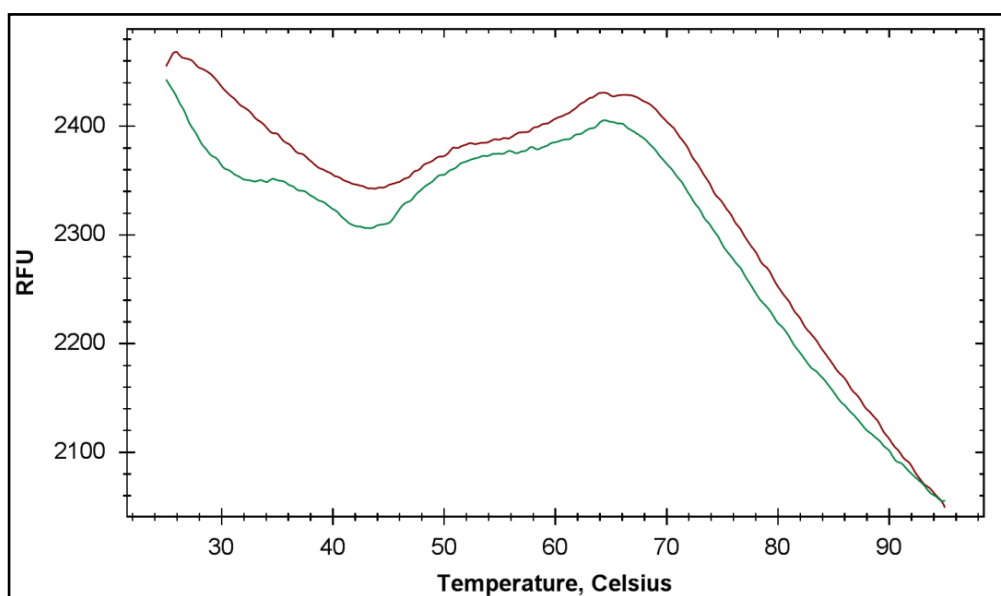


Figure 7.8: DSF experiment for compound **RP07** showing an increase in thermal stability between the recombinant MTB MS protein (pink) and MTB MS protein-ligand complex (green).

Figure 7.8 depicts curves obtained from DSF experiments for protein complexes with compound **RP07**. The positive shift in melting temperature (T_m) for protein-ligand complexes when compared to that of native protein indicates the stability of the complex. Native protein was observed with T_m of 47.2 °C. Protein complexed with compound **RP07** was observed with T_m of 50.9 °C thereby resulting in a positive shift of 3.7 °C in T_m . Compound was found with good stabilization effect over malate synthase thereby correlating to its enzyme inhibitory activity.

7.1.7. Molecular dynamics simulations

Interaction profile of the most active compound RP07 at malate synthase active site is shown in **Figure 7.9**. The compound was found to be involved in hydrogen bonding with residue Val118. Two π - π stacking interactions of the compound were observed with residues Phe126 and Trp541. The top active ligand (RP07) in complex with malate synthase protein was subjected to 20 ns simulation in order to study the protein-ligand interaction stability in dynamic conditions (simulating body conditions) and to generate further theoretical information to support its activity. This ligand-protein complex was simulated explicitly using OPLS_2005 force field in Desmond v3.1.

RMSD analysis for the obtained trajectory was carried out to analyze the stability of protein and ligand in the complex during simulation. **Figure 7.10** shows RMSD for C α atomic positions and heavy atoms for malate synthase-RP07 complex throughout the simulation. An initial jump in RMSD of protein-ligand complex during early stage of simulation may be attributed to the relaxation of protein complex in solvent system. It was observed from the plot; both the C-alpha atoms and heavy atoms of the complex were found to be behaving in similar fashion during simulation with minimal fluctuations.

A simulation of 10 ns was also run for malate synthase in ligand free state and RMSD analysis for all residues is shown in **Figure 7.11**. The plot depicted the highly fluctuating nature of malate synthase in free state. **Figure 7.10** indicated the stabilizing nature of compound **RP07** over malate synthase when compared to protein free state. The root mean square deviation (RMSD) for compound RP07 was analyzed throughout the simulation time period and shown in **Figure 7.12**. The plot illustrates behaviour of the compound in the complex under dynamic conditions. The compound was found to be fluctuating at the initial stages of simulation after which it was found to be equilibrated.

It was observed from the behaviour of both **Figure 7.10** and **7.12**, complex had undergone fluctuations during initial time period after which it was found to be highly stabilized proving the binding affinity of RP07 towards MTB malate synthase and binding stability of complex.

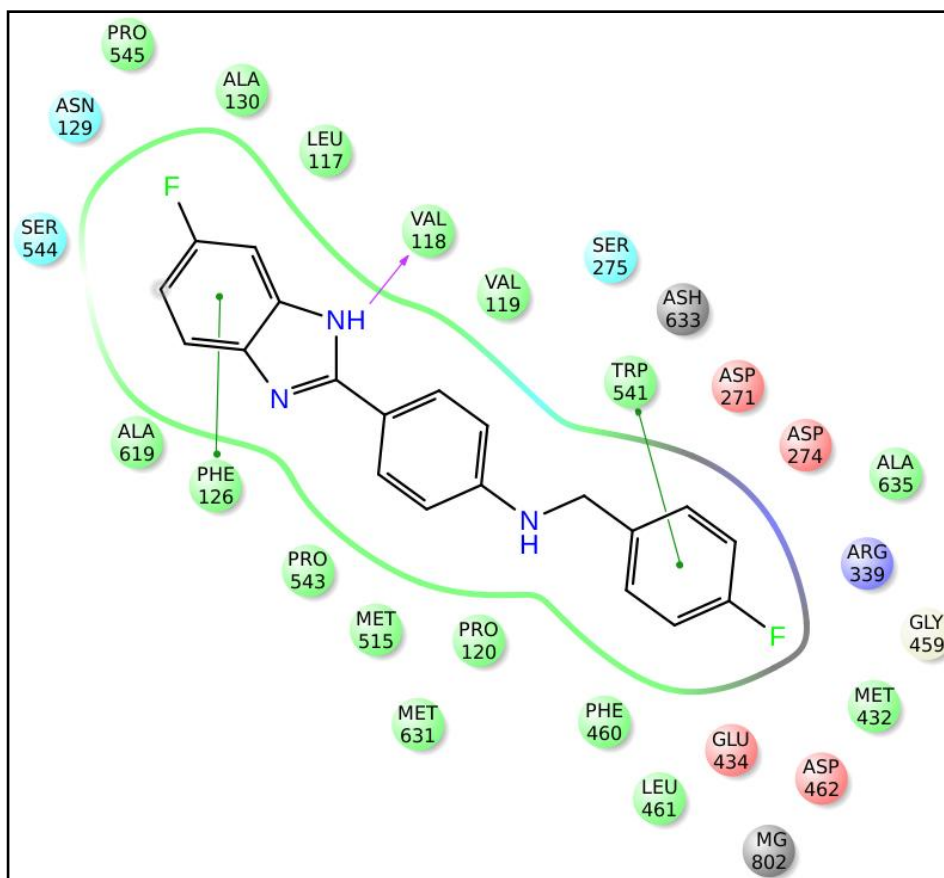


Figure 7.9: Interaction profile of the compound RP07 at malate synthase active site.

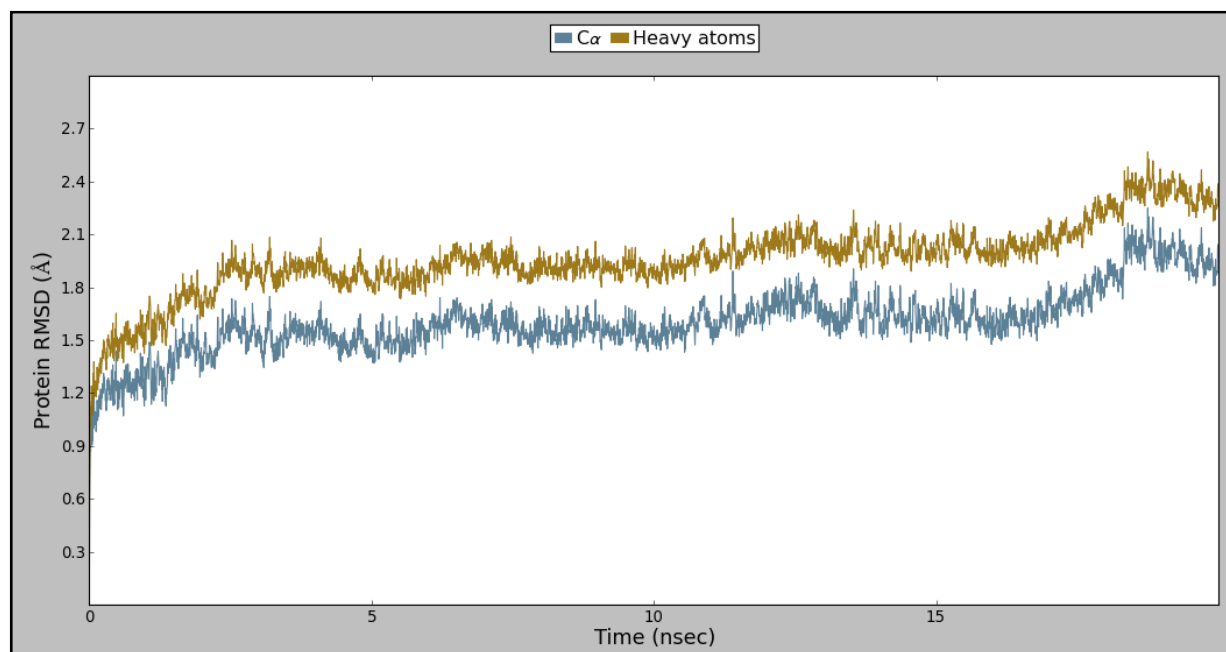


Figure 7.10: RMSD plot of malate synthase in bound state with compound RP07.

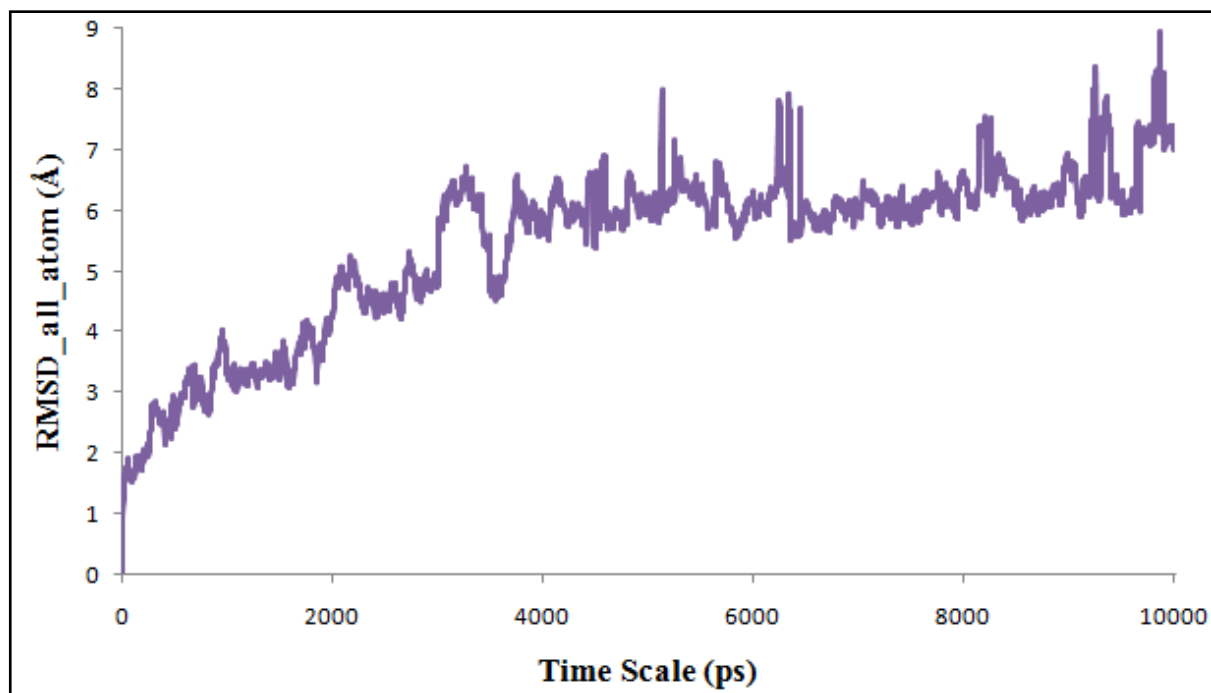


Figure 7.11: RMSD plot of malate synthase in ligand free state.

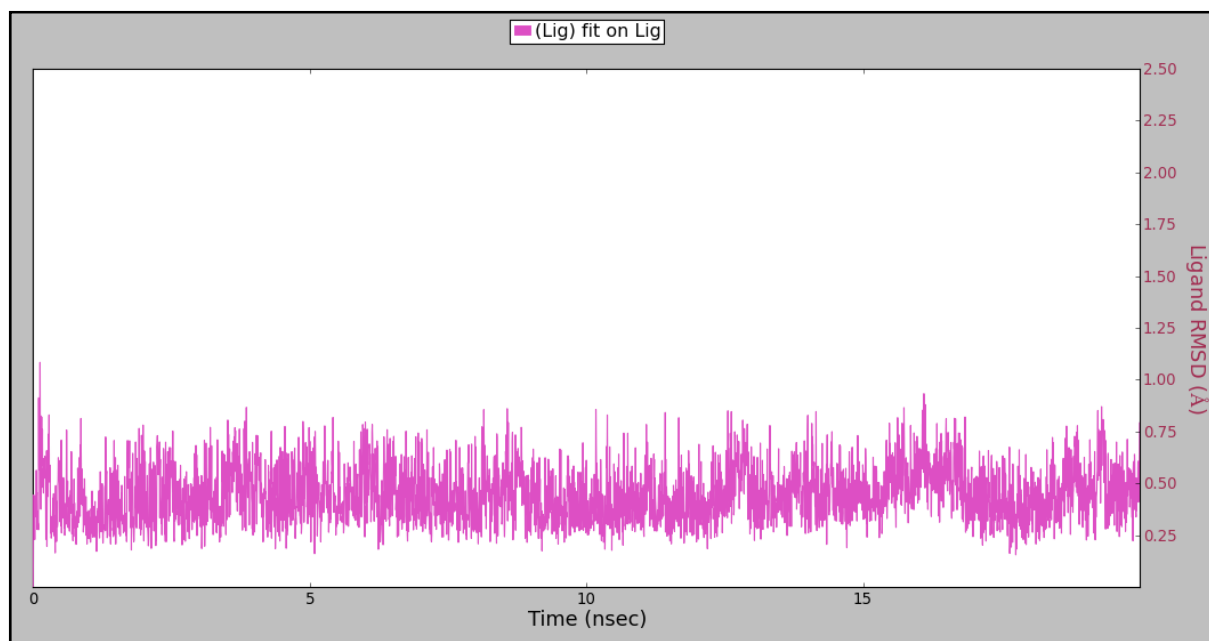


Figure 7.12: RMSD plot of compound **RP07** plotted in complex with malate synthase.

The root mean square fluctuation (RMSF) of protein was analyzed for characterizing local changes along the protein chain during simulation. **Figure 7.13** portrays the RMSF plot for backbone atoms of the protein (green) with respect to their residue index. The plot also

contains the B-factor information of the residues of the protein (red). In this plot, peaks indicate areas of the protein that fluctuate the most during the simulation. Typically, it was observed from the plot that the N- and C- terminals fluctuate more than any other part of the protein. Secondary structure elements like alpha helices (pink shaded) and beta strands (blue shaded) are usually more rigid than the unstructured part of the protein, and thus fluctuate lesser than the loop regions. Protein residues that interact with the ligand are marked with green colored vertical bars. From the plot, it was observed that most of the active site residues were stable with lesser fluctuations. It was also observed that the active site residues interacting with compound **RP07** were stable. The major peaks represent highly fluctuating residues and were observed to fall into the loop regions.

Considering the RMSF for the compound RP07 during the simulation, a plot was plotted for each atom of the ligand with respect to their fluctuation considered throughout the simulation time period and shown in **Figure 7.14**. It was observed that the atoms to both the extremes of the compound were found to be fluctuating while the linker between them was found to be highly stable. The terminal benzimidazole moiety (atoms 1-8) was found to be towards the solvent which was found to fluctuate more. The other terminal of the compound, *para*-fluoro phenyl group (atom 18-25) was found to be aligned into the active site pocket of malate synthase where the moiety was found to fluctuate within the available space. The N-methyl aniline linker between the two terminals was found to be stable with least fluctuations. This part of RP07 was found to interact with the residues Trp541 and Met631 lining the active site.

The torsion angle analysis of the compound RP07 during the simulation time period was carried out to understand the torsional stress undergone by each rotatable bond at the malate synthase active site. The ligand torsions plot summarizes the conformational evolution of every rotatable bond (RB) in the ligand throughout the simulation trajectory (0.00 through 20.00 nsec). **Figure 7.15** shows the 2D schematic of a ligand with color-coded rotatable bonds. Torsion plot for each bond is represented by a dial plot and bar plots of the same color. Dial (or radial) plots portray the conformation of the torsion throughout the course of the simulation. The centre of the radial plot was found to be beginning of the simulation which with time evolution was plotted radially outwards. The bar plots summarize the data on the dial plots, by showing the probability density of the torsion (**Figure 7.15**).

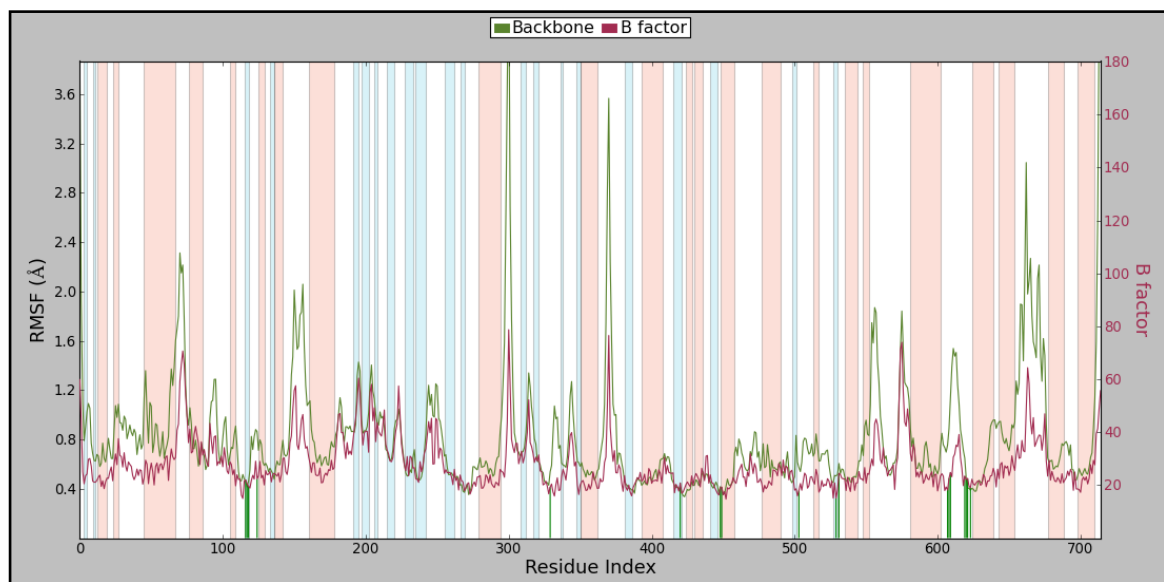


Figure 7.13: RMSF plot for backbone atoms of MS-RP07 complex. Green and red plots indicate backbone RMSF and B factor of residues. Red and blue shaded regions represent α -helix and β -sheet regions of protein. Green vertical lines indicate residues interacting with RP07.

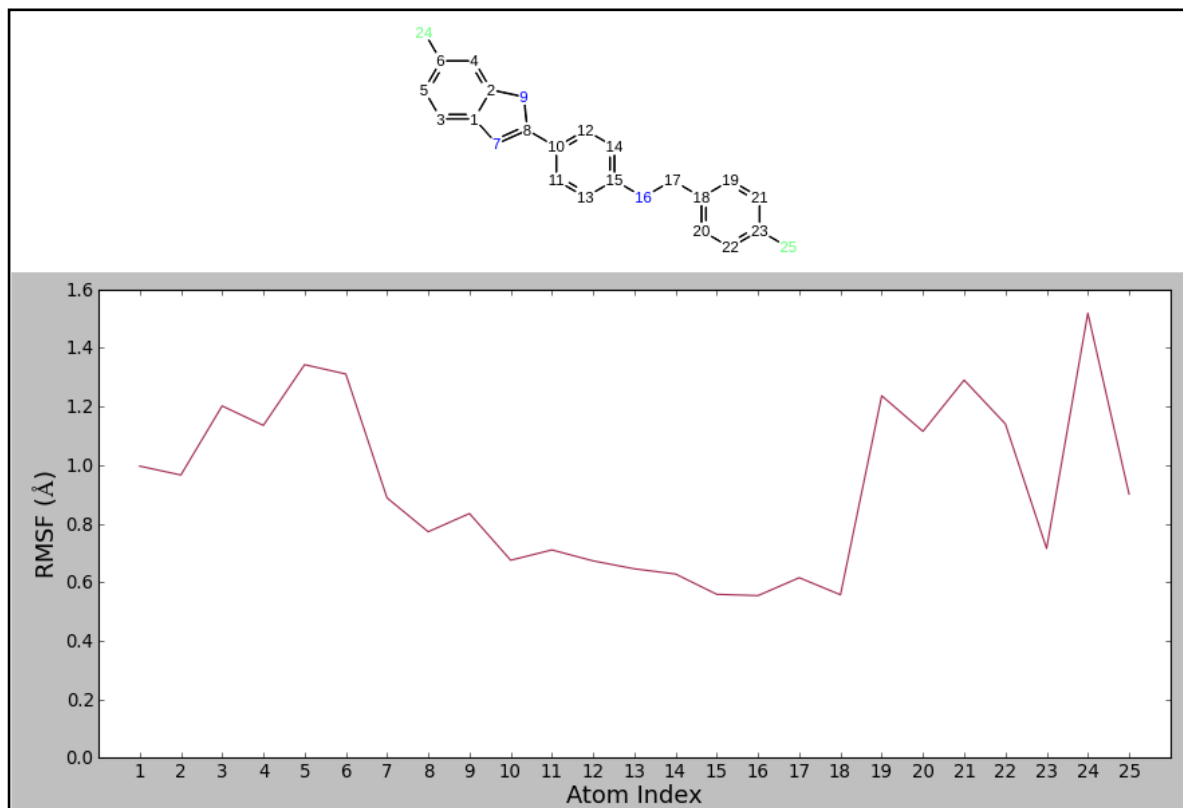


Figure 7.14: RMSF plot for the compound RP07 with respect to its each atom during simulation.

The values of the potential are on the left Y-axis of the chart, and are expressed in kcal.mol⁻¹. Looking at the histogram and torsion potential relationships give the insights into the conformational strain the ligand undergoes to maintain a protein-bound conformation.

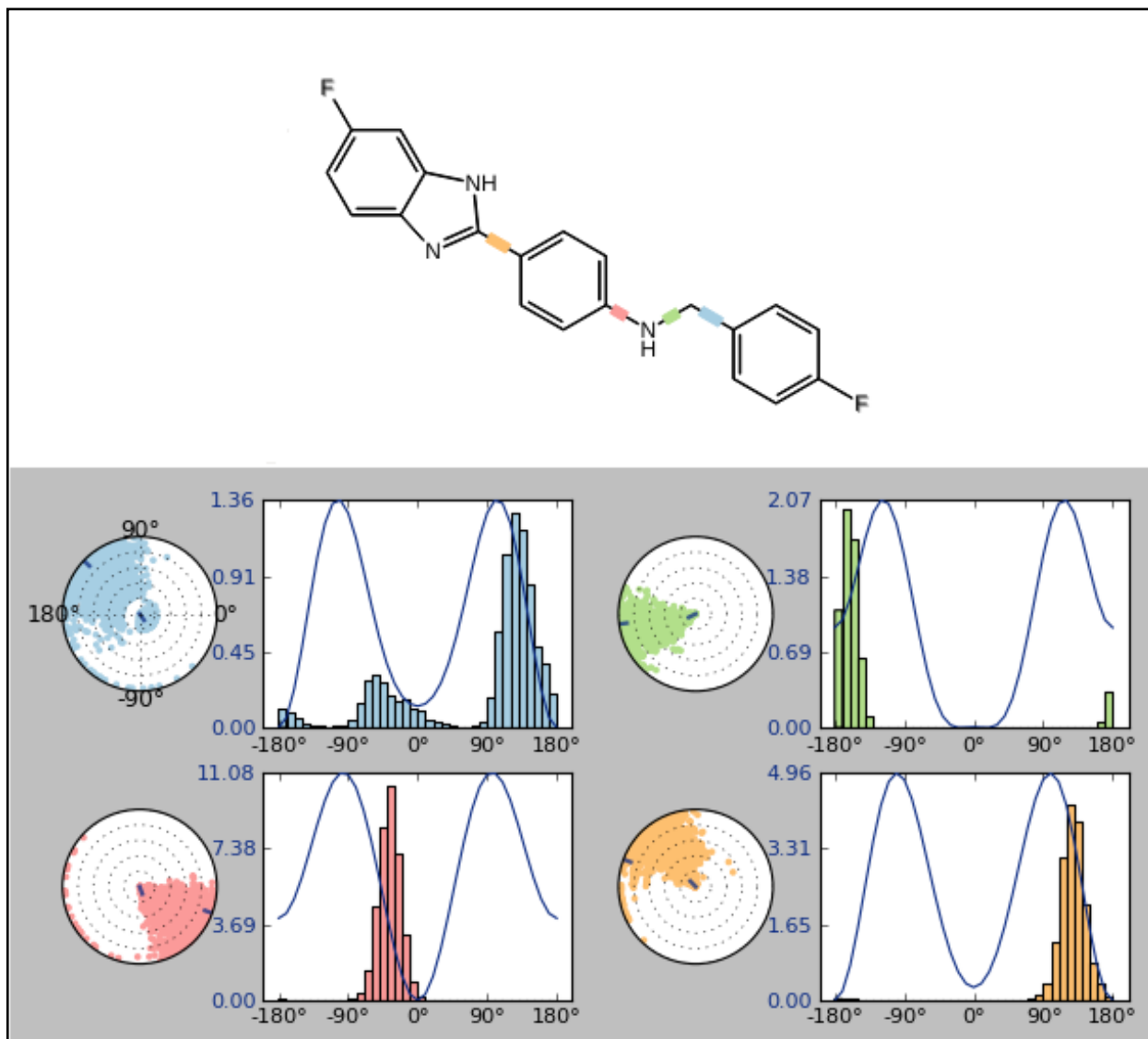


Figure 7.15: The 2D representation of the compound RP07 shows the rotatable bonds of the compound with different color scheme. Torsion angle and torsion potential plotted for each rotatable bond of compound RP07 are shown in radial and bar plot respectively.

Of all torsion analysis plots plotted for four rotatable bonds of the compound RP07, bond between the terminal *para*-fluoro phenyl and methyl group, represented by blue color, was found to undergo more torsional strain to place the compound in stable orientation. This

observation was also supported by high fluctuation of atoms 18-23 in **Figure 7.14**. This fluctuation of *para*-fluoro phenyl moiety may be attributed to the availability of free space in the binding pocket of malate synthase, where the moiety was found to be oriented deep inside the pocket. The remaining three bonds were found to undergo similar torsional strain represent by pink, green and orange colors. The high torsional stress over the rotatable bond between benzimidazole and phenyl moiety (orange colored) was also found to be supported by fluctuating nature of benzimidazole during simulation (atoms 1-8) from **Figure 7.14**. This may be attributed to the orientation of benzimidazole moiety towards the solvent at the entrance of the active site pocket of malate synthase, which offers much space for alignment.

7.1.7.1. Simulation interaction analysis

Interaction profile of compound RP07 at the active site of malate synthase is shown in **Figure 7.16** with the percentage strength of each interaction. It was found that Val118 was the main residue involved in hydrogen bond interaction with about 87% strength with RP07. Also compound was seen to be involved in water mediated interaction with Val118. RP07 was also found involved in π - π stacking interactions with residues Phe460 and Trp541 with strengths of 11% and 47% respectively.

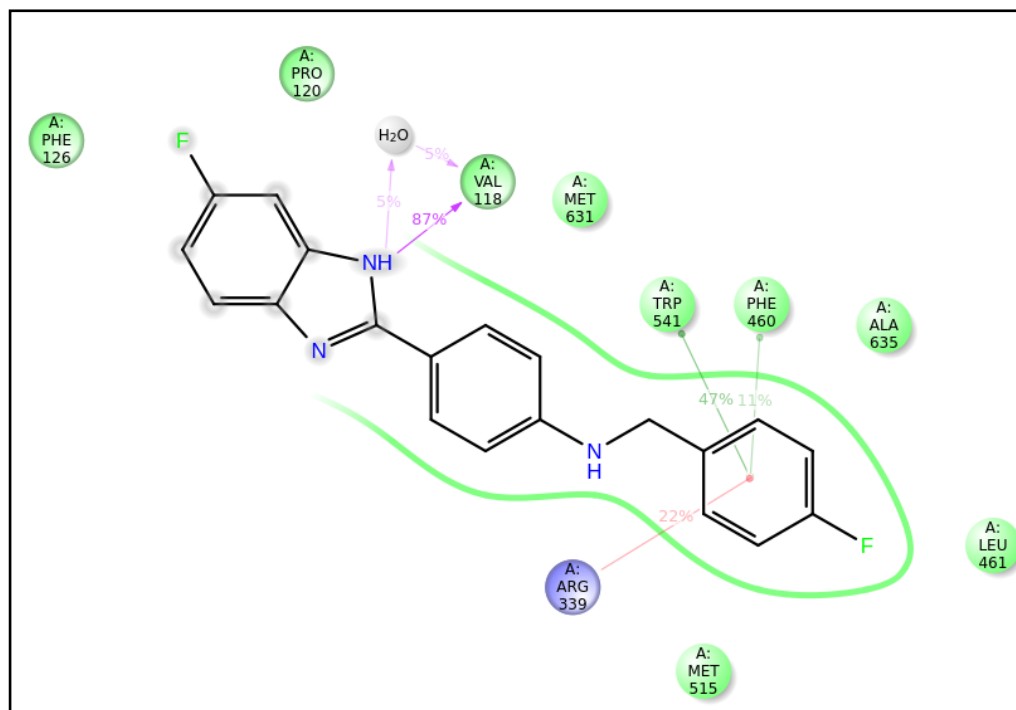


Figure 7.16: Interaction profile of the compound RP07 with malate synthase displaying strength of each interaction.

These interactions were found between *para*-fluoro phenyl of RP07 and phenyl and indole rings of Phe460 and Trp541 respectively. Compound RP07 was also involved in cation- π interaction with Arg339 with about 22% strength analyzed over the simulation time period.

The top panel of the **Figure 7.17** shows the total number of specific contacts the ligand makes with the protein over the course of simulation. The contacts here are categorized into four types: hydrogen bonds, hydrophobic, ionic and water bridges. It was observed RP07 interacted with malate synthase with at least 3-6 interactions throughout the simulation which altered to a maximum of 9 contacts at some particular simulation time points.

Bottom panel of the figure depicts residues interacting with RP07 in a particular time frame. Some residues make more than one specific contact with the ligand, which is represented by a darker shade of orange, according to scale on the right side of plot. From the bottom panel of **Figure 7.16**, it was observed that residues Val118, Phe460, Trp541, Met641 and Ala635 were constantly interacting with RP07 with more than one contact throughout the simulation.

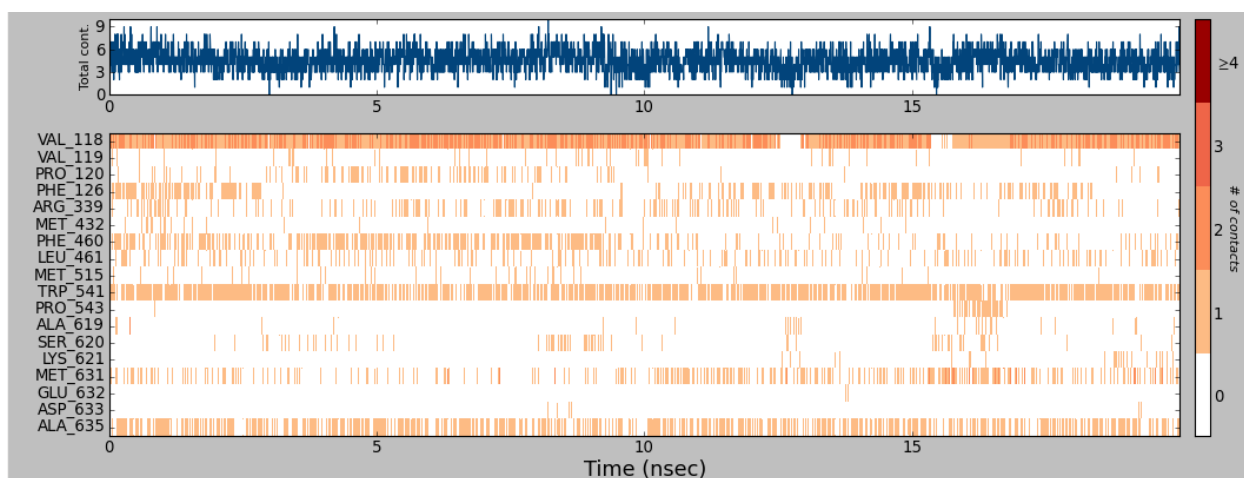


Figure 7.17: Timeline representation of the interactions and contacts (**H-bonds, Hydrophobic, Ionic, Water bridges**) between the compound RP07 and malate synthase. The top panel shows the total number of specific contacts between MTB MS with compound RP07 over the course of the trajectory. The bottom panel shows residues interacting with the ligand in each frame.

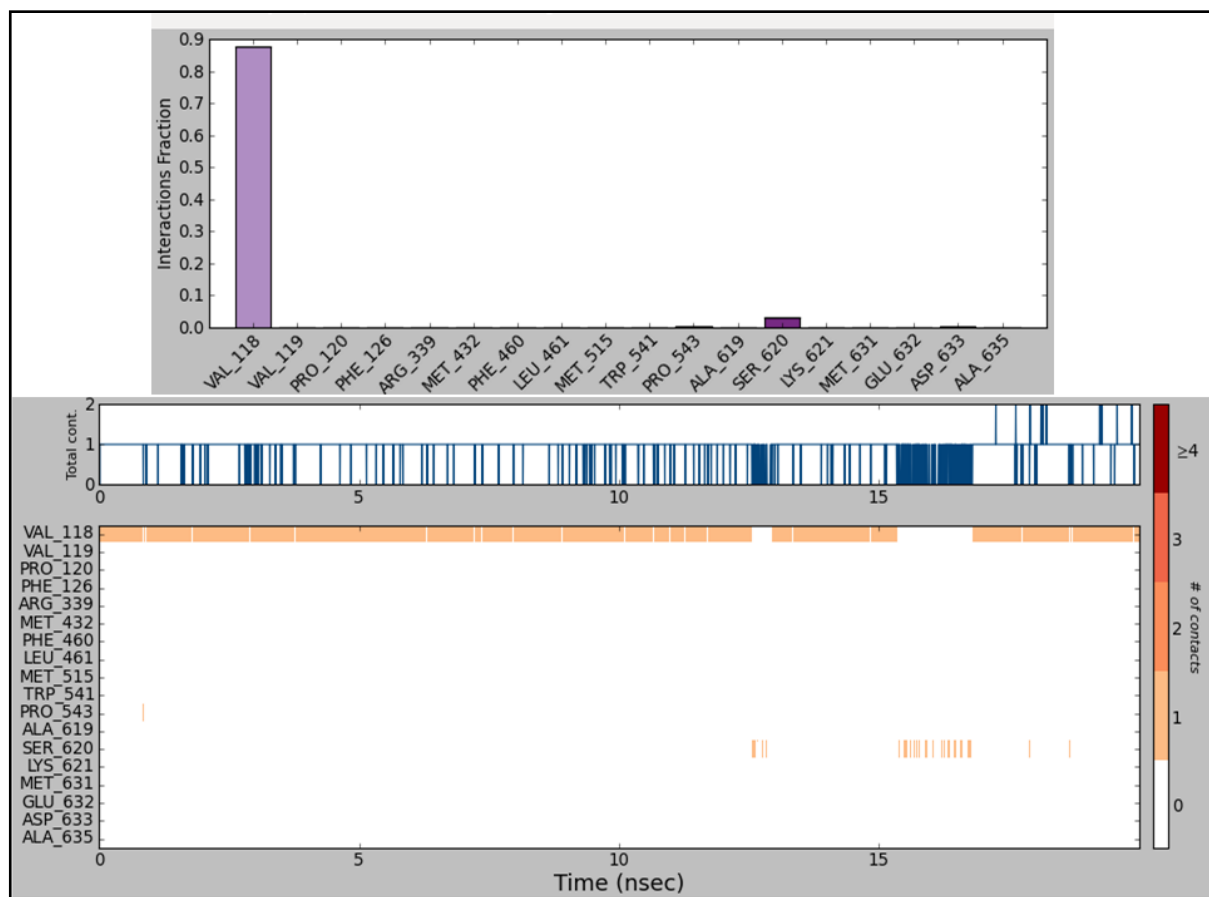


Figure 7.18: Top panel of the figure shows the residues of malate synthase involved in hydrogen bonding with compound RP07. The stacked bar plots indicate the strength of the bond during the simulation time period. The bottom panel shows hydrogen bonding residues interacting with the ligand in each frame.

The hydrogen bond analysis for malate synthase-RP07 complex revealed the presence of hydrogen bond between Val118 and RP07. From the bar plot of **Figure 7.18**, it was understood the strength of Val118 was nearly 90% accounting to the presence of two hydrogen bonds between the carbonyl oxygen of Val118 and hydrogen of amine group (of benzimidazole moiety). In the bottom plot of **Figure 7.18**, hydrogen bonding of residues with the compound in each trajectory was plotted. The hydrogen bonding with Val118 was observed to be strong enough to hold the compound at the malate synthase active site throughout the simulation. Another hydrogen bond was also observed between RP07 and Ser620 which was observed to retain only for a small time period.

The hydrophobic interactions were found to be one of the key interactions at the malate

synthase active site with RP07. The hydrophobic interaction analysis for the complex is given in **Figure 7.19**. From the figure, it was observed that majority of MS active site residues were found involved in hydrophobic interactions with RP07 during the simulation. Of all, interaction between the compound RP07 and Trp541 was found to be the strongest with interaction strength of nearly 75%. The type of interaction with Trp541 was found to be π - π stacking between indole moiety of tryptophan and terminal phenyl group of RP07. Also, it was found that RP07 possessed strong hydrophobic interactions with residues Ala635 and Val118 with almost 60% and 48% respectively. Some other residues involved in hydrophobic interactions were Phe126, Arg339 and Leu461. These hydrophobic interactions were found to be observed throughout the simulation, as seen from the bottom panel of **Figure 7.19**, accounting for the stable malate synthase-RP07 complex.

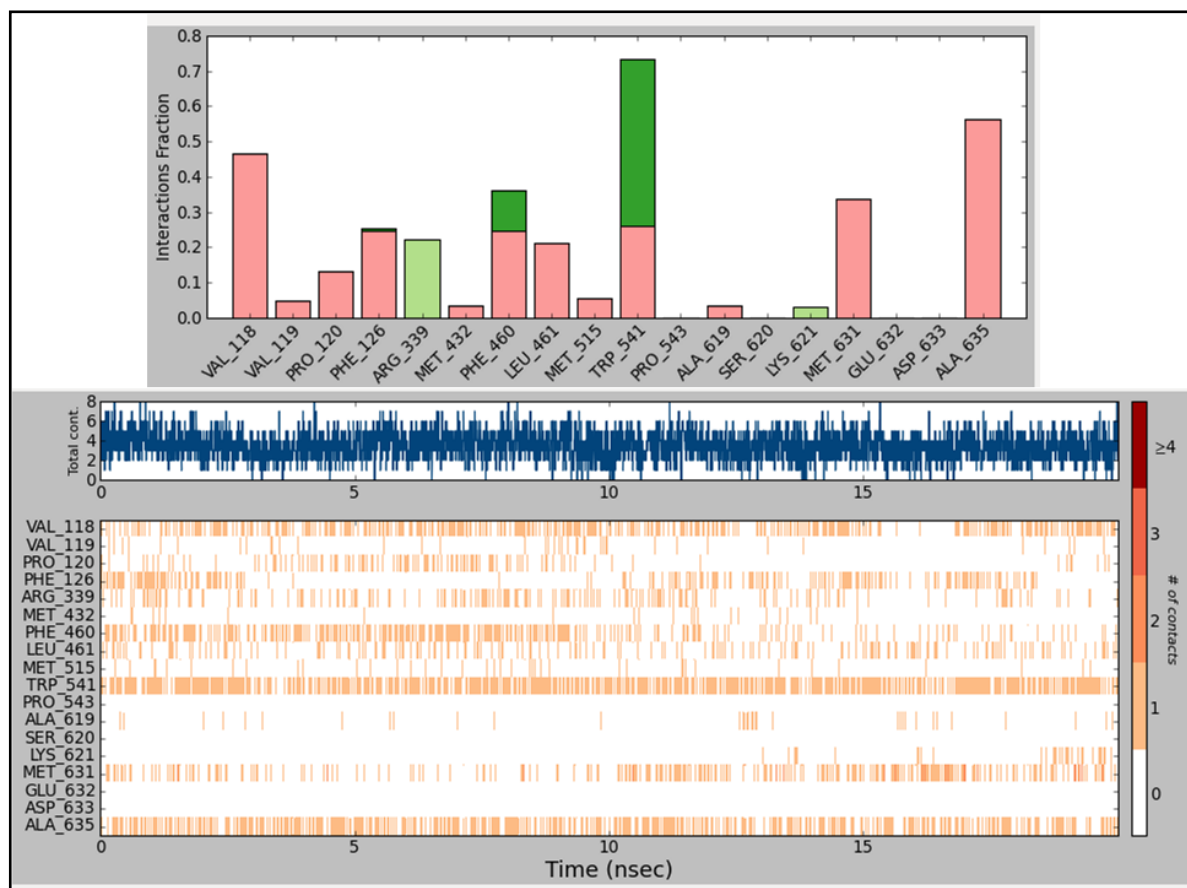


Figure 7.19: Top panel of the figure shows the residues of malate synthase involved in hydrophobic interactions with compound RP07. The stacked bar plots indicate the strength of the bond during the simulation time period. The bottom panel shows residues interacting with the ligand in each frame.

Water mediated hydrogen bonding between the active site residues of malate synthase and compound RP07 was analyzed and given in **Figure 7.20**. The interactions were majorly observed between RP07 and residues Val118, Pro543 and Ser620. Other lesser strength interactions of RO07 were found with residues Ala619, Glu632 and Asp633. These interactions were found to be present at some simulation time periods, disruption of which may be explained by dynamic conditions undergone by the complex during simulation.

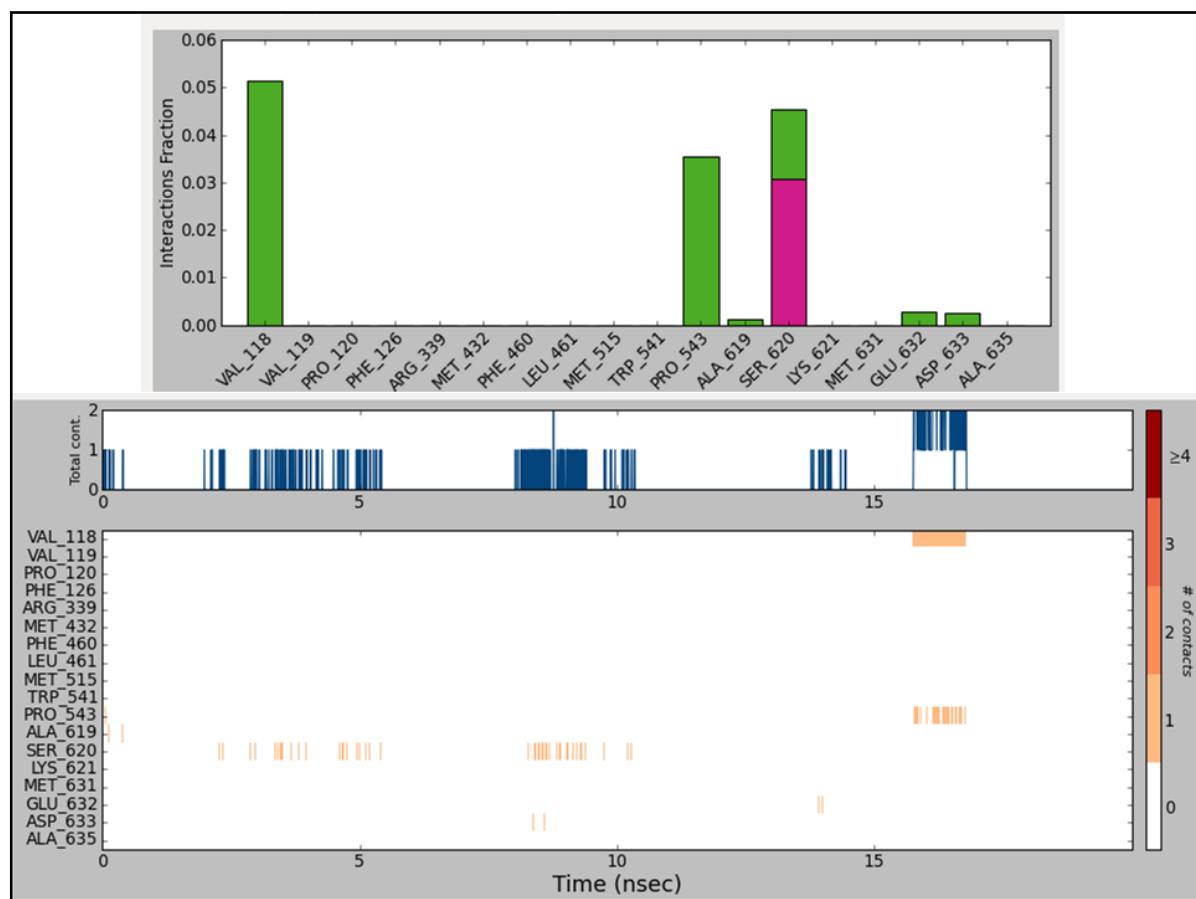


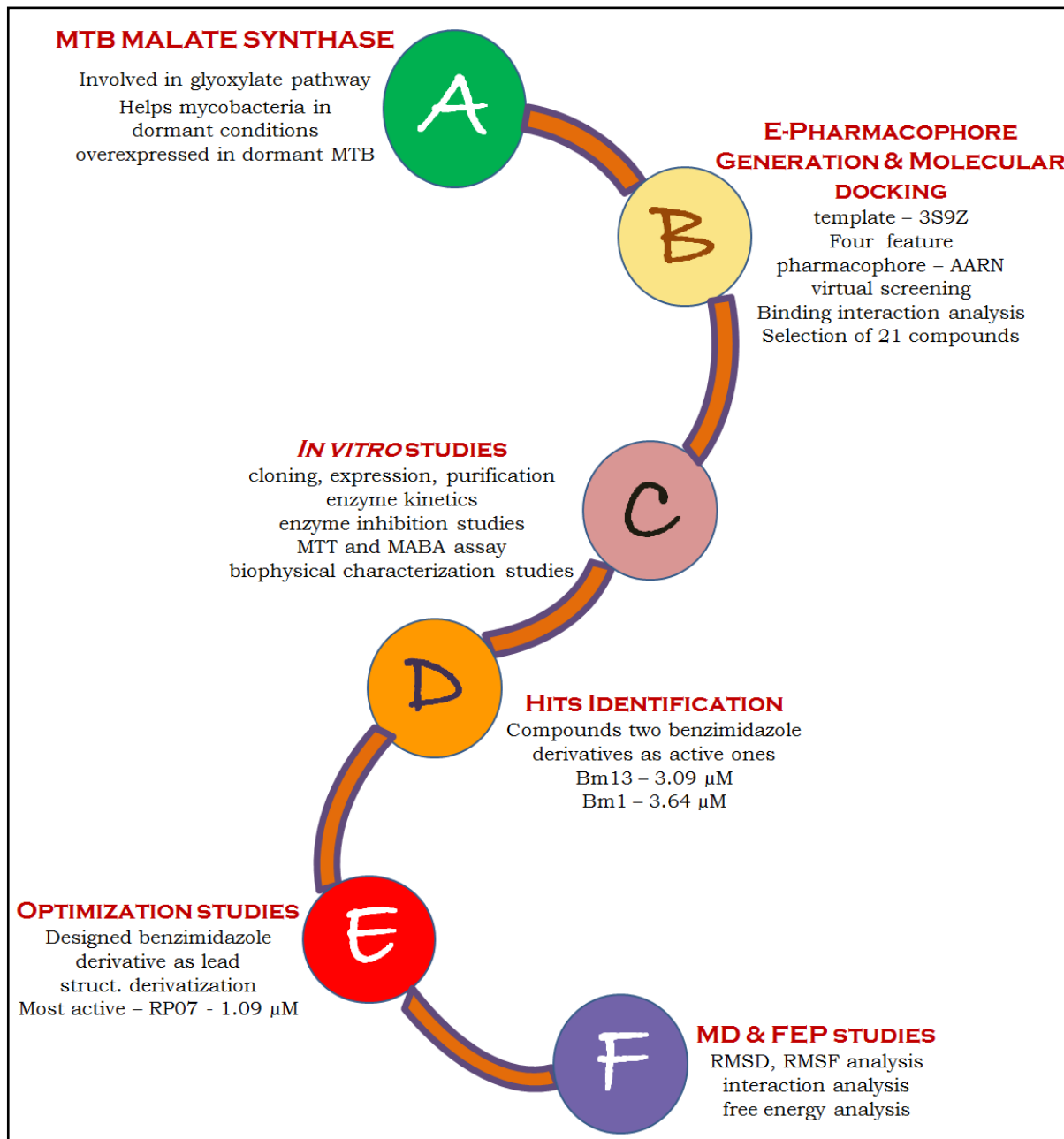
Figure 7.20: Top panel of the figure shows the residues of malate synthase involved in water mediated hydrogen bonding with compound RP07. The stacked bar plots indicate the strength of the bond during the simulation time period. The bottom panel shows residues interacting via water bridge interactions with the ligand in each frame.

7.1.8. Highlights of the study

In the present study, energy optimized pharmacophore was developed based on crystal ligand, 4-(2-bromophenyl)-2,4-dioxobutanoic acid, co-crystallized with malate synthase with PDB code 3S9Z. This model consisting of four chemical features i.e. two hydrogen bond acceptors

(A1, A2), one negative potential (N4) and one ring features (R5) was used as query for screening asinex database and BIT in-house database which led to the selection of 21 compounds as potent *M. tuberculosis* hits based on the glide score, fitness and interaction profile. *In vitro* enzymatic inhibition studies were performed for these 21 hits, of which compounds **Bm13** and **Bm1** from BITS database were found to be top active with 3.09 μM and 3.64 μM inhibitory activities respectively. The benzimidazole derivatives, compound **Bm1** and compound **Bm13** were identified and optimized to generate a chemical library of 25 compounds. Of these 25, compound **RP07** was identified as the most active malate synthase inhibitor with IC_{50} of **1.09 μM** . The behavior of malate synthase-RP07 complex under dynamic conditions was analyzed using molecular dynamics studies which provided many insights into the ligand binding stability over protein. Thus, the overall analysis suggested that the structure based e-pharmacophore model may provided useful information required for proper understanding of the important structural and physicochemical features for designing novel *M. tuberculosis* malate synthase inhibitors.

Overview of malate synthase work



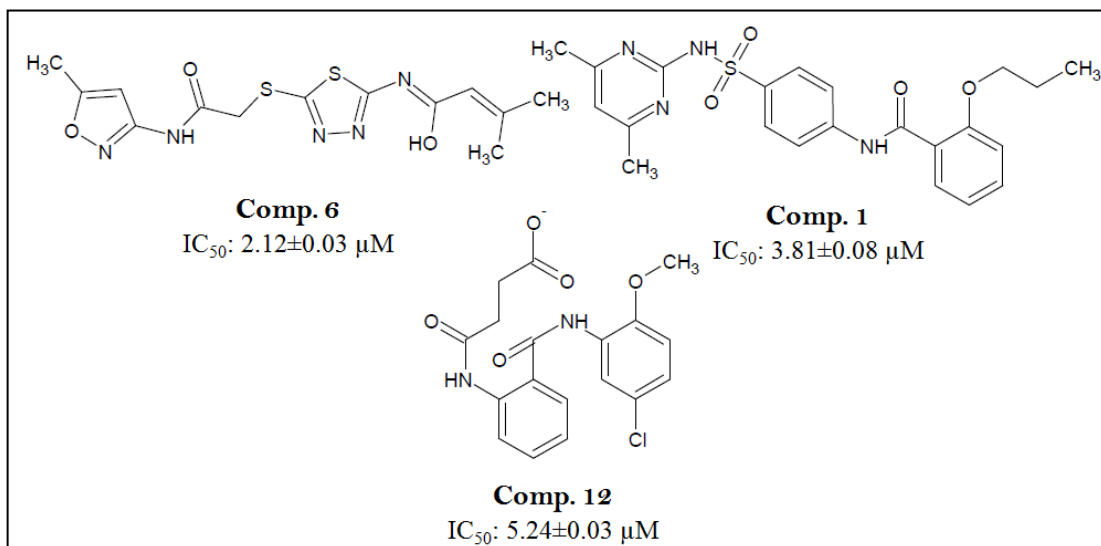
Chapter 8

RECAPITULATION AND CONCLUSION

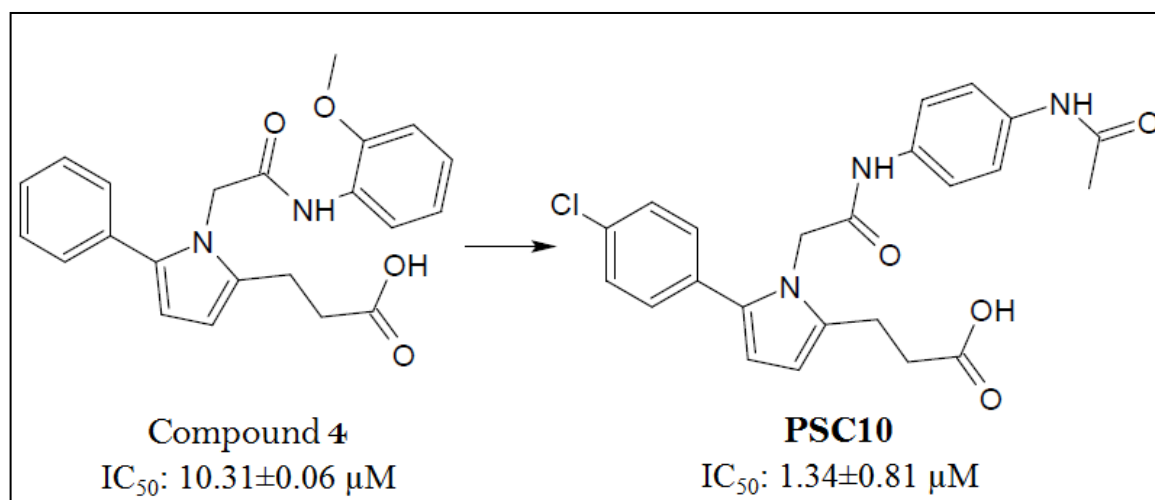
As there is an urgent need of antitubercular drugs for current global population, development of new drugs is of main importance. Based on biological investigation and literature report, glutamine synthetase, glutamate racemase and malate synthase were found to be important targets for the treatment of MTB infection in both active and dormant model (targeting MS). Thus, the present study focused on the design of novel inhibitors targeting these proteins.

8.1. Development of mycobacterial glutamine synthetase inhibitors

In summary, employing an e-pharmacophore based high throughput virtual screening protocol against MTB glutamine synthetase using a compound library comprising 5,00,000 compounds, we successfully identified a novel compound, (1Z)-3-methyl-N-[5-({2-[(5-methylisoxazol-3-yl)amino]-2-oxoethyl}sulfanyl)-1,3,4-thiadiazol-2-yl]but-2-enimidic acid (compound **6**) as MTB glutamine synthetase inhibitor with an IC_{50} of 2.12 μ M against glutamine synthetase. Also compounds **1** and **12** were identified with IC_{50} of 3.81 μ M and 5.24 μ M. Further, the theoretical binding stability of the compound with GS protein was analyzed using simulation experiments.



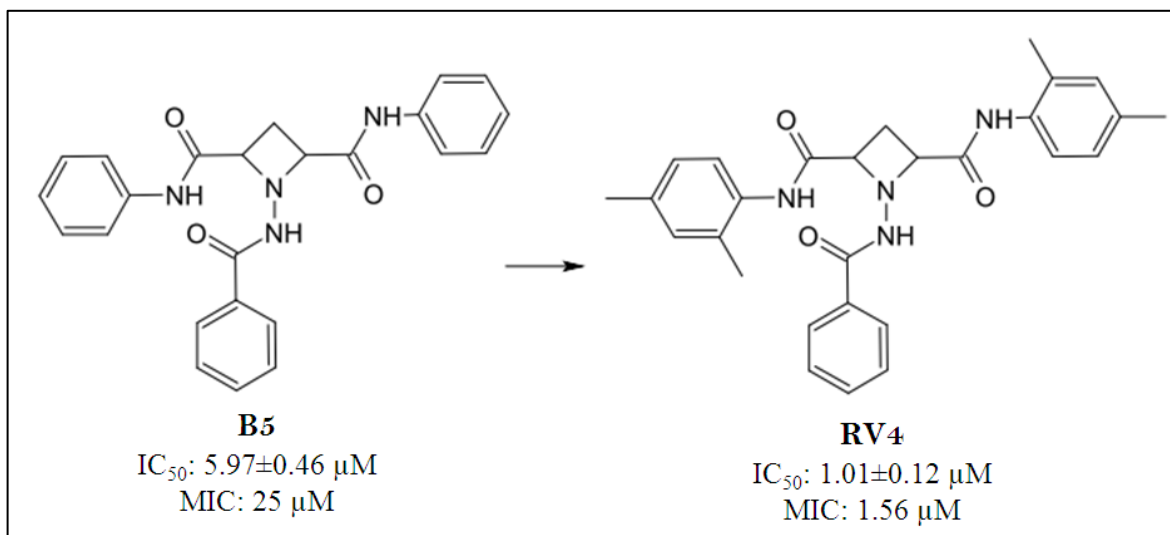
The biophysical characterization was evaluated using differential scanning fluorimetry experiments and theoretical binding energy calculations were performed using FEP studies. Also compound, 3-(1-(2-[(2-methoxyphenyl)amino]-2-oxoethyl)-5-phenyl-1*H*-pyrrol-2-yl)propanoic acid (compound 4; IC_{50} – 10.31 μ M), was identified as lead. Structural optimization of this compound resulted in a series of 40 compounds and evaluated for their biological activity. Compound **PSC10** emerged as the most potent MTB GS inhibitor with the GS inhibitory IC_{50} of **1.34 μ M**. The compounds were found to be inactive against MTB H37Rv strain when tested using MABA assay.



8.2. Development of mycobacterial glutamate racemase inhibitors

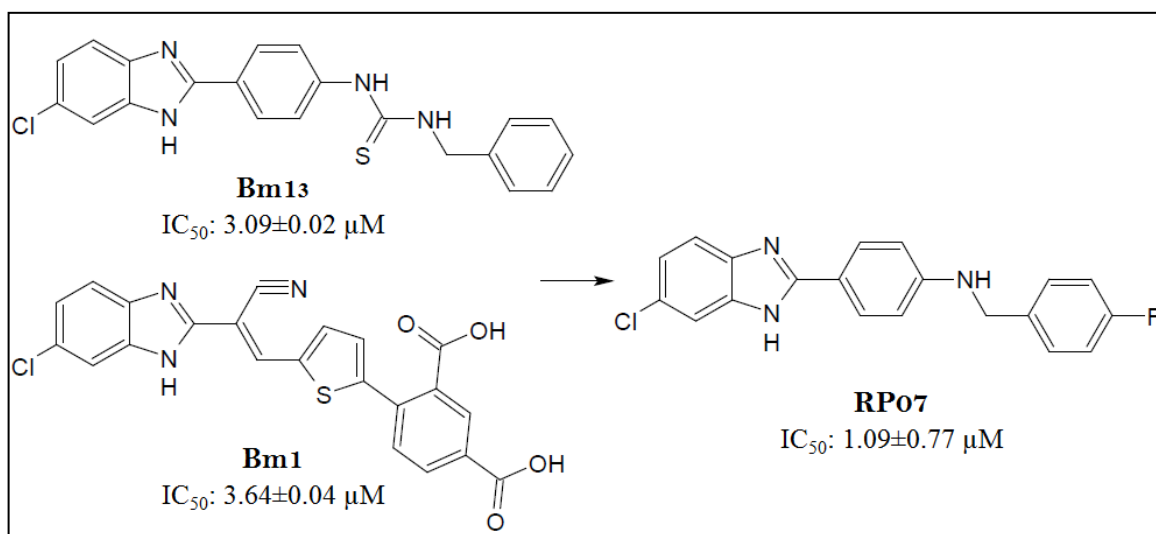
In the case of glutamate racemase, absence of crystal structure provoked us to develop a three dimensional protein structure for the protein using homology modelling. The model was well validated using ramachandran plot and molecular dynamics simulations. The protein model was then employed for virtual screening against the available BITS in-house database which identified 1-(benzamido)- N^2,N^4 -diphenylazetididine-2,4-dicarboxamide (B5) as novel lead against MurI.

The optimization of B5 compound resulted in compound **RV4** with an IC_{50} of **1.01 μ M** and minimum inhibitory concentration of 1.56 μ M against MTB H37Rv strain culture. The further binding affinity of compound **RV4** towards glutamate racemase was analyzed by using differential scanning fluorimetry studies and theoretical studies using molecular dynamics simulations.



8.3. Development of mycobacterial malate synthase inhibitors

In case of malate synthase, a similar protocol as applied for glutamine synthetase was followed. We successfully identified benzimidazole as a novel scaffold which inhibits malate synthase as found from compounds **Bm1** and **Bm13** with IC_{50} s $3.09 \mu\text{M}$ and $3.64 \mu\text{M}$. Based on the identified leads, a series of 25 compounds have been derivatized using synthetic approach and evaluated using biological approaches. Further, in order to confirm the binding of ligand to the protein, differential scanning fluorimetry experiments were performed. Compound **RP07** emerged as the most potent novel MTB malate synthase inhibitors with the inhibitory concentration of $1.09 \mu\text{M}$. The binding stability of complex was analyzed employing molecular dynamics simulations which showed the malate synthase-RP07 complex to be highly stable.



In conclusion, the class of compounds described here are the most promising lead compounds for further optimization and development to yield novel drugs for fast growing bacterial infections and dormant mycobacteria. The study also provides the basis for further chemical and biological optimization of these potent inhibitors as potential antitubercular agents.

FUTURE PERSPECTIVES

Glutamine synthetase and glutamate racemase are some of the crucial enzymes required in the cell wall synthesis of mycobacteria which make them attractive targets for development of antitubercular drugs. The other target, malate synthase, is involved in the survival of mycobacteria in dormant/latent conditions within the host system. This protein serves as an attractive target for development of drugs against dormant form of MTB. The two targets, glutamate racemase and malate synthase, are absent in humans but essential MTB thereby serving as potential targets for the development of novel antimycobacterial compounds. The present study focused on utilizing the pharmaceutically underexplored proteins of MTB as potential antitubercular targets for design and development of effective drugs against tuberculosis, thus offering an excellent opportunity to address the ever increasing problem of mycobacterial resistance.

The study describes the development of chemically diverse series of molecules each for identification of inhibitors against respective target. The compounds reported here displayed considerable *in vitro* enzyme efficacy. The inhibitors identified against glutamine synthetase need to be further optimized as their antimycobacterial potency was observed to be very low. Some compounds against MurI showed satisfactory enzyme inhibitory activity and better bactericidal profile against *M. tuberculosis* H37Rv strain. The compounds are further needed to be studied for macrophage assay and *in vivo* zebra fish studies to acquire a clear picture about their inhibitory profiles. In case of malate synthase, the identified active inhibitors are needed to be evaluated against dormant forms of MTB in order to study their antimycobacterial efficacy as malate synthase is one of the crucial enzymes which over expresses in dormant forms of MTB. Although these results are encouraging, lead optimization is needed to build in an efficient pharmacokinetic and pharmacodynamic profile and to achieve an adequate safety profile to ensure that the dose to man would be in an acceptable range.

The advancement of any of the candidate compounds presented in this thesis along a drug development path would require a significant investigation in medicinal chemistry, preclinical and clinical studies.

BIBLIOGRAPHY

Asselineau J., Lederer E. Structure of the mycolic acids of mycobacteria. *Nature*. **1950**, 166, 782–783.

Andrec M., Harano Y., Jacobson M.P., Friesner R.A., Levy R.M. Complete protein structure determination using backbone residual dipolar couplings and sidechain rotamer prediction. *J. of Struc. Func. Gen.* **2002**, 2, 103-111.

Ashiuchi M., Kuwana E., Komatsu K., Soda K., Misono H. Differences in effects on DNA gyrase activity between two glutamate racemases of *Bacillus subtilis*, the poly-gamma-glutamate synthesis-linking Glr enzyme and the YrpC (MurI) isozyme. *FEMS. Microbiol. Lett.* **2003**, 223, 221–225.

Andries K., Verhasselt P., Guillemont J., Göhlmann H.W., Neefs J.M., Winkler H., Van Gestel J., Timmerman P., Zhu M., Lee E., Williams P., de Chaffoy D., Huitric E., Hoffner S., Cambau E., Truffot-Pernot C., Lounis N., Jarlier V. A diarylquinoline drug active on the ATP synthase of *Mycobacterium tuberculosis*. *Science*, **2005**, 307, 223-227.

Anstrom D.M., Remington S.J. The product complex of *M. tuberculosis* malate synthase revisited. *Protein. Sci.* **2006**, 15, 2002-2007.

ASINEX, ASINEX Platinum and Gold Collection, ASINECorp, Winston-Salem, NC, USA.

Banks J.L., Beard H.S., Cao Y., Cho A.E., Damm W., Farid R., Felts A.K., Halgren T.A., Mainz D.T., Maple J.R., Murphy R., Philipp D.M., Repasky M.P., Zhang L.Y., Berne B.J., Friesner R.A., Gallicchio E., Levy R.M. Integrated Modeling Program, Applied Chemical Theory (IMPACT). *J. Comp. Chem.* **2005**, 26, 1752-1759.

Beard H., Cholleti A., Pearlman D., Sherman W., Loving K.A. Applying physics-based scoring

- to calculate free energies of binding for single amino acid mutations in protein-protein complexes. *PLoS. One.* **2013**, 8, e82849.
- Bennett J.E, Dolin R, Blaser M.J. Mandell, Douglas, and Bennett's principles and practice of infectious diseases. *Elsevier Health Sciences.* **2014**.
- Benson T.E., Walsh C.T., Hogle J.M. The structure of the substrate-free form of MurB, an essential enzyme for the synthesis of bacterial cell walls. *Structure.* **1996**, 4, 47-54.
- Bernstein J., Lott W.A., Steinberg B.A., Yale H.L. Chemotherapy of experimental tuberculosis. Isonicotinic acid hydrazide (Nydrazid) and related compounds, *Am. Rev. Tuberc.* **1952**, 65, 357-364.
- Betts J.C., Lukey P.T., Robb L.C., McAdam R.A., Duncan K. Evaluation of a nutrient starvation model of *Mycobacterium tuberculosis* persistence by gene and protein expression profiling. *Mol. Microbiol.* **2002**, 43, 717-731.
- Binda G., Domenichini E., Gottardi A., Orlandi B., Ortelli E., Pacini B., Fowst G. Rifampicin, a general review. *Arzneimittelforschung.* **1971**, 12, 1907-1977.
- Bloch H., Segal W. Biochemical differentiation of *Mycobacterium tuberculosis* grown *in vivo* and *in vitro*. *J. Bacteriol.* **1956**, 72, 132-141.
- Boshoff H.I., Myers T.G., Copp B.R., McNeil M.R., Wilson M.A., Barry C.E. The transcriptional responses of *Mycobacterium tuberculosis* to inhibitors of metabolism: novel insights into drug mechanisms of action. *J. Biol. Chem.* **2004**, 279, 40174-40184.
- Brennan P.J. Structure, function, and biogenesis of the cell wall of *Mycobacterium tuberculosis*. *Tuberculosis.* **2003**, 83, 91-97.
- Carroll P., Waddell S.J., Butcher P.D., Parish T. Methionine sulfoximine resistance in

- Mycobacterium tuberculosis* is due to a single nucleotide deletion resulting in increased expression of the major glutamine synthetase, GlnA1. *Microb. Drug. Resist.* **2011**, 17, 351-355.
- Chandra H., Basir S.F., Gupta M., Banerjee N. Glutamine synthetase encoded by glnA-1 is necessary for cell wall resistance and pathogenicity of *Mycobacterium bovis*. *Microbiol.* **2010**, 156, 3669-3677.
- Clark-Curtiss J.E, Haydel S.E. Molecular genetics of *Mycobacterium tuberculosis* pathogenesis. *Annu. Rev. Microbiol.* **2003**, 57, 517-549.
- Clemens D.L., Horwitz M.A. The *Mycobacterium tuberculosis* phagosome interacts with early endosomes and is accessible to exogenously administered transferrin. *J. Exp. Med.* **1996**, 184, 1349–1355.
- Cole S.T., Brosch R., Parkhill J., Garnier T., Churcher C., Harris D., Gordon S.V., Eiglmeier K., Gas S., Barry C.E., Tekaiia F., Badcock K., Basham D., Brown D., Chillingworth T., Connor R., Davies R., Devlin K., Feltwell T., Gentles S., Hamlin N., Holroyd S., Hornsby T., Jagels K., Krogh A., McLean J., Moule S., Murphy L., Oliver K., Osborne J., Quail M.A., Rajandream M.A., Rogers J., Rutter S., Seeger K., Skelton J., Squares R., Squares S., Sulston J.E., Taylor K., Whitehead S., Barrell B.G. Deciphering the biology of *Mycobacterium tuberculosis* from the complete genome sequence. *Nature.* **1998**, 393, 537-544.
- Desmond Molecular Dynamics System, v3.1, D. E. Shaw Research, New York, NY, 2012.
Maestro-Desmond Interoperability Tools, v3.1, Schrödinger, New York, NY, 2012.
- Eisenberg D., Gill H.S., Pfluegl G.M., Rotstein S.H. Structure-function relationships of glutamine synthetases. *Biochim. Biophys. Acta.* **2000**, 1477, 122–145.
- Falzon D., Jaramillo E., Schünemann H.J., Arentz M., Bauer M., Bayona J., Blanc L., Caminero

- J.A., Daley C.L., Duncombe C., Fitzpatrick C., Gebhard A., Getahun H., Henkens M., Holtz T.H., Keravec J., Keshavjee S., Khan A.J., Kulier R., Leimane V., Lienhardt C., Lu C., Mariandyshev A., Migliori G.B., Mirzayev F., Mitnick C.D., Nunn P., Nwagboniwe G., Oxlade O., Palmero D., Pavlinac P., Quelapio M.I., Raviglione M.C., Rich M.L., Royce S., Rüsç-Gerdes S., Salakaia A., Sarin R., Sculier D., Varaine F., Vitoria M., Walson J.L., Wares F., Weyer K., White R.A., Zignol M. WHO guidelines for the programmatic management of drug-resistant tuberculosis: 2011 update. *Eur. Resp. Jour.* **2011**, 38, 516-528.
- Flynn J.L., Chan J. Tuberculosis: Latency and Reactivation. *Infect. Immun.* **2001**, 69, 4195-4201.
- Gising J., Nilsson M.T., Odell L.R., Yahiaoui S., Lindh M., Iyer H., Sinha A.M., Srinivasa B.R., Larhed M., Mowbray S.L., Karlén A. Trisubstituted imidazoles as *Mycobacterium tuberculosis* glutamine synthetase inhibitors. *J. Med. Chem.*, **2012**, 55, 2894-2898.
- Friesner R.A., Murphy R.B., Repasky M.P., Frye L.L., Greenwood J.R., Halgren T.A., Sanschagrin P.C., Mainz D.T. Extra precision glide: docking and scoring incorporating a model of hydrophobic enclosure for protein-ligand complexes. *J. Med. Chem.* **2006**, 49, 6177-6196.
- Gising J., Nilsson M.T., Odell L.R., Yahiaoui S., Lindh M., Iyer H., Sinha A.M., Srinivasa B.R., Larhed M., Mowbray S.L., Karlén A. Trisubstituted imidazoles as *Mycobacterium tuberculosis* glutamine synthetase inhibitors. *J. Med. Chem.*, **2012**, 55, 2894-2898.
- Glavas S., Tanner M.E. Active site residues of glutamate racemase. *Biochemistry*, **2001**, 40, 6199-6204.
- Gopal M., Padayatchi N., Metcalfe J.Z., O'Donnell, M. R. Systematic review of clofazimine for the treatment of drug-resistant tuberculosis. *Int. J. Tuberc. Lung. Dis.* **2013**, 17, 1001-1007.

- Gordon A.H., Hart P.A., Young M.R. Ammonia inhibits phagosome-lysosome fusion in macrophages. *Nature*, **1980**, 286, 79-80.
- Grosset J. *Mycobacterium tuberculosis* in the extracellular compartment: an underestimated adversary. *Antimicrob. Agents. Chemother.* **2003**, 47, 833-836.
- Harth G., Horwitz M.A. An inhibitor of exported *Mycobacterium tuberculosis* glutamine synthetase selectively blocks the growth of pathogenic mycobacteria in axenic culture and in human monocytes: extracellular proteins as potential novel drug targets. *J. Exp. Med.*, **1999**, 189, 1425-1436.
- Harth G., Horwitz M.A. Inhibition of *Mycobacterium tuberculosis* glutamine synthetase as a novel antibiotic strategy against tuberculosis: demonstration of efficacy *in vivo*. *Infect. Immun.* **2003**, 71, 456-464.
- Harth, G., Clemens D.L., Horwitz M.A. Glutamine synthetase of *Mycobacterium tuberculosis*: extracellular release and characterization of its enzymatic activity. *Proc. Natl. Acad. Sci.*, **1994**, 91, 9342-9346.
- Höltje J.V. Growth of stress-bearing and shape-maintaining murein sacculus of *E. coli*. *Microbiol. Mol. Biol. Rev.* **1998**, 62, 181-203.
- Höner Zu Bentrup K., Miczak A., Swenson D.L., Russell D.G. Characterization of activity and expression of isocitrate lyase in *Mycobacterium avium* and *Mycobacterium tuberculosis*. *J. Bacteriol.* **1999**, 181, 7161-7167.
- Houben E.N., Nguyen L., Pieters J. Interaction of pathogenic mycobacteria with the host immune system. *Curr. Opin. Microbiol.* **2006**, 9, 76-85.
- Hugonnet J.E., Tremblay L.W., Boshoff H.I., Barry C.E., Blanchard J.S. Meropenem-clavulanate is effective against extensively drug-resistant *M. tuberculosis*. *Science*. **2009**, 323, 1215-

1218.

Hwang K.Y., Cho C.S., Kim S.S., Sung H.C., Yu Y.G., Cho Y. Structure and mechanism of glutamate racemase from *Aquifex pyrophilus*. *Nat. Struct. Biol.* **1999**, 6, 422–426.

Iseman, M. D. MDR-TB and the developing world—a problem no longer to be ignored: the WHO announces ‘DOTS Plus’ strategy [Editorial]. *Int. J. Tuberc. Lung. Dis.* **1998**, 2, 867-867.

James P.E., Grinberg O.Y., Michaels G., Swartz H.M. Intraphagosomal oxygen in stimulated macrophages. *J. Cell. Physiol.* **1995**, 163, 241-247.

Jarlier V., Nikaido H. Mycobacterial cell wall: structure and role in natural resistance to antibiotics. *FEMS. Microbiol. Lett.* **1994**, 123, 11-18.

Johnson M., Zaretskaya I., Raytselis Y., Merezhuk Y., McGinnis S., Madden T.L. NCBI BLAST: a better web interface. *Nucl. Acids. Res.* **2008**, 36, W5-W9.

Jones D., Metzger H.J., Schatz A., Waksman S.A. Control of gram-negative bacteria in experimental animals by streptomycin. *Science.* **1944**, 100, 103-105.

Jones G., Willett P., Glen R.C. Molecular recognition of receptor sites using a genetic algorithm with a description of desolvation. *J. Mol. Biol.* **1995**, 245, 43-53.

Jorgensen W.L. The many roles of computation in drug discovery. *Science*, **2004**, 303, 1813-1818.

Jorgensen W.L., Chandrasekhar J., Madura J.D., Impey R.W., Klein M.L. Comparison of simple potential functions for simulating liquid water. *J. Chem. Phys.* **1983**, 79, 926-935.

Jorgensen W.L., Maxwell D.S., Tirado-Rives J. Development and Testing of the OPLS All-

- Atom Force Field on Conformational Energetics and Properties of Organic Liquids. *J. Am. Chem. Soc.* **1996**, 118, 11225-11236.
- Jorgensen W.L., Ravimohan C. Monte Carlo simulation of differences in free energies of hydration. *J. Chem. Phys.* **1985**, 83, 3050-3054.
- Kar R.K., Suryadevara P., Jana J., Bhunia A., Chatterjee S. Novel G-quadruplex stabilizing agents: in-silico approach and dynamics. *J. Biomol. Struct. Dyn.*, **2013**, 31, 1497-1518.
- Kim K.H., Bong Y.J., Park J.K., Shin K.J., Hwang K.Y., Kim E.E. Structural basis for glutamate racemase inhibition. *J. Mol. Biol.* **2007**, 372, 434-443.
- Kinhikar A.G., Vargas D., Li H., Mahaffey S.B., Hinds L., Belisle J.T., Laal S. *Mycobacterium tuberculosis* malate synthase is a laminin-binding adhesin. *Mol. Microbiol.* **2006**, 60, 999-1013.
- Kirkwood J.K. Statistical Mechanics of Fluid Mixtures. *J. Chem. Phys.*, **1935**, 3, 300-313.
- Kollman P. Free energy calculations: Applications to chemical and biochemical phenomena. *Chem. Rev.* **1993**, 93, 2395-2417.
- Krajewski W.W., Jones T.A., Mowbray S.L. Structure of *Mycobacterium tuberculosis* glutamine synthetase in complex with a transition-state mimic provides functional insights. *Proc. Natl. Acad. Sci. USA.* **2005**, 102, 10499-10504.
- Kräutler V., van Gunsteren W.F., Hünenberger P.H. A fast SHAKE algorithm to solve distance constraint equations for small molecules in molecular dynamics simulations. *J. Comput. Chem.* **2001**, 22, 501-508.
- Krieger I.V., Freundlich J.S., Gawandi V.B., Roberts J.P., Gawandi V.B., Sun Q., Owen J.L., Fraile M.T., Huss S.I., Lavandera J.L., Ioerger T.R., Sacchettini J.C. Structure-guided

- discovery of phenyl-diketo acids as potent inhibitors of *M. tuberculosis* malate synthase. *Chem. Biol.* **2012**, 19, 1556-1567.
- Kwon Y.S., Jeong B.H., Koh W.J. Tuberculosis: clinical trials and new drug regimens. *Curr. Opin. Pulm. Med.* **2014**, 20, 280-286.
- Lechartier B., Hartkoorn R. C., Cole S.T. *In vitro* combination studies of benzothiazinone lead compound BTZ043 against *Mycobacterium tuberculosis*. *Antimicrob. Agents. Chemother.* **2012**, 56, 5790-5793.
- Lamichhane G., Zignol M., Blades N.J., Geiman D.E., Dougherty A., Grosset J., Broman K.W., Bishai W.R. A postgenomic method for predicting essential genes at subsaturation levels of mutagenesis: application to *Mycobacterium tuberculosis*. *Proc. Natl. Acad. Sci. USA.* **2003**, 100, 7213-7218.
- Laskowski R.A., MacArthur M.W., Moss D.S., Thornton J.M. PROCHECK: a program to check the stereochemical quality of protein structures. *J. Appl. Cryst.* **1993**, 26, 283-291.
- Lechartier B., Hartkoorn R. C., Cole S.T. *In vitro* combination studies of benzothiazinone lead compound BTZ043 against *Mycobacterium tuberculosis*. *Antimicrob. Agents. Chemother.* **2012**, 56, 5790-5793.
- Li YJ, Petrofsky M., Bermudez L.E. *Mycobacterium tuberculosis* uptake by recipient host macrophages is influenced by environmental conditions in the granuloma of the infectious individual and is associated with impaired production of interleukin-12 and tumor necrosis factor alpha. *Infect. Immun.* **2002**, 70, 6223-6230.
- Liaw, S.H., Eisenberg D. Structural model for the reaction mechanism of glutamine synthetase, based on five crystal structures of enzyme-substrate complexes. *Biochemistry*, **1994**, 33, 675-681.

Lundqvist T., Fisher S.L., Kern G., Folmer R.H., Xue Y., Newton D.T., Keating T.A., Alm R.A., de Jonge B.L. Exploitation of structural and regulatory diversity in glutamate racemases. *Nature*. **2007**, 447, 817–822.

Lyne P.D., Lamb M.L., Saeh J.C. Accurate prediction of the relative potencies of members of a series of kinase inhibitors using molecular docking and MM-GBSA scoring. *J. Med. Chem.* **2006**, 49, 4805-4808.

Makarov V., Manina G., Mikusova K., Möllmann U., Ryabova O., Saint-Joanis B., Dhar N., Pasca M.R., Buroni S., Lucarelli A.P., Milano A., De Rossi E., Belanova M., Bobovska A., Dianiskova P., Kordulakova J., Sala C., Fullam E., Schneider P., McKinney J.D., Brodin P., Christophe T., Waddell S., Butcher P., Albrethsen J., Rosenkrands I., Brosch R., Nandi V., Bharath S., Gaonkar S., Shandil R.K., Balasubramanian V., Balganesht T., Tyagi S., Grosset J., Riccardi G., Cole S.T. Benzothiazinones kill *Mycobacterium tuberculosis* by blocking arabinan synthesis. *Science*, **2009**, 324, 801-804.

Matsumoto M., Hashizume H., Tomishige T., Kawasaki M., Tsubouchi H., Sasaki H., Shimokawa Y., Komatsu M. OPC-67683, a nitro-dihydro-imidazooxazole derivative with promising action against tuberculosis *in vitro* and in mice. *PLoS. Med.* **2006**, 3, e466.

McKinney J.D., Höner zu Bentrup K., Muñoz-Elías E.J., Miczak A., Chen B., Chan W.T., Swenson D., Sacchetti J.C., Jacobs W.R., Russell D.G. Persistence of *Mycobacterium tuberculosis* in macrophages and mice requires the glyoxylate shunt enzyme isocitrate lyase. *Nature*. **2000**, 406, 735-738.

McNeil M., Wallner S.J., Hunter S.W., Brennan P.J. Demonstration that the galactosyl and arabinosyl residues in the cell-wall arabinogalactan of *Mycobacterium leprae* and *Mycobacterium tuberculosis* are furanoid. *Carbohydr. Res.* **1987**, 166, 299-308.

Mowbray S.L., Kathiravan M.K., Pandey A.A., Odell L.R. Inhibition of glutamine synthetase: a potential drug target in *Mycobacterium tuberculosis*. *Molecules*, **2014**, 19, 13161-13176.

- Muttucumaru D.G., Roberts G., Hinds J., Stabler R.A., Parish T. Gene expression profile of *Mycobacterium tuberculosis* in a non-replicating state. *Tuberculosis (Edinb)*. **2004**, 84, 239-246.
- Niesen F.H., Berglund H., Vedadi M. The use of differential scanning fluorimetry to detect ligand interactions that promotes protein stability. *Nat. Protoc.* **2007**, 2, 2212-2221.
- Nordqvist A., Nilsson M.T., Lagerlund, O., Muthas, D., Gising, J., Yahiaoui, S., Odell, L.R., Srinivasa, B.R., Larhed, M., Mowbray, S.L., Karlén A. Synthesis, biological evaluation and X-ray crystallographic studies of imidazo[1,2-a]pyridine-based *Mycobacterium tuberculosis* glutamine synthetase inhibitors. *Med. Chem. Comm.*, **2012**, 3, 620-626.
- Nordqvist A., Nilsson M.T., Röttger S., Odell L.R., Krajewski W.W., Anderson C.E., Larhed M., Mowbray S.L., Karlén A. Evaluation of the amino acid binding site of *Mycobacterium tuberculosis* glutamine synthetase for drug discovery. *Bioorg. Med. Chem.* **2008**, 16, 5501-5513.
- Pasca M.R., Degiacomi G., Ribeiro A.L., Zara F., De Mori P., Heym B., Mirrione M., Berra R., Pagani L., Pucillo L., Troupioti P., Makarov V., Cole S.T., Riccardi G. Clinical isolates of *Mycobacterium tuberculosis* in four European hospitals are uniformly susceptible to benzothiazinones. *Antimicrob. Agents. Chemother.* **2010**, 54, 1616-1618.
- Pieters J. *Mycobacterium tuberculosis* and the macrophage: maintaining a balance. *Cell. Host. Microbe.* **2008**, 3, 399-407.
- QikProp, v3.5, Schrödinger, LLC, New York, NY, 2012.
- Reece R.J., Maxwell A. DNA gyrase: structure and function. *Crit. Rev. Biochem. Mol. Biol.* **1991**, 26, 335-375.
- Ruzheinikov S.N., Taal M.A., Sedelnikova S.E., Baker P.J., Rice D.W. Substrate-induced

- conformational changes in *Bacillus subtilis* glutamate racemase and their implications for drug discovery. *Structure*. **2005**, 13, 1707–1713.
- Sacksteder K.A., Protopopova M., Barry C. E., Andries K., Nacy C.A. Discovery and development of SQ109: a new antitubercular drug with a novel mechanism of action. *Fut. Microbial*. **2012**, 7, 823-837.
- Sasseti C.M., Rubin E.J. Genetic requirements for mycobacterial survival during infection. *Proc. Natl. Acad. Sci. USA*. **2003**, 100, 12989-12994.
- Schatz A, Bugie E, Waksman S.A. Streptomycin, a substance exhibiting antibiotic activity against Gram-positive and Gram negative bacteria. *Proc. Soc. Exp. Biol. Med*. **1944**, 55, 66–69.
- Schleifer K.H., Kandler O. Peptidoglycan types of bacterial cell walls and their taxonomic implications. *Bacteriol. Rev.* **1972**, 36, 407–477.
- Schnappinger D., Ehrt S., Voskuil M.I., Liu Y., Mangan J.A., Monahan I.M., Dolganov G., Efron B., Butcher P.D., Nathan C., Schoolnik G.K. Transcriptional Adaptation of *Mycobacterium tuberculosis* within Macrophages: Insights into the Phagosomal Environment. *J. Exp. Med*. **2003**, 198, 693-704.
- Sengupta S., Ghosh S., Nagaraja V. Moonlighting function of glutamate racemase from *Mycobacterium tuberculosis*: racemization and DNA gyrase inhibition are two independent activities of the enzyme. *Microbiol*. **2008**, 154, 2796–2803.
- Sengupta S., Nagaraja V. Inhibition of DNA gyrase activity by *Mycobacterium smegmatis* MurI. *FEMS. Microbiol. Lett*. **2008**, 279, 40–47.
- Sengupta S., Shah M., Nagaraja V. Glutamate racemase from *M. tuberculosis* inhibits DNA gyrase by affecting its DNA-binding. *Nucleic. Acids. Res*. **2006**, 34, 5567–5576.

- Shelley J.C., Cholleti A., Frye L., Greenwood J.R., Timlin M.R., Uchimaya M. Epik: a software program for *pKa* prediction and protonation state generation for drug-like molecules. *J. Comp. Aided Mol. Des.*, **2007**, 21, 681-691.
- Sherman D.R., Voskuil M., Schnappinger D., Liao R., Harrell M.I., Schoolnik G.K. Regulation of the *Mycobacterium tuberculosis* hypoxic response gene encoding alpha -crystallin. *Proc. Natl. Acad. Sci. USA.* **2001**, 98, 7534-7539.
- Singh B., Mitchison D.A. Bactericidal activity of streptomycin and isoniazid against tubercle bacilli. *BMJ.* **1954**, 1, 130-138.
- Singh K.K., Dong Y., Belisle J.T., Harder J., Arora V.K., Laal S. Antigens of *Mycobacterium tuberculosis* recognized by antibodies during incipient, subclinical tuberculosis. *Clin. Diagn. Lab. Immunol.* **2005**, 12, 354-358.
- Smith C.V., Huang C.C., Miczak A., Russell D.G., Sacchettini J.C., Höner zu Bentrup K. Biochemical and structural studies of malate synthase from *Mycobacterium tuberculosis*. *J. Biol. Chem.* **2003**, 278, 1735-1743.
- Smith C.V., Sharma V., Sacchettini J.C. TB drug discovery: addressing issues of persistence and resistance. *Tuberculosis (Edinb).* **2004**, 84, 45-55.
- Sriram D., Yogeewari P., Basha J.S., Radha D.R, Nagaraja V. Synthesis and antimycobacterial evaluation of various 7-substituted ciprofloxacin derivatives. *Bioorg. Med. Chem.* **2005**, 13, 5774-5778.
- Stewart G.R., Robertson B.D., Young D.B. Tuberculosis: a problem with persistence. *Nat. Rev. Microbiol.* **2003**, 1, 97-105.
- Sturgill-Koszycki S., Haddix P.L., Russell D.G. The interaction between mycobacterium and the macrophage analyzed by two-dimensional polyacrylamide gel electrophoresis.

Electrophoresis. **1997**, 18, 2558-2565.

Takayama K., Wang C., Besra G.S. Pathway to synthesis and processing of mycolic acids in *Mycobacterium tuberculosis*. *Clin. Microbiol. Rev.* **2005**, 18, 81-101.

Thomas J.P, Baughn C.O., Wilkinson R.G., Shepherd R.G. A new synthetic compound with antituberculous activity in mice: ethambutol (dextro-2,2'-(ethylenediimino)-di-1-butanol), *Am. Rev. Respir. Dis.* **1961**. 83, 891-893.

Trauner, A., Borrell, S., Reither, K., Gagneux, S. Evolution of drug resistance in tuberculosis: recent progress and implications for diagnosis and therapy. *Drugs*. **2014**, 74, 1063-1072.

Tripathi D., Chandra H., Bhatnagar R. Poly-L-glutamate/glutamine synthesis in the cell wall of *Mycobacterium bovis* is regulated in response to nitrogen availability. *BMC. Microbiol.* **2013**, 13, 226-237.

Tripathi D., Kant S., Garg R., Bhatnagar R. Low expression level of glnA1 accounts for absence of cell wall associated poly-L-glutamate/glutamine in *Mycobacterium smegmatis*. *Biochem Biophys Res Commun.* **2015**, 458, 240-245.

Voskuil M.I., Visconti K.C., Schoolnik G.K. *Mycobacterium tuberculosis* gene expression during adaptation to stationary phase and low-oxygen dormancy. *Tuberculosis (Edinb)*. **2004**, 84, 218-227.

Wayne L.G., Lin K.Y. Glyoxylate metabolism and adaptation of *Mycobacterium tuberculosis* to survival under anaerobic conditions. *Infect. Immun.* **1982**, 37, 1042-1049.

Wheeler P.R., Ratledge C. Use of carbon sources for lipid biosynthesis in *Mycobacterium leprae*: a comparison with other pathogenic mycobacteria. *J. Gen. Microbiol.* **1988**, 134, 2111- 2121.

Wilson S.M.H., Sambandamurthy V.K., Jacobs W.R. Survival perspectives from the world's most successful pathogen *Mycobacterium tuberculosis*. *Nature*. **2003**, 4, 949-955.

World Health Organization. WHO Global Task Force outlines measures to combat XDR-TB worldwide. *Geneva, Switzerland*, **2006**, 9.

Zumla A., Nahid P., Cole S.T. Advances in the development of new tuberculosis drugs and treatment regimens. *Nat. Rev. Drug. Discov.* **2013**, 12, 388-404.

ANNEXURE-I

Synthetic procedure and characterization of 3-[1-(2-amino-2-oxoethyl)-5-phenyl-1H-pyrrol-2-yl]propanoic acid derivatives.

1. General procedure for synthesis of substituted (E)-4-(furan-2-yl)-1-phenylbut-2-en-1-one

A solution of 2-furaldehyde (5.85 g, 60.92 mmol) was added to a methanol solution (120 mL) of substituted acetophenone (1equiv), followed by the addition of sodium methoxide (1 equiv). The reaction mixture was stirred at room temperature for 16 h, followed by removal of the solvent in vacuo. The resultant mixture was diluted with water (30 mL) and extracted with ethyl acetate (90 mL). The aqueous layer was re-extracted with ethyl acetate (20 mL). The combined organic layers were dried over anhydrous Na₂SO₄ and the solvent was removed in vacuo to obtain the product *substituted (E)-4-(furan-2-yl)-1-phenylbut-2-en-1-one* as an orange solid.

2. General procedure for synthesis of substituted ethyl 4,7-dioxo-7-phenylheptanoate

ConcHCl(59 mL) was added to a solution of substituted *(E)-4-(furan-2-yl)-1-phenylbut-2-en-1-one* (1equiv) in ethanol (20 ml). The reaction mixture was heated under reflux for 16 h, concentrated, and diluted with dichloromethane (250 mL), and the resultant organic layer was washed with water (25 mL). After phase separation, the organic layer was dried over anhydrous Na₂SO₄ and the solvent removed in vacuo to obtain the crude mixture, which was purified by silica gel flash chromatography to obtain *substituted ethyl 4,7-dioxo-7-phenylheptanoate* in good yield.

3. General procedure for synthesis of substituted 2-(2-(3-ethoxy-3-oxopropyl)-5-phenyl-1H-pyrrol-1-yl)acetic acid

Glycine (1equiv) was added to a solution *substituted ethyl 4,7-dioxo-7-phenylheptanoate* (1equiv) in ethanol (6 mL), followed by the addition of p-toluenesulfonic acid monohydrate (abbreviated TsOH or pTsOH) (0.12 equiv). The reaction mixture was heated under reflux for

16 h, and the solvent removed in vacuo to obtain a crude product which upon purification by silica gel flash chromatography, gives *substituted 2-(2-(3-ethoxy-3-oxopropyl)-5-phenyl-1H-pyrrol-1-yl)acetic acid* in good yield.

4. General procedure for synthesis of *substituted ethyl 3-(1-(2-oxo-2-(phenylamino)ethyl)-5-phenyl-1H-pyrrol-2-yl)propanoate*

The *substituted 2-(2-(3-ethoxy-3-oxopropyl)-5-phenyl-1H-pyrrol-1-yl)acetic acid* (1 equiv) was dissolved in dry DCM (10 mL) and cooled to 0 °C. To this reaction mixture triethyl amine was added drop wise under cool condition. Then EDC HCl (1.5 equiv) and HOBT (0.1 equiv) was added followed by substituted amines. Allowed the reaction mixture to come to RT and stirred for 6 h. The reaction mixture was washed with water (30 ML). After phase separation, the organic layer was dried over anhydrous Na₂SO₄ and the solvent removed in vacuo to obtain the crude mixture, which was purified by silica gel flash chromatography to obtain *substituted ethyl 3-(1-(2-oxo-2-(phenylamino)ethyl)-5-phenyl-1H-pyrrol-2-yl)propanoate* in good yield.

ANNEXURE-II

Synthetic procedure and characterization of N-(2,4-diacetylazetid-1-yl) benzamide derivatives.

1. General procedure for synthesis of 2,4-Dibromopentanedioic acid:

Bromine (4.49 ml, 87.6 mmol) was added drop wise to glutaric anhydride (5.0 g, 43.8 mmol) in a three-necked flask fitted with reflux condenser and CaCl₂ guard tube at 30° C. After the addition of bromine, the reaction mixture was heated to 90° C for 1h and then at 100° C for another 1h. The reaction mixture was cooled to 30° C and formic acid (4 ml) was added slowly. The content of the flask was heated to 100° C for 1h. The reaction mixture was quenched with water and extracted with ethyl acetate (4 x 100 ml). The combined organic layer was dried over sodium sulphate and evaporated to give white gummy solid. The trituration of the gummy solid with diethyl ether give 2,4-dibromopentanedioic acid as white solid (2.7 g, 20.5 %).

2. General procedure for synthesis of amide derivatives:

To a solution of 2,4-dibromopentanedioic acid (1 mmol) in dry dichloromethane (10 ml), various amines (2.2 mmol) was added at 0° C and stirred under nitrogen atmosphere. EDC.HCl (3mmol), HOBt (3 mmol) and triethyl amine (6 mmol) were added at 0° C and stirred at RT for 16hrs. The reaction mixture was quenched with water and extracted with dichloromethane. The combined organic layers were washed with brine, dried over sodium sulphate and concentrated. The crude products were purified by column chromatography to afford respective products.

3. General procedure for final compounds (RV01-11):

To a solution of amide (1mmol) in dry DMF (10 ml), benzohydrazide (0.51 g, 4mmol) was added and heated to 80° C for 2 hrs. The reaction mixture was concentrated to remove DMF and the residue was dissolved in dichloromethane. The organic layer was washed with saturated aq. NaHCO₃ solution, water, brine, dried over Na₂SO₄ and concentrated. The crude product was purified by column chromatography to afford the final product.

ANNEXURE-III

Synthetic procedure and characterization of 4-(1H-benzimidazol-2-yl)-N-benzylaniline derivatives.

1. General procedure for the synthesis of substituted 4-(1H-benzo[d]imidazole-2-yl)aniline

Eaton's reagent (10 vol; wt/vol) was added drop wise to a well pulverised mixture of the corresponding 1,2-phenylenediamine (1 equiv) and 4-amino benzoic acid (1 equiv) at 0°C. The reaction mixture was then heated at 130°C for 10 - 12 h (monitored by TLC and LCMS for completion). The reaction mixture was cooled and neutralised with 10% sodium hydroxide solution to pH of 6-7, the precipitate formed was filtered and washed repeatedly with water and dried. The solid obtained was recrystallized from ethanol to afford the desired product in good yield.

2. Procedure for synthesis of final compounds (RP01-25)

To solution of 4-(1H-benzo[d]imidazole-2-yl)aniline (1 mmol) in 10% methanol DCM, corresponding aldehyde (1.1 mmol) , molecular sieves and catalytic amount of acetic acid were added and stirred for 8hrs. The reaction mixture was then filtered through celite bed and the filtrate was concentrated under argon atmosphere. The resulting residue was dissolved in methanol and cooled to 0 °C followed by the addition of sodium cyano borohydride (1.5 mmol) portion wise. The resultant solution was allowed to attain room temperature and stirred for 4 hrs (monitored by TLC and LCMS for completion). The solvent was evaporated under reduced pressure and the residue was dissolved in ethyl acetate. The organic layer was washed with water followed by brine solution and evaporated in vacuum. The resulting residue was purified by column chromatography using hexane, ethyl acetate as eluent to afford pure product.

APPENDIX

LIST OF PUBLICATIONS

From thesis work

1. **Suryadevara P.**, Soni V., Brindha Devi P., Nandicoori V.K., Sriram D, Yogeeswari P. Computational Sampling and Simulation Based Assessment of Novel *Mycobacterium tuberculosis* Glutamine Synthetase Inhibitors: Study involving Structure Based Drug Design and Free Energy Perturbation. *Current topics in Medicinal Chemistry* (2015), 16(9), 978-995. [PMID-26303425]
2. **Suryadevara P.**, Brindha Devi P., Sriram D, Yogeeswari P. Identification of Novel Inhibitors against Malate Synthase of *Mycobacterium tuberculosis* using Structure-based Drug Design. *Journal of Molecular Graphics and Modelling* (2016) (under review).

Other Publications

1. Soni V., Upadhyay S., **Suryadevara P.**, Samala G., Singh A., Yogeeswari P., Sriram D., Nandicoori V.K., Depletion of *M. tuberculosis* GlmU from infected murine lungs affects the clearance of the pathogen. **PLOS Pathogens** (2015) 11(10):e1005235. [PMID-26489015]
2. Medapi B.*, **Suryadevara P.***, Renuka J., Sridevi J.P., Yogeeswari P., Sriram D. 4-Aminoquinoline Derivatives as Novel *Mycobacterium tuberculosis* GyrB Inhibitors: Structural Optimization, Synthesis and Biological Evaluation. **European Journal of Medicinal Chemistry** (2015) 103:1 DOI: 10.1016/j.ejmech.2015.06.032. [PMID-26318054]
***Contributed equally**
3. Soni V.*, **Suryadevara P.***, Sriram D., OSDD Consortium., Kumar S., Nandicoori V.K., Yogeeswari P. Structure-based design of diverse inhibitors of *Mycobacterium tuberculosis* N-acetylglucosamine-1-phosphate uridyltransferase: combined molecular docking, dynamic simulation, and biological activity. **Journal of Molecular Modeling** (2015) 21(7):2704. [PMID-26078037]
***Contributed equally**
4. Pissinate. P, Rostirolla. D.C, Pinheiro. L.M, **Suryadevara. P**, Yogeeswari. P, Sriram. D, Santos. D.S, Synthesis and evaluation of thiazolyl-1H-benzo[d]imidazole inhibitors of *Mycobacterium tuberculosis* inosine monophosphate dehydrogenase. **Journal of the Brazilian Chemical Society**. (2015) DOI: 10.5935/0103-5053.20150104.
5. Sridevi J.P., **Suryadevara P.**, Janupally R., Sridhar J., Soni V., Anantaraju H.S., Yogeeswari P., Sriram D. Identification of potential *Mycobacterium tuberculosis* topoisomerase I inhibitors: a study against active, dormant and resistant tuberculosis. **European Journal of Pharmaceutical Sciences** (2015) 72:81-92. [PMID-25769524]
6. Jeankumar V.U., Kotagiri S., Janupally R., **Suryadevara P.**, Sridevi J.P., Medishetti R., Kulkarni P., Yogeeswari P., Sriram D. Exploring the gyrase ATPase domain for tailoring newer anti-tubercular drugs: Hit to lead optimization of a novel class of thiazole inhibitors. **Bioorganic Medicinal Chemistry** (2015) 23(3):588-601. [PMID-25541204]
7. Janupally R., Medapi B., Brindha Devi P., **Suryadevara P.**, Jeankumar V.U., Kulkarni P., Yogeeswari P., Sriram D. Design and Biological Evaluation of

- Furan/Pyrrole/Thiophene-2-carboxamide Derivatives as Efficient DNA GyraseB Inhibitors of *Staphylococcus aureus*. *Chemical Biology and Drug Design* (2015) 86(4):918-925. [PMID-25619742]
8. Janupally R., Jeankumar V.U., Bobesh K.A., Soni V., Devi P.B., Pulla V.K., **Suryadevara P.**, Chennubhotla K.S., Kulkarni P., Yogeewari P., Sriram D. Structure-guided design and development of novel benzimidazole class of compounds targeting DNA gyraseB enzyme of *Staphylococcus aureus*. *Bioorganic Medicinal Chemistry* (2014) 22(21):5970-5987. [PMID-25288496]
9. Jeankumar V.U., Janupally R., Pulla V.K., Soni V., Sridevi J.P., **Suryadevara P.**, Shraavan M., Medishetti R., Kulkarni P., Yogeewari P., Sriram D. Development of novel N-linked aminopiperidine-based mycobacterial DNA gyrase B inhibitors: Scaffold hopping from known antibacterial leads. *International Journal of Antimicrobial Agents* (2014) 43(3):269-278. [PMID-24434114]
10. Jeankumar V.S., Alokam R., Sridevi J.P., **Suryadevara P.**, Matikonda S.S., Peddi S., Sahithi S., Alvala M., Yogeewari P., Sriram D. Discovery and structure optimization of a series of isatin derivatives as *Mycobacterium tuberculosis* chorismate mutase inhibitors. *Chemical Biology and Drug Design* (2014) 83(4):498-506. [PMID-24636345]
11. Jeankumar V.S., Renuka J., Peddi S., Soni V., Sridevi J.P., **Suryadevara P.**, Yogeewari P., Sriram D. Thiazole-Aminopiperidine hybrid analogues: Design and synthesis of novel *Mycobacterium tuberculosis* GyrB inhibitors. *European Journal of Medicinal Chemistry* (2013) 70:143-153. [PMID-24148991]

BIOGRAPHY OF PRIYANKA SURYADEVARA

Ms. Priyanka Suryadevara completed her Bachelor of Pharmacy from Acharya Nagarjuna University, Guntur, Andhra Pradesh, India and Master of Science (M.S. (Pharm.)) in Pharmacoinformatics from National Institute of Pharmaceutical Education and Research (NIPER), Hajipur, Bihar, India. She has been awarded INSPIRE fellowship by Department of Science and Technology (DST), India for a period of five years (2013-2018) to carry out her doctoral research work under the supervision of Prof. P. Yogeeswari. She has published 16 scientific publications in well-renowned international journals and presented papers in various conferences.

BIOGRAPHY OF PROF. P. YOGEE SWARI

Prof. P. Yogeeswari is presently working in the capacity of Professor and Associate Dean (Sponsored Research and Consultancy Division), Department of Pharmacy, Birla Institute of Technology and Science, Pilani, Hyderabad Campus. She received her Ph.D. degree in the year 2001 from Banaras Hindu University; Varanasi. She has been involved in research for the last 14 years and in teaching for 13 years. APTI honoured her with YOUNG PHARMACY TEACHER AWARD for the year 2007. In 2010, ICMR honored her by awarding “Shakuntala Amir Chand Award” for her excellent biomedical research. She has been awarded for IASP 2014 “Excellence in Pain Research and Management in Developing Countries” under the basic science research category at Argentina in October 2014. She has collaborations with various national and international organizations that include National Institute of Health, Bethesda, USA, National Institute of Mental Health and Neurosciences, Bangalore, Karolinska Institute, Stockholm, Sweden, National Institute of Immunology, New Delhi, India, Pasteur Institute, University of Lille, France, Bogomoletz Institute of Physiology National Academy of Science, Ukraine, and Faculty of Medicine of Porto, Porto, Portugal,. She has to her credit more than 250 research publications and five Indian Patents. She is an expert reviewer of many international journals like Journal of Medicinal Chemistry (ACS), Journal of Chemical Information & Modeling (ACS, USA), Bioorganic Medicinal Chemistry (Elsevier), Recent Patents on CNS Drug Discovery (Bentham), etc. She has also co-authored a textbook on organic medicinal chemistry with Prof. D Sriram titled “Medicinal Chemistry” published by Pearson Education and three book chapters. She is a lifetime member of Association of Pharmacy Teachers of India and Indian Pharmacological Society. She has successfully completed many sponsored projects and currently handling projects sponsored by DST, DBT INDO-BRAZIL and ICMR-INSERM. She has guided thirteen Ph.D students and currently seven students are pursuing their Ph.D. work.